

Advances in
GEOPHYSICS
VOLUME 35

Seismological Structure of Slabs

ADVANCES IN
G E O P H Y S I C S

VOLUME 35

This Page Intentionally Left Blank

Advances in
G E O P H Y S I C S

Seismological Structure of Slabs

Edited by

RENATA DMOWSKA

*Division of Applied Sciences
Harvard University
Cambridge, Massachusetts*

BARRY SALTZMAN

*Department of Geology and Geophysics
Yale University
New Haven, Connecticut*

VOLUME 35



ACADEMIC PRESS

San Diego New York Boston
London Sydney Tokyo Toronto

This book is printed on acid-free paper. 

Copyright © 1994 by ACADEMIC PRESS, INC.
All Rights Reserved.

No part of this publication may be reproduced or transmitted in any form or by any means, electronic or mechanical, including photocopy, recording, or any information storage and retrieval system, without permission in writing from the publisher.

Academic Press, Inc.
A Division of Harcourt Brace & Company
525 B Street, Suite 1900, San Diego, California 92101-4495

United Kingdom Edition published by
Academic Press Limited
24-28 Oval Road, London NW1 7DX

International Standard Serial Number: 0065-2687

International Standard Book Number: 0-12-018835-X

PRINTED IN THE UNITED STATES OF AMERICA
94 95 96 97 98 99 QW 9 8 7 6 5 4 3 2 1

CONTENTS

Seismological Constraints on the Velocity Structure and Fate of Subducting Lithospheric Slabs: 25 Years of Progress

THORNE LAY

1. Introduction	1
1.1 Slabs and Mantle Convection	2
1.2 How Seismology Provides Information about Slabs	6
1.3 Earthquakes in Slabs	7
2. General Characterization of Slab and Wedge Structures	12
2.1 First-Order Slab Anomalies	12
2.2 Guided Waves	27
2.3 Wedge Structure	31
2.4 Thermal and Mechanical Models	35
3. Travel Time Pattern Constraints on Slab Velocity Structure	51
3.1 Relative Travel Time Patterns and Raytracing Analyses	53
3.2 Residual Sphere Modeling	70
4. Tomographical Imaging of Slab Velocity Structure	88
4.1 Northwest Pacific	90
4.2 Southwest Pacific	104
4.3 South America, Central America, and the Caribbean	108
4.4 Cascadia, Aleutians, and Alaska	110
4.5 Mediterranean and Hindu Kush	114
5. Slab Boundaries: Converted and Reflected Phases	117
5.1 Slab Seismicity and Double Benioff Zones	117
5.2 Constraints on Slab Boundaries and Internal Structure	121
5.3 Seismic Imaging of Phase Boundaries in Slabs	134
6. Focusing, Multipathing, and Diffraction Effects of Slab Structure	138
6.1 Short-Period Defocusing and Multipathing Effects	139
6.2 Long-Period Defocusing and Diffraction Effects	142
7. Future Directions in Slab Imaging and Summary	148
References	154
INDEX	181

This Page Intentionally Left Blank

SEISMOLOGICAL CONSTRAINTS ON THE VELOCITY STRUCTURE AND FATE OF SUBDUCTING LITHOSPHERIC SLABS: 25 YEARS OF PROGRESS

THORNE LAY

*Institute of Tectonics and C.F. Richter Seismological Laboratory
University of California, Santa Cruz
Santa Cruz, California 95064*

1. INTRODUCTION

The recognition that intermediate- and deep-focus earthquakes occur in regions where cold oceanic lithosphere has sunk into the mantle played a major role in the evolution of the theory of plate tectonics in the 1960s (e.g., Isacks *et al.*, 1968). This new dynamical context confronted seismologists and other geophysicists with the challenge of determining the structure and ultimate fate of the downwelling material. The importance of the latter issue for understanding mantle dynamics and thermal evolution of the Earth has spurred the development of many seismological approaches to determining the structure of subducted lithosphere, and rapid advances have ensued over the past quarter century.

The slab imaging problem is especially challenging in that slabs are relatively small-scale three-dimensional seismic velocity heterogeneities embedded in the most heterogeneous regions of the planet. The downwelling material is imperfectly sampled by the sparse seismic wave coverage provided by distributions of natural seismicity and seismological observatories. Controlled seismic experiments to study slabs are logically difficult to implement. Nonetheless, large-scale three-dimensional elastic velocity images of deep slab structures and detailed models of the internal layered seismic velocity structure of slabs have been developed by seismic wave analysis. These models have many implications for the dynamical, thermal, and chemical state of the sinking lithosphere. As might be expected for any such complex undertaking, substantial disagreements persist over the interpretations of the seismic models as well as aspects of the basic seismological data sets and imaging procedures, but there is a clear consensus that progress is being made.

This review, intended for both seismologists and other researchers with interests in earth dynamics, consolidates the substantial 25-year literature on direct seismological measurements of the elastic wave velocity structure and anelasticity of subducting slabs, as these properties provide the primary constraints

on the composition and thermal state of the slabs. The reference list is relatively complete in this regard (through 1993), directing the reader to most major and minor contributions that have been published in the past three decades, although there are undoubtedly additional studies that have accidentally been overlooked.

Many studies relevant to deep slabs will not be considered here. Although studies of focal mechanisms, individual event rupture processes, and seismicity distributions within subducting slabs contribute to our understanding of slab dynamics and geometry, only a few references in these areas are included. Several previous studies have summarized the geometric constraints on slabs revealed by seismicity distributions (e.g., Isacks and Barazangi, 1977; Bevis and Isacks, 1984; Burbach and Frohlich, 1986; Yamaoka *et al.*, 1986; Fukao *et al.*, 1987; Chiu *et al.*, 1991), and these provide extensive bibliographies. Reviews of spatial and temporal distributions of intermediate- and deep-focus earthquake mechanisms in slabs are also available (e.g., Isacks and Molnar, 1971; Vassiliou, 1984; Apperson and Frohlich, 1987; Astiz *et al.*, 1988; Lay *et al.*, 1989; Sugi *et al.*, 1989), and only a few of the corresponding references are discussed here. Tabulations of subduction zone kinematic parameters are available elsewhere (e.g., Jarrard, 1986). Only sparse mention is made of shallow multichannel seismic imaging of convergent margins, which is yielding important information on shallow slab structure. A good introduction to this literature is provided by von Huene and Scholl (1991), who consider the effects of sediment subduction, underplating, and development of accretionary prisms. Although many geodynamical studies of subducting slabs are cited, that extensive literature is not critiqued, for ongoing advances in numerical modeling of increasingly realistic flow models are overturning many previous results. A comprehensive discussion of petrological and mineral physics attributes of deep slab structure is not undertaken here, but ultimately it is of course imperative that any seismological models be interpreted in such a context. Indeed, future efforts to improve slab imaging must increasingly incorporate compositional constraints in addition to thermal models, as discussed in Section 7. The seismic results discussed here represent only the first step. Yet, even with these omissions, the seismological literature on slab velocity structure is substantial and difficult to get a handle on, which provided the original motivation for assembling this review.

1.1. Slabs and Mantle Convection

The Earth's mantle is undergoing subsolidus thermal convection driven by a combination of internal radiogenic heating and about 10–15% heating from below caused by cooling of the core. Good overviews of this large-scale mantle convection context are provided by Silver *et al.* (1988), Jordan *et al.* (1989), and Olson *et al.* (1990). Jordan *et al.* (1989) describe the contemporary perspective

of lithospheric slabs as boundary layer phenomena and define the important notions of chemical, thermal, and mechanical boundary layers, each having different seismic velocity manifestations. This review assumes general familiarity on the part of the reader with the basics of lithospheric evolution and dynamics.

Oceanic lithosphere, the stiff plate formed by the cooling of chemically differentiated material that rises and melts under midocean ridges and spreads laterally in the process called sea-floor spreading, has an ephemeral residence at the surface of the Earth (Fig. 1). Typically, within 100–200 My of its formation, densification of the old oceanic lithosphere associated with its thickening thermal boundary layer leads to a dynamic instability causing it to bend acutely and sink into the interior at a subduction zone, descending as a layered slab with distinct thermal and chemical characteristics relative to the surrounding ambient mantle. The slab includes a thin veneer of surficial ocean floor sediments, on average 50% of which are scraped off and incorporated in the accretionary wedge (von Huene and Scholl, 1991); a 6–8-km-thick layer of basaltic crust; and a 60–90-km-thick layer of olivine-, orthopyroxene-, and clinopyroxene-rich material depleted in the basaltic components (e.g., Ringwood, 1976; Anderson, 1987b; Ringwood and Irifune, 1988). The bottom of the slab is defined rheologically by the transition to predominantly ductile behavior which has increasing shear strain deformation. The slab straightens and heats back up as it sinks, but the warming is sluggish, slow to overcome the effect of more than 100 My of cooling at the surface, and the negative buoyancy of the slab drives its descent. This process constitutes an integral part of plate tectonics, driven by the cooling of the mantle.

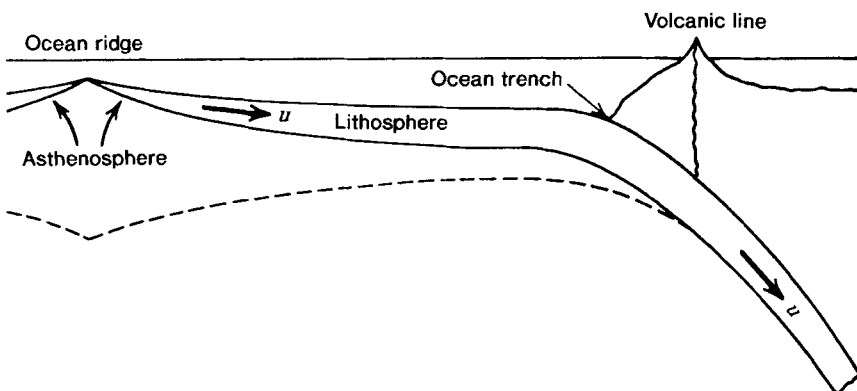


Fig. 1. Schematic evolution of an oceanic lithosphere, which eventually sinks into the mantle as a subducting slab at a subduction zone. The slab can be thought of as a descending thermal boundary layer, but it has also chemically differentiated during its formation, and its low temperature gives it a high viscosity. Reprinted with permission from Turcotte and Schubert (1982).

Increasing pressure and temperature with depth induce various chemical reactions in the slab, including expulsion of water and other volatiles accumulated at the surface, and destabilization of associated hydrous phases. Suites of mineralogical phase transformations occur within the slab's crustal and depleted mantle components. Because the slab has been processed through the melting zone at the ridge, partially hydrated, and cooled significantly, the phase equilibria within the slab differ from those of the surrounding mantle, causing differences in the elastic velocity structure. Material expelled from the slab affects the overlying mantle wedge, with hydration reducing the melting temperature and leading to partial melting that produces subduction zone volcanism. The material property contrasts between the slab and the wedge are enhanced by the localized partial melting, as well as by anisotropic fabrics induced in both the slab and the surrounding mantle by the shear stresses associated with the flow.

As the slab sinks to near 400 km depth an exothermic phase transformation occurs, with $(\text{Mg},\text{Fe})_2\text{SiO}_4$ olivine in the slab converting to the high-pressure modified (β) spinel structure. The spinel transition helps to drive the slab onward, although a central core of metastable olivine may persist to greater depths, with eventual transformational faulting producing deep earthquakes (see Section 1.3). Other phase transitions occur within the transition zone (400–720 km deep). The leading edge of the slab reaches a depth near 660 km about 10 My after leaving the surface. Every year, 80–120 km³ of slab descends below 350 km into the mantle. But now the slab encounters resistance to further penetration, sometimes resulting in distortion of the slab, and there is a buildup of internal compressional stresses oriented in the down-dip direction of the flow. The slab at 660 km depth is still colder than the surrounding mantle by many hundreds of degrees (causing it to have several percent higher seismic velocities than the surrounding mantle) and appears to have sufficiently high viscosity to retain its integrity as a stress guide. An abrupt cessation of all earthquake activity occurs by 680–700 km depth (Stark and Frohlich, 1985; Rees and Okal, 1987). Any slab material that penetrates deeper will undergo an abrupt endothermic dissociative transformation of spinel-structured $(\text{Mg},\text{Fe})_2\text{SiO}_4$ into perovskite-structured $(\text{Mg},\text{Fe})\text{SiO}_3$ and $(\text{Mg},\text{Fe})\text{O}$. Pyroxenes and garnets in the slab will more gradually transform to the perovskite structure, which is the predominant mineral form in the lower mantle.

Whether the slab continues to descend, penetrating deeply into the lower mantle as the downwelling in a whole-mantle convection system, or is deflected and retained in the upper layer of a strongly stratified mantle convective system is still a hotly debated question. Slab chemistry, high viscosity of the lower mantle, a density increase caused by a chemical contrast from the upper mantle to the lower mantle, as well as the presence of the endothermic perovskite phase transformations may all act to inhibit slab penetration into the deep mantle. A variety of scenarios have been advanced (Fig. 2); slabs may penetrate with little

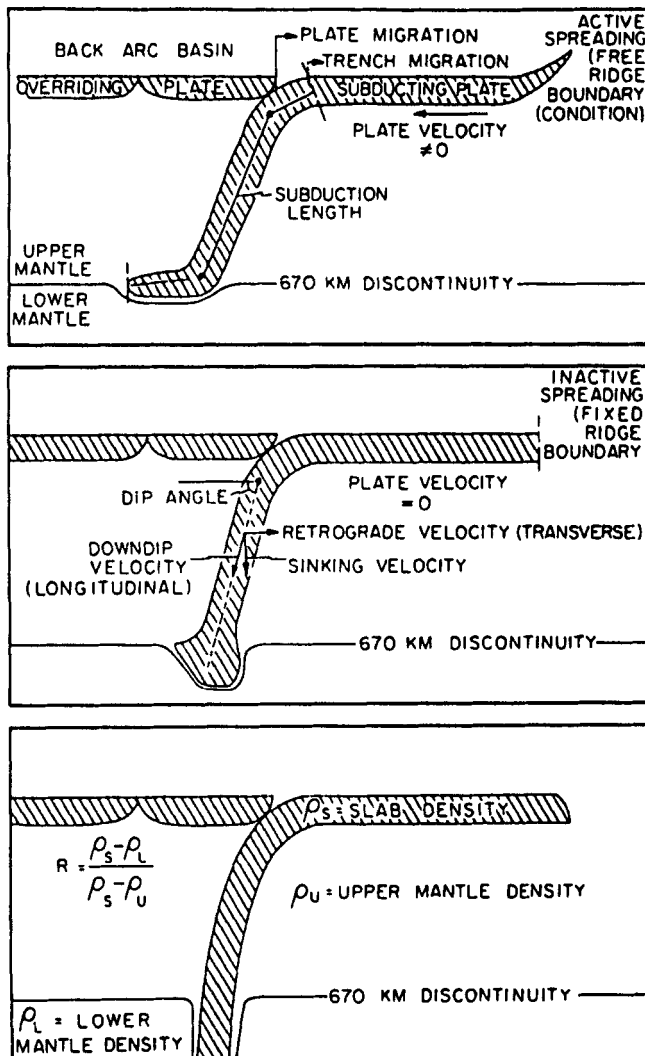


Fig. 2. Several possible fates for subducting lithosphere associated with its ability to penetrate into the lower mantle. The slab may be deflected in the upper mantle of a strongly stratified convection system (top); it may penetrate partially, depressing a phase or chemical boundary between the upper and lower mantle (middle); or it may penetrate readily into the lower mantle (bottom). Additional scenarios include strong broadening of the slab either with or without lower mantle penetration. Reprinted with permission from Kincaid and Olson (1987).

deformation, pile up and overturn catastrophically, penetrate ephemerally with or without significant deformation until they achieve thermal equilibration and rise to depths of neutral buoyancy, or flatten out with deflection but no penetration into the lower mantle. This issue of the fate of subducting slabs has aroused great interest in the Earth sciences, being intimately linked to the chemical cycling and thermal and dynamical evolution of the planet (Silver *et al.*, 1988; Jordan *et al.*, 1989; Olson *et al.*, 1990; Lay, 1993). Fundamental questions about the causes and persistence of geochemical heterogeneity in the mantle, the possible existence of a thermal boundary layer at the base of the transition zone, and episodicity of tectonic motions at the surface are all linked to the issue of whether slabs do or do not ultimately sink into the lower mantle. Observations from numerous disciplines have been brought to bear on this question, yet this remains one of the foremost unresolved questions in geophysics. We will consider this issue in the light of the many studies of seismic velocity structure of deep slabs.

1.2. How Seismology Provides Information about Slabs

Seismological constraints on the elastic velocity structure and anelasticity of any region of the Earth's deep interior are obtained by analysis of seismograms. These are recordings of the transient ground motions produced by the passage of elastic waves that have been excited by a source of elastic strain energy release, such as an earthquake or underground explosion. While seismic waves spread outward from the source over three-dimensional spherical wavefronts, the energy transmitted over any particular path from source to receiver has the significant attribute of being sensitive primarily to material properties along the actual path that is traversed. This enables the seismologist to relate measured travel times, amplitudes, and waveshapes on a given seismogram to a particular path through the Earth. This localized sensitivity of seismic waves enables stable inversion procedures for the source location and origin time as well as for the elastic velocity structure of the interior. The elastic velocity structure depends on the pressure, temperature, composition, and crystallographic orientation of the material encountered along any particular path. Seismic wave paths through the Earth tend to be very long, and identifying any contribution to observable travel times or waveshapes from the short path in the slab near the source constitutes one of the major challenges in all slab investigations.

There is naturally a strong coupling between source locations and velocity structure, and sequential improvements in location accuracy and velocity model complexity have been made throughout the history of seismology, often with initial calibration using known source locations and origin times (as for human-made explosions). The fact that the Earth can be well approximated as a radially layered planet, with its primary elastic properties varying with depth, allows the

use of simple one-dimensional velocity models (available for more than 50 years) in the routine location of all moderate and large earthquakes around the world. These routine locations have absolute uncertainties of about 30 to 50 km, which is adequate for identification of all major seismic belts, such as those within subducting slabs. Improving the accuracy of the locations, for high-resolution work on slab structure, requires either path-specific corrections or three-dimensional velocity models, which have been in development for only 20 years. Nonetheless, it is important to keep in mind that we never know the precise location of any earthquake deep in a slab, for all location estimates are dependent on the seismic velocity model used in the location process, which itself can never be more than an approximation of the true Earth structure.

For the deep slab issue, seismological information comes in three forms: (1) earthquakes occur within the anomalous thermal–chemical environment of the subducted slab, illuminating the flow by their very presence, at least to their maximum depth extent; (2) the strain release in deep earthquakes reflects the deep slab deformational environment; and, most important, (3) the seismic waves radiated from the deep events convey information about the deep structure to surface sensors. We'll consider aspects of the first line of evidence here and then discuss the others in later sections.

1.3. Earthquakes in Slabs

Extracting accurate information about the three-dimensional elastic velocity structure of subducting slabs is a formidable challenge, and it is fortunate that earthquake sources occur within the slabs, in some places persisting to maximum depths of 680–700 km (Stark and Frohlich, 1985; Rees and Okal, 1987). This provides much more complete seismic wave sampling of the slab than is attainable near mantle upwellings (such as under ocean ridges), where earthquakes are confined to depths less than 20 km by the warm temperatures. Having deep sources is critical for imaging the dipping, tabular geometry of the downwellings. Earthquakes below 100 km are found only in regions of current or recent subduction, with anomalously low mantle temperatures being required for any form of abrupt strain energy release. Earthquakes down to depths of 300 km may occur as pore fluid–assisted brittle failure or frictional sliding within the cold downwellings, but the high confining pressures (with resulting high fracture strength and friction coefficient) and probable absence of free fluids in interconnected porosity in slabs at depths greater than about 300 km are generally believed to preclude deeper events from being the same frictional sliding phenomena associated with shallower events (e.g., Kirby *et al.*, 1991). However, the observed seismic wave radiation from deep slab events does require that they involve a predominantly shearing-type process that is virtually indistinguishable

from shallow faulting. Some events deeper than 450 km tend to have more rapid rupture onsets than intermediate-depth events of comparable size (Houston and Williams, 1991), and the overall duration of rupture of deep events generally tends to be relatively short (Vidale and Houston, 1993). Intermediate-depth (70–300 km) and deep earthquakes (300–700 km) do have anomalous statistical behavior relative to shallow events, with less temporal clustering and fewer aftershocks from 100 to 450 km in depth (Frohlich, 1987). Below 450 km the number of aftershocks increases, perhaps as a result of heterogeneity of the stress environment within the slab (Frohlich, 1987).

Deep earthquake occurrence may provide critical information about the thermal and chemical state of deep slabs. Recent experimental work has demonstrated that in the presence of deviatoric stresses, analogues of important upper mantle and slab component mineral phase transformations may occur in association with shear faulting instabilities (e.g., Green and Burnley, 1989; Green *et al.*, 1990, 1992a,b; Burnley *et al.*, 1991; Kirby *et al.*, 1991). Nonhydrostatic stress effects on reconstructive polymorphic transformations in H₂O ice have been documented to show growth and interaction of compressional microinclusions that may coalesce into faults (Kirby *et al.*, 1991). Green and Burnley (1989), Green *et al.* (1992a,b), and Burnley *et al.* (1991) argue that an “anticrack” mechanism in Mg₂GeO₄, an analogue for Mg₂SiO₄, involves a mechanical instability which develops after aseismic nucleation and growth of lens-shaped bodies of the high-pressure phase oriented normal to the compressional principal stress. Abrupt loss of aggregate strength and propagation along a planar zone of transforming material may produce faultlike strain energy release. There has been debate over whether actual acoustic radiation occurs with these transformations (Meade and Jeanloz, 1991), although Green *et al.* (1992a) document the occurrence of acoustic emissions accompanying anticrack faulting in Mg₂GeO₄. Dehydration and amorphization instabilities have been proposed as an alternative source of intermediate and deep earthquakes, based on acoustic emissions in serpentine samples subjected to high pressure and temperature (Meade and Jeanloz, 1991), but it is not known whether faulting is involved. Only the hydrated upper crust of the slab should have any such process, unless hydration occurs along deeper faults produced by bending of the slab.

Particularly important phase transitions which appear to exhibit transformational faulting involve olivine, a significant component of the oceanic lithosphere below the basaltic crust, as it transforms to high-pressure modified spinel or spinel structures (Green *et al.*, 1990). Experimental work has shown that kinetic effects may inhibit the olivine–spinel phase transitions, causing them to occur below their equilibrium depths for a normal mantle geotherm (near 400 km for olivine-modified spinel [α – β] and 520 km for modified spinel–spinel [β – γ]) (e.g., Sung, 1979; Sung and Burns, 1976). A viable hypothesis for deep earthquake occurrence is that transformational faulting takes place in a kinetically

overdriven tongue of metastable olivine within the colder upper central portions of the downwelling slab (Fig. 3). Such a mechanism itself has implications for the thermal and chemical state of the slab. Because the (α - β) transition involves a significant seismic velocity contrast, it is possible to seek evidence for the depressed olivine structure in slabs, as discussed later (Section 5.3). The upper half of the slab is probably enriched in olivine relative to the pyroxene-enriched lower half, which may tend to localize transformational faulting in the upper portion of the lithosphere. From this perspective, deep earthquake activity can be viewed as tracking the coldest regions of the slab and is expected to terminate as the slab heats up sufficiently to overcome the kinetic barriers to transformation or as it goes through higher-pressure phase transitions that do not involve faulting instabilities, such as the spinel-perovskite transition of olivine expected near a depth of 660 km (e.g., Ito and Yamada, 1982; Ito and Takahashi, 1989). An additional important aspect of the phase transition mechanism for deep events is that most of the driving stresses are internally generated within the slab, because the volumetric reduction of the spinel phase surrounding a core of olivine imposes layer parallel compression on the wedge (Goto *et al.*, 1985, 1987). As a result, the pervasive alignment of compressional axes in the down-dip direction

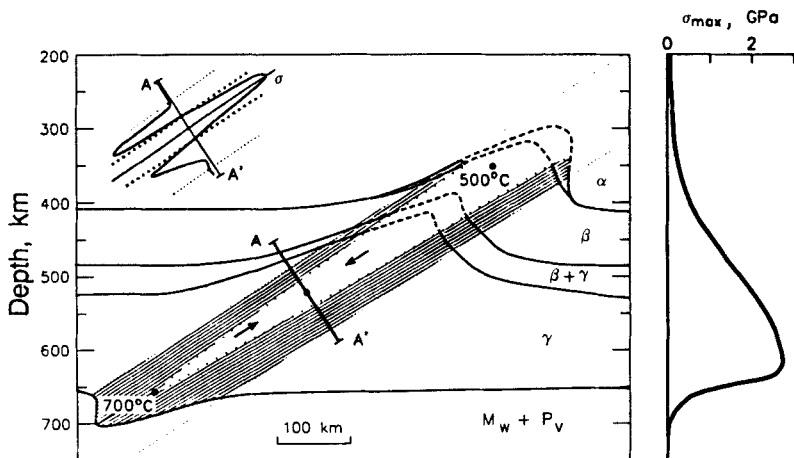


Fig. 3. Possible phase boundary positions for olivine in the vicinity of a subducting slab. If the α - β transition is kinetically suppressed, the central core of the slab may remain olivine down to several hundred kilometers below the equilibrium phase boundary, which is elevated above 410 km depth in the cold slab. The wedge-parallel compressive stress in the metastable olivine wedge derives from the transformation strains in the envelope of lithosphere in which olivine has already transformed to spinel. On the right, the maximum differential stress parallel to the plate and inside wedge is shown. Modified from Kirby, S. H., Durhan, W. B., and Stern, L. A. (1991). Mantle phase changes and deep earthquake faulting in subducting lithosphere. *Science* **252**, 216–225. Copyright 1991 by the AAAS.

in deep slabs (e.g., Isacks and Molnar, 1971; Vassiliou, 1984; Apperson and Frohlich, 1987) may actually have little to do with resistance to sinking of the slab.

The maximum depth of deep earthquake activity is a critical constraint on deep slab processes, but it is hard to exploit this most straightforward of observations until the nature of deep events is fully understood. There have been arguments that the maximum depth of earthquakes corresponds to a critical temperature (Isacks *et al.*, 1968; McKenzie, 1969; Griggs, 1972) associated with thermal assimilation of the slab as it becomes sufficiently weak that it can no longer accumulate or release earthquake-generating strains (see Section 2.4.2). Seismicity in many zones does not extend below intermediate depths, where the inferred cutoff temperatures prove to be close to the temperature estimates near the maximum depth of deep seismicity in other zones. However, there is substantial scatter in plots of lithospheric age (cooling time) versus slab length divided by subduction rate (assimilation time) (Molnar *et al.*, 1979; Wortel, 1982, 1986; Shiono and Sugi, 1985) that precludes a simple interpretation of thermal control on deep seismicity. The minimum in earthquake activity near depths of 300 km in all slabs and the increase to higher levels of activity at greater depths in some slabs (e.g., Vassiliou *et al.*, 1984) require more than simple thermal control on slab seismicity, with the forces on the plate also being important.

Stark and Frohlich (1985) note that in slabs with deep seismicity, the larger events, with magnitudes from 6.5 to 7, occur as deep as 650 km, and smaller events (magnitudes 5.5–6.0) extend to 680 km depth. However, for this deep activity there is not a clear indication of a gradual decrease in activity with depth as would be expected if thermal assimilation controls the termination of deep activity. In fact, some of the largest deep events, such as the July 31, 1970, magnitude 7.5 Colombia event, occur at depths near 650 km. In Tonga there is high earthquake energy release near this depth as well (Richter, 1979). These observations are also difficult to reconcile with the metastable olivine mechanism for deep events, because the deepest slab regions should have been extensively transformed to higher-pressure phases. The stresses at the leading tip of a kinetically overdriven tongue of metastable olivine should be very high, which could account for high earthquake energy release near the maximum depth of seismicity in different slabs.

A variety of mechanisms, including thermal assimilation, lower stress levels due to reduced viscosity of the lower mantle, strong convective stratification that prevents material from sinking into the lower mantle, and phase changes that shut off any earthquake mechanisms, have been considered to explain the termination of the deepest seismicity, but there will not be a resolution of this problem until it is established whether significant volumes of slab material penetrate well below the 660-km phase transition. If slab material does penetrate, the occurrence of the perovskite transformation, which has a moderate negative Clapeyron

slope (dP/dT of the phase boundary), is a likely explanation for the cessation of deep seismicity. Alternatively, thermal assimilation must be invoked if the slab material does not penetrate below the (depressed) phase boundary. Even if this is the case, only partial thermal assimilation is sufficient to inhibit the earthquake capacity of the slab, and significant seismic velocity heterogeneity will still be associated with the cold material of the aseismic deep slab.

Seismicity distributions intrinsically illuminate the slab only where physical conditions allow earthquakes to occur, but analysis of the three-dimensional morphology of the slab in the seismogenic region (Burbach and Frohlich, 1986; Yamaoka *et al.*, 1986; Fukao *et al.*, 1987; Chiu *et al.*, 1991) can constrain deformations above the 660-km mantle discontinuity. Some slabs, such as Tonga, appear to display buckling and imbrication (e.g., Billington, 1980; Giardini and Woodhouse, 1984; Fischer and Jordan, 1991), whereas others, such as the Japan slab, show surprisingly straight orientations all the way to 660 km depth. Of particular interest are regions of isolated deep earthquake activity, displaced laterally from the well-defined deep seismic zones in several arcs. Okino *et al.* (1989) located an isolated event offset from the deep seismicity in the Izu slab, similar to events found under the northern Kuril arc (Glennon and Chen, 1993a), Spain, Peru, and the New Hebrides (Ekström *et al.*, 1990; Lundgren and Giardini, 1992b). Given the special environment required for deep earthquake occurrence, these rare events are usually taken as evidence for horizontal deflection of the deep slab, although the possibility that independent detached slab remnants are responsible for the anomalous events complicates such arguments (Giardini, 1992). Hamburger and Isacks (1987) conclude that interaction between multiple slabs is responsible for the complexity of deep seismicity in Tonga, rather than resistance to penetration. Reconstructing plate motions over intervals of 10 My is important when analyzing complex regions where the geometry of subducting plates has changed, such as along the Vitiaz trench, down-dip of which a detached slab may be colliding with the currently subducting Tonga slab.

Although the spatial distribution of seismicity intrinsically cannot resolve the maximum depth extent of subduction, the shape of the downwellings revealed by seismicity and earthquake mechanisms does provide a boundary condition for modeling slab kinematics for any aseismic extension of the slab (e.g., Zhou, 1990b; Creager and Boyd, 1991; Fischer and Jordan, 1991). These efforts are limited by the fact that the main volume of the subducted material is not seismically active. Zhou (1990b) conducted a systematic study of focal mechanisms for earthquakes in the northwest Pacific and Tonga–Kermadec and found evidence for flattening of the compressional strain axes near 660 km depth beneath the Izu–Bonin and Tonga arc, but no clear evidence for this in the Kuril, Japan, or Marianas slabs. Creager and Boyd (1991) used a kinematic, steady-state model of slab flow along the Aleutian arc, with the geometry constrained by

seismicity locations and results of residual sphere modeling (Section 3.2) to assess the slab geometry. They sought to minimize the dissipation power as the thin slab deforms and found 10% in-plate strain. Using thermal models, they estimate a temperature of 800° at the cutoff of seismicity. Oblique subduction in the western Aleutians results in lateral transport of the slab westward, which predicts the aseismic slab location. Giardini and Woodhouse (1986) examine focal mechanisms, hypocentral distributions, and kinematic reconstructions of slab position to infer that southward shearing of the Tonga slab has distorted the slab geometry by 500 km. Fischer and Jordan (1991) prefer only 300 km of southward displacement based on estimates of slab deformation obtained by summing moment tensor strains from a 10-year catalog. The seismogenic strain can account for up to 50% thickening of the Tonga slab caused by southward shear, although additional thickening could occur aseismically. Along-strike strain decreases toward the south while cross-strike strain increases from north to south. Hamburger and Isacks (1987) also prefer only 300 km southward distortion of the Tonga slab.

Having set the stage for discussing the structure and fate of subducted slabs, we will now conduct a review that is organized loosely parallel to the historical evolution of seismological models for slab structure, from qualitative early seismic characterizations and early and recent thermal–mechanical models (Section 2) to relatively comprehensive modern seismological results (Sections 3–6). This will illustrate both the advances and the continuing uncertainties in our knowledge of the slab’s thermal and compositional structure. Section 7 will consider some future directions for progress in slab modeling, drawing on recent multidisciplinary advances which provide new frameworks for parameterizing deep slab seismic models.

2. GENERAL CHARACTERIZATIONS OF SLAB AND WEDGE STRUCTURES

Catalogs of global earthquake locations defined the existence of Wadati–Benioff zones by the 1940s, well in advance of the notion of subducting lithosphere. It was immediately recognized that anomalous mantle conditions should be associated with the seismogenic regions, given their very limited spatial distribution; however, it was several decades before earthquake location precision and seismic station coverage were sufficient to begin to explore the inhomogeneity around the deep sources. The 1960s brought the first systematic investigation of seismic wave properties associated with the deep seismic zones.

2.1. First-Order Slab Anomalies

Japan was the location of the earliest investigations of seismic wave variations associated with a Wadati–Benioff zone, given the extensive concentration of

both earthquakes and seismometers and the careful documentation of earthquake intensity patterns in the region. Utsu (1971) provided a comprehensive summary of the early Japanese observations relevant to the mantle environment. Since 1918 anomalous patterns of earthquake intensity across Honshu had been noted, with deep Sea of Japan events producing high intensities on eastern Honshu. Azimuthal variations in the frequency content of seismic waves at Japanese stations were detected in 1933, and relatively early arrival times on the east coast of Japan were recognized in station statics by 1931. Systematic investigation of these phenomena was initiated by Katsumata (1960), who studied the amplitudes and travel times of S waves for 19 deep earthquakes near the southern coast of central Japan. He found that the S wave travel times were 10% less to stations to the northeast, along the arc, than to the west, and drew the important conclusion that the seismically active zone transmits seismic waves with higher velocity and lower attenuation than the aseismic zone, now recognized to be the mantle wedge.

Fedotov (1963) observed variations in the absorption of waves from intermediate-depth events along the Kamchatka arc, finding that high attenuation of S waves began for events deeper than 80 km, with more efficient propagation to the eastern side of the arc. Utsu (1966) pursued this notion by systematic investigation of isoseismal patterns for 66 large earthquakes from 1926 to 1965, thoroughly documenting the long history of anomalous wave amplitude patterns for regional events. It was about this time that many of the concepts of global plate tectonics were emerging, prompting new instrument deployments in southwest Pacific island arcs and South America and systematic investigation of the rapidly accumulating data sets being provided by the World Wide Standardized Seismic Network (WWSSN) and other 1960s instrument deployments. The systematic investigation of slab structure in this new context can be associated with several important papers which appeared in press in 1967.

Utsu (1967) and Oliver and Isacks (1967) were the first to articulate clearly the idea that inclined seismogenic zones beneath island arcs are regions with low attenuation and high seismic wave velocity. Utsu (1967) compared Japan Meteorological Agency (JMA) earthquake locations from local Japanese stations with globally determined locations (then provided by the U.S. Coast and Geodetic Survey, USCGS), finding up to 100-km mislocations of the CGS locations, always toward the western side of Japan. This suggested a bias in the mantle velocities affecting the downgoing phases to teleseismic distances. To test this, Utsu analyzed travel times at nine stations for 12 distant intermediate and deep earthquakes, 8 deep events at moderate distances, and 12 nearby intermediate and deep events, finding that P and S velocities were 6% faster on paths up the seismogenic zone to the Pacific side of Japan. These and subsequent estimates of the velocity anomalies associated with deep slabs are tabulated in chronological order in Table 1.

Oliver and Isacks (1967) concentrated on the spectral content of S waves from

TABLE I. TWENTY-FIVE YEARS OF ESTIMATES OF SLAB-MANTLE VELOCITY CONTRASTS OR ABSOLUTE ANOMALIES^a

Reference	Method	Location	Contrast/depth
Oliver and Isacks (1967)	Regional P waves, upgoing S waves	Tonga	1–2% δV_p 1–2% δV_s
Utsu (1967)	Regional P waves, regional S waves	Japan	6% δV_p 6% δV_s
Cleary (1967)	Downgoing P for LONGSHOT	Aleutians	3-s pattern in P times
Kanamori (1968)	Income teleseismic P from LONGSHOT; surface wave group velocities	Japan	4–5% δV_p ; 30–250 km
Kanamori and Abe (1968)	Rayleigh and Love wave group velocities	Japan	–0.4 km/s δV_s ; wedge (30–250 km)
Abe and Kanamori (1970)	Rayleigh and Love wave dispersion	Japan	–0.3 to –0.4 km/s δV_s ; wedge
Ishida (1970)	Local P waves	Japan	2.0–3.0% δV_p (30–250 km)
Jacob (1970)	Upgoing P waves; 3-D raytracing	Tonga	6–7% δV_p (0–600 km)
Kanamori (1970)	Teleseismic P and surface waves	Japan	–0.3 to –0.4 km/s δV_s ; wedge
Katsumata (1970)	Local P and S times	Japan	5–6% δV_p 6–7% δV_s (0–360 km)
Mitronovas and Isacks (1971)	Local P waves Local S waves	Tonga/Kermadec	6% δV_p 6–8% δV_s
Nagamune (1971)	Refracted P Local P and S	Hokkaido, Japan	7% δV_p 7% δV_s
Sorrells <i>et al.</i> (1971)	LONGSHOT times	Aleutians	12–6% δV_p (50–300 km)
Jacob (1972)	Outgoing teleseismic P waves; 3-D raytracing	Aleutians	7.0–10.0% δV_p
Tada (1972)	Local P waves Kaila slowness method	Japan	5.0% δV_p (80–200 km) 3.5% δV_p (200–400 km) 2.5% δV_p (400–600 km)
Barazangi <i>et al.</i> (1972)	Late high-frequency S waves versus depth	Tonga	6% δV_s
Aoki and Tada (1973)	Incoming teleseismic P waves from Cannikin	Japan	–3.0 to –5.0% δV_p ; wedge
Engdahl (1973)	Outgoing teleseismic P	Aleutians	7% δV_p (0–250 km)

Hamada (1973)	Incoming teleseismic P waves from Cannikin	Japan	-4% δV_p : wedge 3% δV_p : slab -1% δV_p : oceanside
Nagamune (1973)	Local P and S travel times	Japan	2-5% δV_p 5-6% δV_s
Pascal <i>et al.</i> (1973)	P travel times; 3-D raytracing	New Hebrides	6% δV_p : slab (0-300 km) -4% δV_p : wedge 6% δV_p (600 km)
Sleep (1973)	Outgoing teleseismic P waves; 3-D raytracing	Aleutians	5-10% δV_p
Yamamizu (1973)	Local 3-D raytracing	Japan	6% δV_p (30-350 km)
Snoke <i>et al.</i> (1974a)	S guided waves	Peru	7% δV_s (70-300 km)
Veith (1974)	Updip P times	Kurile	10-4% δV_p (100-700 km)
Engdahl (1975)	Azimuthal residual patterns	Tonga	10% δV_p (650-700 km)
Fitch (1975)	Master earthquake location	Fiji	5-10% δV_p (540-660 km)
	P wave times	Tonga	
		Peru	
Utsu (1975)	Regional and teleseismic P	Japan	3% δV_p (0-500 km)
Aggarwal <i>et al.</i> (1976)	Outgoing teleseismic P waves	Aegean	5-15% δV_p ; depending on slab length
Noguchi and Okada (1976)	Local P travel times	Japan	4-5% δV_p (0-350 km)
	3-D raytracing		
Robinson (1976)	Updip regional P waves	New Zealand	11% δV_p (0-400 km)
Adams and Ware (1977)	Updip P waves	New Zealand	11% δV_p (0-400 km)
Fitch (1977)	Master earthquake location	Tonga	0% δV_p (500-550 km)
	P wave times	Fiji	10% δV_p (600-650 km)
		Aegean	10% δV_p (600-650 km)
Gregerson (1977)	Outgoing teleseismic P		6-7% δV_p (50-250 km)
Hirahara (1977)	Block tomography with regional and teleseismic P waves	Japan	5.0-6.0% δV_p ; slab (50-250 km) 3% δV_p : slab (350 km) 2% δV_p : slab, (450 km) -2% δV_p : wedge (0-350 km) -1 to -2% δV_p : backside

(continued)

TABLE I. (Continued)

Reference	Method	Location	Contrast/depth
Jordan (1977)	S wave residual sphere	Kurile	Contrasts 7–8% δV_p (50–250 km) 5% δV_p (350 km) 4% δV_p (450 km) 5% δV_s (650–1000 km)
Kasahara and Harvey (1977)	OBS deployment	Japan	8.65–8.97 km/s V_p ; slab (50–230 km) –3% from JB V_p : backside mantle
Okada (1977)	ScSp	Japan	10–15% δV_p
Snoke <i>et al.</i> (1977)	ScSp	Peru, Chile	5% δV_p (150 km)
Fukao <i>et al.</i> (1978)	Reflected P	Ryukyu	8–12% δV_p (200–350 km)
Suyehiro and Sacks (1978)	P times	Japan	–5 to –10% δV_p ; wedge >350 km
Suyehiro and Sacks (1979)	Up-dip P and S times 2-D slab model	Japan	5 ± 1% δV_p 7 ± 2% δV_s
Hirahara (1980)	Block tomography with regional and teleseismic S waves	Japan	6–8% δV_s ; slab (50–250 km) 5% δV_s ; slab (350 km) 2–3% δV_s ; slab (450 km) –2 to –4% δV_s ; wedge (0–400 km) –1 to –2% δV_s ; backside Contrasts 10% δV_s (50–250 km) 8% δV_s (350 km)
Spencer and Gubbins (1980)	Local P wave tomography fixed slab	New Zealand	8% δV_p
Bock (1981)	Outgoing teleseismic P waves to Australia	Tonga	5–6% δV_p (350–400 km) 0% δV_p (400+ km) 3% average δV_p (0–660 km)
Hirahara (1981)	Block tomography with regional and teleseismic P waves	Japan	Pacific slab: 3% δV_p (70–150 km) 1.5% δV_p (200–300 km) Wedge: –1.1% δV_p (70–150 km)

Huppert and Frohlich (1981)	P times along strike	Tonga	-0.5% δV_p (200–300 km) Philippine slab: 2.4% δV_p (70–150 km) Wedge: -1.8% δV_p (70–150 km)
Chiou (1982)	Multiple phases in slab	New Hebrides	5–8% δV_p ; uniform slab 6%–9% δV_p ; layered slab
Horie and Aki (1982)	Block tomography with regional P waves	Kanto, Japan	9–10% δV_p 6–7% δV_p (32–65 km) 2–3% δV_p ; slab -3% δV_p ; wedge
Roecker (1982)	P and S local tomography	Pamir/Hindu Kush	-6 to -8% δV_p ; "slab" (40–80 km) -2% δV_p ; "slab" (80–150 km)
Fukao <i>et al.</i> (1983)	P and S travel times	Southern Honshu, Japan	-14% δV_p (5–7 km thick layer) 4% δV_p (main slab) 7% δV_p (0–330 km)
Spencer and Engdahl (1983)	Joint location and slab tomography	Central Aleutians	10% δV_p ; slab (500 km)
Creager and Jordan (1984)	Residual sphere for ISC P wave times	Kuriles, Japan	10% δV_p ; slab (600 km) 9% δV_p ; slab (800 km) 6% δV_p ; slab (1200 km)
Hasemi <i>et al.</i> (1984)	Block tomography with regional P waves	Tohoku, Japan	3.5% δV_p (65–98 km) 4–6% δV_p (98–131 km) 2% δV_p ; slab (50–150 km) -2% δV_p ; wedge
Ishida (1984)	Block tomography with regional P waves	Kanto-Tokai, Japan	6% δV_p (45–70 km) 3% δV_p (70–95 km)
Ishida and Hasemi (1984)	Block tomography P waves	Kanto-Tokai, Japan	8–10% δV_p (0–20 km) 4–6% δV_p (20–60 km)
Miyamichi and Moriya (1984)	P tomography	Hokkaido, Japan	5% δV_p (20–65 km) 10% δV_p (5–20 km)
Hori <i>et al.</i> (1985)	P and S times	Southwest Honshu, Japan	-14% δV_p (5–7 km layer 30–40 km) 4% δV_p (main slab)

(continued)

TABLE I. (Continued)

Reference	Method	Location	Contrast/depth
Nakanishi (1985)	Block tomography with regional P waves	Hokkaido, Tohoku, Japan	4% δV_p (60–100 km)
Roecker (1985)	P and S relative time method	Izu-Bonin	North of 32.5°N 3–4% δV_p (180–345 km) 4–6% δV_p (400–500 km) South of 32.8°N 8–10% δV_p (325–375 km) 6–7% δV_p (375–410 km)
Ansell and Gubbins (1986)	Fast high-frequency precursors	Tonga	10.0–5.0% δV_p (0–450 km) (reduces with depth)
Creager and Jordan (1986)	Residual sphere for ISC P wave times	Kurile	6% δV_p (200 km) 5.7% δV_p (350 km) 4% δV_p (600 km) 3% δV_p (1000 km)
		Marianas	2.8% δV_p (1150 km)
		Japan	5.1% δV_p (350 km) 3.2% δV_p (1000 km)
Matsuzawa <i>et al.</i> (1986)	P–S conversions	Tohoku, Honshu, Japan	–6% δV_p (5–10-km-thick layer) 6% δV_p (main slab)
Michaelson and Weaver (1986)	Teleseismic 3-D P tomography	North Cascadia Central Cascadia N. Oregon	12% in slab contrast (60–150 km) 6–8% δV_p (30–200 km) 5% δV_p (30–200 km) 3–4% δV_p
Obara <i>et al.</i> (1986)	Block tomography with P and S waves	Northeast Japan	2% δV_p (65–98 km) 6% δV_s (65–98 km) 4–8% δV_p (98–131 km) 6–10% δV_s (98–131 km)
Bock (1987)	Local portable recordings	Tonga	5–7% δV_p (0–250 km) (8–9% maximum in varying slab model) (6–7% in uniform slab)

Engdahl and Gubbins (1987)	Joint location and slab P wave tomography	Central Aleutians	10% δV_p ; slab (80–120 km) −2% δV_p ; wedge (80–120 km) 6% δV_p (120–200 km) 5–6% δV_p (200–400 km) <5% δV_p (30–80 km) 2–12% δV_p (80–130 km) Overall 5–10 δV_p
Kuge and Satake (1987)	Local P wave tomography	New Zealand	<5% δV_p (30–80 km) 2–12% δV_p (80–130 km) Overall 5–10 δV_p
Matsuzawa <i>et al.</i> (1987)	P and S travel times	Northeast Honshu	−6% δV_p (\sim 5-km-thick layer)
Roecker <i>et al.</i> (1987)	P and S local tomography	Taiwan	6% δV_p ; main slab Eurasia slab −2 to −4% δV_p (15–50 km) Philippine
Rasmussen and Humphreys (1988)	P wave tomography	Southern Washington	1–2% δV_p (20–50 km) 2–3% δV_p (30–300 km)
Spakman and Nolet (1988)	P tomography	Oregon	2–3% δV_p (30–150 km) 2–3% δV_p ; slab (0–600 km) −3% δV_p ; wedge (0–600 km)
Spakman <i>et al.</i> (1988)	P tomography	Aegean	3% δV_p (0–200 km)
Hirahara <i>et al.</i> (1989)	Block tomography with regional and teleseismic P waves	Greece, Aegean	Pacific slab 3% δV_p (50–100 km) 1.5% δV_p (100–150 km) Wedge −1.5 to 3% δV_p (50–100 km) −1.5% δV_p (100–150 km) Philippine slab 1.5–3% δV_p (30–250 km) Local wedge anomalies −6% δV_p (100–150 km)
Iidaka <i>et al.</i> (1989)	P–S converted phase	Kanto, Japan	6% δV_p (60 km) 3% δV_p ; slab −3% δV_p ; wedge

(continued)

TABLE I. (Continued)

Reference	Method	Location	Contrast/depth
Kamiya <i>et al.</i> (1989)	Local and teleseismic P wave tomography	Japan Philippine Izu Kuril	-2 to -4% δV_p ; wedge 2-5% δV_p ; slab
Okino <i>et al.</i> (1989)	Travel times	Izu	3.5% δV_p (500-600 km)
Spakman <i>et al.</i> (1989)	P tomography	Kurile Marianas	2-3% δV_p (0-600 km) <1% δV_p (650-1000 km)
Suetsugu (1989)	P tomography P amplitude modeling	Deep Kurile Kurile	2-3% δV_p (650-1200 km) 3.5% δV_p (650-1000 km) 3-1% δV_p ; slab (200-600 km) 4.6% δV_p ; slab (200-300 km) -2.7% δV_p wedge -0.8% δV_p oceanside
van der Hilst and Spakman (1989)	P tomography	Lesser Antilles	2% δV_p (200-400 km) 3% δV_p (400-650 km)
Matsuzawa <i>et al.</i> (1990)	S-P travel times	Middle America Northeast Honshu, Japan	1.5% δV_p (300-1400 km) 6% δV_p (reduces with depth)
van der Hilst (1990)	P tomography	Middle America Lesser Antilles	2-3% δV_p
Zhou and Clayton (1990)	P and S tomography	Northwest Pacific	Slab $\delta V_p \%$ 4-2 4-1 (0-100 km) 3-2 5-3 (100-200 km) 3-1 4-1 (200-300 km) 4-0.5 3-2 (300-400 km) 3-1.5 4-2 (400-500 km) 2-1 2-0.5 (500-600 km) 2-0.5 2-0.5 (600-700 km)

Ambient Mantle			
-2 to -3.5	-2 to -4	(0–100 km)	
-2 to -3	-1 to -4	(100–200 km)	
-1.5 to -2.5	-1.5 to -3	(200–300 km)	
-1 to -2	-2 to -3	(300–400 km)	
-1.5 to -2.5	-1.5 to -2.5	(400–500 km)	
-1 to -2	-1 to -1.5	(500–600 km)	
-0.5 to -1.5	-1 to -1.5	(600–700 km)	
7% δV_p : slab		(35–71 km)	
5% δV_p : slab		(71–121 km)	
13% δV_p : slab		(121–171 km)	
5.8% δV_p : slab		(171–271 km)	
5.7% δV_p : slab		(271–371 km)	
-1 to -4% δV_p : wedge			
1.3% δV_p : slab		(35–71 km)	
3.7% δV_p : slab		(71–121 km)	
3.7% δV_p : slab		(121–171 km)	
4.8% δV_p : slab		(171–271 km)	
5.7% δV_p : slab		(271–371 km)	
7% \pm 2% δV_p (0–400 km)			
4% δV_p : slab (100–300 km)			
3% δV_p : slab (300–600 km)			
2–1% δV_p : slab (600–1200 km)			
Fischer <i>et al.</i> (1991)	P wave residual sphere	Tonga	4–7% δV_p (100–1200 km)
Gubbins and Snieder (1991)	Trapped wave modeling	Kermadec	5% δV_p : (top of slab)
Harris <i>et al.</i> (1991)	2-D P wave tomography	Southern Oregon	3–4% δV_p : slab (0–200 km)
Hasegawa <i>et al.</i> (1991)	P wave tomography	Northeast Japan	-3 to -4% δV_p : wedge
Iidaka and Mizoue (1991)	Along-strike P wave times	Izu slab	6.0% δV_p
			1.5% δV_p : slab upper layer
			2.5% δV_p : slab lower layer

(continued)

TABLE I. (Continued)

Reference	Method	Location	Contrast/depth
Kissling and Lahr (1991) Prévot <i>et al.</i> (1991)	P wave tomography Travel time tomography	Alaska New Hebrides	-3% δV_p ; wedge contrast 4.5–5.5% δV_p 5% δV_p ; slab (50–150 km) V_p slab V_p below slab 7.98–7.99 7.72–7.99 (65–100 km) 8.07–8.08 8.01 (100–170 km) 8.39–8.29 8.26–8.29 (170–270 km) Seismic gap 8.15 7.98 (65–100 km) 7.79 7.94 (100–170 km) 7.58 8.22 (170–270 km)
VanDecar (1991)	Nonlinear, iterative travel P wave tomography	Cascadia	3–4% δV_p ; slab
van der Hilst <i>et al.</i> (1991)	pP and P tomography	Kurile Izu Japan	3–4% δV_p ; slab -1 to -3% δV_p ; wedge

Zhao (1991)	P tomography with 3-D ray tracing	Tohoku	4% δV_p (0–250 km)
Benz <i>et al.</i> (1992)	Block tomography with P waves	N. California	5% δV_p ; slab (50–250 km)
Ding and Grand (1992)	P wave differential residual sphere	Kurile	5% δV_p (100–650 km) 2% δV_p (650–900 km); N. Kurile
Helffrich and Stein (1992)	P reflected	Ryukyu	4–10% 200–350 km
Helffrich and Stein (1992)	ScSp	Japan	–10% δV_p 6 km layer (50–100 km) 8% δV_p 8 km layer in slab –5% δV_p ; wedge 2–3% δV_p ; slab eclogite layer 8% δV_p ; wedge anisotropic layer 4% δV_p ; wedge anisotropic layer 7% δV_p ; elevated phase transition
Iidaka <i>et al.</i> (1992)	Along-strike P travel times	Izu slab	1.5–3.5% δV_p ; slab upper layer 3–5% δV_p ; slab lower layer –3 δV_p ; wedge
Ishida (1992)	Block tomography with regional P waves	Kanto–Tokai, Japan	6% δV_p (45–70 km) 3% δV_p (70–95 km)

^a Contrasts or velocity anomalies are for slab velocity relative to ambient or reference mantle, unless otherwise noted.

deep and shallow events in Tonga and Kermadec. They identified a 100-km-thick, westward-dipping zone along which S waves had little attenuation, enveloping the 100-km-thick band of deep seismicity in the region which had been located by Sykes (1966). The high-Q region, with Q estimates near 1000 versus estimates of about 150 for the surrounding mantle, extended up-dip, continuous with the upper mantle lithosphere to the east of Tonga. The seismograms studied included three-component data from four out of five stations deployed by Lamont Doherty Geological Observatory in Fiji and Tonga in 1964–1965, along with high-frequency portable recordings and data from WWSSN stations AFI (Afiamalu, Samoa) and RAR (Rarotonga; 1500 km east of the island arc).

A suite of qualitative analyses of the data from hundreds of events was performed by Oliver and Isacks (1967), an effort remarkable in that it defined procedures used in dozens of subsequent studies of deep slab structure. Because the earthquake locations were not very precise and there were limitations in the timing accuracy, little attention was paid to seismic velocities, although the high-attenuation paths were found to have 1–2% higher P and S velocities for deep events. Secondary arrivals, attributed to P-to-S conversions, possibly from the upper boundary of the plate, were frequently observed by Oliver and Isacks (1967). They reported low-frequency direct S and P arrivals followed by late high-frequency waves at station RAR for deep Tonga events. With shallow events giving high-frequency arrivals at RAR with high Sn velocities of 4.75 km/s, it was inferred that the late high-frequency energy had propagated up-dip along the seismogenic zone, incurring little attenuation and then propagating horizontally in the ocean lithosphere. Along-slab strike observations to AFI showed early P times and high-frequency observations for shallow events as far as 20° to the south along the arc and for deep events as much as 15° to the south. Undulations of the dipping seismic zone such that some raypaths came out of the high-Q region were inferred to account for events in the depth range 300–400 km having strongly attenuated arrivals at AFI. In addition, incoming patterns of teleseismic arrivals at AFI were considered, with early arrivals for events toward the south. Subsequent analysis of observations at AFI by Barazangi *et al.* (1972) showed that all signals from intermediate- and deep-focus events along the Tonga arc are actually more attenuated than up-dip recordings, indicating that the seismicity delimits the region of high Q and high velocities associated with the northern end of the Tonga slab.

In parallel with these natural earthquake investigations, the detonation of the first of three underground nuclear explosions in the Aleutians, LONGSHOT, occurred in 1966, providing an island arc source with known location and origin time large enough to be observed globally. Cleary (1967) analyzed the teleseismic P wave arrival times, finding a strong azimuthal pattern in P travel time residuals, ranging over 3 s, with early arrivals toward the north. Knowledge of the source position and timing allowed absolute travel time anomalies relative to

a reference Earth model to be determined. He argued that the LONGSHOT pattern was caused by the high-velocity slab dipping beneath the Aleutian arc, with olivine velocity anisotropy being invoked to explain the high velocities. He suggested that the anomaly was large enough to bias significantly the location of earthquakes in island arcs, similar to Utsu (1967), and considered station travel time terms at WWSSN stations MAT (Matsushiro, Japan) and BAG (Baguio, Philippines), both above inclined seismic zones. He argued that azimuthal patterns in the anomalies at MAT and BAG could be caused by fast slab structures similar to that under the Aleutians. Both the near-source and teleseismic travel times of LONGSHOT and the subsequent tests MILROW and CANNIKIN have been extensively studied to constrain slab characteristics (Section 3).

Many studies of slab attenuation remained quite qualitative, with confidence in the interpretations basically being derived from the repeated observation of gross trends. Wadati *et al.* (1969) associated the thin seismic zone under Japan with sinking lithosphere with low attenuation based on transmission efficiency. Molnar and Oliver (1969) observed high-frequency S waves up-dip from deep events in the Marianas, New Britain, Solomon, and South American arcs.

Utsu and Okada (1968) began to bring more quantitative approaches to the analysis of slab phase attenuation, using a spectral ratio analysis of P and S waves from shallow events off the southern Kuril Islands recorded at stations in Hokkaido. The spectra were observed to have large differences, with estimates of $Q_\alpha = 50$ for P waves and $Q_\beta = 100$ for S waves at shallow depths. Investigations of S wave attenuation in South America were summarized by Sacks (1969), with a more complex behavior being found than in Japan or Tonga. Sacks (1969) reported three basic types of S wave from deep events: signals with low-frequency first arrivals, signals with direct S attenuated and slower high-frequency S energy arriving 4–20 s after the direct wave, and direct S waves with no attenuation. He inferred a complex pattern of low Q variations in both the slab and the surrounding mantle. Some high-Q paths up the slab were found as well as high-Q paths to stations far from the coast, while other slab paths did show strong attenuation of the direct wave. Sacks (1971) used spectral ratio methods to measure Q, finding a shear wave attenuation slab model with high Q_β from 0 to 350 km, a patchy region of both low Q_β and high Q_β from 350 to 450 km, and high Q_β below 450 km. The strongly attenuating regions have Q_β as low as 35. A simple, continuous high-Q slab does not appear to be adequate in this region, although Utsu (1971) argued that simple models like those in Fig. 4 are consistent with data from Japan, Kurils, Indonesia, Tonga–Kermadec, and New Zealand.

Mitronovas and Isacks (1971) studied P and S times from deep events in Tonga to stations in the Fiji–Tonga region. Their procedure was to use 38 deep events with locations obtained using only teleseismic data and some intermediate-depth events located using only regional stations, because inclusion of up-dip early arrivals for deep events and down-dip early arrivals for intermediate-depth events

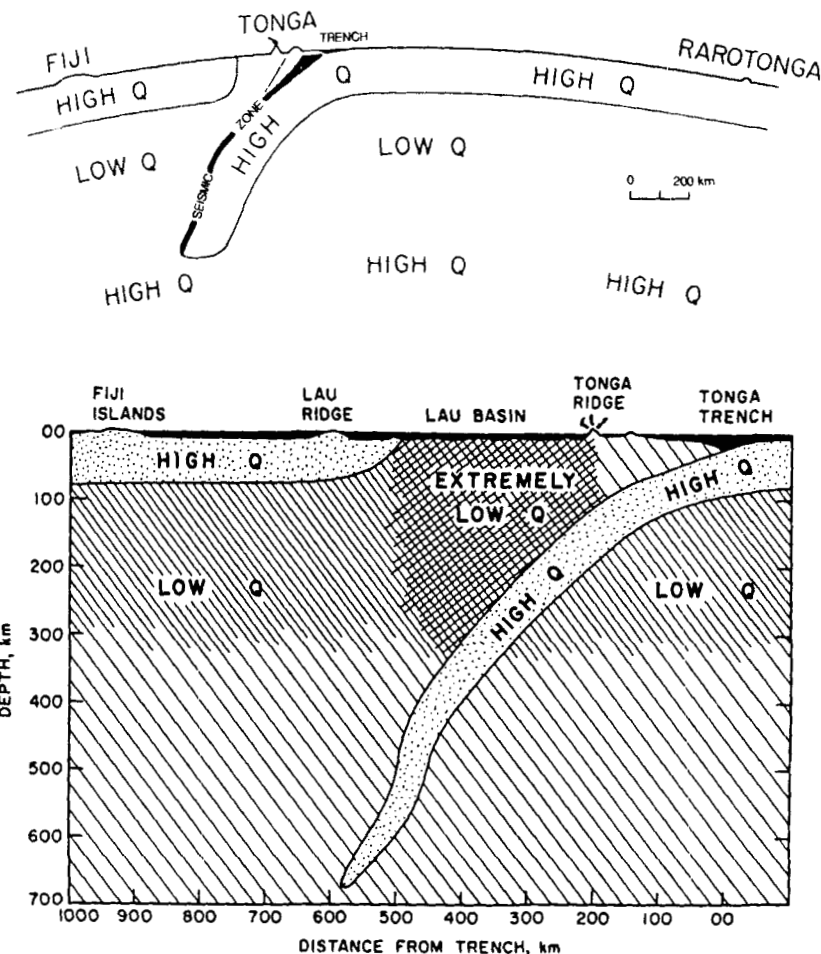


Fig. 4. Early cartoon cross sections through subducting slabs, emphasizing the low-attenuation (high-Q) characteristics of paths up the slab from deep events to stations in the island arc. The upper plot, from Oliver and Isacks (1967), emphasizes the anomalous properties of the slab; the lower plot, from Barazangi and Isacks (1971), reflects the enhanced awareness that the wedge above the slab is anomalous as well, relative to ambient mantle. Reprinted with permission.

can bias the locations by 20 to 40 km. They observed 5-s early anomalies for P waves traveling up-dip along the slab relative to the times to Fiji. Corresponding S times were 10–12 s fast for up-dip paths. This requires that the slab paths be faster by 6–7% than paths through the wedge, and the velocity anomaly must extend the full length of the seismogenic zone to 650 km. Many measurements of slab heterogeneity explicitly involve a relative contrast of this sort, for which any anomalously slow mantle material in the upper wedge will tend to enhance the

contrast estimate (see Section 2.3). Mitronovas and Isacks (1971) found no clear evidence for S wave splitting in their data and chose to interpret the velocity heterogeneity as the result of 1000° temperature variations.

An important emphasis of the early seismicity investigations was to determine the thickness of the deep seismic zone. Initial earthquake relocations indicated fairly thick (50–100 km) planar seismogenic zones (e.g., Sykes, 1966); however, improved earthquake locations constrained the thickness to less than 20–25 km in Tonga (Sykes *et al.*, 1969; Mitronovas *et al.*, 1969), Japan (Wadati *et al.*, 1969; Ishida, 1970; Utsu, 1971), and the Aleutians (Engdahl, 1973; Engdahl *et al.*, 1977). Recent accurate relative locations support such a narrow width under Western Argentina (Smalley and Isacks, 1987), where 90% of the events are within a 12-km-thick zone and the overall thickness is only 20.5 ± 1.5 km. Estimates of the seismogenic thickness based on earthquake rupture dimensions are generally consistent with narrow (10–30 km thick) zones (e.g., Wyss, 1973; Wyss and Molnar, 1972), although the detection of faultlike features in the zone based on multiple ruptures or aftershock distributions has proved challenging (e.g., Wyss, 1973; Billington and Isacks, 1975; Pascal *et al.*, 1978; Giardini and Woodhouse, 1984; Lundgren and Giardini, 1992a; Glennon and Chen, 1993b). Although many deep earthquakes have complex ruptures and multiple subfault orientations, there are examples of quasi-planar alignments on one or both nodal planes apparent in relocated seismicity suggesting large-scale shear failure surfaces in the deep slab (Giardini and Woodhouse, 1984; Lundgren and Giardini, 1992a). The typical narrowness of the seismogenic portion of the slab complicates interpretation of the fate of the slab based on arguments from seismicity alone.

2.2. Guided Waves

The observations of late high-frequency arrivals in seismograms recorded above subducting slabs by Oliver and Isacks (1967) and Sacks (1969) initiated a sequence of many investigations and arguments over the nature of these arrivals. These scattered signals are hard to analyze quantitatively even today, for they intrinsically involve complex three-dimensional geometries and structures which are poorly constrained. They are also puzzling from the point of view that the slab is expected to be faster than the surrounding mantle, effectively providing a poor waveguide which should not readily trap reverberations. The initial interpretations of these arrivals were strongly influenced by early observations of high-frequency P and S waves with long coda durations at large distances in oceanic and continental lithosphere by Shurbet (1962, 1964), as well as the Sn investigations of Molnar and Oliver (1969). Multiple reverberations in the crust and uppermost mantle lid “channel waves” are responsible for these signals, and

persistence of the associated velocity gradients at depth in the slab may explain how the late arrivals occur. If this is correct, lateral continuity of the slab layering should be important for their observability.

Barazangi *et al.* (1972) extended the RAR data set analyzed by Oliver and Isacks (1967) to include events up until 1970, finding very compatible results. The late high-frequency S wave packet was observed 45 s after the low-frequency first arrival for 350-km-deep events and up to 95 s after S for 650-km-deep events. They inferred that the suboceanic lithosphere in the slab produces a continuous waveguide. Isacks and Barazangi (1973) and Oliver *et al.* (1973) argued that high-frequency, late S wave arrivals observed in various subduction zones are best explained by continuous slabs, even in regions with discontinuous seismicity. Barazangi *et al.* (1973) addressed the question of whether the gaps in seismicity in the New Hebrides and New Zealand plates are due to detached plates or low-stress regions (Isacks and Molnar, 1971). They did not find high-frequency signals propagating up the slab for deep events as found in Tonga, and up-dip travel time anomalies for deep events were only 1–2 s, compared to 4–5 s along Tonga. This was taken as evidence that the New Hebrides and New Zealand slabs are detached below 300 km depth, while the Tonga slab is continuous. Tsujiura (1972) observed high-frequency late arrivals for deep earthquakes in Japan, inferring continuous slab structure to the deepest events in that region. More recently, Nagumo and Ouchi (1990) have observed similar high-frequency P and S phases up-dip of intermediate-depth events in Izu, recorded by an ocean bottom seismometer (OBS) array 11–14° east of the trench. The late arrivals appear to have traveled up-dip and then along the ocean lithosphere with apparent velocities corresponding to the upper mantle lid structure.

The largest point of contention has involved continuity of the slab beneath South America. Isacks and Barazangi (1973) analyzed deep events in the Nazca plate, again observing late high-frequency S arrivals. These were observed at WWSSN stations in Peru, ARE and NNA, and the Chilean station ANT. The late arrivals from deep earthquakes in northern Argentina and Bolivia are emergent 1-Hz signals, with apparent velocities of about 4.7 km/s and durations of up to a minute (Fig. 5), similar to the observations at other stations by Sacks (1969). On the basis of these observations, Isacks and Barazangi (1973) inferred that the slab is continuous through the seismic gap from intermediate to deep source regions. No quantitative modeling was conducted, but it was inferred that the slab must be high Q and must have strong reflectors, perhaps associated with the thin eclogitic layer in the crust (basalt transforms to eclogite below 70–100 km) and any overlying melt region in the mantle wedge. A 7% average slab anomaly was assumed in explaining the timing of the late arrivals, but the actual slab velocity anomaly could not be directly measured.

Analysis of data from Carnegie stations in South America and stations NNA and ARE by Snoke *et al.* (1974a) showed that the late high-frequency observations are seen out to distances of 21° but not beyond. The cutoff with distance is

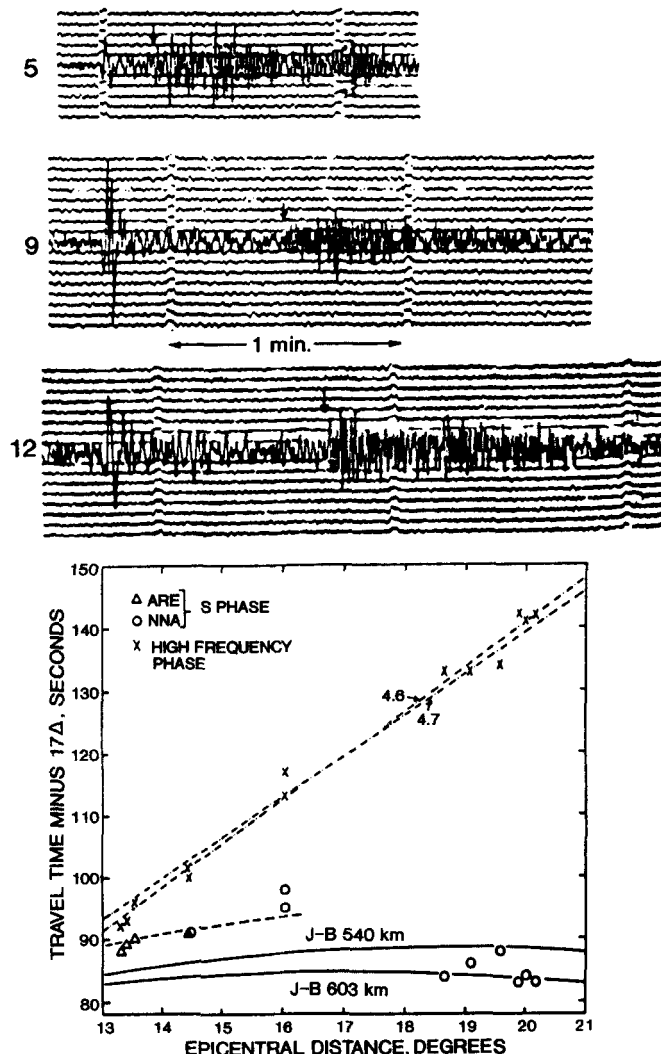


Fig. 5. Examples of short-period S wave signals (first arrival on each trace) from deep-focus earthquakes under South America recorded by up-dip WWSSN stations. Note the high-frequency phase that arrives from 10 to 60 s later. The travel time of the high-frequency signals is plotted as a function of distance in the lower part. Reprinted with permission from Isacks and Barazangi (1973).

not readily explained by the continuous-slab model. They proposed that the late S phases are generated by P waves that travel up to a discontinuity in the slab and then convert to S, subsequently generating the waveguide arrival. P-to-S and PP-to-S conversions from the upper boundary of the slab near depths of 150 km were found to have consistent travel times with the late S arrivals, indicating that the

purely S wave scattering model of Isacks and Barazangi (1973) is not a unique explanation, and in fact continuity of the slab cannot be unambiguously inferred. Snoker *et al.* (1974b) further developed a model which could account for the late shear wave signals under South America, without requiring a continuous slab connecting the intermediate and deep seismic regions. They argued that a sharp reflector extending from depths of 80 to 250 km with about 7% velocity contrast can produce S-to-S reflections of upcoming waves from the deep event, which then reflect multiply in the slab structure and propagate to the surface along a high-Q path.

This question is complicated by strong heterogeneity of Sn propagation in the South American continental lithosphere along the plate boundary. Chinn *et al.* (1980) examined high-frequency lithospheric S waves from shallow and intermediate-depth events along the plate boundary, finding a complex distribution of regions of efficient propagation and strong blockage. Molnar and Oliver (1969) documented similar variations in high-frequency Sn propagation around other arcs. Thus, it is difficult to attribute nonobservability of late high-frequency waves to disruption of the deep slab.

Although down-dip continuity of the South American slab is still open to question, it appears that lateral tears and discontinuities in slabs are not that common, occurring mainly at major geometric disruptions (e.g., Isacks and Barazangi, 1977; Bevis and Isacks, 1984, Burbach and Frohlich, 1986; Yamaoka *et al.*, 1986; Fukao *et al.*, 1987). This conclusion is based on various efforts to fit smooth surfaces to seismicity. Thus, one might expect to observe guided waves at long distances along the strike of a slab. It is surprisingly difficult to find such geometries along the strike of a subduction zone, with the most extensively studied being the paths from Tonga to New Zealand. Huppert and Frohlich (1981) reported early arrivals along this path, and Ansell and Gubbins (1986) followed with an extensive analysis. They found 15-s early P arrivals reported in the ISC bulletins for Tonga and Kermadec events detected by New Zealand stations. Limiting themselves to events south of 22°S and shallower than 350 km, they inspected analog seismograms, finding an early emergent phase with frequencies of 2–10 Hz, followed by a secondary low-frequency phase that arrived at about the Jeffreys–Bullen (J–B) table travel time for a direct P wave. Chiu (1982) observed similar double arrivals in the New Hebrides. Ansell and Gubbins (1986) attributed the early arrivals to propagation through a 5% fast slab, with curvature of the slab limiting the distances at which the precursor is observed. They argue that the high-velocity region must extend to 450 km depth or more in the along-strike region below Kermadec, where there is no seismicity. The arrivals do have variable observability across New Zealand, with slow attenuated arrivals in North Auckland, as noted by Mooney (1970), and the two phases being observed in central New Zealand. They raytraced in a J–B earth model, showing the sensitivity of the multipathing to the slab geometry. The

high-frequency energy was assumed to travel in a thin layer in the slab, with the later low-frequency arrival traveling outside the slab.

Analysis of digital data from New Zealand station SNZO by Gubbins and Snieder (1991) confirmed the dispersive character of the along-slab arrivals from Tonga, with 4% dispersion in the 1- to 8-Hz frequency band. They studied 25 events in Kermadec and Tonga, finding that the precursory high-frequency energy can be observed as far as 20° away. These higher-quality data indicate that the signal is not really two separate arrivals, but more a continuously dispersed arrival spread over a 10- to 15-s window. Propagation in a thin slab model can account for the dispersive character, as shown by acoustic wave modeling of simple layered slab models. However, to match the strong dispersion, a 6–15-km-thick layer of high velocity is needed for simple layered structures. This may correspond to the eclogitic layer, although Helffrich *et al.* (1989) show that the intrinsic velocities of eclogite are not expected to be as fast as the 8.4 km/s layer incorporated in the preferred models. Anisotropy of the layer may need to be invoked, and the thin lid must extend to at least 500 km depth to explain the data. Broadband stations have now been deployed in New Zealand to further study these dispersed along-strike arrivals.

2.3. Wedge Structure

From the initial studies, it became clear that characterizing the slab was complicated by the anomalous properties of the overlying mantle wedge. Most measurements of slab properties are effectively made relative to the anomalous (partially molten, thermally perturbed, hydrated, and strongly sheared) environment in the wedge, rather than relative to normal mantle conditions. This complicates isolation of thermal and chemical effects of slab structure. For example, Oliver and Isacks (1967) noted that a zone of high attenuation above the Tonga slab shifted the frequency content of S waves from the 2–4-Hz observations up-dip to Tonga stations to the 0.5–1-Hz observations in Fiji. Their qualitative estimates of Q_α of 1000 for the slab and 150 for the wedge were based on these relative frequency shifts and thus are a differential measurement, rather than an isolation of the slab effect. But the wedge itself is not uniform. Mitronovas *et al.* (1969) observed large-amplitude, high-frequency P and S waves for deep events in the Tonga arc for paths up the inclined seismic zone as well as for some paths through the wedge, which indicates that the low-Q regions in the wedge are localized in extent. This is similar to Sacks' (1969) observations under South America. Molnar and Oliver (1969) analyzed Sn over 1500 paths, mapping lateral variations in attenuation on the concave side of island arcs and strong contrasts in Sn efficiency across arcs. They found strong wedge attenuation in the Izu–Bonin, Mariana, and Ryukyu arcs. In Table 1, an effort is made to distin-

guish between relative contrast measurements, almost all of which are sensitive to slab–wedge contrasts, and absolute measurements relative to some background model. In many cases the slab heterogeneity relative to normal mantle may be only half of the contrast measurements.

Strong velocity heterogeneity in the mantle under Japan was clearly demonstrated by the study of Kanamori (1968), using incoming P wave arrival times from the Aleutian explosion LONGSHOT recorded by stations in Japan. Eastern Japan recorded early arrivals relative to stations on the Japan Sea side of the country, with J–B anomalies varying by 0.5 s. The P velocity contrasts across the dipping seismic plane were inferred to exist above 250 km depth, with the west side (i.e., the wedge above the slab) being lower in velocity by 0.4 km/s (4–6%). PcP/P differential attenuation estimates were used to estimate a wedge $Q_\alpha = 80$ for the upper 250 km. A thermal contrast of 500° along with about 2% partial melting in the wedge was invoked to explain the heterogeneity. Kanamori (1970) extended this analysis of incoming teleseismic signals with recordings from three Nevada Test Site (NTS) explosions. The travel time anomalies through the wedge increase with increasing path length above the dipping seismic plane, but again the geometry of the paths precluded measuring the velocity anomaly of the slab directly. Slow shear velocities of the wedge above the Japan slab were found by surface wave analysis by Kanamori and Abe (1968) and Abe and Kanamori (1970). The group velocities of Rayleigh and Love waves on the wedge side of the slab require the shear velocity to be 0.3–0.4 km/s slower (~8%) at depths of 30–80 km than on the oceanward side of the slab. This was found to be the case for the wedge regions in the Aleutians, New Zealand, New Britain, the Banda Sea, and near Flores Island. Utsu (1971) discusses early evidence for high-velocity lithospheric and deep structure oceanward of the Japan arc, and Hamada (1973) reported that the oceanic side of the mantle is a few percent faster than the wedge side. The anomalous properties of the wedge must thus be taken into account when any slab–wedge contrast is measured and used to interpret the thermal and compositional state of the slab. The asymmetry in mantle properties on either side of the slab also presents significant difficulties in establishing the actual baseline velocity model about which to calculate anomalies in almost all detailed slab studies.

The importance of anomalous wedge structure in other regions was quickly documented. Fedotov and Slavina (1968) found decreasing P velocities in the uppermost mantle from under eastern Kamchatka (7.4 km/s) to western Kamchatka (7.2–7.3 km/s). Utsu (1969) considered intensity variations in southwestern Japan associated with heterogeneity underlying the Ryukyu arc. Mooney (1970) analyzed frequency content differences in New Zealand recordings of deep Kermadec events and intermediate and a few deep New Zealand earthquakes. Eastern stations tended to have higher frequency content of both P and S waves than western stations, but the pattern did vary with source location. He

inferred the presence of a low-Q zone ($Q_\beta = 40\text{--}80$) under part of North Island and the surrounding oceans, with the preferred model placing the low Q in a layer from 75 to 125 km. The travel time data had a large scatter and placed little constraint on the structure. Dubois (1971) analyzed data from stations in New Caledonia and the New Hebrides, addressing both plate and surrounding mantle structure. He observed late arrivals from LONGSHOT to Melanesian stations, along with a Pn velocity of 7.9 km/s west of the New Hebrides in a region of poor Sn propagation (Molnar and Oliver, 1969), while a low Pn velocity of 7.4 km/s was found along the New Hebrides. Analysis of azimuthal travel time patterns at stations in New Caledonia versus stations along the New Hebrides revealed some travel time effects of the plate, but the results were inconclusive. Rayleigh wave dispersion in the wedge indicated a low mantle velocity of 7 km/s, indicative of a low-velocity wedge region.

Efforts to map the horizontal and vertical variations systematically throughout the wedge were commenced by Barazangi and Isacks (1971), who focused on the Tonga wedge. To constrain the shallow structure, they analyzed variations in Pn and Sn predominant frequencies and amplitudes from Tonga to Fiji, using the propagation efficiency approach of Molnar and Oliver (1969) and short-period instruments deployed by Lamont. They found a high-attenuation zone in the shallow wedge about 300 km wide, extending from the Tonga ridge to the Lau ridge and under the Lau basin (Fig. 4). They attributed this to crustal extension in the back arc. Signals from intermediate and deep earthquakes were used to map high-attenuation zones above the slab, using visual inspection of changes in frequency content and amplitudes for P and S waves. From 150- to 300-km depths, they estimated that Q_α could be as low as 50 and Q_β as low as 20, at least in localized regions, with the low-Q region being offset landward from the volcanic arc, under the Lau basin. High heat flow in the wedge (e.g., McKenzie, 1969; Oxburgh and Turcotte, 1970; Hasebe *et al.*, 1970) was related to these very low Q values.

Quantitative Q measurements of the wedge at teleseismic distances were first made by Niazi (1971), who used spectral ratios for phases recorded at stations in Berkeley and Jamestown. Data from 45 intermediate- and deep-focus events were analyzed in terms of a one-dimensional Q structure, with $Q_\alpha = 80$ found for the New Hebrides wedge. Scatter in the observations was attributed to heterogeneity in the attenuation structure. Wyss and Molnar (1972) estimated $Q_\alpha = 80$ above the Tonga slab using pP/P spectral ratios. Tsujiura (1972) found that for source depths less than 400 km there are strong regional differences in S wave spectra in Japan, whereas for deeper events there is little difference, with all events having depleted high-frequency content, suggesting that the latter paths all traverse an overlying low-Q region in the wedge.

Aggarwal *et al.* (1972) found 15% low P velocities in the upper mantle under the Lau basin west of Tonga, in regions of high seismic attenuation identified by

Barazangi and Isacks (1971). Travel time curves for paths along the Tonga-Kermadec ridge indicate much faster uppermost mantle velocities (8.43–8.48 km/s for P and 4.72–4.78 km/s for S) than paths within the Lau Basin (7.14 km/s for P). The high velocities may correspond to refractions from the top of the subducted oceanic mantle, at a depth of about 50 km. Such pronounced variations in velocity are suggestive of significant partial melting. Dubois *et al.* (1973) also reported low uppermost mantle velocities under Fiji, consistent with strong velocity reductions in the wedge. A very low value of $Q_\beta = 10$ was found on localized paths under Tonga by Barazangi *et al.* (1974).

Sacks and Okada (1974) used spectral ratio techniques to compare the mantle Q structure under western South America and Japan. They estimated that for South America $Q_\alpha = 1000$ –2000 in the wedge down to 350 km, while Japan has lower values of $Q_\alpha = 400$ –500 in the wedge, comparable to the values seaward of the Japan trench measured using pP/P, pPKP/PKP, sScS/ScS, and ScS/SKP spectral ratios. Spectral ratios of pairs of events indicate that Q_α in the Japan and South American slabs is about 1000 at 100 km and increases to about 3000 at 300–400 km. Deeper than 350 km in South America, Q appears to decrease, even in the slab, while high Q values in the seismogenic zone ($Q_\alpha = 3000$) extend to the depth of the deepest Japan earthquakes. A low-Q region above the Japan slab was detected at depths of 350–400 km. The relatively high Q values in the South American wedge were attributed to a thick continental plate.

The use of pP phases to map wedge heterogeneity was extended by Barazangi *et al.* (1975). They inspected 25,000 short-period and long-period waveforms visually, using a bimodal characterization of high and low Q. The Indonesian, South Sandwich, Mexican, Lesser Antilles, Alaska, Izu, and Hindu Kush wedges were not found to have low Q, but the sea of Okhotsk, southern Sea of Japan, Mariana, New Hebrides, Tonga, northern Chile, and southern Peru wedges all showed strong pP attenuation. The absence of sP in regions of strong pP attenuation was the basis for concluding that low Q_α and low Q_β are coupled. The attenuation variations in the upper 200–300 km of the wedge were correlated with low velocities, high heat flow, back arc extension, and regional uplift but not directly with arc volcanism. Regions of inefficient Sn propagation correlate with areas of low Q in the mantle. Small localized magma sources under the arc could not be well sampled by the signals that were analyzed.

P waves from local deep events in Japan were used to infer a low-velocity asthenosphere in the north Hokkaido–Sakhalin region by Naguchi and Okada (1976). Okada (1977) and Hasegawa *et al.* (1979) studied attenuation in the asthenosphere overlying the slab in the Hokkaido and Tohoku regions of Japan, respectively. They used S/P spectral ratios for intermediate- and deep-focus events. They obtained similar models, with a high-Q plate ($Q_\beta = 1000$) below the aseismic front, $Q_\beta = 350$ below the region from the aseismic front to the volcanic front, and $Q_\beta = 100$ below the volcanic front.

Extended mapping of Sn attenuation in the wedge lithosphere near South

America was conducted by Chinn *et al.* (1980). Sn propagates efficiently in the Nazca plate, but has complex behavior in the wedge. Lg propagates efficiently on paths parallel to the structural grain of the Andes. In regions where the slab subducts almost horizontally and there is no wedge, high-frequency Sn waves propagate efficiently, while Sn blockage is intermittent under the Altiplano. Bock and Clements (1982) used spectral analysis to estimate variations in Q values in the wedge above the Tonga slab of 80–240 and slab Q values greater than 630. Chiu *et al.* (1985) analyzed S wave attenuation in the mantle wedge in the New Hebrides, finding comparable strong attenuation.

More recent studies have utilized increasingly high-quality digital data, primarily for the Tonga region. Bowman (1988) analyzed P and S wave attenuation using 77 events recorded by three 3-component stations deployed in Tonga and Fiji during 1983–1985. P wave attenuation was estimated over 100 paths, but S wave attenuation was estimated for only 10 paths because of limitations of signal quality. He obtained fairly consistent Q values using a spectral decay rate method which assumes an ω^2 source model and the predominant frequency shift approach of the early studies mentioned above. For deep events recorded in Fiji he estimates $Q_\alpha = 570$ and $Q_\beta = 200\text{--}400$. For the Tonga slab Bowman estimated $Q_\alpha > 2000$ and $Q_\beta > 1800$, while the average value estimated for the wedge is $Q_\alpha = 240$. Teleseismic analysis of sS and sScS attenuation in broadband waveforms was used to map Q_β under the Lau basin by Flanagan and Wiens (1990). They used time and frequency domain methods, involving waveform equalization and spectral ratios, and found $Q_\beta = 20\text{--}35$ under the Lau ridge. Q can be as low as 30 down to 220 km but increases with depth below 200–300 km. Flanagan and Wiens (1993) have extended this data analysis to Western Pacific subduction zones, again finding very strong attenuation concentrated at depths less than 160 km under backarc basins, with Q_β values of about 36 under the island arcs.

Localized anisotropic properties of the wedge above the Japan (Ando *et al.*, 1983), Tonga (Bowman and Ando, 1987), South America (Kaneshima and Silver, 1992) and Kurile (Fischer and Yang, 1993) slabs have been investigated using shear wave splitting. Anisotropy is potentially a useful indicator of shear flow. Separating out crustal contributions and imaging the structure with high resolution is still a major challenge for such studies. Many additional constraints on wedge structure have been obtained from relative travel time measurements described in Section 3 and tomographic imaging efforts, as described in Section 4. Extensive mapping of velocity and attenuation heterogeneity of the wedge remains a critical aspect of investigations of deep slab properties.

2.4. Thermal and Mechanical Models

As oceanic lithosphere ages, its thickening thermal boundary layer has a predictable temperature structure proportional to the age of the plate. This pro-

vides an initial condition as the plate begins to subduct, allowing calculation of the thermal history of the descending slab as a function of the subduction velocity and geometry. For such calculations, it is necessary to use appropriate thermodynamic parameters and to account for shear strain heating, heat production, adiabatic compression, conductive heating, and kinematics of the surrounding mantle flow. Whereas some early calculations with strong shear strain heating predicted rapid thermal assimilation of the slab, most models now predict that substantial thermal anomalies should persist to depths of 660 km or below, if the slab is able to penetrate into the lower mantle. Such thermal models currently play a major role in predicting the velocity heterogeneity and phase equilibria of the deep slab, and the primary contributions during the past 25 years are mentioned here.

2.4.1. *Slab Thermal Models*

McKenzie (1969) was among the first to consider the problem of subducting slab thermal structure. He used plate theory to calculate the temperature distribution in the lithosphere and argued that plates drive the surface motions. He advanced the idea that the deepest earthquakes in Tonga are bounded by a limiting isotherm, with significant thermal heterogeneity persisting to at least those depths. He also introduced the notion of the “potential temperature” for a slab surrounded by an isothermal mantle in which the effects of adiabatic compression were neglected. This formulation with constant-temperature boundary conditions allowed analytic temperature calculations for the slab. McKenzie began a consideration of the corner flow induced in the mantle wedge and the associated shear heating of the slab. High heat flow measurements in back arc regions of the Kuril, Japan, and Bonin arcs by McKenzie and Sclater (1968) were considered rather enigmatic because the slab was expected to cool the surrounding mantle. McKenzie (1969) related this heat flow to the induced corner flow. McKenzie (1970) expanded on the analytic solutions using the potential temperature approach. He argued that phase changes within the slab are not that important for the temperature field, using the available thermodynamics, but that phase changes can contribute significantly to the buoyancy forces in the slab. The potential temperature model predicts that the maximum depth of seismicity should be proportional to the product of convergence rate and age.

Minear and Toksöz (1970a,b) introduced quasi-dynamic numerical modeling approaches to the thermal slab problem, using two-dimensional finite-difference calculations of the energy equation. In their approach they included adiabatic compression, effects of major phase transitions, strain heating, internal heat sources, and conductive and radiative heat exchange, assuming initial 80- and 160-km-thick slabs. The degree of shear strain heating, which is not independently known, was assigned rather high values, partly in order to induce lo-

calized melting at the top edge of the slab to explain volcanic arc magmatism. This in turn contributed to nearly total thermal equilibration of the slab by depths of 550 km for relatively high subduction rates of 8 cm/yr. The thermal anomalies were transformed into velocity anomalies assuming $dV_p/dT = -0.55 \text{ m/s}^{\circ}\text{C}$, predicting up-dip travel time anomalies of 1–2 s, or more if melting effects are considered. These calculations were related to the travel time anomalies first reported by Oliver and Isacks (1967) and Utsu (1967). These numerical models did not include any induced corner flow and were unable to explain high heat flow in the back arc by conductive heat transport alone.

At around the same time, Hasebe *et al.* (1970) computed two-dimensional time-dependent heat conduction equations for slab models, focusing on observations of high heat flow in the Japan island arc and marginal sea (about 2.5 HFU) versus the low heat flow in the trench (1.0 HFU). They assumed a 100-km-thick lithosphere and generated heat by invoking viscous dissipation by shear stress and penetrative convection of ascending magma. This was moderately successful at overcoming the intrinsically cooling effect of the subducting slab.

The variable degree of thermal assimilation presented in the first generation of slab models prompted a flurry of activity. McKenzie (1971) criticized the finite-difference procedures used by Minear and Toksöz (1970a,b), arguing that short-wavelength errors result in numerical instability that overestimates the temperatures. Hanks and Whitcomb (1971) also took issue with the results, arguing that effects of adiabatic compression were computed incorrectly, there actually being less energy available to heat the slab than had been thought. Griggs (1972) used one-dimensional heat flow calculations to explore slab thermal structure, including the effects of phase transitions, and also argued that Minear and Toksöz (1970a,b) overestimated the strain heating in the boundary layer. Griggs' models have strong thermal anomalies persisting to the depths of the deepest earthquakes very similar to those of McKenzie (1969). Turcotte and Schubert (1973) estimated that frictional stresses on the interplate contact are quite high in subduction zones, on the order of 1.35 kbar. As in the earlier models of Minear and Toksöz, they suggest that the volcanoes lie above regions in the slip zone where the upper part of the descending plate melts due to the high frictional heating, with the magma rising by plastic motion. However, they found lower temperatures in the plate relative to the earlier work, arguing that excessively high thermal conductivity had been assumed.

Minear and Toksöz (1971) responded to the questions about numerical stability of the finite-difference calculations, showing that a 20% temperature overestimation could result, but finer sampling in space and time would eliminate this. Then Toksöz *et al.* (1971) presented additional calculations with a finer grid, with effects of phase transitions and heat sources being revised at every step. No induced flow was yet allowed, but viscous dissipation, adiabatic compression, phases changes, radioactive heating, and a conductive geotherm were all in-

cluded (Fig. 6). These models still predicted thermal equilibration of the slab by 650 km depth for rapidly sinking slabs. These thermal models were used to predict seismic velocity structures used in three-dimensional raytracing calculations, initiating the systematic three-dimensional modeling of travel time anomalies observed for subduction zone events.

The importance of the wedge flow began to receive more attention. Andrews and Sleep (1974) demonstrated that the high heat flow in the back arc can be accounted for by induced wedge flow. They argued against frictional heating at the interplate contact as the source of the heat flow because it is hard to get the heat out of the mantle as the entrained flow drags it downward. They used two-dimensional time-dependent numerical models, with ablation of the plate surface producing island arc volcanism and spreading in the back arc accounting for the high heat flow. Hsui and Toksöz (1979) computed thermal models of slab flow driven by mechanical shearing and thermal buoyancy. They simultaneously computed temperatures within and outside the slab to address the question of why the overall wedge is high in temperature, as indicated by the observations of strong seismic wave attenuation throughout much of the wedge (Section 2.3). The induced flow in the wedge was found to be high because of the small Reynolds number of the material, and it was suggested that viscous shear heating is responsible for generating the large wedge temperatures. Hsui *et al.* (1983) explored whether melting of the subducted oceanic crust due to shear heating and

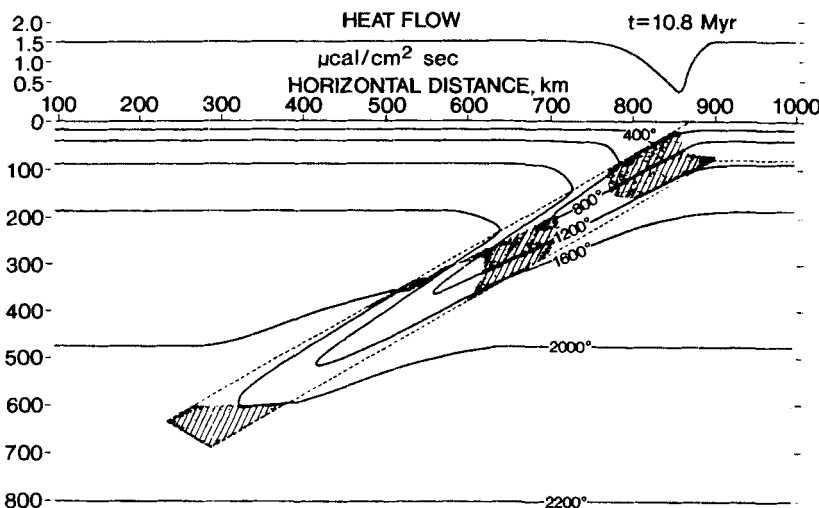


Fig. 6. A model of the thermal regime of a slab with a spreading rate velocity of 8 cm/yr, at a time 10.8 My after it began to sink. Adiabatic compression, phases changes, and shear-strain heating are included in the calculations. Shading indicates the zones of phase changes. Reprinted with permission from Toksöz *et al.* (1971).

dehydration release of volatiles in the slab crust and sediment veneer could contribute to the anomalous wedge properties. They found that the induced corner flow brings in a lot of hot material to the core of the wedge.

Anderson *et al.* (1978) included frictional heating and dehydration in finite-difference modeling of slab thermal structure. Dewatering of subducted minerals in the depth range 80–125 km may help to lower the melting point of the wedge material and possibly the upper slab material, but it was suggested that wedge convection may play a major role in melting localized portions of the wedge. Frictional heating for old subducting slabs was found to be inadequate to melt the slab material, but in young zones the oceanic crust may melt by frictional heating. Anderson *et al.* (1980) performed additional computations in which mass transfer in the wedge was allowed in addition to dehydration and frictional heating. They suggest that a combination of these effects is required to melt peridotite.

2.4.2. Thermal Controls on Seismicity

The progressive heating up of the slab is expected to affect the earthquake distribution in the slab, but the stress environment in the plate must also be considered. Isacks *et al.* (1968) showed that the down-dip length of the seismic zone is basically proportional to the convergence rate and inferred a 10-My assimilation time on the basis of the cutoff of seismicity in different zones. Molnar *et al.* (1979) found that the length of seismic zones correlates with the product of convergence rate times age, albeit with substantial scatter. They estimated that the temperature at the seismicity cutoff is about $600 \pm 100^\circ\text{C}$ at 200 km and $830 \pm 50^\circ\text{C}$ at 650 km. Using the McKenzie model and considering the relative effects of conduction, adiabatic heating, radioactivity, phase changes, and frictional heating, they concluded that conduction is dominant and estimated that the cutoff potential temperature is $800 \pm 100^\circ\text{C}$. Richter (1979) noted the high earthquake energy release in Tonga from 500 to 700 km, suggesting that this is difficult to reconcile with progressive assimilation, and he favored a factor of 10 increase in lower mantle viscosity relative to the upper mantle to provide resistance enhancing the earthquake activity.

Vlaar and Wortel (1976), Wortel (1982, 1986), and Wortel and Vlaar (1988) attribute the termination of slab earthquake activity at different depths in different regions to a depth-dependent critical temperature above which earthquake activity cannot occur (Fig. 7). A pressure effect was invoked by Wortel (1982) to model the increase in temperature at the depth of the deepest earthquake regions mentioned above. The basis of this argument is an observed correlation between maximum depth of seismicity and age of the slab at the trench, A_t (which reflects the initial conditions from which the sinking slab must heat up). A relationship between the time to resorption of the plate to the point where it can no longer

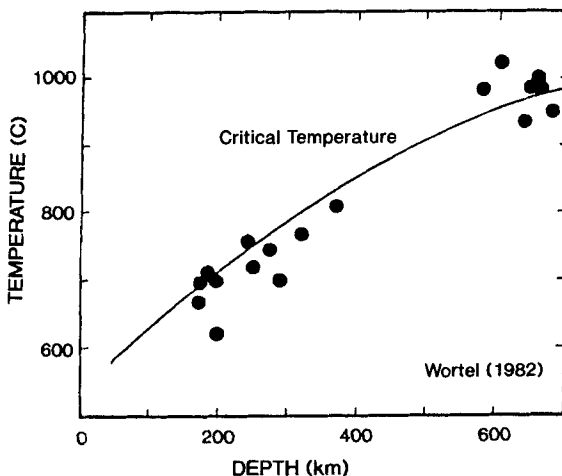


Fig. 7. Comparison of model slab temperature anomalies and maximum depth of earthquakes in different seismic zones with a model of a depth-dependent critical temperature cutoff. Reprinted with permission from Wortel, M. J. R. (1982). Seismicity and rheology of subducted slabs. *Nature (London)* **296**, 553–556. Copyright 1982 Macmillan Magazines Limited.

sustain earthquake failure, t_{res} , and A_t was found: $t_{\text{res}} = (0.12 \pm 0.03)A_t$. Deep events are found only in slabs older than 80–90 My. Wortel (1986) and Wortel and Vlaar (1988) argue that thermal stress associated with reheating of the slab and rheological properties of the elastic core of the slab are responsible for the relatively high seismic activity below the 400-km discontinuity and argue that no barrier at 670 km is required to explain the global cessation of deep activity. Wortel (1986) emphasizes that thermal assimilation does not necessarily imply a gradual reduction in seismicity with depth, for one must consider both the strength of the slab and the forces acting on it. He uses strength laws determined from low P - T environments along with estimates of the forces on deep slabs to suggest that the strength of the slab at 700 km is actually comparable to the strength of surface lithosphere. Interaction between the depth and temperature-dependent forces and rheology of the slab may account for both the relative maxima of deep focus earthquake activity and the termination with depth. Brodholt and Stein (1988) explored whether a limiting strength bounds earthquakes. They considered ductile flow laws, testing whether seismicity is related to sustainable differential stress, and found that seismicity is not readily described by a single lithospheric strength value. Many of these ideas may need to be revisited in the context of phase transition mechanisms for deep earthquakes that may induce local stress environments.

Finite-element models of the stress in slabs have been used to assess the nature of double Benioff zones (Section 5.1) and the relationship of seismicity to the

complex thermal and stress environment (Goto *et al.*, 1983, 1985; Hamaguchi *et al.*, 1983; Honda, 1985). The combined effects of slab deformation, asymmetric heating, internal phase transitions, and deep resistance produce a very complicated environment, and it is not clear which factors dominate the seismicity in any given region.

2.4.3. Convective Models with Chemical and Viscous Stratification

The possibility that the mantle is chemically stratified must be considered in any thermal–mechanical modeling of slabs. Given sufficient intrinsic chemical density contrast between the upper and lower mantle, it is not difficult to develop rigorously stratified mantle convection. Using finite-element time-dependent flow calculations for temperature-dependent non-Newtonian rheology, Christensen and Yuen (1984) estimate that a 5% contrast is sufficient to deflect the slab, preventing mixing between the upper and lower mantle. The compositional boundary should be depressed by 50–200 km. If the chemical density difference is 2–5% the slab can penetrate several hundred kilometers, whereas if it is 2% it may penetrate all the way to the core–mantle boundary (Fig. 8). A chemical density contrast of 5% is near the upper end of estimates of a bulk chemical density contrast between the upper and lower mantles based on mineral physics experiments on silicate perovskite and magnesiowüstite (e.g., Knittle *et al.*, 1986; Jeanloz and Knittle, 1989; Stixrude *et al.*, 1992). Either Fe or Si enrichment of the lower mantle is a viable way to account for the excess lower mantle density. The critical physical parameter underlying these arguments is the thermal expansion coefficient for silicate perovskite at high pressure, which is needed for estimating the density predicted for various lower mantle compositions. Although there is controversy over the experimental determination of the thermal expansion coefficient for perovskite and its extrapolation to high pressures due to possible strong pressure dependence (Chopelas and Boehler, 1989, 1992) most measurements have been made either at atmospheric pressure (Knittle *et al.*, 1986; Ross and Hazen, 1989; Parise *et al.*, 1990) or at pressures below the stability field of perovskite (Mao *et al.*, 1991; Wang *et al.*, 1991). New measurements at simultaneous high pressure and high temperature are just beginning to emerge (Funamori and Yagi, 1993), which indicate less decrease in thermal expansion with pressure than previously thought, strengthening the case for a chemical contrast. Confirmation of these results will be critical for resolving the arguments about any chemical contrast between the upper and lower mantles.

It is very likely that the 660-km seismic discontinuity is primarily the effect of the spinel–postspinel phase transition, for we know that this will occur for the abundant olivine and pyroxene polymorphs in the mantle, but there has been some question about whether an additional chemical contrast is involved. Lees *et*

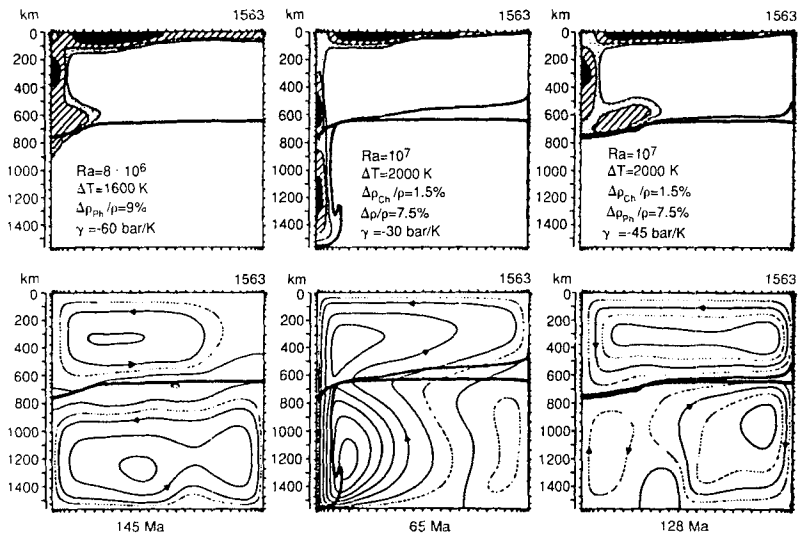


Fig. 8. Thermal convection models for two-layered media with a chemical density contrast and phase change between the upper and lower layers. The ability of downwellings in the upper mantle to penetrate into the lower mantle depends strongly on the strength of the chemical density contrast. Viscosity is shown in the upper diagrams and streamlines in the lower ones. A pure phase boundary with a 9% increase in density and a Clapeyron slope of -6 MPa/K induces layered convection (left). A combined phase and chemical boundary with 1.5% chemical density increase and 7.5% phase change density increase with a Clapeyron slope of -3 MPa/K allows the slab to penetrate (middle). A combined phase and chemical boundary with the same density increases as in the middle, but a Clapeyron slope of -4.5 MPa/K induces stratification. Reprinted with permission from Christensen and Yuen (1984).

al. (1983) argue that the seismic boundary is too sharp, based on seismic reflections, to be an isochemical transition, and they prefer a combined phase and chemical change. They suggested that the lower mantle is enriched in Fe and/or Si, based on the mantle Mg/Si ratio to C1 chondrites. There is still uncertainty in the expected sharpness of the phase boundary, but the small range of global vertical undulations of the 660-km boundary is compatible with a phase transition (see Section 5.3). However, it is not clear that any chemical contrast between the upper and lower mantles must be coupled to the 660-km phase boundary. Jeanloz (1991) considers the possibility that the compositional boundary, which is expected to be very difficult to observe seismically if it involves Fe or Si enrichment, may be present along with a phase boundary. He shows that the transition of polymorphs of olivine and pyroxene to $(\text{Mg}, \text{Fe})\text{SiO}_3$ perovskite and magnesiowüstite can explain the observed contrasts in P and S velocities and density at the 660-km boundary quite well. However, a 5% chemical density contrast could also be present, as needed to reconcile the thermal expansion

determinations, with this boundary affecting the extent of slab penetration. Topography on the chemical boundary would be much higher than on the phase boundary, although the sense of deflection would be the same.

The arguments about whether any chemical contrast exists between the upper and lower mantle are complicated by uncertainty in the composition of the transition zone itself. Bass and Anderson (1984), Anderson and Bass (1986), Anderson (1988), Duffy and Anderson (1989), and Anderson (1991) have suggested models of transition zone chemistry poor in olivine and rich in basaltic components, giving a garnetite transition zone. Such a layer, perhaps accumulating subducted slab crustal components, may have high strength and high viscosity because garnet is a complex cubic mineral. The observed seismic discontinuity at 410 km depth and the seismic velocity gradient through the transition zone appear to be hard to match with material as olivine rich as pyrolite. Although these models are still strongly debated, it is clear that rheological properties of the transition zone are important. Meade and Jeanloz (1990) report diamond-anvil cell experiments indicating that γ -spinel is quite strong, and they suggest that the transition zone may have relatively high viscosity. Future determinations of high pressure–high temperature rheology of upper and lower mantle phases will be important for assessing the dynamics of slabs.

The relative viscosity of the subducting slab influences its ability to penetrate into a chemical contrast, with higher viscosity allowing it to retain a concentrated negative buoyancy that abets penetration. Experimental work using two-layer sucrose solutions with different densities and viscosities (Kincaid and Olson, 1987) indicates that slab geometry also influences slab penetration, with steeper-dipping slabs penetrating more effectively. Kincaid and Olson (1987) define three regimes: penetration with no distortion, limited penetration with development of a thickened root depending on the dip, and negligible penetration of the deep layer with retrograde slab motion and trench migration. Honda (1987) performed numerical modeling of two-layered convection with slab penetration to further explore the effects of chemical layering. Silver *et al.* (1988) argue that penetrative convection, in which the compositionally induced density increase across the transition zone is 2% or less, is a viable explanation for a variety of deep Earth constraints. Continued efforts to quantify any bulk chemistry difference between the upper and lower mantle are critical for assessing the role of any chemical layering, as are efforts to detect any seismic boundary that can be attributed to a compositional contrast.

Viscous stratification of the mantle provides an effective mechanism for resisting slab penetration into the lower mantle and can readily lead to broadened downwellings in the deep mantle. An increase in viscosity across the 660-km boundary by a factor of 10 to 100 has been invoked in several efforts to model the long-wavelength (degree 2–3) geoid, the presence of long-wavelength positive geoid anomalies over subduction zones, and the strong correlation of slab distri-

butions with the degree 4–9 geoid (Hager, 1984; Hager *et al.*, 1985; Hager and Richards, 1989; Hager and Clayton, 1989; King and Hager, 1993). Less abrupt viscosity increases have also been proposed (e.g., Forte *et al.*, 1992). Generally, these models favor lower mantle penetration to achieve a good fit to the geoid, but the results are very dependent on the viscosity model. A combination of a viscosity increase and a chemical contrast can be reconciled with the geoid but requires a substantial accumulation of subducted material at the top of the upper mantle and a deeply (up to several hundred kilometer) depressed compositional discontinuity (e.g., Hager, 1984). Two-dimensional finite-difference calculations with temperature-dependent viscosity by King and Hager (1993) indicated that variable viscosity near the subduction zone changes the amplitude but not the sign of the geoid predictions.

Finite-element numerical simulations also indicate that an abrupt increase in viscosity can strongly deform the subducting slab, causing it to fold over on itself in the uppermost part of the lower mantle (Gurnis and Hager, 1988). These calculations predict that as the duration of subduction increases, the slab dip will decrease. Advective thickening of the slab by a factor of 3, with attendant loss of tabular shape, is predicted for viscosity increases by a factor of 100 from the upper to the lower mantles. Across the viscosity interface the slab can kink and sink at a higher angle (Fig. 9). Viscosity increases by a factor of 10 cause down-dip compressional stress to dominate in the transition zone. The viscous flow models can produce many features similar to those seen in tomographic images (Chapter 4). Thus, this is a viable mechanism for distorting the deep slab and advectively thickening it, but alone it will not prevent eventual sinking of the subducted mass unless extreme viscosity contrasts are invoked. The nature of any seismic velocity anomaly associated with a thickened or buckled slab depends strongly on the extent of heating by viscous deformation, which is poorly known.

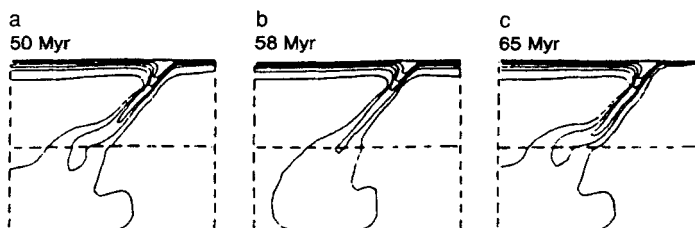


Fig. 9. Isotherms of a slab as it folds in the upper layer during penetration into the lower layer. There is a jump in viscosity by a factor of 30 across the interface (horizontal dashed line). The contour intervals are 0.2, 0.4, 0.6, 0.8, and 0.99. Reprinted with permission from Gurnis and Hager (1988).

2.4.4. Effects of Chemical Buoyancy of the Slab

The distinct phase equilibria of slabs must also be considered when assessing their dynamics. Ringwood (1976, 1982) explored the implications of the pyrolite model for mantle composition on the dynamics of subducted lithosphere. In the pyrolite model, the melting fractionation that occurs at midocean ridges results in a basaltic crust overlying a layer of harzburgite, with a thin underlying region of lherzolite and pyrolite depleted in highly incompatible components (Rb, light rare earth elements). The slab can thus be viewed as a thermal, chemical, and rheological continuum (Fig. 10). The lower interface of the slab may not be defined by an abrupt change in temperature and chemistry as is the upper surface, although the composition of the lower oceanic lithosphere is not precisely known (Anderson, 1987b). Each of the differentiated layers in a slab will undergo a significantly different series of phase transformations compared to the ambient mantle pyrolite; for example, the crust will transform from basalt to eclogite to garnetite.

In 1976, Ringwood argued that as a result of the different phase transformations in each portion of the slab, different densities will exist within the slab and

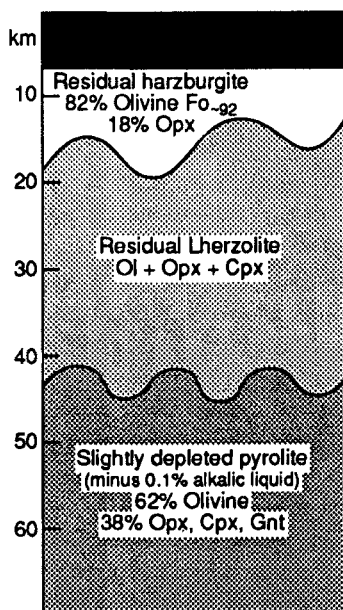


Fig. 10. Idealized petrological structure of oceanic lithosphere with bulk composition equal to pyrolite, showing chemical and petrological zoning developed during partial melting and differentiation at midocean spreading centers. Reprinted with permission from Ringwood (1993).

each portion will sink to a different depth. Since both intrinsic chemistry and temperature variations contribute to the density structure, the ultimate dynamic equilibrium will depend on the density contrast and thermal equilibration. While relatively cold, the entire slab will be denser than surrounding pyrolytic mantle to depths of 650 km. However, Ringwood's calculations indicated that if thermally equilibrated, the harzburgite layer will be buoyant down to depths of 500 km and neutrally buoyant near 640–700 km, which would inhibit further sinking, leading to buckling of the slab and accumulation of a "megalith" of deformed slab products near 650–800 km depth (Fig. 11). Stability of the megalith depends on its intrinsic thermal anomaly and on the erosional effects of thermally coupled convection. Ringwood asserts that upon thermal equilibration the harzburgite will rise from the megalith in diapirs, ultimately finding dynamic equilibration in the overlying lithosphere. Whereas the basaltic component was originally expected to be sufficiently dense that it would sink through the lower mantle (e.g., Ringwood, 1982, 1986), extended experimental data on the density of eclogite relative to pyrolite indicate that it will be neutrally buoyant at depths near 650 km, perhaps forming a 70–100-km-thick layer of garnetite (Ringwood and Irifune, 1988; Ringwood, 1990, 1993; Irifune and Ringwood, 1993). This is similar to the calculations of Anderson (1987b) and the associated model of Anderson and Bass (1986), in which the transition zone from 500 to 650 km is primarily an accumulation of eclogitic material from either accretion or subduction. These ideas also apply to thin, young slabs that are subducted and achieve thermal equilibration at shallower depths. Any accumulation of a garnetite layer above 660 km could act as a barrier to sinking of depleted pyrolite components in slabs, and Ringwood (1993) argues that cold dense slabs will successfully penetrate this layer and sink into the lower mantle, while slabs with seismic zones extending no deeper than 300 km are unable to do so.

The calculations of Ringwood (1990) and Anderson (1987b) predict that if the slab is fully thermally equilibrated with the surrounding mantle, it will be dynamically stabilized in the transition zone. The intrinsic chemical buoyancy can affect subduction and perhaps lead to separation of the slab components. However, numerical calculations of viscous slabs including chemical buoyancy effects indicate that thermal buoyancy predominates, and even if an increase in viscosity with depth leads to strong folding and deformation of the slab, the chemical buoyancy effects are secondary in the overall dynamics of the slab (Gurnis, 1986; Christensen, 1989; Richards and Davies, 1989; Gaherty and Hager, 1994). These calculations indicate that unless the slab material can be held stagnant in the transition zone for sufficient time that full thermal equilibration is achieved, chemical buoyancy effects will not play major role in determining the fate of the slab. Thermal buoyancy appears to dominate, and the slow warming of the slab ensures that even if lower mantle penetration is inhibited by a viscosity increase that slows the rate of descent, thermal equilibration is not

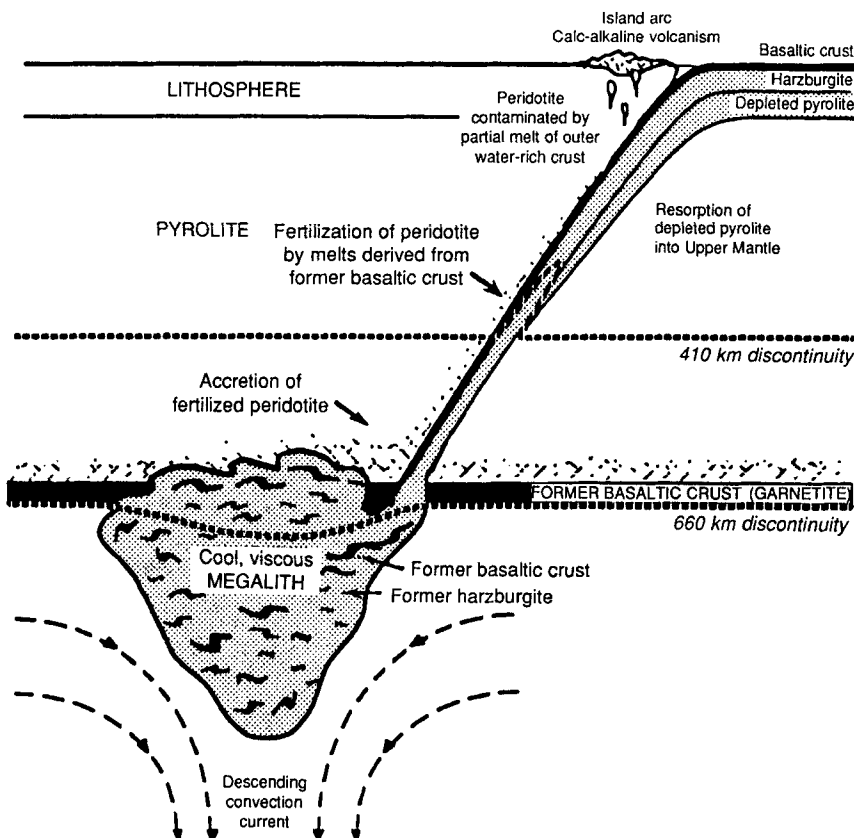


Fig. 11. Cartoon showing possible fate of a deep slab. A gravitationally stable layer of garnetite (550–650 km) and dunite–harzburgite (650–700 km) is present due to previous subduction. The tip of a subducting plate experiences buoyant resistance when it penetrates this layer. The former oceanic crust and harzburgite layers may plastically thicken and buckle to form a large melange (megalith) situated mainly below the 660-km seismic discontinuity. The megalith is a transient feature and ultimately becomes entrained in the convective regime of the lower mantle. The lower layer of ductile depleted pyrolite initially at the base of the descending plate of suboceanic lithosphere becomes resorbed into the upper mantle by convective circulation due to its inability to penetrate the garnetite–harzburgite layer. Reprinted with permission from Ringwood (1993).

achieved before the material sinks into the lower mantle. Physical separation of slab components is inhibited by the high slab viscosity, and one must substantially heat up the slab to achieve separation, presumably by emplacing the slab in a hot thermal boundary layer (Olson, 1988). There is not much evidence for a thermal boundary layer at the top of the lower mantle, so it may be that any slab component separation takes place in the boundary layer above the core. It is

important to note that if the slab material does penetrate below the transition zone, the basaltic component may again become denser than the surrounding mantle, adding negative buoyancy to the slab (Ringwood and Irifune, 1988). Continued work on the high pressure density of slab materials is needed to address this issue.

Anderson (1987b) makes a strong case for the importance of isobaric, thermally induced phase changes in the mantle, particularly given the strong thermal heterogeneity of the subducting slab. He argues, for instance, that low-temperature phases such as ilmenite may exist in the slab and the effects of intrinsic density, velocity, and anisotropy of such unusual phases may have significant contributions to the overall seismic velocity signature of the slab. Anderson suggests that geoid and slab geometry modeling efforts have often underestimated the intrinsic density heterogeneity of the slab by overlooking the chemical effects and contributions from elevated phase transitions. He estimates that slab densities are 5–11% greater than normal mantle between 350 and 550 km, which is much more than thermal expansion alone would predict. The combined effect of chemical and thermal contributions to slab seismic velocity heterogeneity could make slabs as much as 10% faster than surrounding mantle in the transition zone.

2.4.5. Slab and Convection Models with Phase Transitions

The olivine-modified spinel phase transition is expected to be elevated in a cold sinking slab (it has a positive Clapeyron slope), an effect first studied by Schubert *et al.* (1970), and it will liberate heat (it is exothermic), an effect included by Hasebe *et al.* (1970) and Toksöz *et al.* (1971). Turcotte and Schubert (1971) performed analysis of a univariant phase boundary in the presence of uniform convective flow, finding that the α – β transition could be elevated by 150 km in the slab, giving an additional body force in the slab that is of the same order as the thermal contrast, a result similar to the calculations of Griggs (1972). Smith and Toksöz (1972) used finite-difference schemes to calculate stresses for an elastostatic model and estimated that the α – β transition can add 200 bars of shear stress to the slab. Toksöz *et al.* (1973) further explored the effects of phase transitions in the slab, finding that the maximum depth of penetration is strongly affected by the postspinel transition.

More extensive analysis of the effects of phase transitions followed with the studies of Schubert and Turcotte (1974) and Schubert *et al.* (1975), who examined the interaction of solid–solid phase transitions with convection, including the effects of latent heat of transformation and advection of the position of the phase boundary along with the associated body force. They considered linear stability theory for univariant transitions, as in earlier work, as well as for divariant phase transitions (in which olivine and spinel simultaneously exist)

with much larger coefficients of volume expansion. These models, including both olivine–spinel and spinel–postspinel transitions, predicted thermal anomalies as large as 700°C persisting to depths of 800 km. The spinel–postspinel transition was assumed to be endothermic (with negative Clapeyron slope), as is now confirmed by experimental work (e.g., Ito and Yamada, 1982; Ito and Takahashi, 1989; Ito *et al.* 1990). A 115-km elevation of the α – β transition was associated with a large downward gravitational body force adding to down-dip tensional earthquake activity at intermediate depths, and the depression of the spinel–postspinel transition provided a resisting stress that could explain down-dip compressional stress for deep earthquakes. The linear analysis suggested that the endothermic transition would have only a mild stratifying tendency, not providing a major hindrance to slab penetration.

Finite element models of slabs have been used to explore the stress environment associated with kinetically hindered phase transitions as well. Goto and Hamaguchi (1983) and Goto *et al.* (1987) explored stress and temperature distributions in slabs with both equilibrium and nonequilibrium olivine–spinel phase transitions. A depressed tongue of untransformed olivine has a substantial negative buoyancy contribution and gives rise to complex internal stresses in the slab. This effect has not been considered in most other analyses of phase transition effects on slabs.

There have been extensive numerical calculations of the dynamic effects of the endothermic and exothermic phase transformations on upwellings and downwellings in the transition zone. Early time-dependent finite-element convection models with a 660-km endothermic transition (e.g., Christensen, 1982; Christensen and Yuen, 1984, 1985) indicated that a large negative Clapeyron slope (-4 to -8 MPa/K) would be required to induce a leaky double-layered convection. Estimates of the Clapeyron slope vary from -2.8 to -4.0 MPa/K (Ito and Takahashi 1989; Ito *et al.*, 1990) and updated computations at higher Rayleigh number (Ra) have incorporated these values. Calculations with $Ra = 10^6$ – 5×10^7 have been conducted in a two-dimensional Cartesian geometry to assess the effects of the 660- and 400-km phase transitions (Liu *et al.*, 1991; W. Zhao *et al.*, 1992; Steinbach and Yuen, 1992). Increasing Rayleigh number tends to promote layering of the system, as does the coexistence of the two phase transitions. Spherical axisymmetric calculations (Fig. 12) indicate similar phenomena (Machetel and Weber, 1991; Peltier and Solheim, 1992), as well as a tendency for time-dependent behavior involving catastrophic flushing out of the accumulated downwellings in the upper mantle. The geometric configuration of downwellings is important for their ability to penetrate (Bercovici *et al.*, 1993) so fully three-dimensional calculations are needed. Catastrophic overturn is observed in spherical axisymmetric (Machetel and Weber, 1991); Solheim and Peltier, 1994), two-dimensional Cartesian (Weinstein, 1993), and three-dimensional Cartesian (Honda *et al.*, 1993) geometries, but the degree of episodicity of these insta-

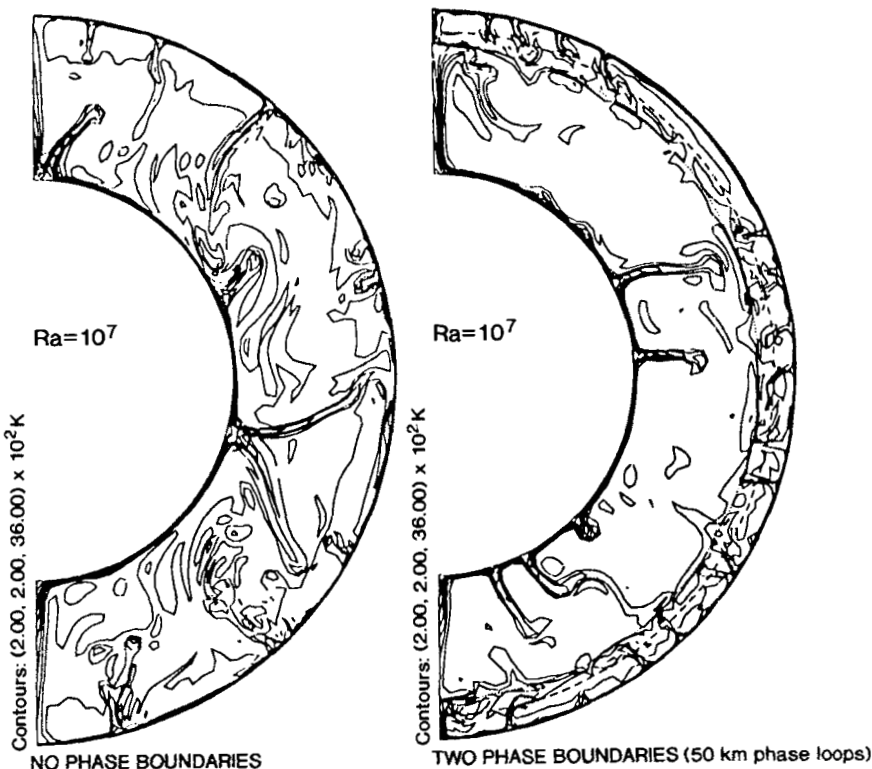


Fig. 12. Instantaneous temperature fields from two axisymmetric simulations of mantle convection at a Rayleigh number of 10^7 . Heating is entirely from below. The calculations on the left do not include any phase transitions; those on the right include both a model olivine- β spinel transition and a model spinel-perovskite transition, with 50-km-thick phase loops. Note that neither hot ascending plumes nor cold descending plumes appear to penetrate the 660-km discontinuity on the right. Reprinted with permission from Peltier and Solheim (1992).

bilities is reduced in fully three-dimensional spherical flow regimes (Tackley *et al.*, 1993), where flushing events are more localized phenomena. The latter calculations are for a realistic mix of bottom and internal heating, with the volume-averaged Rayleigh number from internal heating and superadiabaticity being 1.9×10^7 . The occurrence of intermittent overturning events is an efficient mechanism for producing a heterogeneity spectrum dominated by long-wavelength features, as observed for the Earth. However, it is not clear that upper and lower mantle heterogeneities are as radially decorrelated as expected for the quasi-stratified flow regimes that have been computed (Jordan *et al.*, 1993). At this time, the effects of high-Rayleigh-number flow with strongly temperature-dependent viscosity and phase transitions have yet to be established. It is clear that temperature dependence of viscosity is important for the overall convective

pattern (e.g., Tackley, 1993). It is likely that the stiffness of the slab will strongly influence the ability of the phase transitions to impede their downward motions, as found in the temperature-dependent calculations of Christensen and Yuen (1984) and Zhong and Gurnis (1993), so it is premature to base too many conclusions on these calculations. In addition, the effects of kinetic inhibition of the phase transitions are just beginning to be explored in dynamic calculations (e.g., Daessler and Yuen, 1993).

2.4.6. *Historical Slab Accumulations*

The time-integrated history of subduction places important constraints on the interpretation of seismic models for deep slabs. Estimates of the cumulative subducted material in circum-Pacific regions based on plate reconstructions have been found to correlate with long-wavelength seismic velocity heterogeneity in both the transition zone (Scrivner and Anderson, 1992) and the radially averaged lower mantle (Richards and Engebretson, 1992). Given the long time required for thermal equilibration of the slab material (e.g., Shiono and Sugi, 1985), one expects large volumes of high-velocity material near or below subduction zones, unless the slabs readily sink deep in the lower mantle. Degree 2 harmonic terms of aspherical velocity heterogeneity and accumulated slab volume do correlate rather well in the transition zone and uppermost part of the lower mantle (Scrivner and Anderson, 1992), which can be used to argue either for or against slab penetration into the lower mantle, as long as broadening and thickening of the slab are allowed. Of course, degree 2 is extremely large scale, even relative to the volumes of accumulated slab material, and higher-degree components (admittedly, less well resolved in the current seismic models) show far less correlation. Efforts to relate specific deep slab structures to the history of subduction are just beginning (Engebretson and Kirby, 1992; Grand and Engebretson, 1992; van der Hilst *et al.*, 1992), but this promises to be a fruitful area of research. Calculation of the geoid signature from accumulated slab material allows various models of viscous stratification and slab penetration to be explored as well (e.g., Zhang and Christensen, 1993).

3. TRAVEL TIME PATTERN CONSTRAINTS ON SLAB VELOCITY STRUCTURE

The primary method for establishing the characteristics of subducted lithosphere is to interpret observed seismic velocity structures in conjunction with thermal and petrological models like those discussed in the last section. This is necessary because our understanding of high-pressure mineral physics, slab chemistry, and geodynamic processes is limited, so that all slab models require direct observational constraints, provided mainly by seismology. For example,

velocity heterogeneity in the vicinity of seismogenic zones can be used to place bounds on the thermal structure to test whether the model of a critical cutoff temperature for deep seismicity is accurate. In addition, since huge volumes of slab have descended in the current subduction zones, greatly exceeding the volumes that are presently seismically active, seismological techniques for imaging the aseismic slab material must be used to assess where the slab material has gone. The next few sections will describe how the detailed seismic velocity structure of slabs is determined using refinements of the procedures described in Section 2.

Slabs are thermally and chemically distinct from the surrounding mantle (Section 2.4) and thus have distinct elastic velocity structure. As a result, seismic waves transmitted through the slab incur amplitude and travel time anomalies. The basic idea underlying most seismic travel time modeling of deep slabs is that the cold slab should have higher elastic velocities than the ambient mantle, with the quasi-tabular geometry of the slab (at least above 660 km) giving rise to simple symmetries in the patterns of relatively early and late arrivals, the former having longer path lengths in the slab material. As discussed below, numerous studies indicate that in the transition zone slabs generally do have about 3–5% higher seismic velocities than the surrounding mantle, and stronger contrasts of up to 10% (enhanced by anomalous wedge properties) are found at depths from 50 to 400 km. Realistic thermal models, combined with estimates of temperature derivatives of seismic velocity, can account for much of this heterogeneity (e.g., Creager and Jordan, 1986), with stronger velocity gradients being expected on the crustal side of the slab. However, interpretation of seismic heterogeneity is not a trivial task. There is, unfortunately, still substantial uncertainty in seismic velocity dependence on temperature at high pressures, complicating interpretation of deep slab velocity heterogeneity (Anderson, 1987a, 1988), as discussed in Section 7.

The chemically layered nature of the slab adds detailed velocity structure, such as a high-velocity eclogitic crustal layer, the possible presence of low-temperature phases such as MgSiO_3 -ilmenite, as well as significant ($\pm 5\%$) variations associated with either elevated or depressed equilibrium and/or kinetically suppressed phase boundaries. Anisotropic characteristics of the slab and the surrounding flow may also contribute to the seismic velocity signature of a deep slab (Anderson and Bass, 1986; Anderson, 1987b; Kendall and Thomson, 1993). Finally, there is the intrinsic limitation that seismic wave heterogeneity may have multiple causes. For example, it may be very difficult to distinguish aseismic slab extensions into the lower mantle from induced downwellings in a thermally coupled convection system. Consideration of dynamical models when interpreting seismic images is always crucial.

Efforts to extract information about slab velocity structure from relative travel time patterns for isolated events are discussed in the section. Although the few

nuclear explosions in island arcs have been exhaustively analyzed, most studies of travel time patterns associated with slabs necessarily utilize earthquakes. The greatest challenge in isolating the slab signature in the seismic wave arrival times is that the location of an earthquake source is almost always not known independently. Standard earthquake location procedures project as much as possible of the observed travel time deviations from the reference Earth model into shifting the source location and origin time. Routine earthquake locations are performed with no slab structure in the Earth model, or at best a very simplified slab model, leading to intrinsically biased locations of deep events. Patterns of anomalies with respect to the biased locations can be quite different from patterns relative to the actual location (e.g., Creager and Boyd, 1992), an effect one should account for in any modeling effort, but very few of the studies discussed in the following actually do this. Typically, there is an explicit assumption (almost never demonstrated to be valid) that the earthquake location is determined with enough coverage of the focal sphere that any paths affected by the slab retain their anomalous values.

3.1. Relative Travel Time Patterns and Raytracing Analyses

The three-dimensional geometry of slabs produces complex patterns of body wave travel time residuals with respect to azimuth and takeoff angle from the source. The primary procedure for systematically displaying travel time patterns with respect to the source location is the residual sphere method introduced by Davies and McKenzie (1969). Residual spheres are projections of travel time anomalies onto a source focal sphere, indicating the azimuth and takeoff angle of each raypath corresponding to observed or calculated anomalies. The heterogeneous structure of the slab will cause the raypath orientation to deviate from those calculated for a homogeneous model, which requires that three-dimensional raytracing be performed to produce an accurate residual sphere. Slowly varying patterns of anomalies in the residual sphere can often be attributed to near-source slab structure. Residual sphere displays have been used extensively in both observational and theoretical studies.

Examination of azimuthal patterns of source and station travel time anomalies to infer heterogeneous mantle structure is a classic procedure in seismology (e.g., Cleary and Hales, 1966) and has played a major role in studying subduction zones. Bolt and Nutti (1966) found 2-s azimuthal patterns of station travel time anomalies at Mt. Shasta relative to a control station at Berkeley, which they attributed to heterogeneous mantle structure. This is now associated with the aseismic extension of the subducted Juan de Fuca plate.

The early study of the azimuthal travel time pattern for LONGSHOT by Cleary (1967), described in Section 2.1, initiated the systematic investigation of individ-

ual slab event travel time patterns. Davies and McKenzie (1969) analyzed the LONGSHOT data, addressing the 25-km epicentral mislocation and 50–75-km depth error of routine locations due to slab effects and limited station distribution. They projected the travel time anomalies onto a residual sphere, emphasizing that the pattern is not just an azimuthal pattern, but the fast band corresponds to the dipping plate. To explain the 3-s pattern as a slab structure, they argued that 3–4% heterogeneity over 1000-km paths was needed. Assuming $dV_p/dT = -0.5 \text{ m/s/}^{\circ}\text{C}$, they estimated that a 500° temperature contrast, as in McKenzie's (1969) thermal slab model, would result in a 2.5% fast velocity slab.

The conceptual models introduced by Oliver and Isacks (1967) and Utsu (1967), along with the early thermal slab models described in Section 2.4, indicated that slabs have strong near-source velocity heterogeneity, which motivated development of three-dimensional raytracing capabilities to address slab problems. Numerical integration in spherical geometry of ray equations based on Fermat's principle was introduced by Jacob (1970), Julian (1970), and Sorrells *et al.* (1971), with subsequent development of shooting and bending methods to handle the two-point problem by Julian and Gubbins (1977). These methods have been extensively applied in analysis of earthquake relative travel times, residual sphere methods (Section 3.2), and amplitude focusing and multipathing effects (Section 6).

Julian (1970) did not consider actual data but performed three-dimensional raytracing for raypaths up- and down-dip of thermal slab models, showing the presence of shadow zones produced by wave refraction. Jacob (1970) compared local observations of deep earthquakes (located by teleseismic data) and teleseismic arrivals from shallow events (located by local stations) to estimate slab velocity anomalies for the Tonga–Kermadec slab. Using a planar slab model with slab thickness from 100 to 200 km, he modeled the up-dip observations with a 6% fast slab model, although allowance for a low-velocity wedge pushed this to 7–10%. Anomalies of 5–6 s for the entire slab path were observed for both up-dip and down-dip observations. The presence of a 7% fast slab anomaly predicts about 4-s relative time trends for downgoing teleseismic phases alone. Jacob (1970) suggested that systematic relocation using slab models and raytracing should improve absolute earthquake locations.

Three-dimensional raytracing in a layered medium separated by planes and spherical interfaces (rather than smooth inhomogeneity) was performed by Sorrells *et al.* (1971) to analyze LONGSHOT travel times. They applied station corrections to reduce the scatter in the sinusoidal azimuthal travel time pattern and then modeled the resulting 1.4-s pattern with a fast slab. They favored slab models with 6–12% fast P velocities extending to 300 km. Comparable results for the Aleutian slab were found by Jacob (1972), who used his raytracing method to investigate the LONGSHOT travel times. He analyzed P wave times in the distance range 20–100°, using about 300 observations. By exploring different

reference models he established that their effects could be significant. His slab-related residuals, ranging from -0.1 to -2.0 s, yielded a preferred model with an 80-km-thick plate extending to 250 km with a P velocity anomaly of 7–10%. The higher velocity value was obtained when a -5% anomaly was assigned to the wedge. The range of slab velocity anomaly was reduced to 6–8% for slab models extending to 300 km depth. Correction of the travel times by the slab model produced more sensible systematic relations between station residuals and tectonic province, giving confidence that the source contribution was being isolated.

Confidence in the slab structure explanation for the LONGSHOT times grew quickly, largely because there was no uncertainty in the source location, and even small irregularities of only 1–2 s in the azimuthal pattern were used to infer detailed structure. For example, Abe (1972) argued that travel times in the limited 10 to 30° azimuthal range are 1 to 2 s later than expected for the smooth pattern and attributed this to a tear in the underthrust lithosphere intruded by relatively low-velocity asthenospheric material with a contrast of 0.3–0.6 km/s relative to the slab. The tear was associated with lateral contortion of the slab reflected in the Bowers ridge topography on the overriding plate and the kink in the Aleutian arc near Amchitka. Sleep (1973) was the first to use a thermal model (from Toksöz *et al.*, 1973) in constructing the velocity structure parameterization for the LONGSHOT data. That study and numerous other studies concentrated on the amplitude and multipathing effects of the slab and are discussed in Section 6.

McKenzie and Julian (1971) were the first to study the deep velocity structure of the subducted Juan de Fuca slab under Washington State. They used travel times for the well-located, 65-km-deep 1965 Puget Sound earthquake. When plotted on a residual sphere, a high-velocity zone dipping about 50° toward the east was apparent in the residuals, with no pattern being found in the residual spheres from a nearby event in Vancouver away from the slab. They attributed the high-velocity region to an aseismic extension of the subducted plate. They examined about 100 other earthquakes in subduction zones but had little success in identifying slablike features due to large scatter in the data. They indicate that slab structures were apparent in the Aleutians, Kurils, and Tonga–Fiji, in addition to the Pacific northwest subduction zone, but noise prevented systematic modeling of these patterns. At the time there were no aspherical earth models or reliable station corrections with which to suppress deep mantle and near-receiver effects, so the limited success in constraining slab structure with early residual sphere approaches is not surprising (more sophisticated approaches are discussed in the next section). Solomon and Butler (1974) examined teleseismic P residuals at Washington and California stations, seeking a slab effect. They found eastward-dipping early arrivals on the west flank of the Sierra Nevada and the California Cascades that could be related to the subducted Juan de Fuca slab, but the evidence was not compelling. Analysis of anomalies at station LON led them

to conclude that any slab feature detected by McKenzie and Julian (1971) does not extend deeper than 200 km.

One of the fundamental obstacles to isolating the near-source slab-associated travel time anomaly in teleseismic signals is the need to suppress the travel time anomalies that accumulate at large distances from the source, as the raypath travels through the heterogeneous mantle and crust beneath the recording stations. Errors in the reference model can produce systematic patterns in residuals which may be misinterpreted as slab effects and which contribute to event mislocation. A standard seismological approach to isolating the near-source contributions is the use of differential travel time anomalies for two observations which differ in raypath primarily near the source. Toksöz *et al.* (1971) introduced the idea of using differential travel time anomalies between P waves recorded at common stations for events at different depths in the slab. They analyzed 13 Tonga events, using deep event patterns to correct the teleseismic times of shallow and intermediate-depth events, which reduced the residuals considerably in size. A fast band of residuals with 1.5–2.0-s advances was observed in residual sphere displays for shallow and intermediate-depth events, which appears to be due to the slab, but this pattern disappeared with depth. This “relative residual technique,” which is similar to modern differential residual sphere methods described in the next section, empirically accounts for all deep mantle and near-receiver effects but does have the danger of eliminating any common pattern that may originate near the source.

Toksöz *et al.* (1971) used thermal models and Julian’s (1970) raytracing approach to explore the bending effects on rays and to compare theoretical and observed residuals, especially in the two-dimensional down-dip orientation. They found that total travel time anomalies for shallow events could be 4 s, with about 2.5 s being due to the slab and 1.5 s due to the slow wedge. They used $dV_p/dT = -0.5 \text{ m/s}/^\circ\text{C}$ in converting from thermal to velocity structure. The data available at the time were quite limited and led to inconclusive results regarding the slab heterogeneity below 500 km.

Another approach to isolating the near-source velocity structure was proposed by Kaila (1969) and has been applied to various subduction zones in a sequence of studies. This method involves determining the linear segment of a travel time versus distance curve for an event at depth in a slab, which will correspond to initially horizontally oriented raypaths. If the travel times are dense enough and have small enough scatter to identify the constant ray parameter segment, and if the depth is well constrained, the constant ray parameter directly reveals the velocity at the source. This provides a method by which the velocity as a function of depth in the slab can be determined, including the depths at which any velocity discontinuities due to phase transitions are located. This procedure has been applied to events in Tonga–Kermadec (Kaila and Krishna, 1978), Japan (Kaila *et*

al., 1971, 1974), Taiwan (Krishna and Kaila, 1984a), and New Guinea (Krishna and Kaila, 1984b). These studies find P and S velocity structures which show monotonically increasing velocities from 40 to 360–400 km depth in each region, with abrupt velocity discontinuities near 400 and 650 km. There is no evidence of an upper mantle low-velocity zone, indicating that the velocities that are inferred are actually those of the slab and not the surrounding mantle. The absolute P velocities appear to vary from slab to slab, with those in the Solomon Islands being 3–6% higher than in Japan but lower than in Tonga, and there are apparent variations in the depths of the discontinuities (360 km in Japan and 600 km in Tonga). The reliability of these models is hard to assess, as every region has very different regional seismic station distributions and the procedure does not include corrections for heterogeneity surrounding the slab.

Following Utsu's (1967) analysis of up-dip travel times to Japan (Section 2.1), Ishida (1970) used travel time anomalies from 410 relocated hypocenters for Japanese events at intermediate and deep depths to estimate that the slab under Japan is 2–3% faster than surrounding mantle. This is among the lower estimates of the slab–wedge contrast. Tada (1972) analyzed P wave travel times from events in the Japan slab at regional stations and used the ray parameter method of Kaila (1969) to arrive at estimates of slab velocity contrast at different depths. He argued that the slab heterogeneity decreases from about 5% near 200 km to 3.5% at 400 to 2.5% at 600 km. The enhanced velocity contrast at shallow depth appears to reflect the unusually low velocity in the wedge above the Japan slab. Analysis of the times from deep earthquakes led Utsu (1975) to estimate an average P velocity contrast between the slab and upper mantle of at least 3%. In southwestern Japan the complex geometry of the overlapping Philippine Sea and Pacific slabs also began to receive study. Shiono (1974) explored up-dip travel time patterns from intermediate-depth events to see the effects of the Philippine Sea plate.

Aoki and Tada (1973) and Hamada (1973) followed the earlier work of Kanamori (1968) in examining travel time patterns across Japan from the 1971 Amchitka Island explosion CANNIKIN. Aoki and Tada inferred that the mantle wedge region is 3 to 5% lower in velocity than the corresponding region in the mantle on the seaward side of the subducting plate on the basis of the travel time variations from east to west across Japan. Hamada used three-dimensional raytracing with a simple slab model to characterize the velocity contrasts on either side of the subducting Pacific plate. He preferred a model in which the 100-km-thick slab was 3% faster than a reference model, while the wedge down to 275 km was 4% slower (for a contrast of 7%) and the seaward mantle was 1% slower than the slab to depths of 350 km.

Engdahl (1973) presented equations for raytracing in a three-dimensional slab structure and applied them to the Aleutian slab. He assumed an 80-km-thick slab

model, 250 km long with 7% fast slab material, and used this model to relocate seismicity. He found a very thin seismic zone, only 10 km thick, consistent with the narrow zones found in other regions (Section 2.1).

The gap between intermediate-depth and deep seismicity in the New Hebrides arc was studied by Pascal *et al.* (1973), using up-dip P and S residuals from deep events. Stations in the New Hebrides record arrivals 3 s early compared to stations in New Caledonia, and the three-dimensional modeling method of Jacob (1970) was used to explore associated slab models. The New Hebrides slab was estimated to be 6% fast from 0 to 300 km and 6% fast near 600 km depth, with the wedge being 4% slow. The events were located with teleseismic observations including pP and pPKP surface reflections to minimize bias. Since the up-dip anomalies are smaller than the 5-s anomalies observed in Tonga by Mitronovas and Isacks (1971), Pascal *et al.* (1973) concluded that the New Hebrides deep earthquake activity is in a detached, nearly horizontal zone. Barazangi *et al.* (1973, 1974) presented evidence that the gap in the seismicity is a region of strong attenuation, supporting this idea.

Veith (1974, 1975) developed an earthquake location procedure including parameterization of systematic spatially varying source and station effects, which he applied to more than 200 earthquakes at depths from 10 to 650 km in the Kuril slab region. Data from 25 nearby and 149 distant stations were used, with slowly varying systematic trends in station and source terms along the arc being allowed for. His results show 6–7-s arrival time variations due to the plate and wedge heterogeneity. Surface phases pP and sP were used to help constrain the depths. The parameterized source and station terms were then used to locate more than 3000 events in the slab. Up-dip travel time anomalies of –5 s to Kamchatka and Kuril Island stations were modeled using the method of Sorrells *et al.* (1971). Veith estimated that the slab is 10% fast from 100 to 300 km and about 4% fast at 650 km. Raytracing estimates of the epicentral bias due to the slab heterogeneity indicated that epicenters can be in error by 60 km for events 50 km deep, 5–45 km for events 150 km deep, 25 km for 300-km-deep events, 10 km for 500-km-deep events, and 5 km for 600-km-deep events. Depth biases can be 30 km too shallow for 600-km-deep events (if regional data are included) and 5 km too deep for events at 50 km depth. Veith also observed a double Benioff zone, with the upper plane having down-dip compressional events and the deeper plane having down-dip tensional events (see Section 5.1).

A master earthquake relative location method was applied to deep events in Fiji, Peru–Brazil, and Tonga by Fitch (1975, 1977). He used P and pP phases and parameterized the relative locations to explicitly include the near-source absolute velocity, in an attempt to determine the *in situ* structure. The choice of near-source velocity affects the takeoff angles, particularly for stations with nearly horizontal takeoff angles, so there is a strong dependence of the raypath on the model. Fitch attempted to solve this problem by dividing the raypaths into

two groups, including paths greater than a cutoff distance which had constrained ray geometry and those within the cutoff distance (20–30° for deep events) for which the geometry was included in the inversion. He obtained estimates of near-source P velocity structure of 10.7–11.4 km/s in the different deep zones, which is 5–10% fast relative to typical reference models at depths from 540 to 660 km.

Solomon and U (1975) used the down-dip travel time residuals at stations CAN, CTA, PMG, and BRS for events at different depths in the Tonga slab to infer near-source velocity anomalies. ISC data and locations for 475 events in the depth range 70–650 km were used, with the mean residuals showing a (negative) peak near 250–350 km depth. Solomon and U advanced the interpretation that the particularly high velocities in this range result from elevation of the olivine– β spinel phase transition by about 100 km in the cold slab, and they inferred a 1000°C contrast between the slab and normal mantle at 250 km depth. A careful consideration of possible biases due to defocusing or mislocation effects did not provide an alternative interpretation. They did not find any evidence for the high-velocity material reported from 540 to 600 km in the Tonga slab by Fitch (1975). Fitch (1977) extended his analysis and estimated that in Tonga the slab is 10% fast deeper than 600 km, but not fast from 500 to 580 km depth. He interpreted this in terms of an elevated postspinel phase transition (the sign of the Clapeyron slope was not yet well established to be negative) or 1000°C thermal heterogeneity and inferred that the slab penetrates about 100 km below the deepest events. This method is apparently not very sensitive to the reference model or the master event depth, but the nonlinear sensitivity of the raypaths to the structure appears to be a problem.

While seeking temporal patterns in station anomalies, Engdahl (1975) examined relative time residuals between Aleutian and Alaskan stations recording deep Fiji–Tonga events, finding the presence of strong near-source anomalies. He observed 2-s differences in station anomalies over a 12° azimuthal range and 17° distance range, persisting to source depths of 600–700 km. He inferred the presence of 10% velocity contrasts near the source down to depths below 600 km in the Tonga slab.

Studies of the seismicity and slab structure in the central Aleutians were conducted by Engdahl (1973), Engdahl *et al.* (1977), and Engdahl (1977), using data from the Amchitka network. Thermal slab models were used along with seismic raytracing to explore the slab effects. The absolute position of the thermal slab model was controlled using LONGSHOT travel time and amplitude patterns, and the model was used to relocate the regional seismicity. This yielded a thin, 10–20-km-thick seismic zone, with locations found using the slab model and only local data shifting by 20 km north and 20 km shallower than routine teleseismic locations. The local locations also indicated a sharp change in dip of the seismic zone near 100 km depth, in contrast to teleseismic locations, which was to persist as a controversy for several years.

Robinson (1976) analyzed relative travel times from Tonga-Kermadec events recorded at stations across New Zealand, which vary by 2.5 s, to infer that up to 11% velocity anomalies exist in the New Zealand slab at depths from 0 to 400 km. Adams and Ware (1977) obtained similar estimates of the slab anomaly for New Zealand. Joint hypocentral determinations for deep events in Tonga were used to provide accurate relative locations, with relative travel time patterns indicating -3.3 -s P anomalies up-dip to station NIU (Sondergeld *et al.*, 1977). Sondergeld *et al.* (1977) reported that they examined residual spheres to look for deep velocity anomalies in Tonga, expanding the data set of Toksöz *et al.* (1971), but were unable to find convincing evidence for near-source anomalies below 300 km depth due to large scatter and poor coverage. They concluded that if any deep near-source anomaly is there it must be weak.

Thermal models were used by Engdahl *et al.* (1977) in raytracing analyses of the Kuril, Aleutian, and Alaskan slabs, with the raypath refractions being examined to see how takeoff angle perturbations bias focal mechanisms. Slab velocity models were computed using the relatively high value of $dV_p/dT = -0.9$ m/s/ $^{\circ}$ C from Sleep (1973), which predicts 8–10% slab velocity anomalies. The procedure involved a two-dimensional grid with cylindrical symmetry, to account for the slab shape. Local data from Amchitka and Alaskan networks and WWSSN and bulletin times were used. Analysis of 39 intermediate-depth events in the central Aleutians was performed, with relocation in the slab model using the regional and teleseismic data. The calculations of Jacob (1972) and Sleep (1973) were used to position the slab. A thin zone of seismicity near the top of the slab was found, with composite focal mechanisms revealing compressional and along-strike tensional mechanisms rather than the expected down-dip tensional solutions. Relocation of seven events under Alaska also showed that the seismicity is located near the top of the slab velocity anomaly. Consideration of ray bending effects for five events showed that shallow thrust event focal mechanisms are hardly affected by perturbation of the takeoff angles because the steep seaward takeoff angles which usually constrain one nodal plane are not affected much by the slab.

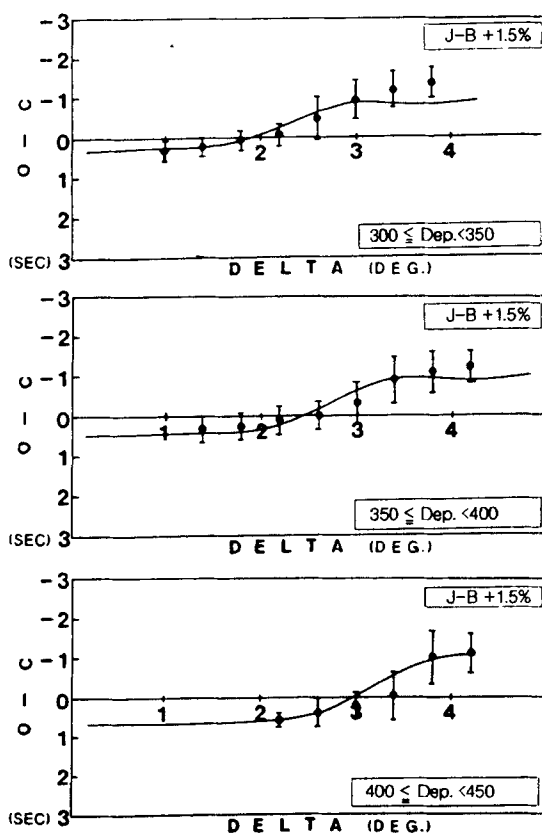
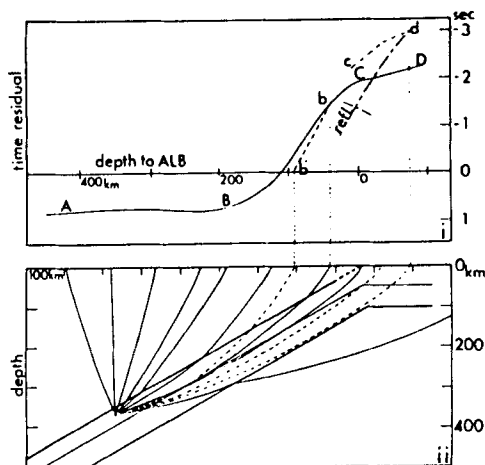
Efforts have also been made to use relative times to constrain structure on the oceanward side of the Japan and Kuril plates. Nagumo *et al.* (1970) placed an OBS seaward of the Japan trench and inferred from travel time anomalies that the P and S velocities of the slab are 8–12% higher than under the Japan Islands. Subsequently, Kasahara and Harvey (1977) deployed an OBS seaward of Hokkaido to examine travel time patterns oceanward of the Kuril trench. For seven earthquakes located by the USGS, of which five are in the Kuril slab, they observed high velocities in the slab, exceeding 8.5 km/s for P and 4.8 km/s for S in the upper 230 km of the slab. In some cases the velocities in the slab can be as high as 8.65–8.97 km/s in the range 50–230 km. Two deep events in Izu were used to obtain paths that dive under the slab. They estimated that the as-

thenosphere on the Pacific side of the slab is 3% slower than J-B to 390 km, while the upper limit for average velocities of the oceanic mantle is 8.4 km/s for P and 4.7 km/s for S above 390 km. These velocities are higher than those reported by Nagumo *et al.* (1970) or Nagamune (1973). Fukao (1977) analyzed $dT/d\Delta$ measurements in Japan from 69 Kuril events at distances from 13 to 30° to determine a velocity model down to 800 km depth below the oceanward side of the Kuril arc. He found a high-velocity lid extending to a depth of 85 km, a moderate low-velocity zone with velocities only decreasing to 8.1 km/s, and a high-velocity gradient from 165 to 200 km. This is consistent with the absence of strong velocity contrasts on the seaward side of the slab.

In the travel time study of Suyehiro and Sacks (1979) two-dimensional up-dip raytracing with a dipping slab was performed assuming that the seismicity is located about 20 km below the boundary between the slab and asthenosphere based on work by Yamamizu (1973). Patterns of P and S travel time residuals versus depth of the upper plate boundary were used to constrain the slab dip and velocity model. The P wave travel times have a smooth pattern varying by 2.5 s, while the S waves vary by 5 s with the same simple pattern. Single-layer slab models gave velocity anomalies of 5% for P and 9% for S. A two-layer slab model was proposed, motivated in part by the shallow oceanic lithospheric model of Shimamura and Asada (1976), obtained by wide-angle reflections and refractions. Suyehiro and Sacks (1979) found that the upper 40–50 km of the slab was 1% slower than the lower portion, with the overall contrast relative to the wedge being $5 \pm 1\%$ for P velocity and $7 \pm 2\%$ for S velocity. This study was extended by Iidaka and Mizoue (1991), using 26 deep events from 314 to 433 km deep with locations from the JMA. They also performed two-dimensional raytracing to model patterns of up-dip travel times and favor a two-layer slab model 1.5% fast (relative to the J-B model) in the upper layer and 2.5% fast in the lower layer, with –3% slow velocity in the wedge and below the slab. The upper layer is 30 km wide and the overall slab is 100 km thick (Fig. 13.).

Suyehiro and Sacks (1978, 1983) found evidence in P wave times from deep earthquakes in the Kuril and Japan slabs for a low-velocity region above the slab below 300 km, with 5–10% low velocity, possibly correlated with the low-Q region reported by Sacks and Okada (1974) (Section 2.3). The 1983 study used events deeper than 200 km reported in the ISC bulletin from 1964 to 1976. Using the ISC anomalies, they compared the travel times with a subducted slab model and a 3% slow asthenosphere. They note that such a low-velocity region can influence travel times from deep events as well as estimates of slab anomalies. This feature does not show up in recent tomographic images like those of Fukao *et al.* (1992) (Section 4).

The issue of slab effects on earthquake locations was explored further by Barazangi and Isacks (1979), who compared ISC and USGS locations with those



of local networks in Japan and the Aleutians. Overall, they found no substantial bias or distortion for events in Japan deeper than 50 km, mainly because the shallow-dipping slab does not have much effect for teleseismic signals. For the steeply dipping Aleutian slab they found 50 km northward mislocations of the events relative to the local solutions, consistent with the results of Jacob (1972) and Davies and Julian (1971), but Barazangi and Isacks (1979) argue that the teleseismic locations are actually closer to the absolute positions. This is because of the strong effect of the slab on local locations for the Adak region, based on the results of Engdahl (1973) and Engdahl *et al.* (1977), who showed that the Benioff zone is displaced northward by up to 30 km and is less steep when slab effects are accounted for.

Differential times between P, S, PcP, ScS, and ScP for deep Tonga events were analyzed by Frohlich and Barazangi (1980) in an attempt to isolate upper and lower mantle source and receiver side contributions. They used recordings at distances less than 60° in Fiji, New Caledonia, and Australia. Differential times reduced origin time and near-receiver effects, but the nature of the data precluded locating the anomalous material. For example, the P times on the near-source leg were consistent with 10% slab anomalies extending to 1000 km or with 1% anomalies over the entire path. Differences between S and P times on down-going (ScP–PcP) and up-going (ScS–ScP) legs were combined with S–P anomalies to try to account for receiver effects. Down-going rays at a low angle to the plate show large positive S–P residuals, and overall the S wave times indicate no anomaly over the path segments where P is fast. This is very puzzling, as any slab thermal effect would be expected to produce a correlation in P and S times, and it appears that no slab feature was isolated.

Bock (1981) analyzed travel times of P waves at the Warramunga seismic array in Australia from 49 earthquakes in the Tonga slab with depths from 42 to 679 km. This array is fortuitously located such that P waves from shallow Tonga slab events travel down the slab dip on the path to the array. Bock's procedure was similar to that of Toksöz *et al.* (1971) and Solomon and U (1975), but source depth control was provided by pP observations at the array. Locations of the events were determined after removing stations at distances that appear to be strongly influenced by slab structure, following the suggestion of Mitronovas and Isacks (1971). This involved identifying distance and azimuthal ranges in

Fig. 13. Geometry of the up-dip relative travel time analysis in the Japan slab by Suyehiro and Sacks (1979) and Iidaka and Mizoue (1991). The two upper panels show expected travel time anomalies and corresponding raypaths for an idealized two-layered slab model. Reflection arrival times from slab boundaries are shown by the dotted lines. The lower three panels show the fit to observed data from events at different source depths in the Japan slab for the models of Iidaka and Mizoue (1991) described in the text. Reprinted with permission from Suyehiro and Sacks (1979) and Iidaka and Mizoue (1991).

which the anomalies vary strongly with source depth. Bock found that the Warramunga travel time anomalies are more negative (early arrivals) for events with depths from 40 to 260 km than for events below 400 km depth, by 1.5–2.3 s. There is no significant variation with depth from 400 to 670 km. Data between 250 and 350 km depth are sparse, so he could not look for an elevated olivine- β spinel phase transformation in the slab. Using differential residual times between shallower and deeper events and assuming that the location of the anomaly is in the intervening inclined seismic zone, an estimated slab velocity contrast of 5–6% above 400 km was derived, along with an estimate of $1000 \pm 450^\circ$ temperature contrast relative to normal mantle. For this slab velocity contrast estimate, the deeper event in each differential pair was located from 350 to 400 km. If the deeper event is as deep as 680 km the total slab anomaly is estimated as 2–3%, assuming that the raypath from the shallow events remains completely within the slab. The lack of variation of anomalies at depths from 400 to 680 km requires that the raypaths exit the slab rather quickly or have common path lengths in the slab (requiring a lower mantle extension of the slab below the deepest events) over this depth range or that the slab velocity anomaly is very reduced at these depths. Steepening of the slab dip could affect the interpretation, and the neglect of raypath perturbations due to the slab heterogeneity may also bias the velocity estimates.

Huppert and Frohlich (1981) analyzed travel time anomalies along strike of the Tonga slab, finding up to 12 s fast arrivals at AFI and RAO (Raoul Island). They analyzed 39 events with depths of 70–300 km at distances up to 1200 km. To constrain the locations they reread P times at 11 stations and, together with pP-P times, performed joint hypocentral determinations. Using a modified version of Jacob's (1970) raytracing, they modeled the data with an 8% fast uniform slab model or a layered model with a 27-km-thick 6% fast upper layer, a 14-km-thick transition, and a 69-km-thick 9% fast lower layer. They attributed the velocity contrast to a 700° temperature contrast, with combined effects of the slab and wedge thermal structure. A differential anomaly method, using observations at the teleseismic station ALQ, was used to desensitize the analysis to origin time and location errors, yielding a 5% fast slab in the upper 300 km. Multiple arrivals and a small precursor at AFI were interpreted as effects of internal reflections in the slab. (Further analyses of the along-strike precursors in the Tonga slab are discussed in Section 2.2.)

An attempt to develop a systematic correction procedure for slab effects to use in earthquake location procedures was made by Fujita *et al.* (1981). They used raytracing in thermal models to compare observed and predicted anomalies for the central Aleutians, finding that slab corrections reduce mislocations between teleseismic and local solutions to about 20 km and the addition of empirical station corrections reduces this to 10–15 km. They assumed $dV_p/dT = -0.9$ m/s/ $^\circ$ C in mapping thermal models into velocity structures, and by modeling

residuals as a function of distance to the arc pole they estimated a 300-km-deep slab model. By making many raytracing calculations, they developed smoothly varying source corrections as a function of distance and azimuth from the source, along with station corrections based on local network source locations.

Raytracing by Frohlich *et al.* (1982) and McLaren and Frohlich (1985) demonstrated that local event locations of main thrust zone activity in the Aleutians are quite reliable, but slab effects cause local estimates of outer rise locations to be poor. Engdahl *et al.* (1972) pursued the comparison of local and teleseismic locations in the central Aleutians. They argued that the amount of mislocation depends on the position in the arc and the data coverage, with locally determined locations for intermediate-depth events being biased up-dip and teleseismic locations biased downward by up to 50 km. They compared earthquake locations in thermal models with Joint Hypocentral Determination (JHD) locations for shallow thrust events, concluding that slab models are not well enough known to locate accurately without including some local data. One effect of neglecting slab structure is an apparent increase in dip of the seismic zone below 50 km. They also compared the JHD locations with locations obtained using the smoothly varying source terms developed by Fujita *et al.* (1981), with the local solutions as a reference. Teleseismic location accuracy with a slab model can be quite good if station corrections are calibrated using local solutions.

A method of simultaneous inversion for the position of the slab structure and earthquake locations introduced by Spencer and Gubbins (1980) was applied to Aleutians data by Spencer and Engdahl (1983). The slab fitting was performed using 205 intermediate-depth events from 1974 to 1977. The slab geometry was assumed *a priori*, with the inversion used to shift the slab position from an initial position given by Sleep (1973), without actual raytracing. Then the slab velocity anomaly was estimated at 7–8% fast for a length of 300–400 km, and the velocity model was used to relocate locally recorded events, which reduced the dip of the intermediate zone, bringing the local and teleseismic locations into improved agreement. Subsequently, Hauksson (1985) used three-dimensional raytracing to relocate local earthquakes near the Shumagin Islands. Nieman *et al.* (1986) performed additional three-dimensional raytracing in Aleutian slab models, using varying thermal coefficients and depth of penetration of the slab. Based on comparisons of teleseismic locations with a slab model and the local locations, they preferred a short slab, extending to 360 km depth, with a maximum velocity anomaly of 10% and an average velocity anomaly of 6%, but could match the data with a slab extending to 600 km depth with lower anomalies. Little mislocation was found for events deeper than 100 km in the slab.

Roecker (1985) extended the near-source velocity inversion procedure of Fitch (1975), merging it with an *a priori* slab model similar to that of Spencer and Gubbins (1980). This procedure uses arrival time differences to determine *in situ* slab velocity and hypocentral relative locations. An approximate raypath scheme

was used, its validity being confirmed by raytracing. This was applied to 200–600-km-deep events in the Izu slab, where dense travel time measurements were available from Japanese stations. Clusters of events within ± 100 km along strike of a master event were relocated. Using data from stations in central and southwestern Honshu, progressive inversions with parameter separation were performed beginning with specified slab velocity anomalies and a 100-km-wide slab. Seven master events were used in the depth range 300–400 km and five in the range 400–500 km, with an attempt being made to detect any elevation of the α - β phase transition in the slab. There was slight sensitivity to the positioning of the master event in the slab, as well as to slab dip. For events from 27 to 31°N the P velocity from 400 to 500 km is 4–6% higher in the slab. North of 32.5°N the slab was 3–4% fast in the range 180–375 km, while south of 32.5°N the slab was 7–10% fast from 325 to 375 km and 6–7% fast from 375 to 410 km. Roecker suggests that 50-km elevation of the phase transition may occur toward the southern region. It is not clear why it would differ in the north.

Travel times from deep Izu events were further analyzed by Okino *et al.* (1989), in a study of an isolated deep event in July 1982 at 545 km depth. This event is located 200 km west of the seismic zone (Fig. 14), suggesting that the slab is deflected horizontally. Travel time patterns across southwest Japan were modeled to test whether there is any evidence for a horizontal slab. Travel times from two events in the main seismogenic zone of the slab north and south of the unusual event were used to construct differential residual patterns. Three-dimensional raytracing was used to test whether a horizontal high-velocity region is present near the isolated event, assuming a 3.5% fast slab with a -1.5% slow wedge. Because of different path lengths in the slab structure from each source, a better fit was achieved for the horizontal slab model.

Travel time patterns observed in Japan for paths along the strike of the Izu arc

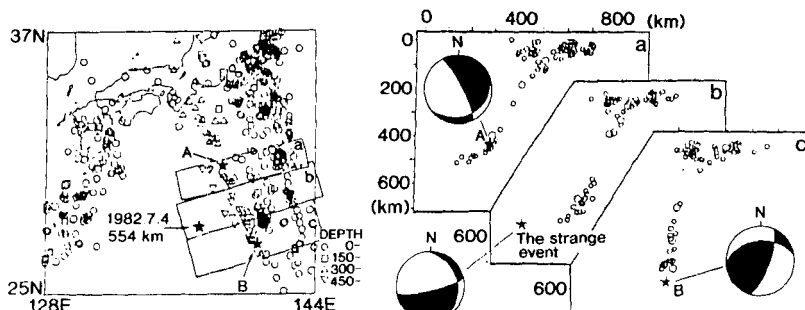


Fig. 14. Example of a rare, isolated deep-focus earthquake. The July 4, 1982 event occurred at a depth of 534 km, offset about 200 km west from the primary zone of deep activity associated with subduction of the Izu (Pacific) slab. Reprinted with permission from Okino *et al.* (1989).

have been analyzed by Iidaka *et al.* (1989a, 1992). In the first of these studies, Iidaka *et al.* (1989a) analyzed seven earthquakes 300–600 km deep recorded by stations in the Kanto region. Holding the locations fixed to the ISC determinations, they modeled the patterns of relative times across Kanto, with corrections for crustal structure and effects of the Philippine Sea and Pacific slabs which underlie Kanto. A slab model was obtained by three-dimensional raytracing, with a rapid increase in velocity in the upper few tens of kilometers in the slab, followed by a gradual decrease. The surrounding mantle was given a −3% velocity anomaly, while the maximum slab anomaly was +3%. The patterns of residuals were found not to be too sensitive to source mislocation. The stronger gradient near the surface of the slab was associated with the stronger thermal gradient expected there. This modeling was extended by Iidaka *et al.* (1992) using data from 19 events. They incorporated a two-layer slab model, following Suyehiro and Sacks (1979), and modeled 2-s patterns of P residuals across stations in the Tokai and Kanto regions. Their three-dimensional raytracing indicates that with the wedge being held at −3% slow velocity, the upper layer of the slab is 1.5–3.5% fast over a 40-km-thick region, with the lower half of the slab having lower velocity gradients and smoothly diminishing velocity, and the oceanside mantle must be at least 3% slower than the peak velocity in the slab (Fig. 15).

Ohtaki and Kaneshima (1994) examined deep events in the southernmost Izu slab, using three-dimensional raytracing to obtain a model in which these events lie within high-velocity material. With the evidence from Okino *et al.* (1989) for flat lying slab further to the north, they concluded that the Izu slab continuously distorts from flatlying to steeply dipping along the arc. This is supported by residual sphere studies (Creager, 1984) as well as tomographic inversions (van der Hilst and Seno, 1993).

Deployment of four mobile stations in Tonga in 1981–1982 and 1984 provided up-dip travel times from intermediate- and deep-focus events analyzed by Bock (1987). He used JHD locations of groups of events with master events located only by teleseismic data to minimize the slab effect on the locations. Of course, any deep aseismic slab structure could still bias the source parameters. pP observations from the ISC were used to constrain the depths, and then three-dimensional raytracing using the methods of Julian and Gubbins (1977) was used to constrain the slab heterogeneity. This is probably the most comprehensive up-going raytracing effort to date, with a number of slab velocity distributions being considered and slab geometry being varied. However, the results are somewhat ambiguous. Velocities up to 8% fast were found for models with the velocity varying across the slab, and uniform-velocity models are 6–7% fast. The data are equally well fit if the velocity anomaly decreases below a depth of 400 km, so there was no resolution of the velocity anomaly in the transition zone.

Prasad and Bock (1987) compared signals from shallow Tonga events re-

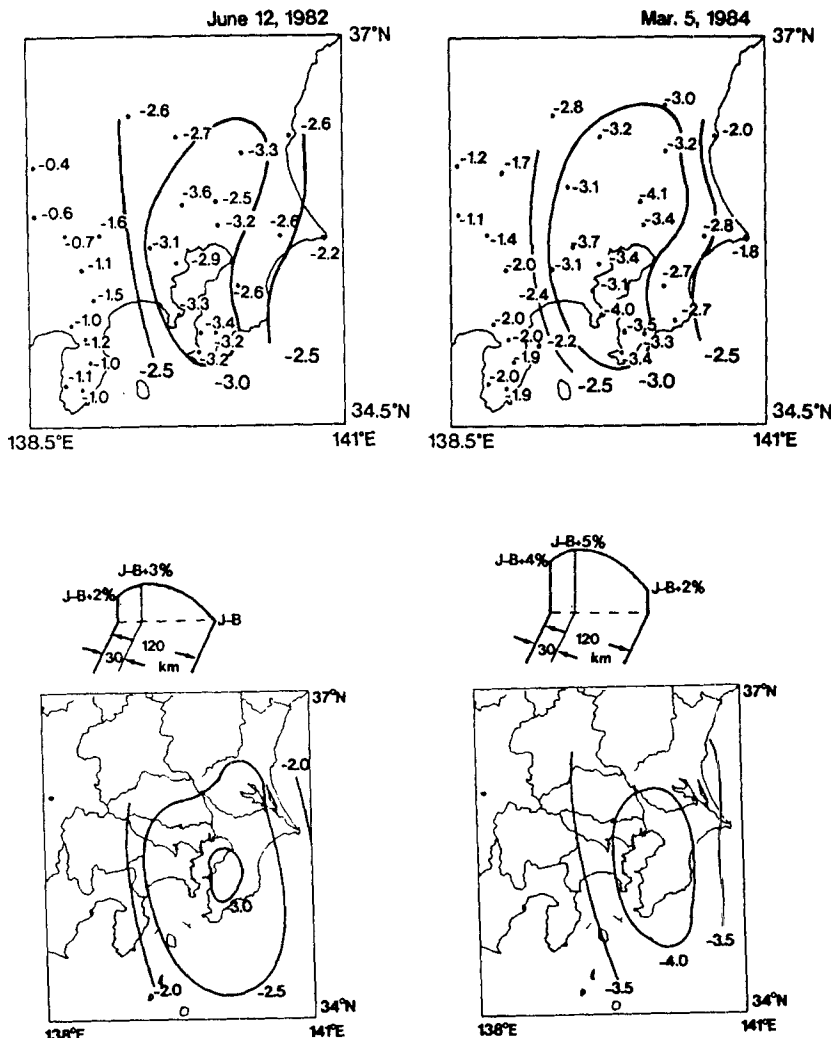


Fig. 15. Comparison of observed travel time patterns across southeastern Honshu from events in the Izu slab (top) with slab models and theoretical travel time patterns for the models of Iidaka *et al.* (1992) described in the text. Reprinted with permission from Iidaka *et al.* (1992).

corded at stations RAR and NUE (Niue). NUE lies much closer to the trench than RAR and thus has a more pronounced along-strike path for most Tonga events. Relative to the diving raypath observations at RAR, early P anomalies of -10 s are found at NUE for shallow events, but for depths greater than 100 km the anomaly suddenly decreases rapidly, to about -2.5 s at 200 km depth. This

suggests that the oceanic lithosphere has a base near 100 km. Analysis of ISC times for 105 events from the surface to 644 km shows that NUE records early times for events down to 300 km. Three-dimensional raytracing indicates that at least a 90-km-thick high-velocity region is needed to match the times from 15 relocated events. A thin lithospheric lid, as proposed by Anderson and Regan (1983), appears to be less consistent with the data.

A deployment of nine OBS stations in the Lau Basin and station VAV on Tonga Island provided recordings of 2 intermediate and 10 deep-focus events analyzed by Bock *et al.* (1991). These were used to measure the contrast in P velocity between the slab and the wedge. No S waves were observed at the OBS stations. The events were relocated relative to those studied in Bock (1987), yielding depths 14 ± 15 km deeper than the ISC. Using three-dimensional raytracing to account for the slab path to VAV and to the OBS stations, the P velocity in the slab was estimated to be $7 \pm 2\%$ higher in the depth range 0–400 km.

The New Hebrides slab may have a gap in it, revealed by seismicity and seismic wave propagation. Pascal *et al.* (1978) performed JHD of events from 1962 to 1973 showing that there is an uncontorted zone of intermediate-depth seismicity about 20 km thick for 700 km along the strike of the arc, with one central gap in activity from 50 to 150 km. Grasso *et al.* (1983) and Prévôt *et al.* (1991) find that the aseismic region has relatively slow velocities, and Marthelot *et al.* (1985) show that it has strong attenuation. Chatelain *et al.* (1992) further explore the seismicity gap, finding that no S waves traverse the gap. They argue that localized detachment of the slab occurred within the last 1 My, causing uplift of some of the central New Hebrides Islands.

Relative travel time patterns have also been used to study deep lower mantle heterogeneities which may be related to subducting slabs. Jordan and Lynn (1974) analyzed ScS–S and PcP–P differential travel times from two deep Peruvian earthquakes recorded at North American stations. A localized (15°) azimuthal anomaly ranging over 1.5 s for PcP–P and 5 s for ScS–S anomalies was detected and inferred to result from a high-velocity region in the mantle under the Caribbean. The velocity anomalies were estimated as about 1%, with the relative perturbation of P and S velocity being the same, based on the ratio of P and S anomalies. It appears that the direct P and S waves are responsible for the anomaly, because their travel times correlate with the differential times, whereas the core reflection travel times do not. This indicates that the anomaly is from 600 to 1400 km deep and about 500 km broad. Jordan (1975) suggested that this deep Caribbean anomaly is a deep mantle expression of subducted slab. He related the heterogeneity to multipathing of signals from a Colombian event recorded at LASA and array mislocations of Mexican events by NORSAR.

Lay (1983) analyzed a greatly expanded data set of ScS–S differential travel times recorded in North America from deep earthquakes in Peru, Bolivia, Argen-

tina, and the Sea of Okhotsk. The Caribbean anomaly was shown to extend from at least 1000 km to about 1900 km depth. Other deep heterogeneities were also detected, one being a low-velocity region from 1700 to 2700 km below Brazil, which produces up to 4-s S wave anomalies and 30–100% amplitude enhancements for long-period S waves resulting from the approximately 2% heterogeneity. A broad region of fast shear velocity structure below 2000 km under the western United States was also inferred from the differential travel times. These studies of localized travel time patterns have gained confidence by the similarity of features in tomographic images. For example, Grand (1987) finds a high-velocity tabular structure extending from 600 to 1000 km under the south-central United States, and from 750 to 1900 km under the Caribbean, which closely corresponds to the early results. He associates this feature with the subducted remains of the Farallon plate. More recent tomographic models (Steve Grand, personal communication, 1992) show low velocities under Brazil from 2000 to 2500 km and a broad region of fast material near the base of the mantle under Central and North America, generally consistent with the results of Lay (1983). These models also show high-velocity material from 600 to 1300 km directly below the deep earthquake zone in Peru. Bokelmann and Silver (1993) observed travel time variations of 3 s for P waves and 8 s for S waves across a 1500-km-long seismic line, for paths sampling the Caribbean anomaly. They infer that the western edge of the anomaly has a gradient about 300 km wide. The relative velocity ratio for the anomaly is estimated as $\delta \ln V_s / \delta \ln V_p = 1.7$. Some evidence for multipathing of the S waves traversing the structure was also found.

3.2. Residual Sphere Modeling

The residual sphere display introduced by Davies and McKenzie (1969) not only is a convenient display of three-dimensional travel time anomalies but also, as they pointed out, is a natural representation for considering earthquake location effects in terms of spherical harmonics of the residual pattern. The origin time is found by eliminating the zeroth-degree, or mean anomaly over the entire data set, while the location is found by eliminating the first-degree harmonic. An important problem for residual sphere modeling is that a tabular slab structure can impart travel time patterns with a substantial degree 1 harmonic as well as a moderate degree 0 harmonic, and these components will not be retained in the residual sphere (Fig. 16). The magnitude of such “lost” components depends strongly on the slab geometry and its sampling by the raypaths. This effect can be mitigated, but not avoided, by attaining as complete coverage of the residual sphere as possible. Removing the degree 0 and 1 terms usually substantially modifies the pattern of relative anomalies in the residual sphere, and in the case of sparse raypath coverage strong “far-side” effects can result, with the location

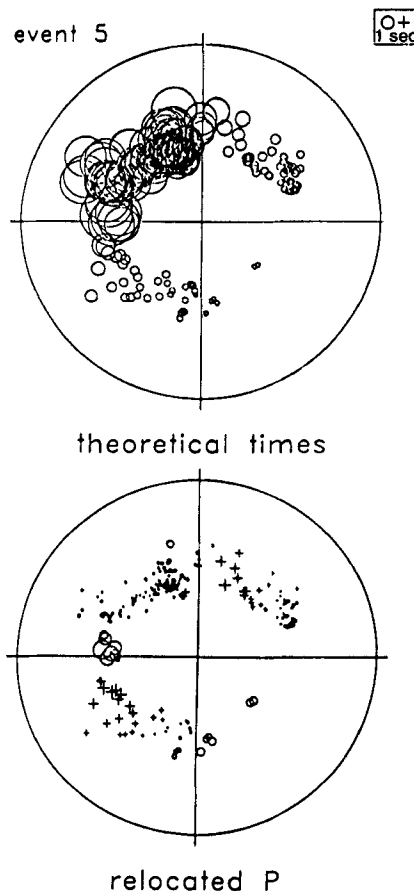


Fig. 16. Residual sphere projections of theoretical travel time anomalies at teleseismic stations for a model with a slab dipping about 50° toward the northwest. The upper plot shows the total travel time anomalies for each path, which are all negative due to the presence of fast material in the slab. Larger anomalies correspond to longer paths in the slab. The plot below shows the pattern as it might actually be observed with the effects of locating the earthquake being removed. The residuals now have zero mean, and much of the strong degree 1 pattern induced by the moderately dipping slab has been suppressed. The lower plot is typical of data that would be modeled by residual sphere analysis, and clearly the pattern caused by the slab is obscured from what would be measured were the position of the source independently known (top). From Ken Creager, personal communication (1991).

process producing large anomalies where there had been none in sparsely sampled regions of the focal sphere. Again, the key to reducing this is increasing coverage of the sphere and explicitly accounting for the effect in any modeling effort.

Several early studies of residual sphere patterns were mentioned in the previ-

ous section, but the first effort to model comprehensively a residual sphere anomaly pattern was conducted by Jordan (1977). He analyzed the deep-focus event of January 29, 1971 in the Kuril slab, using S waves. S waves have three to four times larger travel time anomalies than P waves and thus should have higher signal-to-noise ratio and greater sensitivity to slab velocity structure. A total of 142 hand-measured teleseismic S and ScS arrival times from primarily short-period WWSSN recordings were used, with teleseismic station corrections being applied. Some efforts were made to pick SH arrivals, to avoid S to P conversions at the receiver. The source location from Veith (1974) based on P wave times and spatially varying source to receiver corrections was assumed. The resulting S wave J-B residuals show a smoothly varying pattern of anomalies, ranging more than 10 s over the limited portion of the focal sphere spanned by the down-going data. No relocation was performed, which implicitly assumes perfect compatibility of the P and S travel time variations, but the pattern of S wave anomalies, with a dominant degree 2 azimuthal term, is such that relocation would not have a large effect (as later demonstrated for this event by Creager and Jordan, 1984). A complicated smoothing and interpolation algorithm was developed to isolate the near-source contribution from the path and station anomalies, which results in a saddle-shaped pattern with early arrivals along the strike of the slab. An approximate raytracing method neglecting ray bending was used to predict anomaly patterns for slab structures extending below the 540-km-deep source. A 100-km-thick slab model with uniform 5% fast velocities and an 85% dip extending to 1000 km depth can match the saddle-shaped anomaly. Slight asymmetry of the observed residual pattern to the NE versus the SW was attributed to along-strike truncation of the slab toward the NE.

Residual sphere modeling for P waves was pursued by Creager and Jordan (1984), who analyzed 14 intermediate- and deep-focus events in the northwest Pacific, using 4040 ISC Bulletin times for teleseismic P and PKIKP arrivals. In this study, preliminary versions of station corrections from Dziewonski and Anderson (1983) were used, depth-dependent ellipticity corrections (Dziewonski and Gilbert, 1976) were made, and the events were relocated using the down-going phases and the Herrin (1968) travel time tables. Relocations relative to the ISC locations involved 0.9- to 8.4-s origin time shifts, -8 to +65 km depth shifts, and less than 10-km epicentral shifts. The exclusion of up-going arrivals, used in the ISC locations, is largely responsible for the large relocation effects. The motivation for restricting the data to a narrow cone of down-going raypaths was to avoid complications of upper mantle triplications and complex structure of the shallow slab and wedge regions. Relocation was accomplished by applying an operator to the observed residuals that annihilates the subspace that can be contaminated by event location, with the same operator being applied to the synthetic travel times. No corrections for lower mantle structure were applied, because while the model of Dziewonski (1984) was shown to predict up to 1-s

variations, most corrections would be less than 0.25 s. A smoothing procedure similar to that of Jordan (1977) was applied to enhance the slowly varying (presumably near-source) anomaly pattern, with the large scatter in the ISC P wave data giving much greater influence to the smoothing operation than in the initial S wave study. For the six deep Kuril events an NE–SW trough of negative anomalies was found, with orientation consistent with the strike and dip of the steeply dipping slab, with smoothed anomalies ranging over 1.5 s. For shallow Kuril events early times are observed at shallower angles toward the northwest, whereas a shallow event in the Kormandorski Islands showed fairly little pattern, suggesting that deep mantle effects are not responsible for any long-wavelength pattern for events in this region. For the January 29, 1971 event the ratio of S to P anomaly patterns was found to be 3.5:1, similar to that found for lower mantle differential times by Jordan and Lynn (1974) and Lay (1983).

Creager and Jordan (1984) modeled the P wave residual spheres by using kinematic thermal slab models, based on the codes of Minear and Toksöz (1970a) and Sleep (1973), and used $dV_p/dT = -0.9 \text{ m/s/}^\circ\text{C}$ to convert to velocity models. Effects of shear strain heating were ignored, giving rise to models with strong thermal heterogeneity persisting to large depths. Three-dimensional raytracing was used to calculate travel times for P wave raypaths corresponding to actual data sampling, anomalies relative to a homogeneous model were computed, the pattern of residuals was relocated, and the smoothing operation was applied. Relocation of the theoretical times ensures that any patterns in the observed anomalies associated with relocation are mimicked in the model, which of course is the case only if the model is correct. Relocation was also found to reduce sensitivity to positioning of the event within the slab model, and the sources were assumed to be in the coldest part of the slab. Comparisons with the smoothed data for deep events, with good matches being obtained, led to the conclusion that the Kuril slab must penetrate to 900–1000 km, with a dip of 75°. Ray refraction precludes assessment of whether the slab extends deeper. Modeling of intermediate-depth residual spheres with a 55° dipping slab provides fair fits to the data, with significant differences in the residual spheres relative to the deep events being accounted for by the difference in ray geometry and dip of the slab. Modeling of two deep events in the Sea of Japan suggested a 60° dip of the slab extending to greater than 800 km. The P velocity heterogeneity predicted by these models is very strong, with a 10% fast slab at 500–600 km, 9% at 800 km, and 6% at 1200 km. However, it appears that the raytracing calculations in this paper were in error, with the velocity heterogeneity being overpredicted by more than a factor of 2 (e.g. Anderson, 1987b).

Creager (1984) and Creager and Jordan (1986) explored subduction zones in the northwest Pacific and Marianas and used empirical comparisons of intermediate- and deep-focus events to estimate the value of dV_p/dT in the slabs as –0.4 to –0.6 m/s/°C, which was used in their residual sphere modeling. This

lower value of the temperature derivative largely compensates for the errors in raytracing in the work of Creager and Jordan (1984), and basically similar models with reduced velocity heterogeneity were proposed by Creager and Jordan (1986). In the latter study corrections were made for the lower mantle aspherical P velocity model L02.56 of Dziewonski (1984), because this model predicts P anomalies of up to 2 s for the Marianas source region. In the vertically dipping Marianas slab residual spheres for events from 149 to 572 km depth were considered (Fig. 17). The anomaly patterns decrease in magnitude with depth, largely

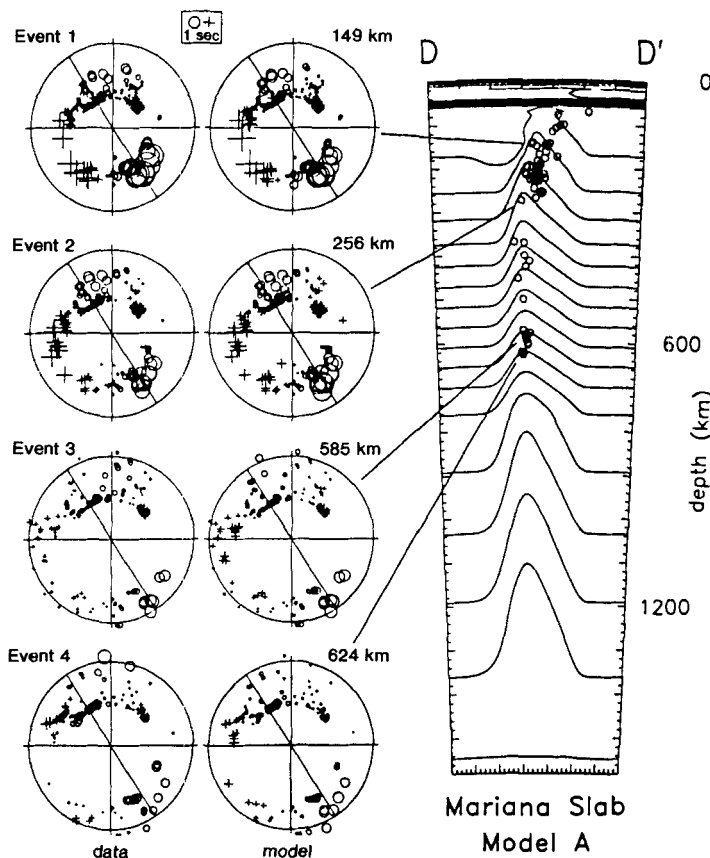


Fig. 17. Comparison of observed (left column), relocated and smoothed residual spheres, for events at different depths in the Marianas slab, with theoretical calculations (middle column) for the slab velocity model associated with the cross section shown on the right. Note the decrease in residuals with depth and the good match of observed and synthetic patterns for events at all depths. Fitting the travel times from the deeper events requires high-velocity material below depths of 660 km, which is modeled as a fast slab extending to more than 1200 km deep. Reprinted with permission from Creager and Jordan (1986).

due to the fact that the travel time anomalies are proportional to $\delta V_p/V_p^2$, with the denominator changing by nearly a factor of 2 over the depth range, while the slab thermal anomaly is expected to vary far less, changing δV_p by only 15% for the thermal parameters chosen by Creager and Jordan (1986). There is a small additional effect of increasing take-off angles for deeper events reducing the travel path in the high velocity slab at azimuths away from the strike. The preferred value of $dV_p/dT = -0.5 \text{ m/s/}^\circ\text{C}$ was used in modeling the Marianas slab, although inclusion of phase changes in the model gives a slightly reduced value of $dV_p/dT = -0.4 \text{ m/s/}^\circ\text{C}$. These values are close to laboratory measurement on mantle minerals at high temperatures and low pressures. The presence of the postspinel phase change can cause the slab velocity heterogeneity relative to surrounding mantle almost to vanish in the slightly depressed phase boundary (the thermal effect is comparable to the phase transition effect), while an elevated α - β transition enhances the slab velocity just above 400 km. Although the theoretical residual patterns did not prove very sensitive to the thickness of the thermal boundary layer, a width of 180 km was preferred.

Creager and Jordan (1986) calibrated the Kuril slab $dV_p/dT = -0.6 \text{ m/s/}^\circ\text{C}$ using events from 129 to 175 km depth and performed kinematic slab modeling using the algorithm of Toksöz *et al.* (1971). Their preferred model (Fig. 18) has a slab that steepens in dip near 500 km, as in the locations of Veith (1974), with a 10° steeper dip in the northeast than in the southwest. The deep slab model extends to 1200–1300 km depth, with P velocity heterogeneity of about 4% near 600 km depth and 3% near 1000 km depth. For the Japan slab the same temperature derivative was found, with a velocity anomaly of 4% at 600 km depth. A model with a deep extension of this slab with dip increasing from 25 – 30° in the upper mantle to 55 – 65° in the lower mantle was preferred. For the Marianas, the slab model extends to a depth of at least 1000 km, with about 2.8% velocity anomaly at that depth. A similar model is proposed for the southern Izu slab near 26°N , based on five residual spheres for events from 142 to 572 km deep (Creager, 1984). On the basis of their modeling, Creager and Jordan (1986) conclude that models of mantle convection that do not have lithospheric slab penetration into the lower mantle to depths exceeding 1000 km should be rejected or downweighted. They estimate that at the rate of current subduction, the volume of the upper mantle is thrust into the lower mantle about once every billion years or less, depending on the extent of entrainment.

The issue of how well residual sphere modeling can constrain the thickness of the deep slab was explored by Fischer *et al.* (1988). They considered kinematic Kuril and Marianas slab models that thicken perpendicular to the plane of the slab (Fig. 19), and analyzed four residual spheres for deep events. Slab thickening could result from reduced flow velocity with depth due to an increase in lower mantle viscosity (e.g., Vassiliou, 1984; Vassiliou *et al.*, 1984; Hager, 1984; Hager *et al.*, 1985; Vassiliou and Hager, 1988; Gurnis and Hager, 1988) or resistance from the endothermic phase transition at 660 km. Thickening by

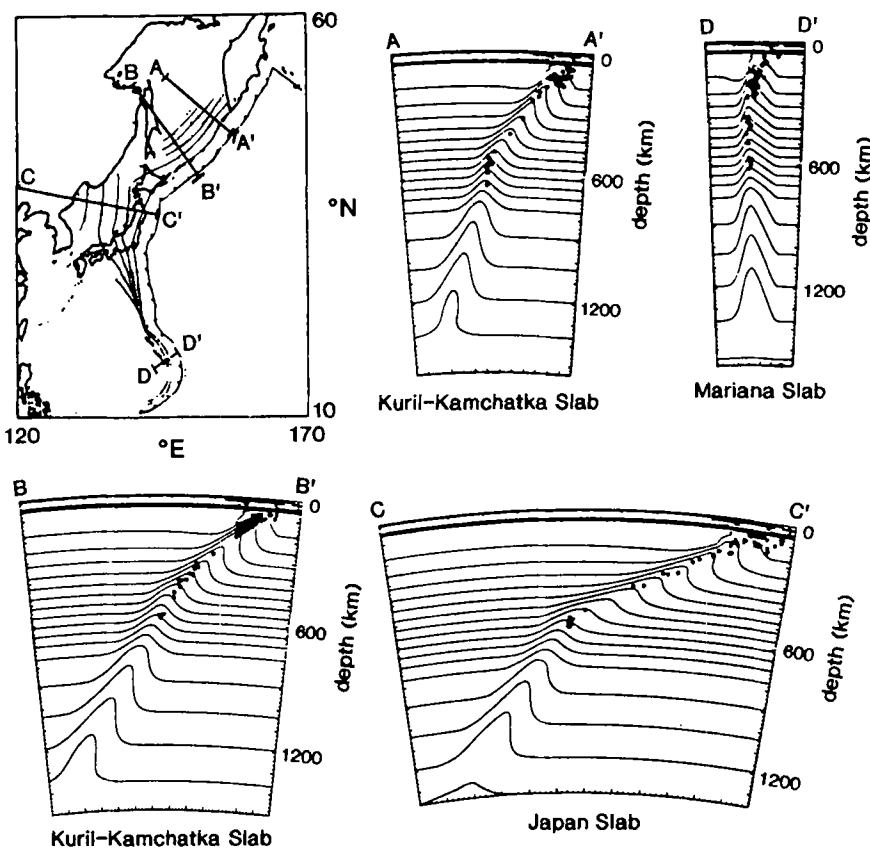


Fig. 18. Cross sections through three-dimensional slab velocity models derived by residual sphere analysis of several intermediate- and deep-focus earthquakes in the western Pacific subduction zones. The seismic zone in the map is contoured in 100-km intervals. In all cases, the slab models are shown extending to 1350 km depth, although penetration depths below 1000–1200 km cannot be resolved by the data. The contour interval is 0.25 km/s. Reprinted with permission from Creager and Jordan (1986).

thermal conduction is expected to produce only a 20% slab width increase over 10 My, so some mechanical process must be involved if slabs thicken significantly. Strong shear strain heating was not included in these models, so the velocity heterogeneity persists in the deformed plate. In each region the best fit to the data was achieved with no thickening; however, for the Marianas the vertical geometry is such that the slab can thicken by a factor of 5, while the Kuril slab can thicken by a factor of 3, and the models can still be reconciled with the data (within the 90% confidence region on the variance reduction). This lack of sensitivity is due to the compensating effects of ray bending. Effectively, a weak,

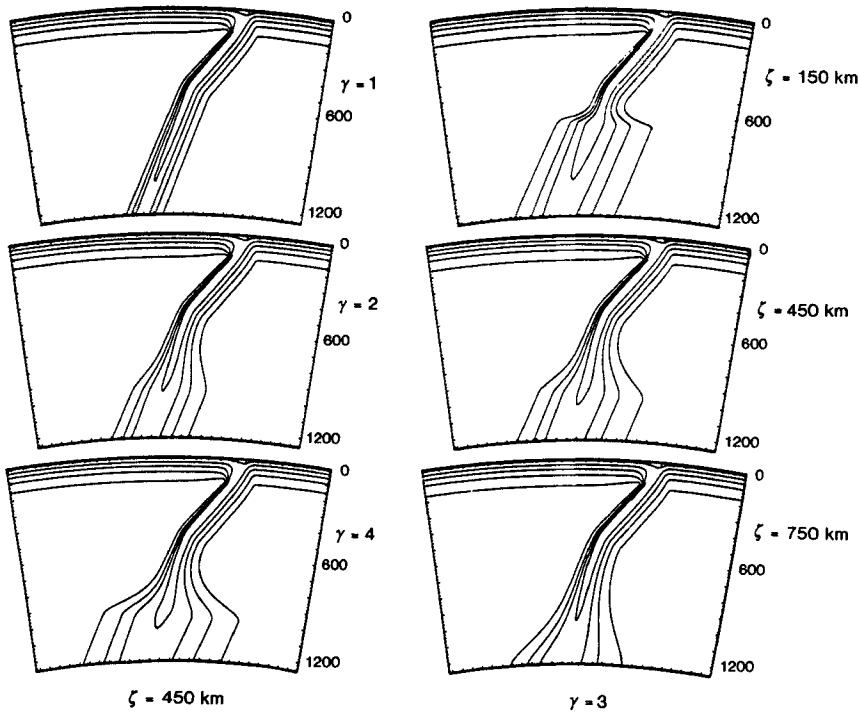


Fig. 19. Examples of deep slab models that include rapid broadening of the slab anomaly in the lower mantle (left column) and broadening over a vertical transition length ranging from 150 to 750 km. These types of models are consistent with residual sphere observations, although undeformed slabs appear to fit some residual sphere data best. Reprinted with permission from Fischer *et al.* (1988).

broad anomaly produces the same travel time patterns as a concentrated narrow one, but in either case the slabs must penetrate to 900–1000 km. Broadened slabs could perhaps explain the 500-km broad features detected in the lower mantle beneath North America and the Caribbean by Jordan and Lynn (1974), Lay (1983), and Grand (1987). In addition, the very large scale regions of fast material in the lower mantle beneath subduction zones in tomographic models (e.g., Dziewonski and Woodhouse, 1987) can be related to slab accumulations only if significant slab thickening occurs. However, any significant thickening must occur largely aseismically, for the deep seismic strain release even in the most seismogenic zone (Tonga) can account for less than a tenth of the deformation required to broaden the slab by a factor of 3.

Residual spheres from 25 intermediate- and deep-focus events in the Tonga slab were analyzed by Fischer *et al.* (1991) to map out the geometry (strike and dip) and deformation of the slab. The data analysis procedure included ellipticity

correction, station correction, aspherical model correction (Dziewonski, 1984), and smoothing. The same thermal modeling procedure as described above was used, with $dV_p/dT = -0.5 \pm 0.2 \text{ m/s/}^\circ\text{C}$ being estimated from the data. The associated velocity variations in the slab are 3–7%. Unless the thermal derivative is doubled or tripled, this analysis suggests that the Tonga slab must extend to minimum depths of 800–900 km, and it may thicken by up to a factor of 3, although there is no resolution of such thickening. The preferred models extend to 1300 km depth. The residual spheres indicate along-strike contortion of the slab, with curvature in the northern end tracking the seismicity and truncation of the slab near the northernmost events. The slab appears to steepen in dip in the south, where the models indicate that it must penetrate to 825–875 km, although it is not required to steepen in the north, where the penetration must be at least 725–775 km. The imbrication and distortion of the slab may explain why, of the various residual sphere studies, this one shows the most scatter and the strongest effects of smoothing of the residual spheres. The final fits to the heavily filtered residual spheres are quite good, but they do represent a minor fraction of the total variance in the unsmoothed residuals.

The Aleutians slab was studied using 11 earthquake residual spheres and anomalies for CANNIKIN by Boyd and Creager (1991). Individual event determinations of dV_p/dT range from -0.37 to $-0.85 \text{ m/s/}^\circ\text{C}$, with the preferred value again being $-0.5 \pm 0.1 \text{ m/s/}^\circ\text{C}$. Depths of the events were initially specified by waveform modeling studies, but all other procedures were the same as in Fischer *et al.* (1991). The local strike and dip of the slab, along with the depth extent, were determined by forward modeling, optimizing a norm measuring the fit of synthetic model times to the data. The best fits give 41–94% variance reduction of the smoothed residual spheres. It appears that the geometry can be quite robustly determined, to within $\pm 5^\circ$ in dip and $\pm 10^\circ$ in strike. The depth of penetration trades off with the thermal derivative, but the preferred models all have long aseismic extensions to at least 600 km depth. For CANNIKIN and an earthquake with a precise locally determined location, the unrelocated residual spheres have strong degree 1 terms. The best slab model can account for 65% of the variance of the unrelocated residual spheres and 82% if relocated. Forty-three PcP times were included for one event, providing better coverage of the central portion of the corresponding focal sphere. These data were used to argue for a change in slab dip from 60° to 80° in the lower mantle, with the slab extending to 1200 km depth. The PcP waveforms are rather simple and impulsive, with -1.5 s anomalies. It seems difficult to reconcile these simple waveforms with energy that has propagated over 1000 km through the defocusing structure of the slab. Another possibility is that high-velocity structure deep in the mantle is responsible for the early PcP arrivals. In order to produce slab models that do not extend to below 600 km, thermal derivatives of -0.6 to $-1.1 \text{ m/s/}^\circ\text{C}$ had to be used. Sleep (1973) modeled the LONGSHOT

travel times with a 200-km-long slab using a value of $-0.9 \text{ m/s}^{\circ}\text{C}$, suggesting that this modeling is very dependent on the exact positioning of the slab and the processing of the data.

Various concerns have been raised about the surprisingly clean results obtained in the group of residual sphere studies that have been mentioned, involving details of the processing (e.g., the heavy filtering used to enhance the low-amplitude, slowly varying patterns in the data, which are assumed to be induced by near-source structure), the data selection (e.g., the use of "noisy" catalog travel time measurements from nonstandard stations for only down-going P arrivals which span a very limited portion of the focal sphere), the model parameterization (e.g., neglect of possible slab anisotropy), and the heterogeneous Earth correction procedures (e.g., use of low-resolution earth models which probably underestimate actual deep heterogeneity components of path effects). Several recent studies have attempted to overcome some of these possible difficulties.

The existence of systematic bias in bulletin data sets associated with variations in instrument magnification was explored by Grand (1990), who found that low-gain stations tend to report late arrivals in the ISC Bulletin. This was based on comparison of Dziewonski and Anderson's (1983) station corrections and the instrument gains for about 900 stations. A possible explanation is that low-gain stations may not detect small precursors seen at high-gain stations. There can be feedback between intrinsic noise levels and station gains as well. Perhaps a greater concern about the bulletin travel times is the intrinsically large scatter in the data. Gudmundsson *et al.* (1990) analyzed ISC travel time statistics, separating spatially coherent and incoherent variance, finding low signal-to-noise ratios (≈ 2) for P waves at teleseismic distances. The signal-to-noise ratio is even lower at local and regional distances. By examining the variance in ray bundles and relating it to the spherical harmonic power spectrum of the slowness variations, they infer that most mantle heterogeneity is concentrated in the upper mantle, with the lower mantle being relatively devoid of small-scale structure. Aliasing of strong small-scale structure into long-wavelength models of slab heterogeneity and tomographic inversions is a source of concern, but the effects of random noise appear most serious. Efforts to measure arrival times manually (e.g., Takei and Suetsugu, 1989; Ding and Grand, 1992) tend to reduce substantially the range of anomalies in residual spheres for deep events relative to the catalog values.

To isolate the near-source contribution of deep slab heterogeneity to travel times, it is important to suppress contributions from mantle heterogeneity far removed from the source region. Given the predominance of large-scale heterogeneity in both the upper and lower mantles (e.g., Su and Dziewonski, 1991, 1992), one cannot safely assume that any slowly varying pattern in a residual sphere must be caused by near-source structure. For example, Zhou and Anderson (1989b) showed that relative travel time anomaly patterns for the Tangshan,

China earthquake and nine of its large aftershocks actually resemble those for deep events in the Kuril slab, suggesting a common component of lower mantle or near-receiver heterogeneity on paths to teleseismic stations. Grand and Ding (1989) found similar travel time residual patterns for deep Kuril events and explosions at Amchitka, after correcting the latter for effects of the Aleutian slab.

Confronted with the difficulty of isolating near-source travel time anomalies, there are two different procedures. As they become available, one can use higher-resolution aspherical earth models (e.g., Inoue *et al.*, 1990; Vasco *et al.*, 1993) to make deep path corrections, or one can adopt an empirical calibration strategy, using data from nearby events to establish improved path corrections, free from the damping and smoothing effects of tomographic inversions. Both approaches were tried by Zhou and Anderson (1989a), who analyzed residual spheres for 33 events in the northwest Pacific. Data with takeoff angles up to 90° were included to stabilize the slab anomaly pattern in the relocated residual sphere, with ellipticity corrections and two types of propagation corrections being applied. In the first case, average station anomalies from 94 events deeper than 300 km in the northwest Pacific were used, effectively providing empirical, azimuthally dependent station corrections. The strategy is for the variation in slab orientations among the 94 events to average out any near-source effects and to isolate the common deep mantle and near-receiver effects. The resulting station anomaly pattern proves to have a nearly slablike feature in it (Fig. 20), so that application of these corrections tends to reduce the strength of slab anomalies in several regions. This does raise concern about whether too much near-source pattern is being removed. The second type of path correction was made using the Clayton and Comer (1983) aspherical mantle model (see Hager and Clayton, 1989), which has far more small-scale features than the heavily filtered model of Dziewonski (1984).

The residuals corrected separately for both types of path corrections were used to fit a symmetric surface of the form $dt(\Theta) = C_0 + C_1 \cos(\Theta) + C_2 \cos(2\Theta)$, where Θ is the colatitude with respect to an axis normal to a fast plane of anomalies. For a tabular slab well sampled by raypaths, the C_2 term should correspond to the fast velocity region. For Marianas events fast regions were found to correspond to the seismic plane for depths from 149 to 255 km, but for events from 585 to 623 km there is much scatter, with no simple pattern. Similar results were found for 12 events in the Izu slab, with reasonable slab patterns to a depth of 400 km but scattered behavior from 450 to 540 km. For Japan a shallow dipping fast plane is found down to depths of 370 km and possibly below. Some differences in C_2 terms are found for the two corrections, mainly due to the large scatter in the data. Residuals spheres for the seven deep Kuril events considered show little evidence for a fast slab. No smoothing was applied, so it is difficult to compare directly with the results of Creager and Jordan (1986), but Zhou and Anderson (1989a) argue convincingly that the limited ray coverage in the earlier

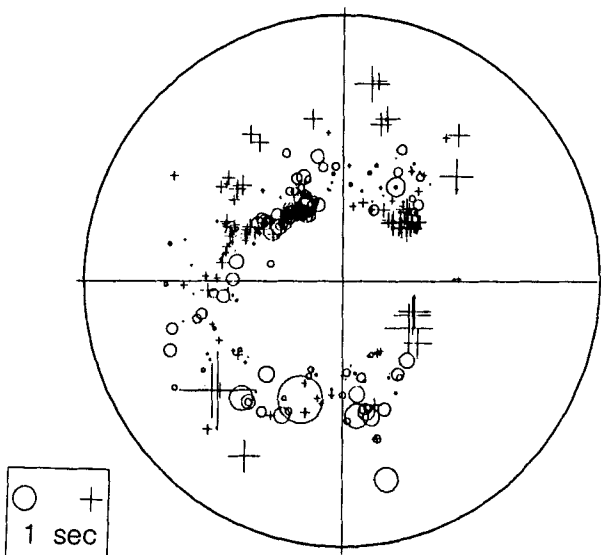


Fig. 20. Stereographic plot of station/path anomalies empirically determined by averaging anomalies from many events in the western Pacific. The path residuals show slowly varying patterns that are similar to those seen for some deep events in the Kuril arc, suggesting that lower mantle and receiver effects may contaminate the deep-event residuals. Reprinted with permission from Zhou and Anderson (1989a).

study would preclude detection of any horizontal slab structure and that the heavy smoothing intrinsically leads to a good fit to the data.

Zhou *et al.* (1990) used whole mantle (Clayton and Comer, 1983) and regional northwest Pacific (Zhou and Clayton, 1990) tomographic models to compare path anomalies with 145 residual spheres for events in the western Pacific. The ray parameter coverage of the focal sphere was again extended substantially by including close-in observations. Many of the coherent features in the residual spheres that give rise to the simple slab structures shown in Fig. 18 are apparent in the path terms for the tomographic models. There is evidence for horizontal flattening of some slabs, particularly the Japan and southern Kuril slabs, which is revealed only by the extended ray parameter coverage. This analysis, like that in Zhou and Anderson (1989a), did not invoke any *a priori* slab model and did not include three-dimensional raytracing. Zhou *et al.* (1990) argue that for the deep events, fast slablike features in the residual spheres are often caused by diffuse heterogeneity in the deep mantle and near the receiver, with heterogeneity below the slabs in the depth range 650–1500 km not being any more pronounced than in other regions. Long paths through weak heterogeneity can accumulate large anomalies, and it is not safe to assume that slowly varying patterns must be near

the source. The relatively small size of corrections for the aspherical model of Dziewonski (1984) was attributed to heavy damping of that model, so that it underpredicts deep effects. There is also a systematic tendency for high-velocity regions below the circum-Pacific to project onto residual spheres, fortuitously yielding patterns that have the correct geometry for slabs. Zhou *et al.* (1990) filter their data using a degree 6 filter and compare the smoothed and unsmoothed residual spheres with the predicted patterns from the tomographic models. They argue that the filter used by Creager and Jordan (1986) has such a large half-width (42°) that it corresponds to a spherical harmonic degree 3, which has very few degrees of freedom and necessarily gives rise to an excellent model fit. They also criticize the use of a cosine taper with takeoff angle by Creager and Jordan (1986) as this suppresses any horizontal patterns. There is some concern about how much of the scatter in the residual spheres remains unaccounted for by the tomographic models, despite the huge number of parameters in those models (Boyd and Creager, 1991), but one must allow for the large intrinsic noise in the ISC data base for any isolated event.

Several additional studies have presented clear evidence for lower mantle and near-receiver contributions to deep earthquake travel time residuals being underpredicted by standard station corrections or integration through low-resolution aspherical earth models. Following up on preliminary work by Lay (1983), Schwartz *et al.* (1991a) examined relative SH wave arrival times from 16 Kuril slab events in the 60° azimuth range to North America. They used ISC locations as a reference, lacking the azimuthal coverage to relocate the events, and observed very similar relative residuals, corrected for station anomalies, across North America for groups of events in the depth ranges 100–200 km, 350–500 km, and 500–600 km. The same trend is apparent in sS travel times, suggesting that this pattern is produced by deep mantle heterogeneity. If the common pattern is removed, there is a significant effect on the residual sphere pattern analyzed by Jordan (1977), indicating that lower mantle corrections need to be applied prior to modeling. As much as 6–7 s of the relative travel time pattern in the S residuals may be due to deep mantle structure. Analysis of the residuals as a function of takeoff angle suggests that fast structure near the base of the mantle can produce ScS–S differential time anomalies, which can also be misinterpreted as near-source effects. Schwartz *et al.* (1991b) further demonstrated that the common pattern in the S times from the Kuril events was well predicted by integration through a completely independent aspherical shear velocity model for the mantle under North America. The observed and predicted path anomalies have a 0.87 correlation. Schwartz *et al.* (1991b) note that application of path corrections can greatly reduce the anomaly pattern attributed to the near-source environment (Fig. 21) and suggest that the common assumption that $dVs/dT = dVp/dT$ may overestimate shear wave heterogeneity in the low-temperature environment of the slab.

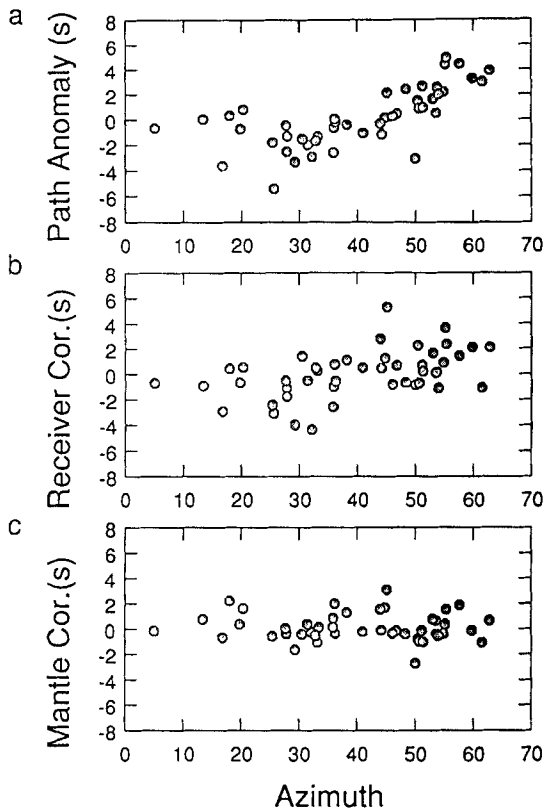


Fig. 21. Relative S wave travel time anomalies across North America from events in the Kurile slab with no corrections (top), the same anomalies after correction for station anomalies (middle), and the same anomalies after further correction for a high-resolution lower mantle shear velocity model (bottom). Almost 6 s of the relative trend is eliminated by the corrections, indicating that residual spheres which have not been corrected for high-resolution tomographic models may be seriously biased. Reprinted with permission from Schwartz *et al.* (1991b).

Analysis of 260 WWSSN long-period tangential component signals with S, ScS, sS, and sScS arrivals from 25 intermediate- and deep-focus events in the Kuril and Japan slabs was performed by Gaherty *et al.* (1991). The data were from stations in Europe, near planes perpendicular to the slabs, effectively providing two-dimensional geometries. Although the limited azimuthal coverage precluded relocation of the events, the general patterns in the S and ScS times across Europe, after correction for the station corrections of Toy (1989) and Wickens and Buchbinder (1980), were found to be similar to those in Jordan (1977), with relatively early ScS phases arrivals. Relocations of azimuthally complete data sets for several of these events produce only minor effects on the

down-dip patterns for the steeply dipping Kuril slab (Eckhardt and Lay, in preparation). This is not the case for shallow events or shallow dipping slabs, where the relocation effect can reverse the sense of relative travel time patterns in the down-dip direction. Similarity in patterns of ScS-S and sScS-sS differential anomalies (Fig. 22), with the core-reflected phases being relatively fast, suggests that deep mantle structure produces ray parameter variations that may be partially responsible for features such as the steepening of dip for deep slabs in the residual sphere models of Jordan (1977) and Creager and Jordan (1986). Empirically determined station corrections based on both up- and down-going phases are much stronger than standard station locations, suggesting that azimuthal terms in the station corrections are also important. Gaherty *et al.* (1991) modeled the down-dip travel time patterns for seven deep events, with and without corrections for lower mantle effects from sScS-sS patterns. They considered a suite of slab structures with deep shear velocity heterogeneity of about 5%. The corrected travel times give a slight preference for broadened slab models, or slabs that do not extend into the lower mantle. Further analysis with complete azimuthal coverage is needed to confirm these results.

Creager and Boyd (1992) considered in detail the issue of earthquake mislocation effects in residual sphere modeling. As shown in the many studies of mislocation effects associated with slabs described in the last section, ISC epicentral mislocations of as much as 40 km for shallow events in the Aleutian slab are to be expected. Using residual spheres for event locations constrained by local networks, Creager and Boyd estimate that as much as 2 s of the actual slab anomaly pattern is lost in the relocation process, and the relative pattern of residuals can change significantly (Fig. 16). The nature of the effects varies with position in the slab. They estimate that for shallow dipping slabs, relocation using only teleseismic P waves can cause 85% of the variance in the slab related pattern to be lost in projecting out the degree 1 term. This emphasizes the dangers of comparing unfiltered (unrelocated) theoretical times with data that have usually been filtered by the location process. The potential problems with using S wave anomalies computed relative to a source location based on P waves were also considered. The stronger variations in S wave times can enhance the relocation effect relative to P times, so that a bias can remain if the P wave location is adopted. This could affect relative S wave patterns like those analyzed by Schwartz *et al.* (1991a,b) possibly explaining why variations in the residuals with depth do not correspond to those seen in P wave residual spheres; however, the consistency of those patterns with deep mantle tomographic models and with sS relative times argues against this. It is clear that the most stable procedure is to always locate the source using the data being studied, which requires good azimuthal coverage. Comparisons of residual sphere patterns with slab orientations like those of Zhou *et al.* (1990) can be misleading if the effects of relocation on the expected patterns are not accounted for. Similarly, tomography, which uses the residuals relative to a homogeneous model, may fail to converge on a

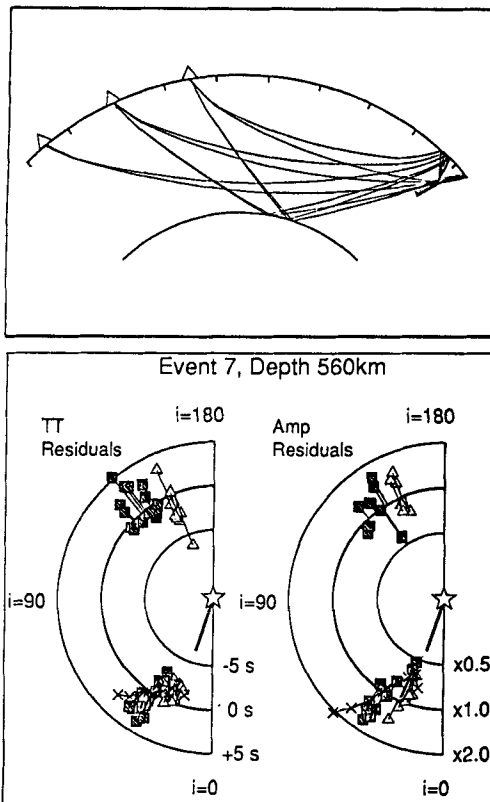


Fig. 22. Illustration of one approach to eliminating distant lower mantle and receiver effects using up-going sS and sScS arrivals to correct down-going S and ScS relative times. The raypath geometry in the down-dip direction of a slab is shown at the top. Observed travel time and amplitude anomalies in the vertical plane in the slab dip direction are shown for SH data below, with anomalies plotted in a radial diagram such that fast arrivals lie closer to the center (negative anomalies) and slower arrivals lie farther away, with the data being shown at the correct takeoff angles in the two-dimensional geometry. Theoretical predictions for the Kuril slab model of Creager and Jordan (1986), scaled to an S wave structure, are shown by the \times s. Note that down-going ScS phases (triangles below the source) are fast relative to S (squares below the source) as predicted by the model, but this may in fact be a distant effect because sScS phases (triangles above the source) are also fast relative to sS (squares above the source), giving the same trend with ray parameter. Fast material near the core–mantle boundary could affect ScS and sScS in similar ways, giving rise to the apparent near-source pattern. Amplitudes are well predicted by the slab model, and the up-going phases do not show a similar pattern. Reprinted with permission from Gaherty *et al.* (1991).

realistic structure because the initial anomalies are strongly distorted relative to the actual slab patterns. For example, the “far-side” effect in residual spheres can lead to errors in the tomographic image, because large anomalies produced purely as a result of relocation will be included in the back-projection analysis. This problem can be reduced by using good focal sphere coverage, and iteration

with raytracing and event relocation is the best way to build up the actual slab model.

Differential residual spheres, first introduced by Toksöz *et al.* (1971), can be computed for events at different positions in the same slab to cancel distant path effects. Although the travel time anomalies that result are substantially reduced relative to those found by the early residual sphere analyses, such studies have tended to favor the presence of high-velocity material in the lower mantle along portions of the down-dip extension of the Japan and Kuril slabs (Takei and Suetsugu, 1989; Okano and Suetsugu, 1992; Ding and Grand, 1992). Takei and Suetsugu (1989) used hand-read times from WWSSN recordings of nine events in the Japan slab, six of which were deeper than 550 km and three at intermediate depth. Given the shallow dip of the plate at intermediate depth, empirical path corrections were determined using the average anomalies from the intermediate-depth events, with differential residual spheres being computed by subtracting these from the average residuals for the deep events. The patterns in the differential residual sphere correlate with the deep event patterns, with a band of fast times with -1 s anomalies to the west (Fig. 23). Relocation of the events did not

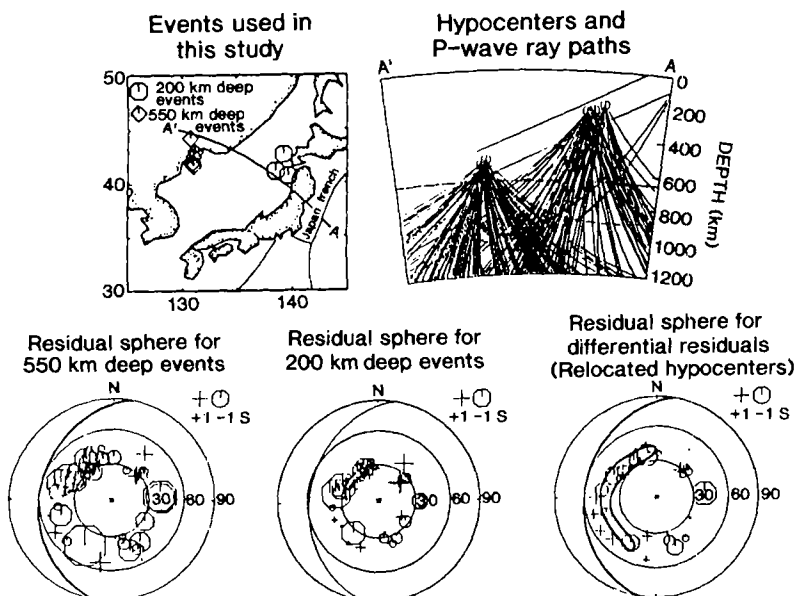


Fig. 23. Example of differential residual sphere analysis for events in the Japan slab. The position of the events is shown on the map and in the slab cross section at the top. Residual spheres for averaged data from deep and intermediate-depth events are shown on the lower left, and the differential residual sphere between these two groups, after relative relocation, is shown on the lower right. A band of negative (fast) arrivals is seen, dipping about 60° toward the west. Reprinted with permission from Takei and Suetsugu (1989).

change this pattern, and they infer a narrow slab structure dipping 50–60° into the lower mantle, consistent with the model of Creager and Jordan (1986) and the tomographic results of Kamiya *et al.* (1988) (Section 4.1.2). Comparison of the measured times with ISC Bulletin times indicates much larger scatter in the ISC times, which is one argument for heavy filtering of the ISC data.

For the Marianas, application of the differential residual sphere method by Okano and Suetsugu (1992) appears to eliminate the high-velocity region below the deepest events, consistent with the results of Zhou and Anderson (1989a). P and PKIKP travel times read from WWSSN stations were measured for three Kuril and nine Mariana slab events. Differential spheres were computed between deep and shallow events in both regions. The travel times were corrected for station corrections and ellipticity and pP–P times were used to constrain the depth when relocations were performed. Perhaps the most surprising result is that PKIKP arrivals for the Marianas deep events do not show early arrivals, despite nearly vertical paths through what should be a high-velocity vertical slab extension, given the model of Creager and Jordan (1986). Differential residual spheres for intermediate-depth Marianas events near 240–250 km do show a slab feature, but no pattern is observed for events from 600 to 650 km. A model with a 5% fast slab extending to 670 km depth in the Marianas was obtained by three-dimensional modeling. The shallow event travel times were first assumed to be free of any slab effect, and then corrections were made for the slab model, but in both cases no deep extension of the slab was found. The differential residual sphere for the Kuril slab shows a scattered pattern, with some evidence for fast velocities along a 50° dipping aseismic extension into the lower mantle, rather than the steeply dipping model preferred by Creager and Jordan (1986).

The most complete differential residual sphere analysis thus far has been for the Kuril slab, for which Ding and Grand (1992) favor a model with substantial advective thickening of the plate and lower mantle penetration in the northern part of the arc but flattening of the plate to subhorizontal in the southern arc. Hand-measured WWSSN travel times for 30 deep, intermediate-depth, and shallow events were analyzed, significantly reducing the scatter relative to ISC data. The lower mantle velocity anomaly in these models is only 2%, about half that in the models of Creager and Jordan (1986), mainly due to the decreased range of the anomalies in the hand-measured data and the explicit path correction effects of the differential residuals. The differential travel times were modeled using a numerical method that accounts for three-dimensional ray bending effects, and the observed and theoretical differential residual spheres were computed for events that had been relocated relative to each other.

While most of these procedures for improving corrections for distant propagation effects lack the comprehensive three-dimensional raytracing and careful handling of relocation artefacts that characterize the work on residual spheres by Creager and Jordan (1984, 1986), Fischer *et al.* (1988, 1991), and Boyd and Creager (1991), it is clear that the reliance of these studies on low-resolution

aspherical models for correcting for distant effects is inadequate. It is also clear that constraining the focal sphere coverage to down-going teleseismic signals severely limits the types of slab effects that can be detected. Interpretation of differential patterns is somewhat more complicated than for individual events, but the confidence gained in the isolation of near-source contributions is substantial. Of course, there is a danger in differential residual sphere and other empirical path calibration procedures of eliminating the desired near-source signal if the path separation is not sufficient. Given the complex three-dimensional geometry of all subduction zones, this is a serious consideration.

4. TOMOGRAPHIC IMAGING OF SLAB VELOCITY STRUCTURE

A logical extension of the studies of relative travel times for isolated events described in the last section is to merge data from many events to determine the near-source velocity structure of the slab and its environs. This is the basic strategy underlying seismic tomography—the development of an image of the heterogeneity from the constructive and destructive interference of travel time anomalies along different paths (e.g., Nolet, 1987; Hirahara, 1993). There are many possible parameterizations of the velocity model, ranging from simple block models with minimal *a priori* information to detailed models such as thermal slab structures (as used in residual sphere modeling) which invoke strong *a priori* constraints on the geometry of heterogeneity. Basic inversion strategies introduced by Aki and Lee (1976) and Aki *et al.* (1977), expanded to handle vastly increasing data sets and model sizes (e.g., Clayton and Comer, 1983; Nolet, 1985; Van der Sluis and van der Vorst, 1987; Spakman and Nolet, 1988), have been applied in numerous tomographic imaging studies of global structure and regions near subducted slabs. The vast travel time data sets provided by the ISC Bulletin have been the primary data source for these inversions, although regional network data in several arcs have also been used, as well as digital waveform data in some global inversions.

Most global tomography models involve large-scale mantle structure and do not resolve the relatively localized velocity gradients associated with subducted slabs (e.g., Dziewonski and Woodhouse, 1987; Woodward and Masters, 1991). However, these models are important for the slab problem in several ways. First of all, the derivation of the global models usually involves determination of station statics which can be used for travel time corrections or may show systematic patterns above slabs directly (e.g., Hager and Clayton, 1989). The global aspherical models can also directly provide path corrections for portions of raypaths far removed from a slab, for use in regionalized imaging or residual sphere modeling. There is some danger of circularity in this, in that the limited raypath coverage associated with all global models may smear some near-source

heterogeneity into the deep parts of the model, which can then be incorrectly removed in the regional modeling (e.g., Frohlich and Grand, 1990). The lower mantle P velocity model of Dziewonski (1984) has been used extensively for corrections in residual sphere modeling, and the higher-resolution P wave models of Clayton and Comer (1983) and Inoue *et al.* (1990) have also been used in slab investigations (Section 3.2). The latter two mantle models and the models of Vasco (1991), Pulliam *et al.* (1993), and Vasco *et al.* (1993) use block models with either $5^\circ \times 5^\circ$ or $6^\circ \times 6^\circ$ blocks with thicknesses of 100–200 km, which can directly reveal some slablike structures as well as back arc low-velocity regions, but clearly these must involve substantial averaging with surrounding regions, precluding definitive analysis of the slab structure or precise determination of slab velocity heterogeneity.

Low-resolution global models are useful for examining the lower mantle below subduction zones, to assess whether there is evidence for cold downwelling material (i.e., high-velocities). For example, Pulliam *et al.* (1993) find high-velocity regions in the lower mantle under Tonga and the New Hebrides down to depths of 1670 km, under Japan and East Asia to the core–mantle boundary, and under the Caribbean and Central America down to 2070 km. Similar features are found in the models of Inoue *et al.* (1990) and Nenbai (1990). The heterogeneity near 650 km is stronger in the model of Dziewonski (1984) than it is at greater depth. Waveform tomography studies of lower mantle shear velocity structure reveal large-scale regions of high-velocity material below subduction zones suggestive of large-scale downwellings that may be associated with thickened slabs with entrained material (e.g., Dziewonski and Woodhouse, 1987; Su *et al.* 1994); however, any such interpretations are highly conjectural. Alternative processes such as thermally coupled convection and chemical heterogeneity must be considered. The preliminary nature of many of the global models must also be kept in mind; for example, it has often been asserted that there is a coherent circum-Pacific ring of high-velocity material throughout the lower mantle, but this feature is very disrupted and not apparent in more recent high-resolution images, undermining some early inferences about dynamic processes in the lower mantle.

Whereas early high-resolution tomographic models (e.g., Hirahara, 1977) addressed upper mantle slab structure alone, many recent studies include the lower mantle below the seismogenic regions, providing a basis for assessing the fate of deep slabs. Accounting for source mislocations and deep mantle and near-receiver effects are always major problems, as is the vertical smearing in tomographic images associated with limited crossing ray coverage below the deepest sources (Spakman *et al.*, 1989; Zhou, 1988). Limited efforts have been made to solve the simultaneous location and velocity determination problem (e.g., Engdahl and Gubbins 1987), but most tomographic studies utilize an iterative procedure, initiating with catalog locations and relocating in a homogeneous model,

followed by, at least in some studies, relocating in the first-step tomographic model using simplified raytracing. Only recently have fully nonlinear iterative inversions with three-dimensional raytracing been applied to slab imaging. As discussed in the last section, a major problem is that much of the slab signal may be lost in the initial location process and the pattern of residual travel time anomalies can be strongly distorted (see Section 3.2), unless the raypath coverage is extensive enough to eliminate the trade-off between slowly varying slab anomalies and slowly varying relocation effects. In the future, inversions starting with an initial slab structure may overcome much of this difficulty, as in the studies of Spencer and Gubbins (1980) and Zhao (1991). Strategies for eliminating heterogeneity outside the model space have included omitting teleseismic raypaths altogether (Zhou and Clayton, 1990), correction for mean station residuals at teleseismic distances (e.g., Kamiya *et al.*, 1988; van der Hilst *et al.*, 1991), and simultaneous inversion for the complete global structure using a variable block size for the near-source and deep mantle portions of the model (Fukao *et al.*, 1992). Improvements in the source location problem have been achieved by including both regional and teleseismic data, as well as surface reflections (pP, PP), which enhance the focal sphere coverage and reduce errors in source depth (van der Hilst and Engdahl, 1991, 1992). Important high-resolution tomography studies of subduction zones are discussed in the following.

4.1. Northwest Pacific

A large number of tomographic inversions for structure near subduction zones have been produced in the northwestern Pacific. The high concentration of earthquakes and seismic stations in the region and the good azimuthal distribution of teleseismic stations have provided fairly high-quality data sets. The Pacific and Philippine Sea slabs sink in the Kuril, Japan, Ryukyu, Izu–Bonin, and Marianas subduction zones, and tomographic models have been obtained for all of these regions, many of which are discussed in the review by Hirahara and Hasemi (1993). That review present many figures from the diverse tomographic inversions.

4.1.1. *Localized Studies in Japan*

In a very early study, Zandt (1975) performed a three-dimensional inversion of travel times in southwest Japan, probably the first such application in the region. This was followed by the work of Hirahara (1977) and Watanabe (1977), who both studied the P velocity structure under Japan. Hirahara (1977) was the first to develop a large-scale three-dimensional velocity model for a subducting slab including a complete resolution analysis. He applied the method of Aki and Lee

(1976) and Aki *et al.* (1977) in a block model inversion of structure below Japan extending to a depth of 650 km. This damped least-squares inversion involved calculating perturbations to slowness in blocks traversed by raypaths along with relocation of the events. The raypath perturbations caused by velocity heterogeneity were ignored. This pioneering application involved 3500 travel time residuals reported in the ISC Bulletin from 20 intermediate- and deep-focus earthquakes. 104 Japanese stations and 232 teleseismic stations were used. Average travel time anomalies to teleseismic stations were calculated and used as path corrections to suppress deep mantle and near-receiver effects. Given the relatively small number of events, this procedure may have projected some near-source structure onto the teleseismic station corrections, and indeed the distribution of average residuals found by Hirahara (1977) (his Fig. 4) somewhat resembles the residual spheres of individual events, but it was important to suppress distant contributions to the residuals. The block sizes were 50 km in the uppermost layer and 100 km at greater depth, with ray coverage providing constraints on heterogeneity only to a depth of 450 km.

The high velocity anomalies of the slab found by Hirahara (1977) were on the order of 5 to 6% at depths from 50 to 250 km, decreasing to 3% near 350 and 2% near 450 km. The wedge region was about 2% lower velocity down to 350 km. The seismicity proved to be located in the upper portion of the high-velocity material, with the upper boundary of the plate being more sharply defined than the lower boundary. The same data set was analyzed by Hirahara and Mikumo (1980), using smaller block sizes in the vicinity of the plate to give a more detailed model. The high-velocity feature of the slab is present at depths from 150 to 550 km, with the relative sharpness of the upper surface of the plate again being apparent. Three-dimensional raytracing was used to test the stability of the model, by comparing observed and calculated patterns, but raytracing was not introduced into the inversion, so the effects of path perturbation on the model are not fully understood. The predicted gravity anomaly for the tomographic model was compared with the observed Bouguer anomaly under Japan, with much of the large positive Bouguer anomaly in northwestern Japan being attributed to the subducting slab.

Hirahara (1980) performed a similar block inversion of S wave arrival times at Japanese stations for the same 20 events used in his study of P velocity heterogeneity. The times were taken from the Seismological Bulletin of the Japan Meteorological Agency (JMA), with 876 residuals being used. Teleseismic data were not used, and the source locations were fixed to be the relocated positions found in the P wave study. The nonuniform nature of the data sets for P and S makes comparisons questionable, but similarities in basic heterogeneity patterns were found. The slab is fairly well defined down-dip from Hokkaido and central Honshu to depths of 350 km, but deeper structure is poorly resolved. The highest shear velocity anomalies in the plate are 6–8% from 50–250 km depth, 5% near

350 km, and 2–3% near 450 km, which are systematically higher by 1–2% than corresponding P anomalies. The wedge has shear velocity anomalies of –2 to –4% at depths above 400 km, giving slab–wedge velocity contrasts of 10% (50–250 km) and 8% (350 km) for shear velocity. The P and S velocity anomaly models were combined to give images of Poisson ratio variations with depth, which tend to show low Poisson ratios near the slab and higher values in the wedge, but there is substantial uncertainty in the absolute values due to differences in damping in the inversions and varying resolution of the models.

Many studies have concentrated on more localized regions of the Japan subduction zone; these will be discussed moving roughly from south to north. A detailed three-dimensional block model of the mantle underlying the southwestern Japan was obtained by Hirahara (1981), using ISC data. The subducting Philippine Sea and Pacific plates under Kyushu were imaged to depths of 150 km, with very contorted slab geometry being suggested. The subducting Pacific plate was found to have 3% high velocities in the depth range 70–150 km, with the wedge velocity anomaly at depths of 100–200 km being –2%, while the Philippine Sea plate was 2.5% fast with the wedge being –2.2% slow under Kyushu. The same data set was analyzed by Hirahara and Ishikawa (1984), with transverse isotropy being included in the block inversion formulation. The effects of anisotropy were restricted to a velocity spheroid to reduce the number of parameters. Although resolution of the anisotropic parameters is very marginal, there is some indication that fast directions tend to be perpendicular to expected magnetic lineations in the subducted slab. Somewhat better constrained is an indication that regions of the wedge above the slab are anisotropic, with P velocity anisotropy being found to correlate with regions in which Ando *et al.* (1983) have observed shear wave splitting. Tanaka (1987) performed a high-resolution tomographic inversion of the P velocity structure beneath southwestern Japan, under Shikoku and Chigoku. A thin, seismogenic low-velocity layer was found at the top of the high-velocity Philippine Sea slab, which extends to 150–200 km depth along the plunging seismic zone.

The study by Ando *et al.* (1983) used three-component stations above the Japan slab. Analysis of 89 records revealed two localized regions of anisotropy 50–100 km wide at depths of 50–200 km under western Honshu. Shear wave splitting with 1-s time delays between fast and slow waves, corresponding to 4% anisotropy over 100-km-long paths, was observed. Crossing raypaths were used to bound the region of anisotropic material. The orientation of the fast direction rotates by 90° over the 100-km separation between the two anisotropic zones. Crack alignment and olivine orientation were invoked to explain the observed splitting. Hirahara (1993) discusses anisotropic P wave travel time tomography in some detail, showing that the large number of parameters and the nonuniform ray coverage yield only half as much resolution as in the isotropic case. He

argues that independent *a priori* knowledge of the symmetry is needed to stabilize such inversions.

The structure under the Kanto district is remarkably complex, due to the overlap of the Philippine Sea and Pacific plates, and seismic imaging has played a major role in unraveling the complexity. Horie and Shibuya (1979) began to study this region using explosion and earthquake travel times, and there were many studies of the crustal structure, including the study of P and S velocities by Ukawa and Rukao (1982). Horie and Aki (1982) performed the first localized block model inversion for the structure in the upper 65 km under the Kanto District. They found 6–7% P velocity variations in the depth range 32–65 km, with some indication of the Philippine Sea and Pacific plates. Their model suggests that the slab is 3% fast and the mantle wedge –3% slow in the region. Ishida (1984) developed a three-dimensional block model for the upper 145 km of the mantle below the Kanto–Tokai region, as an extension of the work of Horie and Aki (1982). She relocated 5000 events in the region in a six-layer block model to study the plate configuration. Although crustal velocity variations greater than 10% were found, the velocity fluctuations are about 6% at depths from 45 to 70 km, in agreement with the earlier work, and 3% from 70 to 95 km. Ishida and Hasemi (1984) extended this effort, using 25-km blocks to develop a three-dimensional P wave model. They found evidence for a 30-km-thick Philippine Sea slab subducting in the Sagami and Suruga troughs. Yamazaki and Ooida (1985) further examine the configuration of the Philippine Sea plate under central Japan.

The detailed P velocity structure under Kanto–Tokai was further investigated by Ishida and Hasemi (1988) and Ishida (1992). Ishida and Hasemi (1988) performed simultaneous damped least-squares inversion for structure and event locations for 91 events using data from 61 stations. Their model extended to a depth of 212 km with seven shells in a 10×17 grid of blocks 0.25° on a side. Inversions with half-grid-width shifts of the grid were conducted to establish stability of the inversions. They found that a 75% variance reduction in the residuals was achieved by including the three-dimensional model and that strong, up to 20%, lateral velocity variations were imaged. A clear 30-km-thick zone of 4–6% high velocity, extending to the northeast and west of the Izu Peninsula, is associated with the Philippine Sea plate, which extends to 40–70 km depth. The resulting model was used to relocate 23,000 earthquakes from 1983 to 1985, revealing a complex pattern associated with collision of the Philippine Sea and Pacific slabs. Ishida (1992) refined this model using 244 events, modifying the interpretation to favor a 30 ± 5 -km-thick Philippine Sea slab that sinks northwestward under the Sagami and Suruga troughs above the westward-dipping Pacific plate, but a bump in the Philippine Sea plate beneath the Izu Peninsula causes a rotation to a northward dip. In the northeastern region under the Sagami

trough the Philippine Sea and Pacific slabs are in direct contact. The tomographic model was used to relocate 47,500 events from 1980 to 1988. Overall, the model is consistent with the oblique convergence in the region and with regional focal mechanisms and clustering of earthquakes.

Hirahara *et al.* (1989) performed a detailed block model inversion using 7490 P wave travel times for paths traversing the wedge overlying the subducting Pacific and Philippine Sea plates in central Japan. They find that regions of low P velocity tend to correlate with regions inferred to have low Q on the basis of intensity data (Hashida and Shimazaki, 1985). The high-velocity region associated with the plate extends to 150 km depth, well below the 60-km maximum depth of seismicity.

The region below Tohoku (northeast Honshu) is geometrically the simplest portion of the Japan arc and has received extensive study. Hasemi *et al.* (1984) inverted regional P wave recordings from the Tohoku University network for three-dimensional structure in the upper 164 km beneath Tohoku. Their block model shows clear low-velocity features in the upper 65 km beneath volcanic and geothermal areas of the crust, with the subducting Pacific slab being apparent at depths greater than 65 km. They suggest that the slab is 2% fast from 65 to 98 km, with the wedge anomaly being -1 to -1.5% , while from 98 to 164 km the slab is 1–3% fast and the wedge is -3% slow. However, their raypaths travel directly up from the slab, so the resolution of the slab anomaly is very poor. Recognizing this, they performed inversions in which they assumed a 4–6% fast slab with specified geometry and found comparable heterogeneity in the wedge. They have no resolution of deeper structure in their model. A tomographic inversion of the upper 100 km of mantle under Tohoku and Hokkaido (Nakanishi, 1985), using 7600 P travel times from the JMA, revealed slab–wedge contrasts of 4% at depths of 60–80 km, in agreement with Hasemi *et al.*, (1984). Obara *et al.* (1986) also performed inversion of Tohoku network recordings for the P and S velocity structure under the northeastern Japan arc, finding low P/S velocity ratios in the plate with slab–wedge velocity contrasts at depths of 65–98 km being 2% for P and 6% for S, while from 98 to 131 km the contrasts were 4–8% for P and 6–10% for S. The slab seismicity in this region has a clear double zone (see Section 5.3), with the upper zone locating near the top of the high-velocity region. T. Sato *et al.* (1989) found similar features in the northern Tohoku region. These studies detected low velocities in the crust and upper mantle below the active volcanoes in central Japan.

Tomographic inversions including crustal and mantle discontinuity topography have also been conducted in Tohoku. Horiuchi *et al.* (1982) used a power series representation of the Conrad and Moho surfaces in inversion for locations of local events and depth of the discontinuities. Zhao *et al.* (1990a) pursued this, allowing for variation of the Conrad and Moho depth under the entire Tohoku

region, using S-to-P and P-to-S converted phases to determine the position of the boundaries, without allowing for velocity variations. This requires three-dimensional raytracing. They find that generally the boundaries are deep under the land and shallow under both the Japan Sea and Pacific coastlines. Zhao *et al.* (1990b) discuss the P velocity structure of the uppermost mantle off the Japan Sea coast.

Seismic tomography including the effects of mantle velocity discontinuity topography was performed for northern Honshu by Zhao (1991) and Hasegawa *et al.* (1991). These studies used P and S waves, with the depth of the Conrad and Moho boundaries being given by Zhao *et al.* (1990a) and the slab boundary constrained by precise earthquake locations. Three-dimensional raytracing was used in iterative tomographic inversion of 50,919 times from 512 shallow and 688 intermediate and deep events from 40 to 650 km. The inversion was directed at high resolution of the wedge structure under central Honshu and refined imaging of the low-velocity zones underlying the volcanoes. An 80-km-thick plate was found, consistent with reflections off the base of the plate (see Section 5.2.2) by Umino *et al.* (1990). The overall contrast between the wedge and plate is about 6%, and there is no indication of a zone of low velocities right at the plate surface. Zhao and Hasegawa (1993) discuss the full model, extending to a depth of 500 km beneath Japan, with 25–50 km spatial resolution. The Philippine Sea plate is estimated to be about 30 km thick. Zhao (1991) and Zhao *et al.* (1992a,b) obtained a model with good resolution above 200 km and very good resolution from 40 to 90 km depth. The slab is about 4% fast, with overall 6% V_p and 10% V_s heterogeneity in the model, with low velocities beneath volcanoes (Fig. 24). They used 18,679 P and S arrival times from 470 shallow and intermediate-depth events. Inversions with and without specifying a fast slab in the starting model give large differences in the slab structure below 200 km depth, indicating lack of deep resolution. The patterns in the wedge vary in amplitude depending on the starting model, and the variance reduction is better when the slab is specified, indicating that use of an initially heterogeneous model based on *a priori* information is probably necessary for resolving the three-dimensional structure. Kamiya (1991a,b) has inverted Japan University Network Earthquake Catalog (JUNEC) and JMA data for models of the Japan slab using one-step inversions, without raytracing. He obtained models similar to, but less coherent than those of Zhao (1991). The JMA data have less variance than the ISC data.

The three-dimensional structure under Hokkaido has also been explored. Takanami (1982) and Miyamachi and Moriya (1984) found evidence for a dipping low-velocity zone below southern Hokkaido, inferred to be subducted crust associated with the collision between the Kuril and northeastern Japan arcs. The structure has –10% anomalies from 5 to 20 km and –5% anomalies from 20 to

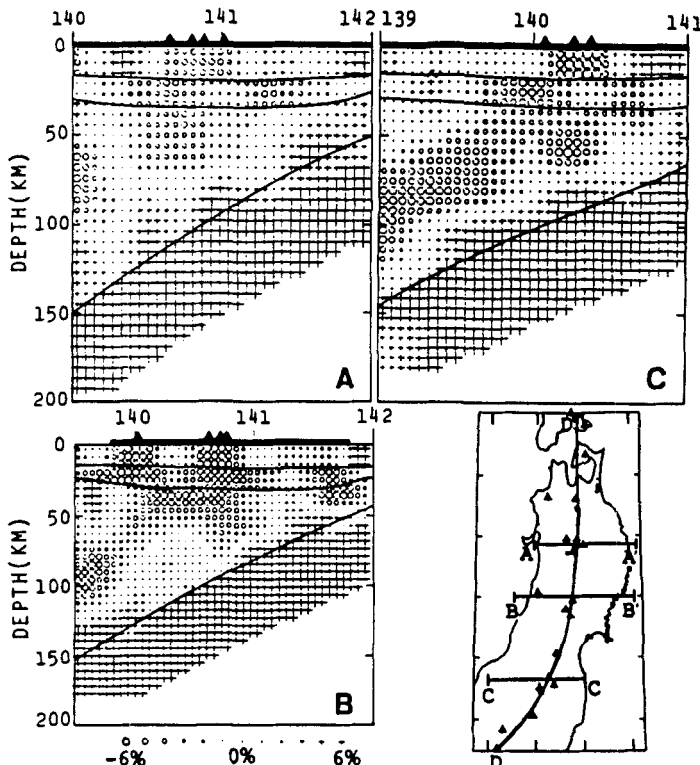


Fig. 24. E-W vertical cross sections of P wave fractional velocity perturbations (in percent) along the three lines shown in the insert map. Filled triangles and heavy horizontal lines represent active volcanoes and land area, respectively. The position of Conrad, Moho, and slab upper boundaries is shown. These models included an a priori slab structure, and the model is most resolved only in the wedge. Reprinted with permission from Zhao *et al.* (1992a).

60 km depth. Inversion of pulse-broadening measures of attenuation for three-dimensional structure under Hokkaido indicates that the low-velocity regions correspond to low-Q regions (Furumura and Moriya, 1990).

A detailed P velocity model for all of Japan was obtained by Zhao *et al.* (1993a), using local, regional, and teleseismic data simultaneously. They used 45,318 P wave arrival times from 1241 shallow and deep earthquakes under Japan, as well as 4211 travel times from teleseismic events. Low-velocity regions in the mantle wedge extend to about 200 km, and the slab is imaged as 80–90 km thick with 4–6% higher velocity than the surroundings.

Seismic intensity patterns have also been the subject of crossing path and tomographic analysis. Nakanishi and Horie (1980) extended the early seismic intensity studies (Section 2) by Katsumata (1960) and Utsu (1966), by analyzing

the intensity distribution in Kanto from 1949 to 1978. They found high intensities on the eastern side of the Izu Peninsula, which were attributed to a high-Q path through the Philippine Sea slab. On the basis of the intensity patterns, a northeast-dipping slab in the Sagami trough was postulated, extending 60–80 km deep to the top of the Pacific slab. This region was subsequently targeted for tomographic inversion of seismic velocities in the studies described above. A tomographic inversion for shear wave attenuation under Kanto was performed by Hashida and Shimazaki (1985). They used 4500 seismic intensity reports as measures of maximum ground acceleration, with a block model with $50 \times 60 \times 30 \text{ km}^3$ blocks, extending to a depth of 180 km. Lacking knowledge of the source radiation, it was assumed to be isotropic, with all amplitude effects being attributed to attenuation. The model shows a low-attenuation zone in the Philippine Sea slab, with an aseismic region extending to about 120 km toward the north. Under northeast Kanto a region of low attenuation extends to 60 km depth, as a root of the overriding plate, with high-attenuation zones on the continental side of the volcanic front. Similar intensity data were analyzed for the Tohoku region by Hashida and Shimazaki (1987). Hashida (1989) extended the intensity inversions to include the upper 90 km under most of Japan. He found high Q on the Pacific side of northeast Japan and high Q in southwest Japan with a small low-Q region on the Pacific side.

Spectral amplitude ratio measurements have been used instead of intensities in several three-dimensional attenuation investigations. Umino and Hasegawa (1984) inverted for attenuation under Tohoku, finding a high $Q_\beta = 1500$ in the slab, low $Q_\beta = 150$ between the volcanic front and the Japan Sea, and medium $Q_\beta = 500\text{--}800$ between the Pacific plate and the volcanic front. Very low Q was found under volcanic regions. Sekiguchi (1991) measured differential attenuation values and inverted for three-dimensional Q structure under Kanto–Tokai. Using P/S power spectral ratios to measure differential t^* values and the assumption that $Q_\alpha/Q_\beta = 2.25$, 3610 measurements were inverted. A one-dimensional model was used to compute the raypaths, and no correction for three-dimensional focusing associated with the tomographic models was used because the location of caustics is probably not reliable. He again found high Q in the region of the Philippine Sea plate, as well as in the Pacific plate. High Q was found east of the volcanic front and low Q west of the volcanic front, but no low Q was found under the volcanoes.

4.1.2. Kuril Slab and Large-Scale Regional Inversions

Several tomographic studies have directly addressed the Kuril slab structure. Suetsugu (1987, 1988, 1989) inverted teleseismic P waves from intermediate- and deep-focus events in the Kuril slab. His data were taken from ISC Bulletin reports for 1971–1982 for stations at distances less than 10° and $30^\circ\text{--}90^\circ$ from

the sources. Corrections for ellipticity and Dziewonski and Anderson (1983) station terms were made, and the events were relocated in the J-B model. Clear slablike anomaly patterns are shown in the resulting residual spheres, largely because the inclusion of local stations reduces the trade-off between location and slab patterns. To avoid multipathing problems, the emphasis was on the down-dip direction. A parameterized slab model with a smooth cosine velocity structure across the slab was used in the depth range 0–650 km, with an increase in dip to 55° at 300 km depth, overlying a block model of 1° × 1° × 100 km blocks from 650 to 1250 km. Different velocities were allowed above and seaward of the slab. Inversion was then performed for the locations of the events and the up-going station anomalies as well as the block model parameters. No raytracing was performed. In the depth range 200–400 km a slab contrast of 7% was found, and from 500 to 600 km 4% was found. A high-velocity extension of the slab with 2–3% anomaly was found to a depth of 1200 km. A low-velocity region under the deep extension was also imaged. No correction was made for lower mantle path effects, and the model explicitly precludes any flattening of the slab above 650 km. The high-velocity slab extension does not change in dip as in the residual sphere models of Creager and Jordan (1986).

Yamanaka (1990) and Yamanaka *et al.* (1992) performed block tomography inversion for the Kurils using the inversion method of Hirahara (1988). Their models involve 0.5° × 0.5° blocks from 33 to 50 km thick, extending from 0 to 1200 km depth. ISC data from 1964 to 1985 were used. For the S wave inversion by Yamanaka *et al.* (1992) the 1994 events were not relocated, and average station anomalies were used to remove distant slab effects. Simulations with a 5% slab model show that the basic geometry can be recovered, but the model underpredicts the amplitude with increasing depth. Similar features were found in the P and S structures, and the authors suggest that the Kuril slab involves four segments, with the southwestern end extending no deeper than 500 km, with a dip of 35°. North of this region the slab dips 50° and flattens to horizontal near 650 km. Farther to the north the slab has a weak anomaly from 200 to 350 km, and high S velocity from 350 to 850 km and high P velocity from 350 to 1000 km, with no bend in the slab. The deep extension of the slab does not steepen in dip as in the residual sphere models of Creager and Jordan (1986), consistent with the model of Suetsugu (1989). In the far north the slab anomaly is weak from 100 to 500 km depth, with a steeply dipping slab extension into the lower mantle.

The Kuril, Japan, Izu, and Mariana slabs have also been imaged in larger-scale, high-resolution inversions. Kamiya *et al.* (1988) and Kamiya *et al.* (1989) performed an inversion for the upper 1200 km of the mantle in the region from 20 to 50°N and 120 to 150°E. They used 0.5° × 0.5° × 33–50 km blocks and 103,032 teleseismic travel times from 833 earthquakes in the ISC Bulletins from 1971 to 1983. Use of only down-going phases greatly limits the potential resolu-

tion of any horizontally deflected slab structures. Selecting only impulsive arrivals, ellipticity, elevation, and station corrections were applied, with average station anomalies being used for stations outside the model space. Relocation parameters and 64,197 velocity unknowns were inverted for using a row-action matrix inversion with 30 iterations. The model indicates that the Sea of Japan slab steepens in dip below 500–600 km and extends to 1100–1200 km with a dip of 45–50°, but there is strong along-dip streaking due to lack of crossing path coverage in this region. This structure is similar to the model of Creager and Jordan (1986), which has a 55° dipping lower mantle extension. North of 29°N the Izu slab appears to flatten, whereas south of 26°N the Izu slab may penetrate vertically to 850 km depth, as suggested in the residual sphere analysis of Creager (1984). Low velocities 2–4% lower than the average were found above the Pacific and Philippine Sea slabs, and blotchy high-velocity regions extend below the Ryukyu arc to 600 km deep.

This model was extended by Miyatake and Hirahara (1989b) using 0.24 million ISC P times and 1672 pP times from 2060 events. The grid was expanded to include the Kuril slab as well. As in the study of Suetsugu (1989), data in the distance range <10° and 30°–90° were used. Synthetic simulations with a 3% fast slab and Gaussian noise with a standard deviation of 0.8 s indicate relatively mild down-dip smearing of the slab anomaly for the Japan slab in the study of Miyatake and Hirahara (1989b). Their basic results are very close to those of Kamiya *et al.* (1989).

Spakman *et al.* (1989) inverted a huge data set of 1.4 million local, regional, and teleseismic ISC P wave travel times for the Pacific Northwest. They used only data from events in the model region, which encompassed the Marianas, Izu, Ryukyu, Japan, and Kuril slabs. The block model has 51,832 1° × 1° cells varying in thickness from 33 to 100 km, extending to a maximum depth of 1400 km. Relocation terms and station statics were inverted for, but no raytracing was performed. The images for the Kuril, Marianas, and Japan (the latter are shown in Hirahara and Hasemi, 1993) slabs all have substantial high-velocity regions extending below the maximum depth of seismicity. The Mariana slab shows a broadened extension to about 1000 km, and the fast velocity region below the Japan slab is suggestive of some steepening of the dip. High-velocity regions around the Kuril slab could be taken as evidence for either slab flattening or deep penetration. However, simulations with synthetic slab models based on thermal slab structure and the same raypath coverage also show severe smoothing and streaking of the slab heterogeneity down-dip into the lower mantle. In addition, van der Hilst and Spakman (1989) show that use of an incorrect reference model can yield horizontal streaking in the tomographic images, possibly confused with flattening of the slab. Interpretation of these tomographic images is thus very equivocal. Hirahara (1993) suggests that the larger variance in the data used by Spakman *et al.* (1989), which was used to select the variance of noise in the

simulations, results in greater smearing effects in the simulations and actual inversions.

In a study which used only regional and local observations, Zhou (1988, 1989) and Zhou and Clayton (1990) obtained P and S wave models for the northwest Pacific from 0 to 60°N and 115 to 164°E, again using ISC data. They analyzed 130,000 P times and 56,000 S times, using block models $1^\circ \times 1^\circ \times 50$ km and $2^\circ \times 2^\circ \times 50$ km, extending to a depth of 1200 km. Only rays within the model space were used, which does give a few teleseismic rays but not much down-going coverage. No source relocations were performed, but source statics and receiver corrections were iteratively removed. The models indicate 7–8% velocity contrasts in the shallow mantle, with somewhat intermittent fast velocity structures associated with the deep seismogenic zones. Estimates of resolution from synthetic calculations using the raypath coverage of the data were made, but no relocation effects were accounted for. Hirahara (1993) and Spakman *et al.* (1989) argue that omission of realistic noise and relocation effects in the resolution test probably overestimates the spatial resolution, because in that case the simulations preserve the total anomaly, which is not actually measurable.

The resulting velocity images suggest a complex pattern of flattening and fingering of some slabs, with intermittent lower mantle penetration by others. Under the Kuril slab, there is some evidence for fingering around 600 km depth and some high-velocity extension to 700–850 km in the north, but no deep slab in the central Kurils. This is contrary to the results of Suetsugu (1989) and Yamanaka *et al.* (1992). The Japan slab shows some evidence for flattening, although there is some fast material just below the deepest events. Zhou and Clayton (1990) argue that down-dip smearing is responsible for the images of Kamiya *et al.* (1989). The Izu slab is inferred to flatten above 600 km, while a broad region of fast velocity material down-dip of the Mariana slab extends to 800–1000 km depth. Comparison of the P and S velocity models indicates that $d(\ln V_s)/d(\ln V_p) = 1.5$, but without relocation of the sources this estimate has large uncertainty.

It appears that the characteristics of deep slabs are hard to resolve using only up-going or down-going phases, but use of all phases is difficult unless a good strategy is used to suppress distant path effects. Rather than relying on average station statics or corrections from global models, Fukao *et al.* (1992) solved for a complete global model with a variable grid size in the vicinity of the western Pacific subduction zones. They used the ISC data set and adopted the global block model parameterizations of Nenbai (1990) and Inoue *et al.* (1990). This allowed direct solution for distant effects, without use of *ad hoc* corrections. Iterative relocation initiated with the model of Inoue *et al.* (1990) was performed, with the western pacific subdivided into $150 \times 150 \times 50$ km³ blocks, which is much smaller than in the rest of the model ($5.6^\circ \times 5.6^\circ \times 100$ km). Even finer blocks, with dimensions halved relative to the smaller size, were used

in the vicinity of slabs. A total of 410,000 P times was incorporated in the inversion, with reference models with and without 400- and 670-km discontinuities being used. Little dependence on the starting model was found, in contrast to the results of van der Hilst and Spakman (1989). Checkerboard test patterns were used to test the potential resolution provided by the ray coverage, and the smoothing algorithm of Inoue *et al.* (1990) was used to suppress fluctuations. The procedure did not include three-dimensional raytracing but did include effects of the aspherical model. This involved computing an average radial model at each step and then relocating in this average model with corrections for the 3D structure.

The images that result from this inversion are quite impressive (Fig. 25), with rather continuous high-velocity structures in the seismogenic zones, well-defined low-velocity regions in the wedge, and rather large accumulations of high-velocity material in the transition zone and down to depths of 800 km or so below the Kuril, Japan, Izu, Mariana, and Java slabs. Under Japan there is evidence for both a broad, flattened anomaly and some fast material extending to 1000 km depth below the deep seismicity. This contorted geometry may correspond to the separate regions imaged by Kamiya *et al.* (1989) and Zhou and Clayton (1990) using down-going and up-going phases, respectively. Under the southern Kuril and northern Izu regions the slabs tend to deflect to subhorizontal and extend landward for over 1000 km. The flattening of the velocity anomalies under Izu is consistent with the results of Miyatake and Hirahara (1989b), Zhou and Clayton (1990), and Okino *et al.* (1989). Under the northern Kuril arc, a broad zone of fast velocity material may extend to 900 km, but this does not appear to be a simple tabular structure. This is consistent with broadened high-velocity region imaged in the differential residual sphere modeling of Ding and Grand (1992). The Mariana slab is poorly manifested at upper mantle depths, but there is a broad fast velocity region down-dip from 800 to 1200 km. This is similar to the model of Spakman *et al.* (1989) and suggests significant broadening relative to the thin slab model proposed by Creager and Jordan (1986). This region does have rather poor resolution, so smearing of a concentrated anomaly is plausible. A broad fast velocity region is found from 800 to 1200 km deep, along the down-dip direction from the Java slab. The images show an interesting low-velocity region seaward of the Japan and Izu slabs at depths from 300 to 700 km. It is unclear whether this may be an artifact of the reference model. Tests with synthetic data sets show some horizontal smearing of the input velocity structures but not too much vertical smearing. The authors interpret these images as evidence for strong deformation of subducting slabs, accumulation of large piles of slab material, and eventual sinking of each pile into the lower mantle.

van der Hilst *et al.* (1991, 1993) performed another inversion of ISC P wave travel times for the northwest Pacific using an improved reference earth model and a high-quality data set of pP observations. By comparisons with inversions

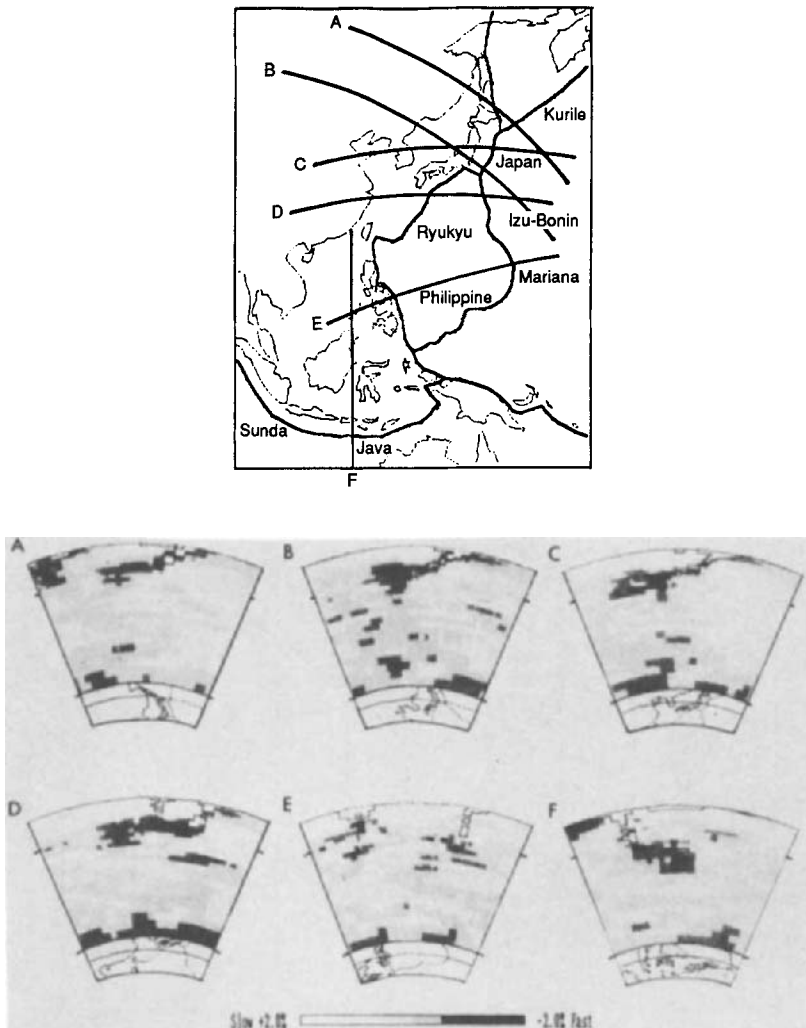


Fig. 25. Cross sections in the slowness model of Fukao *et al.* (1992) extending from the Earth's surface to the core-mantle boundary on the six vertical sections shown by the index map (top). Faster velocity regions are dark. The depth of the 670-km boundary is shown by the tick mark on each frame. The location of hypocenters is indicated by the blocks overlying the shallow regions. Reprinted with permission from Fukao *et al.* (1992).

using the smooth J-B model, they established that inclusion of the 410- and 660-km discontinuities significantly affects horizontal and even vertical features in the models, with the amplitude of high-velocity anomalies also being influenced by the reference model. They included the pP phases, corrected for water depth and topography, to relocate events in the IASP91 earth model, giving better

depth constraints. The variance of the P wave residuals after location in the IASP91 model is 17% less than for the J-B model, which is comparable to the variance reduction provided by the tomographic inversions (van der Hilst *et al.*, 1991, 1993; Engdahl *et al.*, 1993). The pP data also provide better raypath coverage of the model, particularly in the shallow mantle. Two million P wave residuals and about 100,000 pP residuals from 40,000 earthquakes in the study region were used, for 2300 global stations. The block model has $1^\circ \times 1^\circ$ dimensions, with layer thicknesses varying from 33 to 200 km and a total depth extent of 1600 km. Station corrections were determined for stations outside the model to suppress distant effects. The resulting models (Fig. 26) show strong evidence for deflected high-velocity material near the northern Izu and Japan slabs, with vertical extension of the Marianas slab to about 1100 km. van der Hilst and Seno (1993) attribute rapid trench migration along Izu to the flattening of slab structure there in contrast to nearly vertical penetration of the slab below the Marianas. The northern Kuril slab appears to extend at a steep dip into the lower mantle to a maximum depth of about 1050 km. The central Kuril slab broadens and flattens near 500–600 km, with a narrow extension to 800 km depth. The southern Kuril slab flattens with no clear extension into the lower mantle. The images are generally very compatible with those of Fukao *et al.* (1992); thus there appears to

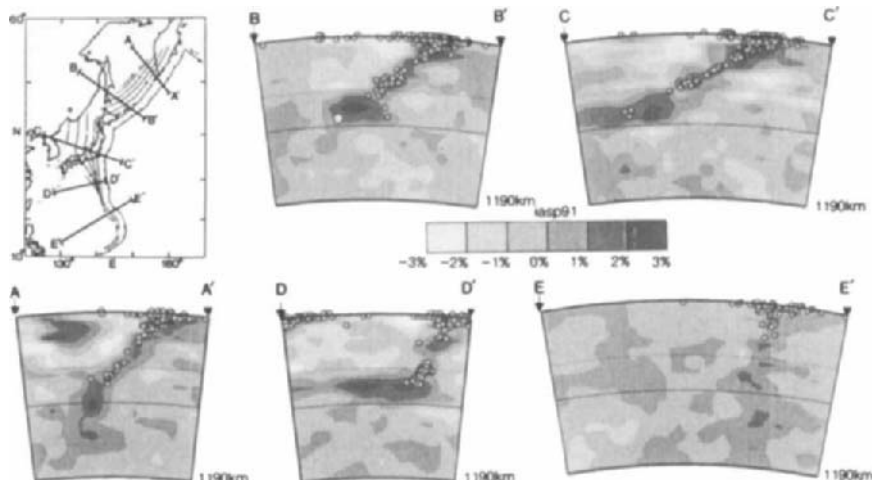


Fig. 26. Cross sections through three-dimensional tomographic P wave velocity models for western Pacific subduction zones. The seismic zone in the map is contoured in 100-km intervals. Faster velocity material (relative to the reference iasp91 model) is darker, with shading in 1% velocity variations. Dots are earthquake hypocenters along each of the cross sections. Mantle discontinuities at depths of 410 and 660 km are shown. Note that high-velocity material correlates with the deep seismic zones and shows evidence for both penetration (AA',EE') and flattening (CC',DD') at the top of the lower mantle. Reprinted with permission from van der Hilst *et al.* (1991, 1993).

be some convergence in the tomographic imaging of velocity structure in the vicinity of the western Pacific deep slabs.

4.2. Southwest Pacific

The subduction zones of the southwest Pacific are less extensively studied than those to the northwest, mainly due to more limited seismic coverage at both regional and teleseismic distances. However, the complexity of these regions, including uncertain geometry of both ancient and present slabs, makes the tomographic models quite important for understanding the subduction process in this region.

4.2.1. *Tonga–Kermadec–New Zealand*

There have been several tomographic inversions of the Tonga–Kermadec convergent zone. Miyatake and Hirahara (1989a) performed block tomography inversion for Tonga using the method of Hirahara (1988), but have not yet published any details. Zhou (1990a) performed a P velocity inversion for a broad region including Tonga–Kermadec, New Zealand, and the New Hebrides. He used 3220 events deeper than 80 km with 201,745 P arrival times from the ISC Bulletin for 1964–1982. Summary rays were formed to reduce this to 953 events and 82,518 average times. Stations corrections and aspherical model path corrections for the structures of Clayton and Comer (1983) and Zhou and Clayton (1990) were used to reduce distant propagation effects. An iterative relocation and velocity inversion method was used, with two-dimensional raytracing being used for paths within the model for each iteration. The final block model has $1^\circ \times 1^\circ \times 50$ km blocks. Impulse tests indicate that only 50% of the anomaly amplitudes are recovered. The model shows low velocities, 5% slow, in the back arc of Tonga down to depths of 300 km, while the Tonga slab has high velocities that decrease in amplitude with depth, vanishing near 550 km. There is a region with about 1.5% high velocity from 800 to 1000 km deep, along the down-dip extension of the Tonga slab, but this is not continuous along strike. The New Zealand slab has high-velocity material down to 500–550 km depth, while the Kermadec high-velocity zone appears to flatten near the base of the upper mantle.

The relationship of 776 earthquake focal mechanisms, mainly from the Harvard CMT catalog, to the tomographic images for Tonga–Kermadec and the northwest Pacific slabs was explored by Zhou (1990b). He observes that in general the fast slab anomalies align with the deep compressional stress axes. The slab models are not sufficiently well resolved to detect any internal slab structure related to the transition from tensional to compressional down-dip stress orientation. Zhou (1990b) argues that apparent fingering of some slab structures

is associated with rotation of the deep event compressional axes toward more horizontal orientations.

The shallow three-dimensional P velocity structure under North Island, New Zealand was studied by Spencer and Gubbins (1980), Robinson (1983, 1986), and Kuge and Satake (1987), and Satake and Hashida (1989) inverted intensity observations for the three-dimensional Q structure in the region. Spencer and Gubbins (1980) assumed an *a priori* slab model and used ISC travel times at local stations from 56 earthquakes to position the slab and to estimate its velocity structure along with simultaneously determining the earthquake locations. This was one of the first joint slab structure–earthquake location tomographic inversions using a parameterized form of the slab (rather than blocks). The slab model was specified by five parameters giving the orientation and slowness contrast of the slab. The amplitude of the slab anomaly found in several inversions was 8–8.6%, but the inversions could not determine the width of the slab or how the velocity anomaly varies with depth.

Robinson (1986) also obtained a three-dimensional velocity model by simultaneous inversion of P and S arrival times from 129 local events for velocity structure and hypocenters, extending an earlier study (Robinson, 1983). The model was parameterized as a horizontally segmented layered crustal model overlying a dipping slab structure with uniform velocity internal layers, extending to 60 km depth. Approximate raytracing was used and a constant V_p/V_s ratio was assumed. The position of the dipping plate boundary was iteratively determined. The slab structure has a crustal velocity of 6.75 km/s overlying deeper layers with 7.82, 8.17, and 8.68 km/s and shows some evidence for a tear between northern and southern regions with different dip. The very high lower slab velocities of 8.68 km/s were poorly resolved. Along-strike observations of P waves from events in the crust of the Pacific plate subducting under North Island, New Zealand also indicate very high internal velocities in the slab, 8.8–9.0 km/s (Galea, 1992). The fast material appears to be located either at the base of the crust or about 12 km deeper, and the high velocities are comparable to the high Pn velocities found in southeast North Island by Kayal and Smith (1984). The P waves show a high-frequency initial phase with a small, long-period precursor, followed by a secondary arrival 4 s later. Three-dimensional raytracing with a curved slab geometry indicates that it is difficult to explain the data with internal slab velocities less than 8.8 km/s, with the initial arrival being associated with a head wave along the internal boundary in the slab.

The velocity inversion by Kuge and Satake (1987) used 513 local arrival times at 15 stations for 67 events and a model with $90 \times 90 \times 30\text{--}50 \text{ km}^3$ blocks extending down to 256 km in five layers. Simultaneous inversion for structure and earthquake locations was performed, and the grid was shifted to explore stability. The inversion shows evidence for a slab steeply dipping under North Island in the northeast and gently dipping in the southwest, also consistent with

the existence of a tear in the slab. Comparison with the Q inversion of Satake and Hashida (1989) shows that high Q and high velocity are correlated in the depth range 30–80 km in southeast North Island, there being <5% velocity perturbations on average. At depths from 80 to 130 km the slab velocity variations range from 2 to 12%, with some correlation between velocity and Q variations. Kuge and Satake (1987) estimate that the slab velocity anomaly is mostly about 5%, with localized regions having anomalies up to 10%.

4.2.2. *New Hebrides, Solomon Islands, New Britain*

The complex tectonic history of the convergent zones lying between Tonga and Indonesia, where there have been reversals of subduction direction and collisions of island arcs with oceanic plateaus and continental crust, makes these regions of particular interest for tomographic studies. Goula and Pascal (1979) performed a block inversion for shear velocity structure on the convex side of the slab subducting in the New Hebrides trench. Travel times of outgoing teleseismic S waves were measured for 30 shallow and intermediate-depth events at 11 teleseismic stations using long-period recordings. Deep earthquakes in Tonga and the New Hebrides were used to compute station/path corrections. They found two zones of low shear velocity, 5–10% lower than the J–B model between 150 and 350 km, one near the central part of the arc below the d'Entrecasteaux fracture zone, the other at the southern end of the arc below the Loyalty Islands. Variations in attenuation of pP phases traversing the region were measured or taken from Barazangi *et al.* (1975), and paths with strong attenuation were found to correlate with the low-velocity regions. This heterogeneity on the seaward side of the plate cautions against interpreting all observed velocity contrasts as resulting from slab or wedge variations.

Taniyama *et al.* (1990) studied the upper mantle structure beneath the New Hebrides using the inversion method of Hirahara (1988). The model extended to 1200 km depth, with a 20° (longitude) by 40° (latitude) region. The effectiveness of suppressing distant effects by removing an average residual for teleseismic stations was examined. This appears to work fairly well, based on comparisons of the mean residuals with calculations through three-dimensional aspherical structures. Details of the model have not yet been published. Zhou (1990a) included the New Hebrides in his inversion, finding that the slab is not defined as a continuous high-velocity region. He observed relatively low velocities in regions that are gaps in seismicity. A more localized tomographic study in this arc was conducted by Prévot *et al.* (1991). One-dimensional and three-dimensional P and S velocity models were obtained for the region from 15 to 20°S, extending to a depth of 250 km. The one-dimensional modeling reveals the presence of a low-velocity zone from 75 to 100 km deep, with velocities about 9% low. Local data from 27 land stations and 8 OBS stations for the years 1978–1988 were com-

bined with regional ISC data from 38 stations out to 40° distance, to provide 35,816 P travel times and 29,014 S travel times from 4181 events. The method of Roecker (1982) and Abers and Roecker (1991) was used in the inversion, with blocks in the shallow layers being adjusted to accommodate *a priori* information about crustal structure. The model reveals a somewhat patchy high-velocity slab structure, with a low-velocity zone corresponding to a seismic gap in the central portion of the arc. This region has P velocities as low as 7.6–7.8 km/s in the slab from depths of 170–270 km, in contrast to surrounding mantle velocities of 8.1–8.3 km/s (see Table 1). This zone was found to have strong attenuation by Marthelot *et al.* (1985) (see Section 3.1), and it was suggested that a strong thermal anomaly of about 750°C is located in the slab. The slab contrast with the underlying mantle was found to be weak.

Abers and Roecker (1991) performed a block inversion for P and S wave velocity structure in the region of the New Guinea arc–continental collision zone. Their data base included 10,961 ISC arrival times (with 2081 repicked times) from regional stations recording 957 earthquakes between 1967 and 1984. The method of Aki and Lee (1976) was followed in a joint inversion for locations and seismic velocities in constant-velocity polyhedra. The model was used to relocate 1916 events in the region, with the number of events satisfying the selection criteria being doubled by the use of the improved velocity model. The relocated events define a vertical zone from 125 to 250 km depth under northern New Guinea which appears to be continuous with the New Britain arc seismicity rather than with a narrow zone of seismicity that extends along the Papuan peninsula. The crustal heterogeneity in the region appears to dominate the seismic travel time variations, with mantle heterogeneity models reducing variance in the inversions by only 10%, while crustal variations account for 40%. A region of 1–4% low P velocities at depths of 35–171 km beneath the Bismarck Sea indicates typical wedge heterogeneity. Maximum travel time contrasts between the wedge and plates are 3.5–4% at depths from 71 to 271 km under New Britain and 6–13% at depths of 35–171 km beneath New Guinea. The high-velocity zones appear to offset from the deep seismic zones as indicated for some other regions, but the spatial resolution of the mantle heterogeneity is not good enough to demonstrate this convincingly or to define the sharpness of the plate boundaries. The structure at depths greater than 371 km is poorly resolved due to inadequate ray coverage.

4.2.3. Taiwan, Indonesia, Philippines

The three-dimensional velocity structure under Taiwan was analyzed by Roecker *et al.* (1987). They studied P and S wave travel times from 1260 events using the method of Roecker (1982). An approximate raytracing method was used in the inversion. The velocity model shows evidence for subduction of

Eurasian crust under Taiwan in a 6–16-km-thick zone of low velocities extending to 50 km depth. There is also a 1–2% fast velocity feature associated with the Philippine Sea plate which subducts in the Ryukyu trench. The earthquakes appear to be located in the slightly slow upper region of this slab.

The Indonesian region is one of the more tectonically complex convergent zones, and slab tomography is useful for studying the distorted slab structures. Puspito *et al.* (1993) developed a P wave tomography model beneath Indonesia, based on inversion of 118,203 ISC P wave times for local and teleseismic events. They used the inversion method of Hirahara (1988). The model extends from 15°S to 15°N and 90 to 140°E and from 0 to 1200 km in depth, with 25 layers and 0.5° × 0.5° blocks. 2268 local events and 1247 teleseismic events were studied. Mean anomalies to teleseismic stations were used to reduce deep mantle and receiver effects. The geometry is somewhat limited, but fast velocity features corresponding to the deep seismic zones are clearly imaged in the model. The results show the high-velocity zone along the Philippine Sea plate extending down to about 450 km, 200 km beyond the maximum depth of seismicity. The eastward-dipping Molucca Sea slab can be traced down to about 400 km, while the westward-dipping slab may penetrate to the lower mantle. A high-velocity region that trends NE–SW beneath the Molucca Sea may represent a slab remnant. The Indian slab appears to extend to about 300 km in the Andaman–Sumatra region and has a continuous fast velocity structure down to the deepest seismicity, with an apparent aseismic extension to about 900 km depth. This roughly corresponds to the fast velocity region found in the model of Fukao *et al.* (1992) from 800 to 1200 km deep beneath Borneo.

4.3. South America, Central America, and the Caribbean

A large-scale inversion for shear velocity heterogeneity under North America was performed by Grand (1987). This model, based on long-period S and SS travel times, provides fairly poor resolution of upper mantle slabs (blocks have 500 km dimensions) but did provide evidence for a roughly tabular high-velocity structure at depths from 700 to 1700 km below the southeastern United States and the Caribbean. The southern portion of this structure corresponds to the anomaly studied by Jordan and Lynn (1974) and Lay (1983). Further development of this model (Grand, in preparation) shows a strong high-velocity anomaly under western South America extending from 700 to 1200 km depth, which also appears to have a roughly tabular structure aligned in the north–south direction. This feature has been attributed to the lower mantle expression of the subducted Farallon slab.

One of the few high-resolution tomographic imaging studies in South America was performed by Cunningham *et al.* (1986). P and S wave arrival times from

microearthquakes recorded by an 18-station regional array deployed in 1981 were used to image shallow mantle and crustal structure in southern Peru above the transition in easterly dip of the Nazca plate from nearly horizontal toward the north to near 30° toward the south. The model extended to 190 km in eight layers but mainly provides coverage of the wedge above the slab. Crustal thickening from 40 to 70 km was indicated between the coast and the Cordillera Occidental, with low shear velocities in the depth range 70 to 130 km above the 30° dipping portion of the slab. Whitman *et al.* (1992) have examined patterns of high-frequency seismic wave attenuation under the central Andean plateau. High- and low-Q regions in the upper plate and wedge were mapped in three dimensions, with a thin low-Q region just above the slab (similar to Sack and Okada, 1974) or a variable asthenospheric window being proposed to vary along the arc from north to south.

High-resolution tomographic inversion for the structure under the Caribbean was performed by van der Hilst and Spakman (1987, 1989), van der Hilst (1990), and van der Hilst and Engdahl (1991). The studies of van der Hilst and Spakman (1987, 1989) used ISC data to invert for three-dimensional P wave velocity structure to a depth of 1300 km. These models revealed the high-velocity extension of the Lesser Antilles slab to a depth of 600–650 km. Sensitivity to the one-dimensional reference structure was documented in this inversion, by comparison of inversions using the J–B model versus a model with discontinuities at 390 and 660 km. It was shown that nonlinear effects are important for this inversion, and apparent flattening of the deep Lesser Antilles slab in the J–B model inversion is eliminated in the inversion using a reference model with transition zone discontinuities. These images suggest that the deep Central America slab broadens and extends to 1400 km, connecting up to the shear wave anomaly in the model of Grand (1987).

To improve the data coverage for this inversion, van der Hilst (1990) and van der Hilst and Engdahl (1991) included pP and PP data in the inversion. They used only earthquakes located within the model but stations both within and outside the model. The 15-layer block model has $1.25^\circ \times 1.25^\circ \times 33\text{--}225$ km blocks extending to 1325 km depth. 650,000 arrival times from ISC and NEIC catalogs, along with some hand-measured PP data, were combined into 331,273 composite rays. Relocations were performed prior to solving for the model parameters, which included station corrections to account for distant propagation effects. Inclusion of the pP and PP data provides better source depth constraints as well as raypath coverage at angles oblique to the P waves. This appears to affect mainly the resolution of shallow mantle structure. Still, the model is poorly resolved above 33 km depth, and from 33 to 185 km only patchy slab structures are visible in the Lesser Antilles, northern South America, and Central America. From 185 to 470 km the main high-velocity feature is a continuous ring from the Lesser Antilles to northern South America, and at greater depths a high-velocity

band from Central America to South America develops as the Lesser Antilles feature weakens. From 660 to 760 km the north-south high-velocity band is about 1.5–2.5% fast, and it weakens and broadens as it extends to 1325 km (Fig. 27). Tests with harmonic patterns indicate 60–80% recovery of anomaly amplitudes, so actual heterogeneity in the upper portion of the lower mantle is quite strong. The agreement of the P tomography with the S velocity model of Grand (1987) is best in the range 760–1000 km, but there are rather poor correlations between the models in the upper mantle. van der Hilst (1990) discusses the tomographic images in the context of a model in which the Caribbean plate underthrusts northern South America, but there is also a broad high-velocity structure extending northward from Venezuela under the central Caribbean.

4.4. Cascadia, Aleutians, and Alaska

The lithospheric structure of northern California was explored by P wave tomography using recordings of 120 earthquakes recorded by the U.S. Geological Survey California seismic network in a study by Benz *et al.* (1992). Strong P wave velocity variations were found in the depth range 30–100 km, with velocities ranging from −5.5% to +9.5%. The Gorda plate has about 9% fast anomalies above 100 km, and on average 5–6% fast velocity from 100 to 250 km. It

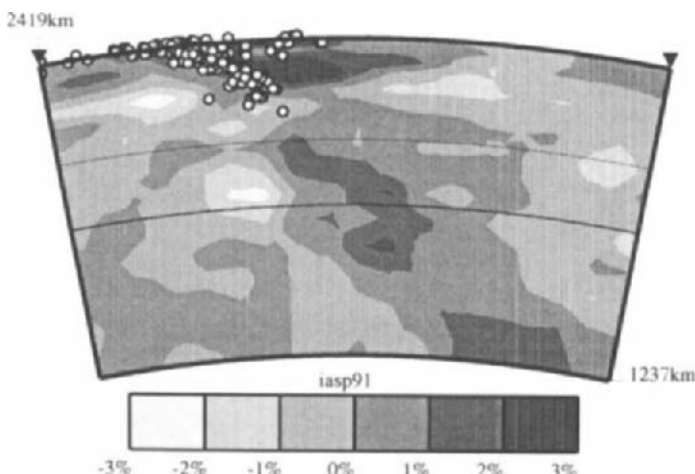


Fig. 27. Cross section through a three-dimensional tomographic P wave velocity model for the Middle American trench and Caribbean. The plot has the same conventions as in Fig. 26, with the fast velocity region suggesting a slab dipping toward the east, extending downward from the seismicity. The fast region below 1000 km is centered under the Caribbean, in a region where both P and S velocities are fast. From van der Hilst, personal communication (1993).

dips at about 70° below 100 km depth. A 9% high-velocity structure observed near the northern Great Valley and south of the current slab location was inferred to correspond to a detached segment of the Gorda plate. Two-dimensional raytracing was used to confirm the basic features of the tomographic model. It appears that the main Gorda plate extends to 100–150 km depth below Mount Shasta and Mount Lassen, with a narrow, possibly detached tongue extending to 250 km. A low-velocity region under the northern Coast Ranges is associated with the slabless window. Zandt and Carrigan (1993) have performed thermal calculations and convection modeling to explain some of the general features in the tomographic image beneath California. They argue for time-dependent small-scale convection associated with the tectonic disruption of the upper mantle, as the Gorda plate is displaced toward the north.

The mantle velocity structure beneath Washington and Oregon has been studied to determine the fate of the Juan de Fuca plate ever since McKenzie and Julian (1971) performed a residual sphere analysis in the region. Iyer and Rite (1981) and Iyer *et al.* (1982) studied teleseismic P residuals under the northern and central Oregon Cascades, finding evidence for a steeply dipping (60°) high-velocity body extending to 220 km depth. Three-dimensional inversion of teleseismic P wave residuals beneath Washington and northern Oregon was performed by Michaelson and Weaver (1986). They analyzed 4160 relative residuals from 67 events at 104 stations using the method of Aki *et al.* (1977), imaging the structure to 300 km depth in $50 \times 50 \times 50$ km 3 blocks. The residuals range over only 1.8 s but show azimuthal patterns as strong as 2.6 s. The model shows evidence for the Juan de Fuca plate dipping 45° to the ENE beneath the central Cascades, with 5% velocity anomaly, while the dip is $65\text{--}70^\circ$ toward the east under Oregon, with 3–4% velocity anomaly. Under the northern Cascades the slab heterogeneity is 6–8%, with 45° dip. The imaged structure is not particularly tabular, but some high-velocity material does extend from 45–300 km depth. Two-dimensional raytracing was performed with slab models with laterally varying crust to confirm the basic model features. Detachment of the slab was suggested to explain the model under northern Oregon.

Additional P tomography beneath the Cascades was performed by Rasmussen and Humphreys (1988). They used 4900 relative residuals from 100 teleseismic earthquakes to invert for an 11-layer block model with $30 \times 30 \times 50$ km 3 blocks extending to 400 km depth. Their model shows evidence of a 60–120-km-wide slab with 2–3% fast velocities dipping 65° to the east extending to 150 km under northern Oregon and to 300 km under southern Washington. Inversions of synthetic data sets indicate 60% amplitude recovery for the steep slab geometry, with the lack of raytracing probably partly responsible for underestimating the heterogeneity. Harris *et al.* (1991) used data from a 366-km-long seismic array deployed in southern Oregon in 1982 to image the Juan de Fuca slab. They used 434 relative residuals from 35 events in a two-dimensional (long block) model

using the method of Aki *et al.* (1977). Their images are not very compelling, with strong streaking artifacts, but there is weak evidence for a 3–4% fast high-velocity zone dipping 65° toward the east, extending to 200 km depth. Some low-velocity regions were found in the wedge as well.

An iterative, nonlinear travel time inversion was performed for the Cascadia subduction zone using arrival times from the Washington Regional Seismic Network (WRSN) by VanDecar (1991). P velocity perturbations to a depth of 500 km were obtained, with nonlinearity associated with ray bending being accounted for by updating raypaths and travel time partial derivatives in each step. The raypaths became stable after three iterations. The model shows a clear high-velocity tabular structure, presumably the Juan de Fuca plate, with 3 to 4% fast velocities, extending from 50 to about 300 km depth. The same nonlinear algorithm was applied by Neele *et al.* (1993) in a simultaneous inversion of P wave travel times and amplitudes recorded by the WRSN. Using the model of VanDecar (1991) as a starting model, to stabilize the nonlinear sensitivity of the amplitudes to the velocity structure, it was found that inversion with a carefully processed set of amplitude anomalies added little constraint to the tomographic images, largely due to the small size and high variance of the amplitude data and the ability of very small short-scale slowness perturbations to account for the amplitude fluctuations. The disparate sensitivity of travel time and amplitude data to the slab velocity structure was confirmed by inversion of synthetic data sets. The amplitude data were used to confirm the basic characteristics of the model of VanDecar (1991) by simple forward comparisons.

The upper mantle velocity structure of the northern Cascadia arc was studied by Zhao *et al.* (1992c), who inverted 32,876 P arrival times and 20,525 S arrival times from 3174 earthquakes recorded by the Geological Survey of Canada. They used the raytracing inversion method of Zhao (1991), finding some evidence for the subducted slab extending northward from central Washington. Kissling and Lahr (1991) analyzed the P velocity structure of the Alaskan subduction zone using 110,000 arrival times from 4,928 earthquakes. They found a 5% fast slab overlain by a tabular zone of 10% reduced velocities. The method of Zhao (1991) was applied to 166,000 P and S wave arrival times from 9327 earthquakes recorded by the Alaskan Earthquake Information Center, in a tomographic study of the Alaskan subduction zone by Christensen *et al.* (1992). High velocities associated with the slab are seen to depths of 200 km. Zhao *et al.* (1993b) have extended this study, using 142,908 P wave arrival times from 12,237 events. They found a 45–55-km-thick Pacific plate 3–6% faster than surrounding mantle.

Tomographic inversions with simultaneous determination of parameterized slab velocity structure and earthquake locations were conducted for the central Aleutians by Spencer and Engdahl (1983) and Engdahl and Gubbins (1987). Spencer and Engdahl (1983) parameterized the slab with cylindrically symmetric structure and used P and S arrivals at local distances and teleseismic P waves in

the joint inversion. The length of the slab was not well resolved, but 7% velocity anomalies were found for a model extending to 334 km depth. Engdahl and Gubbins (1987) extended this effort using 151 central Aleutian events and including teleseismic pP and sP phases corrected for structure at the reflection points to tighten source depth control. A total of 15,565 arrival times from the ISC and local reports were used, with azimuthally dependent station corrections of Dziewonski and Anderson (1983) being used to correct for distant path effects. The parameterized slab model was two-dimensional (cylindrically symmetric), and no raytracing was used, with iterations being performed on the locations but not on the velocity parameters. The difficulty of such simultaneous inversions is illustrated by the fact that the locations of 37 events had to be fixed to prevent eliminating all of the slab anomaly in the inversion. The results for an 80–100-km-thick slab show 10–11% slab velocity anomalies near 90 km and 4–6% at greater depth, down to 400 km (Fig. 28). The events locate near the upper plane of the high-velocity slab, with a region of low velocity just above the slab giving

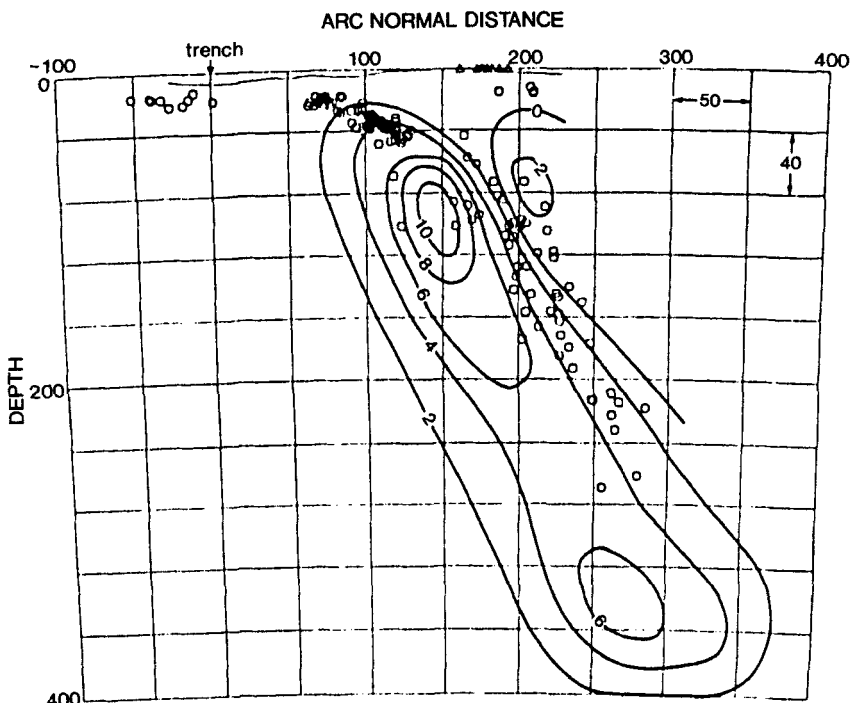


Fig. 28. Cross section through the slab model in the Aleutians obtained by simultaneous inversion for slab structure and earthquake locations. The contours are in 2% velocity anomaly. Note that the seismicity locates in the upper portion of the slab and that there is locally a 10–12% velocity gradient. The maximum depth of the slab is not resolved in this model. Reprinted with permission from Engdahl and Gubbins (1987).

rise to strong contrasts. The depth phases provide important constraints on the structure above and at the top of the slab. The inversion resolves the velocities down to 250 km depth, but not below. The lack of raytracing seems questionable given the strong velocity heterogeneity found in the model. Nakanishi and Yamaguchi (1986) demonstrate with numerical tests that when 5–7% velocity contrasts are involved, use of actual raypaths increases the resolution in tomographic inversions.

4.5. Mediterranean and Hindu Kush

The first large-scale inversion of P velocity structure under Europe was a low-resolution inversion by Romanowicz (1980). This inversion of ISC data extended down to 700 km and revealed the presence of some fast velocities north of the Mediterranean where slabs have been subducted, but the large block size ($4^\circ \times 4^\circ$ and $5^\circ \times 5^\circ$) precluded resolving any slab structures. Hovland and Husebye (1981) inverted a four-layer model for P velocity perturbations in the upper 600 km of the mantle below France, Germany, and northern Italy, and Hovland and Husebye (1982) extended the model to the Aegean. Some high-velocity regions are seen extending to 550 km depth, but these were not associated with any dipping slab structures. Waveform inversion of scattered surface waves by Snieder (1988) also produced low-resolution shear velocity models across Europe, with some high S wave velocities below Greece, the Adriatic, and northern Italy. Further analysis of large-scale shear velocity structure under Europe by waveform and travel time inversion was performed by Zielhuis (1992). A large-scale P wave velocity inversion extending to 1200 km beneath Europe and the Mediterranean was performed by Granet and Trampert (1989), using 10,890 teleseismic arrival times collected by the Euro-Mediterranean Seismological Center. They used the SIRT algorithm, a row-action inversion procedure introduced to global tomography by Clayton and Comer (1983). A central volume of the model with a $3^\circ \times 3^\circ$ grid was used throughout western Europe. The images show some evidence for high velocities beneath the Hellenic trench, with a possible detachment of the slab at a depth of 250 km.

Higher-resolution models were produced for the Mediterranean by Spakman (1986a,b). Using an extensive model with $1^\circ \times 1^\circ \times 33\text{--}130$ km blocks in nine layers extending down to 670 km, Spakman (1986a,b) inverted 550,000 P wave arrival times for structure under Europe, the Middle East, and the Mediterranean. These models provided the first strong indication of extensive subduction in the Aegean and Tyrrhenian arcs, with evidence of high-velocity lithosphere at depths of 250–600 km extending from Spain to Iran. Using the conjugate gradient (LSQR) row-action inversion method described by Nolet (1985), the inversions provide fairly good resolution in the upper portions of the 9360-block

model. A broad high-velocity zone, 250 km wide is imaged dipping northward under the Aegean Sea, and a broad fast region is found from 200 to 500 km under Italy. A poorly resolved structure is apparent under Spain as well. Spakman (1988, 1990, 1991), Spakman and Nolet (1988), and Spakman *et al.* (1988) refined these inversions, using 480,000 ISC arrival time measurements, and compared the LSQR and SIRT algorithms, leading to a preference for the former. Spakman (1988) emphasizes the important point that the residuals going into such inversions are the "numerical waste" resulting from the location process, and hence it is difficult to produce accurate models of the interior. To suppress contributions from outside the model space independent station corrections were applied to about one third of the data, with additional station corrections being determined in the modeling. A total of 20,069 unknowns were solved for, including the event relocation parameters. Random permutation of the data and block model resolution tests were used to explore the stability of the inversions. These tests indicated that only 30–40% of the input amplitude is recovered even in the noise-free case; thus the $\pm 1^\circ$ anomalies in the final models are poor estimates of actual slab heterogeneity. The resulting model indicates a rather continuous Aegean slab, extending to 600 km, about 400 km deeper than the seismicity. Spakman *et al.* (1988) and Wortel *et al.* (1990) infer subduction for a duration of 26–40 My, much greater than prior estimates of 5–13 My for closing of the Tethys. It is disturbing that the structure follows the pattern of cell hit counts. A low-velocity zone under Greece suggests detachment of the slab in that region near 200 km depth. Blanco and Spakman (1993) further investigate the north-dipping high-velocity zone under Spain, relating it to the isolated region of deep earthquake activity. They developed a model extending to 1400 km and found a 1.5–2% fast slablike structure dipping steeply beneath the Iberian peninsula.

A tomographic model for the Europe–Mediterranean region extending down to 1400 km depth was obtained by Spakman *et al.* (1993). This study incorporated teleseismic signals, with a source term being estimated to eliminate distant path effects, and used ISC data from 1964 to 1987, with about 1.7 million times from about 60,000 events and 2259 stations. A regional reference model with mantle discontinuities at 405 and 670 km depth was used, and the model involved 49,600 cells $0.8^\circ \times 0.8^\circ \times 33\text{--}100$ km. Significant differences are seen in models using the J–B and the regional reference model, indicating that raypath effects are important. A broad lower mantle extension of high-velocity material down-dip of the Aegean slab is apparently resolved in this inversion, and it is suggested that the slab may extend down to 800–900 km. In the less well-resolved region under Spain, the high-velocity structure extends from 150 to 670 km, with somewhat less vertical smearing of high velocities into the lower mantle. Under Italy, high-velocity material extends in a broad structure from 150 to 400 km depth. A broad zone of fast material extends to about 1000 km depth below the northern Alps, but the exact relationship of this to subducted plate

material is uncertain. Wortel and Spakman (1992) considered the evolution of the Mediterranean and used these tomographic images to infer a complex subduction history and an intriguing tearing and detachment of aseismic slab extensions.

In addition to large-scale tomographic inversions of the Mediterranean region, smaller-scale inversions for shallow structure have been performed. Scarpa (1982) inverted for velocity structure under Italy, finding high velocities from 200 to 500 km in the Tyrrhenian region. Oncescu (1984) made a three-dimensional P wave velocity model below the Carpathian arc. Amato *et al.* (1993) have performed teleseismic arrival tomography under Italy, providing better resolution of this structure. Early work on the Aegean slab was performed using teleseismic travel time patterns by Agarwal *et al.* (1976) and Gregerson (1977), who observed 1–2 s fast arrivals for paths sampling the mantle below Rhodes and Crete. Gregerson (1977) used outgoing P waves, recorded in Greenland, which he found to be about 2 s fast. Assuming a slab model 100 km thick extending from 50 to 250 km depth, he estimated a slab velocity anomaly of 6–7%. Incoming teleseismic arrivals at stations in the Aegean showed Rhodes and Crete to overlie fast mantle, with 1–2 s early arrivals (Agarwal *et al.* 1976), which again was interpreted as evidence for a slab from 5 to 15% higher velocity, depending on the depth extent of the slab.

Additional tomographic inversions in the Aegean region were performed by Christodoulou and Hatzfeld (1988), who studied the structure beneath northern Greece, and by Ligdas *et al.* (1990). The latter study inverted for three-dimensional structure under the Aegean using 5000 teleseismic and local P wave travel times. The model was divided into $1^\circ \times 1^\circ \times 33\text{--}100$ km cells with 10 layers extending to 600 km depth. As in the study of Spakman *et al.* (1988), a continuous high-velocity region was found, extending down-dip and curving around the Hellenic trench. Strong heterogeneity was found in the lithosphere above 100 km depth, with low velocities under the Aegean Sea. Ligdas and Main (1991) performed synthetic simulations with input slab structure to assess vertical resolution in this tomographic model. Some artificial stretching of the high velocities was found, by as much as a factor of 2 down-dip, so it is unclear how far below 200 km the Aegean slab extends, but the simulations with a slab extending only to 280 km do not predict the observed peaking of anomalies near 480 km depth. Drakatos and Drakopoulos (1991) applied a block inversion to 3973 regional travel time residuals at 62 stations from 166 earthquakes in the Aegean region. Their images also indicate the presence of the high-velocity plate dipping northward along the Hellenic arc and low velocities under the Aegean Sea. These velocity inversions show some similarities to the tomographic inversion of seismic intensity data in the same region by Hashida *et al.* (1988). The latter study found low Q in the upper 40 km beneath the Aegean, with high Q in the surrounding arcs, particularly under Crete where the African plate is subducting.

The convergent zone between India and Eurasia has been investigated in

several tomographic studies, but slab structure in the area is hard to determine because of the thick overlying crust. Roecker (1982) analyzed 8800 P and S arrival times from 580 earthquakes in the Pamir–Hindu Kush region, determining one- and three-dimensional structures for the upper 230 km. The three-dimensional inversions indicate 10% low-velocity regions at depths from 70 to 150 km, which Roecker (1982) associates with large quantities of subducted crust. He used a simultaneous source location and velocity model inversion, with a parameter separation and progressive inversion method. This resulted in confidence that the earthquakes are actually located in relatively low-velocity material, which he interpreted as eclogitic continental crustal material. Ni *et al.* (1991) used the same method to invert for three-dimensional P and S velocity structure in the western Hazara arc of Pakistan. This inversion was performed for only the upper 36 km, using 2699 P and 1478 S times read from 15 vertical component stations. The model indicates a shallow dipping Indian plate with a 6.0 km/s crust in the area. A 14-km-deep detachment surface was inferred to be the thrust contact.

5. SLAB BOUNDARIES: CONVERTED AND REFLECTED PHASES

The constraints on slab velocity structure provided by tomography and residual sphere modeling discussed in the last two sections are limited to measures of the gross volumetric heterogeneity of the slab. Even if detailed thermal models are specified, as in residual sphere modeling, the travel time information simply does not provide resolution of the detailed structure (e.g., velocity gradients at the upper side of the slab), and one must be cautious about the apparent resolution of the resulting models. Trade-offs with source locations and intrinsic effects of tomographic imaging procedures generally lead to underprediction of the actual heterogeneity. More detailed characterization of slab velocity structure is needed for separation of the thermal, chemical, and mineral phase equilibria contributions to the seismic heterogeneity. This is attained primarily by analysis of velocity gradients and discontinuities within and at the surface of the slab, using phases reflected and converted at these boundaries. This provides localized, high-resolution information about the slab velocity structure which can then be interpreted in the context of models for the chemical and thermal state of the slab. In addition, it is important to consider the relationship of the structure to the intraplate seismicity, to understand the mechanical properties of the slab.

5.1. Slab Seismicity and Double Benioff Zones

The interpretation of converted and reflected phases associated with subducting slabs often requires knowledge of the relationship of the slab boundaries to

the slab seismicity. In some deep zones the seismicity defines a very thin single layer, as discussed in Section 2.1, usually located in the upper portion of the slab velocity anomaly imaged by tomography (Section 4). An important feature of intermediate-depth seismicity is that it sometimes occurs in two spatially offset planes, called a double Benioff zone, with the upper plane being very near the top of the slab. Detection of double zones requires accurate event locations, which delayed the recognition of these structures. Sykes (1966) noted the presence of two intermediate-depth zones 30 km apart in the Kurils but did not have very precise locations. In Japan, Tsumura (1973) was the first to discuss the double Benioff zone under Kanto, and Umino and Hasegawa (1975) first reported a double plane in Tohoku.

Subsequent work by Hasegawa *et al.* (1978a,b) has provided detailed characterization of the double zone under Tohoku, using microearthquake hypocenters and composite focal mechanisms (Fig. 29). In this region the planes are 30 to 40 km apart, with composite focal mechanisms for events in the upper plane having primarily reverse faulting, some with down-dip compressional orientation, while the lower plane has down-dip extensional stress. The double zone begins by 70 km depth and the two planes merge by 175–200 km depth. Below that depth the seismic zone is very thin, on the order of 10 km. A 200 × 300 km region shows the two zones clearly. Yoshii (1977, 1979) examined the same region using pP data from the ISC catalog and found two layers at depths from 80 to 150 km, which he attributed to sagging or unbending of the slab. In Hokkaido the double planes are 25–30 km apart in the depth range 80–150 km (Suzuki *et al.*, 1983), and a double zone is also found under Kyushu (Ishikawa, 1985).

Using the improved location accuracy provided by spatially varying source

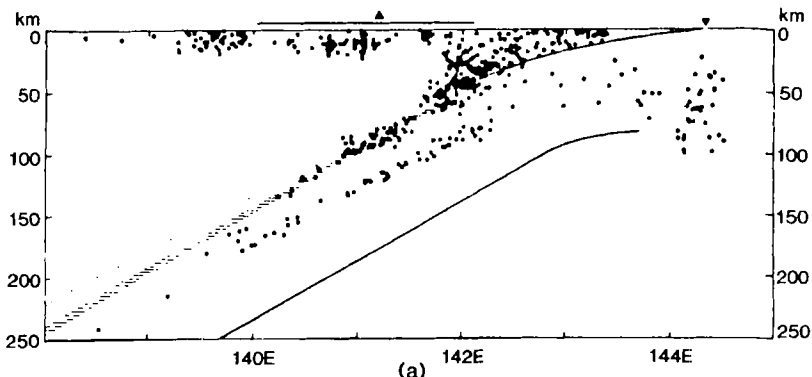


Fig. 29. Cross section through the Japan slab under Tohoku, Japan, showing the presence of the double seismic zone. The hatched region indicates the position of the surface where SeSp phases convert, presumably at the top boundary of the slab. Reprinted with permission from Hasegawa *et al.* (1987b).

and receiver anomaly parameters, Veith (1974) improved the resolution of the double zone in the Kuril slab. He found evidence for the upper zone having compressional down-dip mechanisms. The lower zone is about 30 km deeper and extends over the depth range 70–200 km. Veith suggested extreme elevation of the olivine–spinel phase transition to 120 km depth as a mechanism for putting the center of the slab under tension. Kao and Chen (1993, 1994) investigated the development of the double seismic zone in the Kuril–Kamchatka region, in the down-dip and along-strike directions, finding that this feature is not present along the entire slab.

There have been mixed observations of double Benioff zones in other regions. Ansell and Smith (1975) performed accurate relative locations and found that intermediate-depth activity in the slab below New Zealand is confined to a 9-km-wide band with no evidence for a double zone. Engdahl and Scholz (1977) suggested that a double zone exists below Adak, in the Aleutian slab, but the data were not very convincing. Fujita and Kanamori (1981) argue that this apparent double zone was the result of an artifact in projecting the seismicity, and subsequent work by Engdahl and Gubbins (1987) clearly shows that improved locations with a slab model cause this feature to go away. Hasegawa and Sacks (1981) found no evidence for a double zone under Peru, although Isacks and Barazangi (1977) suggested that one is present. Samowitz and Forsyth (1981) relocated events in the Marianas slab using a master event method with spatially varying station corrections and proposed the existence of a double zone on the basis of three events found 30–35 km deeper into the slab, which are separated from a clear upper zone less than 20 km thick with concentrated activity. The deeper events are down-dip tensional, while the upper plane activity is down-dip compressional, and unbending was considered as a possible mechanism. Engdahl and Fujita (1981) consider the Marianas as well, and argue that extreme care must be taken in locating events because of slab effects as well as any station variations. Small variations of event position within the slab can cause several seconds of travel time variation, so it is best to use a slab model when studying double zones.

Isacks and Barazangi (1977) considered seismicity cross sections in many slabs and argued that thickening of the seismic zone at intermediate depth is a manifestation of slab unbending. Unbending of an elastic slab should produce very large stresses in the elastic core of the slab, on the order of 30 kbar, so some other rheology is needed if unbending is invoked to explain the double zone (Sleep, 1979). Following the early suggestion of Smith and Toksöz (1972), Sleep (1979) proposed sagging of the slab under its own weight, with lower support from the transition zone, as a mechanism to produce the double zone. He used his numerical method (Sleep, 1975) to show that sagging does not require huge internal slab stresses. A summary of the global observations of double zones by Fujita and Kanamori (1981) was used as a basis for considering their basic

mechanism. Consideration of 243 focal mechanisms for intermediate-depth events led to a general relationship between intraplate stresses and kinematic characteristics of the slab. The underlying argument is that stress in the slab is controlled in part by the age and rate of convergence, with the extent of in-plate compression increasing with convergence rate or decreasing age, although there is not a simple relationship. Old, slow slabs are tensile, while relatively uncommon old, fast slabs tend to show double Benioff zones. Young and fast slabs are also tensile, an exception to the general trend. Fujita and Kanamori (1981) argue that unbending and phase changes are unlikely to explain double zones, with sagging or thermal effects or possible asthenospheric flow being more likely. A good case is made for double zones being indicative of a state of near stress equilibrium within the slab, a condition which is not often satisfied, giving rise to the variability of double zones.

A double zone in the central Aleutians near the Shumagin Islands was suggested by Reyners and Coles (1982). The upper plane, extending from 45–100 km, has composite focal mechanisms with down-dip tension, contrary to observations in other regions. The lower plane, 25 km deeper, extends from 65 to 125 km. Loading from the overriding plate was suggested as a factor in controlling the intraplate stresses. House and Jacobs (1982) suggest that thermal stresses due to the differential heating of the plate may be responsible for the double zone in the Aleutians, and Goto *et al.* (1985) further show that thermoelastic stresses can be substantial within the plate.

Fitting of a smooth spherical harmonic surface to seismicity distributions was applied by Bevis and Isacks (1984) to search for double zones. The double zone under Tohoku was found to be offset by 33 km in their study, but no double zones were detected under Cook Inlet, Alaska or in southern Peru. No double zone was found under western Argentina, where Smalley and Isacks (1987) analyzed S-P differential times from a local network to locate events in a subhorizontal segment of the Nazca plate. They found a zone 107 ± 5 km deep, with 90% of the events in a 12-km-wide band, and noted that there are other regions where a single plane of seismicity is observed. Comte and Suárez (1994) found a double seismic zone under Chile, again with tensional events in the upper layer. They suggest that basalt to eclogite phase transition plays a role in the local stress state.

A clear double zone is apparent under New Zealand at shallow depths of 50–80 km for events located in a slab model (Robinson, 1986). Kawakatsu (1985, 1986b) made a careful study of earthquake mechanisms in the Tonga region, which previously was generally assumed to be primarily in down-dip compression at intermediate depths (e.g., Billington, 1980; Fujita and Kanamori, 1981), and found that tensional events do exist and they tend to be deeper within the slab. The evidence for a double zone is not uniform along the trench, and there are complications due to contorted geometry of the northern Tonga slab and subduction of the Louisville Ridge in central Tonga, but there is fair evidence for

a double zone in some regions. The locations were determined using a method similar to that of Samowitz and Forsyth (1981). Kawakatsu (1986b) estimates that thermoelastic strain rates are too low to account for the double zone, while unbending, sagging, or mantle flow effects are viable. Further modeling (Kawakatsu, 1986a) of the kinematics of a slab confirms that unbending strain rates are large enough to account for the seismic strain rate at intermediate depths in the Tonga slab obtained by summing the seismic moments of events between 1965 and 1983. A plastic–brittle lithosphere model like that of Tsukahara (1980) was used along with thermal modeling of the slab to estimate the strain rate of unbending. It is clear that all slabs do in fact unbend, attaining nearly straight geometries at intermediate depths, so this modeling seems to provide an adequate explanation for double Benioff zone occurrence. Variations in slab thermal and kinematic properties, as well as surrounding mantle flow, may explain the intermittent observation of double zones.

A deeper double Benioff zone may exist within a subducting slab, if the hypothesis of transformational faulting of a kinetically suppressed olivine– β spinel phase transition (Section 1.3) is correct. Phase transition–induced earthquakes occurring along the margins of a tongue of depressed olivine could conceivably occur in a double band at depths from 380 to 660 km. There is some evidence for a double layer of seismicity at these depths revealed by high-resolution relative locations in the Japan slab (Iidaka, personal communication, 1992) and in two locations of the Tonga slab (Wiens *et al.*, 1993). The latter study finds a double zone from 380 to 470 km deep in the northern part of the slab and one from 340 to 420 km deep in the southern part of the slab, both separated by about 30 km. However, no double zones were found in other slabs at this depth in a global reconnaissance by Wiens *et al.* (1993).

5.2. Constraints on Slab Boundaries and Internal Structure

Strong velocity gradients near a subducted slab cause seismic waves to reflect and convert in mode type, just as they do for other discontinuities and gradients in the Earth's interior. The three-dimensional geometry of dipping slabs makes observation and modeling of slab-related conversions and reflections more challenging than for nearly horizontal boundaries. Many raypath geometries have been considered for such boundary interactions, including arrivals incident from below, within, and above the slab (Fig. 30).

5.2.1. *ScSp Conversions: Waves Incident from Below the Slab*

Perhaps one of the first observations of a slab converted phase was by Katsumata (1953), who observed a longitudinally polarized precursor to ScS, strong-

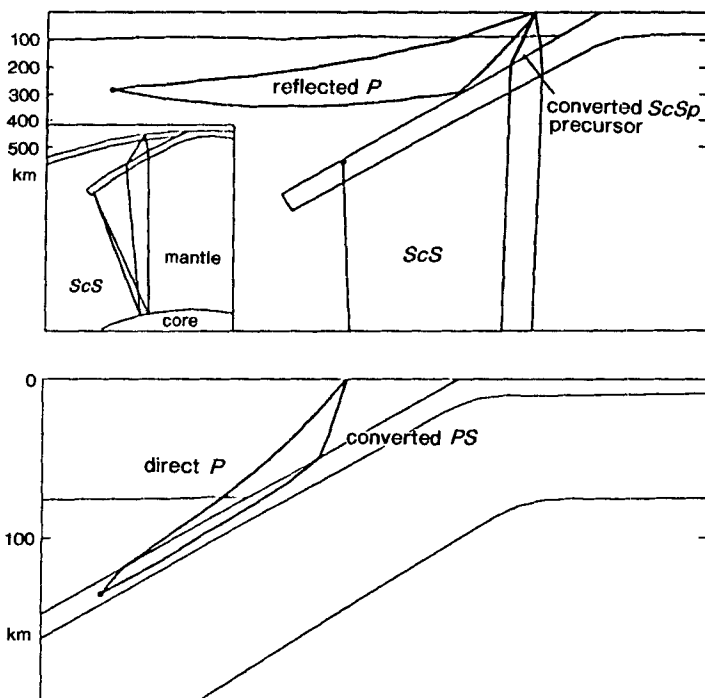


Fig. 30. Examples of raypaths associated with slab boundary interactions for topside, bottomside, and internal reflections and conversions. Reprinted with permission from Helffrich and Stein (1993).

est on the vertical component, for a deep event under Korea observed at Japanese stations. The ScS phase travels downward to the core and then back to the surface, and for stations up-dip from the source and above a slab the wave incident from below can interact with the slab structure. Katsumata (1953) found an 8–10-s precursor time suggesting conversion of the up-going ScS phase near 80 km depth, producing the phase called ScSp. Okada (1971) made further observations of ScSp from deep events at stations in Japan, again finding about 8-s ScS–ScSp differential times. He noted that the polarization direction of the phase corresponds to the dip direction of the slab, supporting the interpretation of the phase as ScSp conversion from near the upper surface of the plate.

Okada (1973, 1977, 1980) pursued analysis of ScSp phases for Japan and South America. A clear indication that these arrivals involve a dipping interface is that they are sometimes very large, with ScSp/ScS ratios of up to 0.5, whereas in other cases the arrivals are very weak. Based on 7.5–21-s ScS–ScSp differential times at 11 stations in Hokkaido, Okada (1973) found evidence for conversions at depths of 80–350 km in the dipping Japan slab. Analysis of observa-

tions at WWSSN stations ARE, LPB, ANT, and NNA in South America resulted in detection of ScSp phases at ARE and NNA, with paths under southern Peru. ScS–ScSp lag times of 10–11 s indicate a boundary 100–250 km deep. No spectral difference was found between ScSp and ScS, and modeling showed that a dip of 30–35° with a sharp velocity contrast of about 5–10% is required to account for the larger ScSp observations. The dip and depth of the boundary are inconsistent with early ideas about a shallow, flat slab in this region (Isacks and Molnar, 1971), and possible detachment or conversion from the bottom of the slab were considered. Stations ANT and LPB did not show ScSp, indicating that geometry is very important for the observation of the phase.

The relationship between double seismic zone seismicity and ScSp conversions was explored by Hasegawa *et al.* (1987b), who performed three-dimensional raytracing through an 80-km-thick slab model with 6% high velocity to constrain the depth of ScSp conversions observed 9.7–14.1 s ahead of ScS under Tohoku. ScSp was not observed in western Honshu. Combined with raytracing relocation of the local microseismicity in the same model, which proved to have little change in the position of the upper plane of seismicity, it was found that conversions occur very close to the upper plane of the double seismic zone. ScSp/ScS amplitude ratios of about 0.2 were observed and explained by the slab model.

Nakanishi (1980) analyzed ScSp phases from seven deep nearby events across Japan. In southwestern Japan he found evidence for arrivals 3 s ahead of ScS under Shikoku, where the slab dips steeply, and 5.3–4.6 s ahead under the Chugoku district of Honshu, presumably converted from the Philippine Sea plate. Using the suggestion of Sacks and Snoker (1977), he modeled the polarity of the arrivals to obtain the velocity contrast, finding that the velocity must decrease with depth, with lower S velocity in the uppermost slab than in the overlying mantle. This is compatible with a subducted crustal layer. A variety of transition zone models for the slab boundary were considered, with second-order discontinuities being used to fit the frequency content and amplitude of the ScSp arrivals. Difficulty was experienced in matching the observed amplitudes, with the preferred model having an asymmetric low-velocity channel in the upper slab with width of 40 km.

Extension of this analysis was presented by Nakanishi *et al.* (1981), with more complete coverage of Japan being provided by four deep events with clear ScSp observations along the entire eastern coast. Using envelopes of the short-period signals to measure ScS–ScSp time differences automatically, evidence was found for conversions from 80 to 350 km deep with the differential time varying from 5 s to more than 30 s. The amplitudes of the ScSp phases decrease toward the west, as found by Hasegawa *et al.* (1978b), with the ratios varying from 1 to 0, decreasing with increasing ScS–ScSp differential time. Using a Q model obtained by Hasegawa *et al.* (1979), the differential attenuation between ScS and

ScSp was estimated, but the lack of systematic difference in predominant period of the two phases relative to the depth to the conversion point suggests that the effect of differences in attenuation are not great. A 30° dipping slab with 5–10% higher slab velocity is needed to match the ScSp/ScS amplitudes for conversions that occur fairly deep in the slab, but the presence of a low-velocity zone near the conversion interface was again inferred from the polarity at stations in easternmost Japan. Sharp transition zones, with widths less than 10 km, were required to match the frequency content of the ScSp phases.

ScSp phases at South American stations were used to define the geometry of the subducting plate by Snook *et al.* (1977), who inferred that 5% boundary velocity contrasts are required to explain observations at ARE and NNA in Peru and PEL in central Chile. The polarity of the conversions is such that the boundary must go from high velocity to low velocity, consistent with up-going conversion at the top of a high-velocity slab. They argue that conversions from a 28–38° dipping boundary near 180 km depth under southern Peru are consistent with the seismicity pattern, contrary to the model of a shallow dipping plate in this area proposed by Isacks and Molnar (1971). The shallow seismicity in the region was attributed to intraplate activity in the upper plate rather than in the slab. Under central Chile the dip of the plate estimated by modeling ScSp is only slightly steeper than the dip defined by seismicity at a depth near 120 km. Absence of ScSp phases at other stations above the slab (LPB and CUZ) was taken as evidence for disruption of the plate or absence of a strong velocity contrast. Barazangi and Isacks (1979) examined station NNA and found no ScSp conversions, but then Snook *et al.* (1979) presented some observations of weak ScSp phases at NNA. The latter study advocates a model of constant slab dip from central Peru to central Chile to a depth of at least 120 km, primarily based on the ScSp observations. Hasegawa and Sacks (1981) provide additional ScSp modeling, favoring a 10% velocity contrast and a slab dip of 26° in southern Peru, before the slab flattens to nearly horizontal. Subsequent relocations of earthquakes, analysis of focal mechanisms, and fitting of surfaces to the regional seismicity support continuity of the slab from southern Peru to Chile (Bevis and Isacks, 1984; Schneider and Sacks, 1987).

In a recent study, Iidaka and Obara (1991) analyzed ScSp phases from the deep May 12, 1990 Sakhalin earthquake, at 70 stations under the Kanto–Tokai region of Honshu. ScSp was well observed in northeast Kanto, but not in southern Kanto or Tokai. They used the conversion points to locate the slab relative to seismicity, finding that the conversion interface lies just above the seismic plane at depths of 75–100 km, about 5 km deeper than the estimate from S reflections by Obara (1989) (Section 5.2.3). Helffrich and Stein (1993) examine 22 ScSp amplitudes at WWSSN stations in Japan using the envelope method of Nakanishi (1980) and find 5.6 and 23-s ScS–ScSp differential times at SHK and MAT, respectively. The ScSp/ScS amplitude ratios corrected for radiation pattern are

0.39 at MAT and 0.19 at SHK. Correction for the Q model from Okada (1977), which has $Q_\beta = 150$ in the wedge versus $Q_\alpha = 345$, along with Fresnel zone effects due to conversion from the dipping slab, changes these ratios to 0.12 at MAT and 0.14 at SHK. This emphasizes the importance of the three-dimensional geometry.

In summary, ScSp conversions reveal sharp slab interface contrasts from depths of 50–340 km in the Japan slab and somewhat more intermittently in other slabs. Below 100–120 km the conversions are from a velocity decrease of 5–10% encountered along the up-going path, while at shallower depths at least some of the conversions are from a velocity increase.

Other up-going phases may convert from slab structure under a station. Single-station, three-component analysis of receiver functions was first applied to study slab converted phases by Langston (1981). This procedure involves isolating P to S conversions in the crust and upper mantle under a station for a teleseismic signal using the relative strength of arrivals on the vertical and horizontal components of the P wave ground motion. The source function is estimated by assuming that the vertical signal has a single impulse transfer function, which allows the source to be removed from the horizontal signal by deconvolution. Langston (1981) studied signals at WWSSN station COR and found that a 20° dipping high-velocity contrast 45–50 km deep, at the base of a low-velocity zone, produces P-to-S conversions. This was interpreted as the oceanic plate Moho in the Juan de Fuca plate. Crosson and Owens (1987), Owens *et al.* (1988), and Lapp *et al.* (1990) attempted to constrain the shallow geometry and velocity contrasts of the dipping Juan de Fuca plate beneath Washington using detailed receiver function analysis. Crosson and Owens (1987) proposed that there is an arch in the slab under Washington and British Columbia. The structure dips 10–12° under Puget Sound and 15–20° north and south of the shallow dipping region. Broadband stations were deployed south of the Olympic Mountains to constrain the dip and depth of the boundary by P-to-S conversions. Lapp *et al.* (1990) interpret the deconvolved horizontal signal at a station 30 km east of Mt. Ranier as P-to-S conversions from a dipping oceanic crustal Moho at a depth of 53 km with a 16° dip to the southeast. The oceanic crust is modeled as a 6.7 km/s layer overlain by continental upper mantle of 7.7 km/s, giving a low-velocity waveguide in the subducted crust. Detailed receiver function analysis of the northern Cascadia subduction zone has also been performed by Cassidy and Ellis (1993).

5.2.2. *P and S Conversions for Waves Traveling within the Slab*

Most studies of conversions within slabs use up-dip observations, although Sleep (1973) did observe some teleseismic complications which may be due to near-source conversions. Several early studies of slab phases traveling up-dip in the slab were discussed in Sections 2.1 and 2.2, primarily involving observations

of high-Q paths and packets of multiple reflections traveling up the slab. Very early studies of isolated arrivals generated at boundaries in the slab included those of Mitronovas *et al.* (1969) and Mitronovas and Isacks (1971), who argue that a sharp velocity contrast at the top of the subducting lithosphere in Tonga was responsible for P-to-S conversions at depths of from 50 to 200 km. Mitronovas and Isacks (1971) observed two arrivals between P and S on horizontal component recordings, the first about 3–4 s after P and the second 6–12 s after P. They infer that the first is converted from the Moho and the second is a P-to-S conversion from near the slab. A third converted phase, believed to be an S-to-P conversion from the slab, arrives on the vertical component about 6–10 s ahead of S. Along-strike observations of P waves in the Tonga slab at station AFI show secondary arrivals which may correspond to reflections from the top of the slab (Huppert and Frohlich, 1981).

In the up-dip travel time study of Suyehiro and Sacks (1979) for the Japan slab (Section 3.1), two later arrivals were observed, the first of which was attributed to refraction or reflection from a midplate boundary, and the second arrival could be a wide-angle reflection from the lower boundary. The internal reflection influenced their parameterization of the slab as a two-layer model and was related to the larger lithospheric discontinuity in the wide-angle reflection study of the old Pacific lithosphere by Shimamura and Asada (1976).

Fukao *et al.* (1983) attempted to constrain the depth at which the basaltic layer in the underthrusting crust of the Philippine Sea plate below the Kii Peninsula converts to eclogite. Their approach was to analyze late phases found for events that locate in the subducting crust. For events down to a depth of 60 km, they observe late secondary arrivals with apparent velocities of about 6.6 km/s only at stations up-dip of the underthrust zone. The first arrivals for these events tend to be weak. The interpretation that the secondary arrivals have traveled by paths up the oceanic crust leads to the conclusion that a coherent low-velocity waveguide exists at least to depths of 60 km, which requires some suppression of the equilibrium depth for basalt-to-eclogite transformation. A 5–7-km-thick crust with about –14% velocity anomaly overlying a 4% fast mantle was proposed for the shallow slab. The maximum depth of the low-velocity crustal layer is not well established because deeper-focus events may be occurring within the oceanic mantle rather than in the waveguide, reducing the strength of any secondary phases.

Subducted crust of the Philippine Sea plate was examined by Hori *et al.* (1985). Distinct late P and S phases with apparent velocities of 7 and 4 km/s, respectively, were observed for sources less than 50–60 km deep at stations where the subcrustal seismic zone is in contact with the continental crust. Initial P and S phases from 52 subcrustal earthquakes below the Kii Peninsula have weak arrivals with apparent velocities of 8 and 4.6 km/s, respectively. The apparent velocities were estimated by event common and station common pro-

files, and raytracing was used to explore models for the late phases including Moho conversions and wedgelike structures. It was inferred that a low-velocity channel less than 10 km thick, corresponding to untransformed basaltic crust, extends to 50–60 km depth. This could correspond to the low-velocity layer producing ScSp conversions studied by Nakanishi (1980). Simultaneous location and velocity estimation provides support for the presence of low-velocity subducted crust under Honshu (Hurukawa, 1987; Hurukawa and Imoto, 1987, 1992).

Internal slab conversions from intermediate-depth events deeper than 70 km in the New Hebrides were analyzed by Louat *et al.* (1979) and Chiu *et al.* (1985). In addition to a small-amplitude first P arrival with a high apparent velocity of 7.7 km/s, presumably refracted up the high-velocity region of the slab, Chiu *et al.* (1985) observed two extra arrivals. The first is an impulsive arrival within a few seconds after the initial P wave, with an apparent velocity of 6.9 km/s, which is apparently refracted in the slightly lower-velocity upper portion of the slab. The other arrival is 8–13 s after P, with SV-type motion, similar to the observations of Mitronovas and Isacks (1971). This was interpreted as a P-to-S conversion, with its observed highly variable frequency content being attributed to pockets of low attenuation as imaged by Chiu (1982). No evidence for a high-velocity layer of eclogitic material at the top of the plate was found, but the interpretation of the raypaths is very qualitative and this possibility cannot be ruled out.

An attempt to determine the distance from the plate surface of a 181-km-deep event in the Kuril slab was made by Stefani *et al.* (1982). The event was located in the lower plane of a double Benioff zone, with the upper seismic plane expected to lie within 15 km of the boundary. Teleseismic observations were inspected for existence of P-to-P reflections or S-to-P conversions from the upper layer. The azimuthal variation of such an arrival should be only about 1.5 s at teleseismic distances, and it was necessary to look at stations with nodal direct P waves because the event was too large (magnitude 6.2) to use the short-period signals. Observations of a secondary arrival were found with timing and polarity consistent with a distance of 38 ± 5 km from a sharp reflecting boundary. The event is a double event, with the source complexity making the interpretation rather uncertain, but it was claimed that change in mechanism of the two sub-events could not explain the secondary arrival. This experiment is complicated by the possible existence of slab diffraction and multipathing effects along strike, which were not considered.

Clear converted phases between P and S were observed in New Zealand for local events by Kayal (1986). S-to-P and P-to-S conversions at the Moho of the Indian and Pacific plates were observed for events deeper than 50 km under North Island. A high-velocity S refraction appears to originate along the plate boundary, or on the Moho within the slab, along with an S-to-P conversion.

Honda (1984) analyzed travel times of P-to-S converted phases originating

near the upper surface of the Pacific plate under northern Kanto, and additional P-to-S conversions at the upper plate boundary in the Tohoku district were studied by Matsuzawa *et al.* (1986). Late phases with SV motion and high apparent velocities similar to those of the P waves were observed for intermediate-depth events, with the time shift between the phases being shorter in eastern Honshu and longer in central western Honshu and the phase disappearing in the far west. The P-to-S conversion can be as large as half the amplitude of the P wave. In addition, a secondary P phase arrives about 3 s after P on the vertical components. The arrivals were seen for earthquakes in both the upper and lower planes of the double seismic zone. Matsuzawa *et al.* (1986) modeled these phases with a two-layer plate model with a thin low-velocity (having a -6% velocity anomaly) upper layer 5 to 10 km thick overlying a 6% fast velocity lower layer. The events in the upper seismic plane were located in the low-velocity layer. P-to-S conversions appear to take place at depths from 60 to 150 km, with the position of the boundary being located by differential travel time inversion. This low-velocity zone could be responsible for the ScSp phase studied by Okada (1980) and Nakanishi (1980), with the zone being too small and close to the sources to have been imaged in tomographic models such as that of Hasemi *et al.* (1984). Modeling of these phases with synthetic waveforms by Matsuzawa *et al.* (1987) showed that the two-layer model can match the amplitudes of the converted phases, but the polarities are hard to identify.

Iidaka *et al.* (1989b) observe anomalous phases following direct P for events in the Pacific slab beneath Kanto. They interpret these as P-to-S conversions off of a sharp interface near 60 km, just above the top of the double Benioff zone in this region. They use a model with a 3% fast slab surrounded by 3% slow mantle (for a 6% velocity contrast) in modeling the timing and moveout of the observed arrival. Iidaka *et al.* (1990, 1991, 1992) followed up on earlier observations of S-to-P conversions from the Philippine Sea slab by Mizoue *et al.* (1981) and Kanjo (1987). Iidaka *et al.* (1990) analyzed impulsive phases on vertical component recordings that arrive about 2.5 s after P and often have amplitudes equal to or larger than that of the initial arrival. Using data from 29 events, they found that the secondary phase is observed only when the raypath crosses the contact between the upper plate and the Philippine Sea slab, and it does not move out with respect to P as the distance varies. These observations and two-dimensional raytracing rule out explanations other than S-to-P conversion at the upper boundary of the Philippine Sea slab. The observations are used to contour the upper surface of the plate, yielding a dip of 50° at depths shallower than 20 km, although the dip estimate is probably unstable. Iidaka *et al.* (1992) further analyze the S-to-P conversions, as well as P-to-S conversions in signals recorded on the east coast of the Izu peninsula. The P-to-S conversion is strongest on the horizontals and again is seen only when the raypath crosses the interplate con-

tact. The depth of the Philippine Sea plate boundary is found to be 28–35 km, and a more reasonable dip of 12.9° was estimated for the slab.

Hori (1990) analyzed late phases following weak P and S initial arrivals for 127 events 40–60 km deep under Kanto, somewhat north of the area studied by Hori *et al.* (1985). In this region the Philippine Sea plate overlies the Pacific plate. The weak initial arrivals appear to dive into the plate and have slightly steeper angles of incidence than the later phases. The secondary arrivals appear to propagate up the basaltic/gabbroic crust of the slab. Hori infers that conversions or refractions occur where the slab crust comes in contact with the lower continental crust.

Late P and S phases have been found for events under Shikoku and northern Kyushu in studies by Tanaka and Oda (1988), Okura and Takeuchi (1989), and Oda *et al.* (1990). Using a station in southwestern Honshu, Oda *et al.* (1990) analyzed P and S phases with weak initial arrivals followed by stronger arrivals. The precursors were observed only for limited geometries along the strike of the Nankai trough, for events in the upper 40–60 km. By using events at different distances to estimate apparent velocities of the phases, they found that the early arrivals have high velocities of 8 and 4.9 km/s for P and S, respectively, and the later arrivals have corresponding velocities of 6.6 and 3.8 km/s. The interpretation, based on raytracing, is that the events are in the subducted oceanic crust, with the emergent precursors refracting in higher-velocity regions of the slab. The presence of a low-velocity layer is consistent with the ScSp conversions in the region observed by Nakanishi (1980) and with the high-resolution tomographic imaging by Tanaka (1987), who used finer blocks than in the original model by Hirahara (1981) (Section 4). The absence of double arrivals for deeper events indicates that either the low-velocity zone does not extend below about 60 km or the events are located below any such region.

Matsuzawa *et al.* (1990) examined additional S-to-P conversions under eastern Honshu, finding that events in the lower seismic plane show strong conversions from a boundary just above the upper seismic plane. Events in the upper seismic plane do not show this arrival. The time differences between direct S and the S-to-P conversion for 567 recordings of 213 events were used to locate the upper plate boundary in the depth range 30–130 km. The timing of the P-to-S conversions studied by Matsuzawa *et al.* (1986) gives consistent positioning of the upper plate boundary (Fig. 31). Assuming that there is a low-velocity zone in the upper plate, with the conversion boundary being at the top of this zone, they conclude that there is a gradual velocity gradient across the lower boundary of the low-velocity zone, since no S-to-P conversions are observed from that region.

Analysis of broadband P wave recordings for two deep focus events in the Nazca plate below Peru–Brazil shows a large-amplitude arrival 1.5 s after the

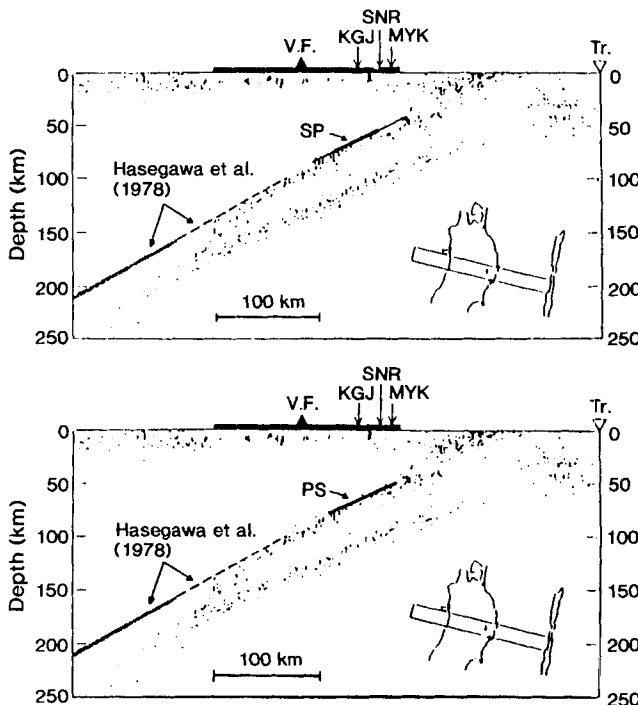


Fig. 31. Comparison of the double seismic zone seismicity beneath Tohoku, Japan, and the position of boundaries inferred from S to P and P to S conversions at the top of the slab. It appears that the upper plane of the seismicity lies just below the conversion boundary. Reprinted with permission from Matsuzawa *et al.* (1990).

direct P wave (James and Snoke, 1990). This phase has reversed polarity and is 1.5 times larger than the direct phase, and the incidence azimuth is rotated by 20° relative to the direct P. Raytracing and modeling of the secondary phase indicate that it may originate as a wide-angle reflection within the subducting slab, with a sharp (<10 km) discontinuity at a velocity reduction being needed. Slab models with 3 and 5% fast velocity anomalies, as well as elevated olivine–spinel transitions, indicate that the reflection occurs near the upper surface of the Nazca slab at depths from 150 to 400 km, which is in the seismicity gap in the Benioff zone. This tends to support the argument by Isacks and Barazangi (1973) that the slab is continuous, rather than the alternative models proposed by Snoke *et al.* (1974a,b). It is unclear why there is a gap in seismicity even if strong velocity heterogeneity associated with the slab is present in the gap.

The possibility of significant intraplate structure near the lower plane of double seismic zones was supported by the study of Ando *et al.* (1989), who observed S-to-P conversions possibly from near the lower seismic zone. Iidaka

and Mizoue (1991) extended the analysis of Suyehiro and Sacks (1979) for up-dip travel times in the Pacific plate under Japan and observed late high-frequency P arrivals, which they model as reflections from an internal boundary inside the plate of their two layer model (Section 3.1). The 30-km-thick upper layer of their slab model is close to the thickness of the double zone, and they predict that reflections from the midplate boundary can be observed only for events deeper than 250 km, which exceeds the depth to which the double zone extends. Their model has a 1% velocity increase in the plate, sufficient to produce wide-angle P wave reflections in the up-dip geometry. Nakamura *et al.* (1992a,b) analyzed recordings from the 30-station Kyoto network for events in the Izu slab, finding secondary P wave arrivals 2 and 13 s after direct P for events deeper than 300 km. The apparent velocities of these phases are the same as P, so they originate near the source. The 2-s arrival is interpreted as a S-to-P conversion from a discontinuity 20 ± 3 km above the source. The 13-s arrival is interpreted as a P-to-S conversion from 50 ± 5 km below the source in northern Izu and 80 ± 5 km below the source in southern Izu. If correct, this provides further evidence for a sharp lower boundary of the slab, similar to that of Suyehiro and Sacks (1979). Three-dimensional raytracing indicates that the slab is about 4% faster than the surrounding mantle. The sharp upper boundary was inferred to be a chemical contrast, but the nature of the sharp lower boundary was considered puzzling. The distance between the seismicity and the upper boundary suggests that the events are not in the crustal layer of the slab, and therefore the deep Izu event is unlikely to involve transformations in serpentine (Meade and Jeanloz, 1991). A secondary arrival from shallow (< 100 km deep) events in the upper plane of the double Benioff zone in the Izu slab has been studied by researchers at the Disaster Prevention Research Institute of Kyoto University (Nakamura, personal communication, 1992). The timing of this arrival indicates that it is an S-to-P conversion off of a velocity contrast 30 km deeper into the slab, arriving about 9 s after P. This places the structure near the lower plane of the double Benioff zone.

5.2.3. *P and S Conversions for Sources above the Slab*

Numerous studies have reported direct observations of reflections and refractions off dipping subducted structures at shallow depths. Nagamune (1971) observed large-amplitude, low-frequency phases arriving 10–20 s after small-amplitude, high-frequency S waves for shallow earthquakes above the slab in the southern and central Kurils. He inferred that the initial arrivals were refracted from the top of a 7% fast slab. Shiono (1974) argued that high phase velocity P waves observed below Shikoku represent P waves refracted from the top of a dipping Philippine Sea plate. On the basis of these observations he argued that the leading edge of the plate is 150–200 km inland from the trench. Mizoue

(1976) also found P waves reflected from the upper boundary of the descending Philippine Sea plate. Hurukawa and Hirahara (1980) argued for the presence of a thin low-velocity layer, slower than the surrounding mantle by 5–6%, based on additional observations of reflections from the descending Philippine Sea plate.

A wide-angle reflection off the Izu–Bonin slab was detected by Fukao *et al.* (1978), with an apparent velocity of 16.5 km/s. This phase arrives 10–20 s after P for three events in the Ryukyu arc and appears to be associated with a postcritical reflection from the 410-km discontinuity. The phase is observed in the range 12.5–14° and is strong near 13.5°. Two-dimensional raytracing with a 4–12% fast slab can explain the travel times. For an assumed 10% contrast the reflecting boundary must be no thicker than 10 km.

Following analysis by Horiuchi *et al.* (1982) of the Moho P wave properties under Tohoku, Obara and Sato (1988) found evidence for an S wave reflector in the form of clear S arrivals 15–45 s late in the S wave coda. This horizontal component arrival has an 8-Hz dominant frequency, an emergent onset, and a high apparent velocity toward the west. The location of the reflector was found by fitting a dipping plane to the travel times from eight stations, with the preferred position being near the upper plane of the double seismic zone at depths from 80 to 100 km. The late arrival often has high amplitudes, requiring a reflection coefficient averaging around 0.5 after corrections for geometric spreading, attenuation, and focal mechanism, which may indicate the presence of melt or liquids near the reflector. Obara (1989) analyzed additional observations of late S wave reflections under southern Kanto. He found that the reflector extends from 60 to 120 km depth and does not appear to cause reflections from less than 60 km depth. Obara examined data from 61 earthquakes in 1987, finding the reflection at all stations except along the east coast of Honshu. It appears that the reflector exists under the Philippine Sea slab, as well as farther to the north. The reflection is strong in regions where the Philippine Sea slab overlies the Pacific slab, which may be due to enhancement of the contrast between a low-velocity layer at the top of the Pacific plate and the overlying mantle.

Many reflection seismology studies reveal the complexity of very shallow slab structure. For example, Green *et al.* (1986) and Clowes *et al.* (1987) use multi-channel seismic reflection profiles across Vancouver to argue that the subducted plate has imbricated, producing a laminated structure. The underplated structures with layered sediments and volcanics produce substantial reflectivity. Discussion of many of the shallow imaging efforts is provided by von Huene and Scholl (1991).

5.2.4. Modeling Slab Structure Using Results from Reflections and Conversions

There have been numerous attempts to characterize the thermal and petrological conditions of subducting slabs at shallow depths, using models and field observations (e.g., Peacock, 1987). Modeling studies are critical for interpreting

the deeper slab as well. Taking the collective constraints on slab interface properties from 10 to 350 km depth provided by the studies described above, Helffrich *et al.* (1989) attempted to find viable petrological and thermal models to account for the diverse observations. Their approach was to assume a pyrolite mantle composition, a thermal slab model including corner flow but no shear heating, and Birch–Murnaghan equation of state calculations using available thermoelastic data for upper mantle mineral phases. It proves to be particularly challenging to explain 5–12% contrasts over sharp (<10 km) boundary transitions because the major rock types such as peridotites and eclogite are not expected to have large velocity contrasts in the upper mantle, and temperature variations are not expected to make strong contrasts over 10-km widths. Of course, there is substantial uncertainty in many of the thermodynamic parameters and even in the thermal models, so such calculations are still tentative.

Attempts to model the deeper (>300 km) ScSp conversions and P reflections, which require sharp 5–12% velocity increases from the mantle wedge into the slab, were made using a 10-km-thick eclogite layer over a layered harzburgitic/lherzolitic slab. It was concluded that an elevated olivine– β spinel transition is needed, as the 4–8% P and S velocity increase of the phase transition can provide 70% of the total contrast, with temperature differences accounting for 20% and composition differences accounting for 10%. The shallow (<100 km) ScSp conversions and reflections, along with the evidence for a low-velocity waveguide in the slab, can be reconciled with a gabbroic ocean crust having a kinetically inhibited eclogite transition, since large velocity contrasts are involved in that transformation as well.

To explain the strong contrasts from 100 to 300 km depth is difficult because there are no significant phase changes available to enhance the slab–mantle contrast. It is estimated that at these depths a 400° increase across the upper 10 km of the slab is reasonable, which can account for only 1.75% velocity increase. The chemical contrast is expected to contribute only 0.5%, so other mechanisms must be invoked to make a strong contrast (Fig. 32). Melting of a thin layer above the slab, perhaps due to expulsion of fluids associated with dehydration in the slab, can enhance the contrast and perhaps explain some of the deeper ScSp conversions involving a velocity increase along the path. Alignment of olivine in the hot wedge induced by the shear flow may cause a difference in anisotropic fabric relative to any alignment in the peridotitic portions of the slab, accentuating the contrast in properties, but this will not provide a low-velocity region above the slab. It remains unclear whether neglect of viscous heating near the top of the slab is justified, and given the difficulty of matching the observed behavior one must also be concerned about the reliability of the thermodynamic parameters.

Helffrich and Stein (1993) conduct a careful analysis of ScSp amplitudes using Thomson–Haskell matrix models and raytracing of P reflections off the slab to further quantify the interface conditions. They confirm the basic results of Fukao

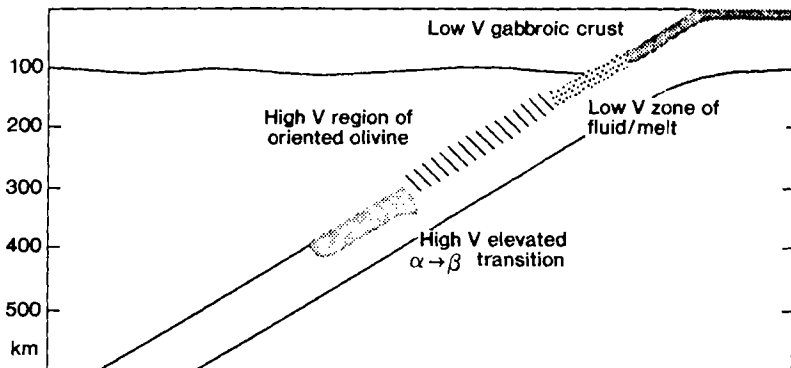


Fig. 32. Schematic of upper plate processes that appear to influence the strength of velocity boundaries at intermediate depths. The variety of processes is required to account for low-velocity regions in the top of the slab and strong conversion boundaries. Reprinted with permission from Helffrich *et al.* (1989).

et al. (1978), and estimate that a 4–10% increase in slab velocity is needed to match the travel times and amplitudes of the reflection off the slab. Modeling of the corrected ScSp/ScS ratios at stations MAT and SHK described above yielded first-order discontinuity models with unrealistically high velocity contrasts of 15–25%, and gradational transitions require even larger contrasts. Following Nakanishi (1980), attempts were made to model the data with layered interfaces, to exploit constructive interference between phases arising from different boundaries. The data at SHK can be modeled with a 6-km-thick 10% low-velocity layer overlying a 2% fast deeper slab. An 8% increase in a thin 8-km-thick layer can model MAT, but this is very hard to explain petrologically. A model with an eclogitic layer with low shear velocity at the upper surface of the slab or hybrid models with the velocity effects of the olivine- β spinel phase transition or anisotropy in the overlying wedge and deep slab superimposed on thermal and chemical effects can also explain the data, so there is no unique interpretation. Better constraints on P and S velocities of the various mineral types of interest are needed, along with improved constraints on the actual boundary properties.

5.3. Seismic Imaging of Phase Boundaries in Slabs

Seismic mapping of phase boundaries in the slab and surrounding mantle can also place important constraints on the subduction process. Both the 410 and 660-km discontinuities are important in this regard, because they are good indicators of the thermal heterogeneity in the downwelling as well as providing buoyancy forces favoring and opposing subduction, respectively. Several efforts

to detect any additional contribution to the volumetric high-velocity anomaly of the slab associated with elevation of the 410-km discontinuity were discussed in Section 3.1, with the results being rather ambiguous. There have also been efforts to detect directly reflections from the olivine– β spinel phase boundary in the vicinity of slabs. Sacks and Snook (1977) analyzed local recordings of deep-focus events in South America, finding arrivals between P and S that they attributed to up-going S-to-P conversions at the 410-km boundary. They found the rather curious result that the velocity discontinuity should involve a velocity increase on the up-going path, which is of course contrary to the expected decrease. This is based on the polarity of the observed phase and was attributed to a very deep lithosphere–asthenosphere boundary.

Vidale and Benz (1992) analyzed teleseismic observations of deep events, examining the interval between P and the surface reflection pP for any underside reflections from discontinuities above the source. They used a large short-period array with 881 stations in the western United States to stack the signals, enhancing detectability of any small reflections or conversions. Analysis of six deep events (one in South America, one in the Marianas, two in Tonga, and two in the Bonin slab) showed evidence for about 15 km elevation of the phase boundary near the core of subducted slabs for P reflections and S-to-P conversions from the boundary. It is possible that dip of the boundary may obscure the true position of the phase transition.

The possibility of kinetic inhibition of the 410-km transition was explored in a travel time study by Iidaka and Suetsugu (1992). They examined up-dip travel times in the Pacific slab under Japan, comparing observed patterns of anomalies with calculations for slab models with equilibrium (elevated) and kinetically suppressed (depressed) phase boundaries. The dense network in Japan provides better coverage than in earlier travel time studies in Tonga (Solomon and U, 1975) and Izu (Roecker, 1985) (see Section 3.1). Recordings at 63 stations in southeast Japan for 29 events between 300 and 500 km depth were used. The events were relocated relative to four master events located using pP times from the ISC Bulletin. No slab model was used in the locations because this tends to have little effect in Japan. Travel time patterns across Honshu vary by 1–1.5 s and were modeled using two-dimensional raytracing beginning with the model of Suyehiro and Sacks (1979). Events from 300–350 km depth show no preference between models, whereas events from 400–500 km depth indicate a preference for a depressed transition compatible with the metastable olivine model (Fig. 33). This result is not very dependent on the heterogeneity in the slab and wedge indicated by tomographic models. Geller (1990) discusses the relationship between this model and the experimental work of Green *et al.* (1992a) and Kirby *et al.* (1991).

The 660-km boundary beneath subduction zones has also been studied. This seismic discontinuity is most likely the result of the spinel–perovskite phase

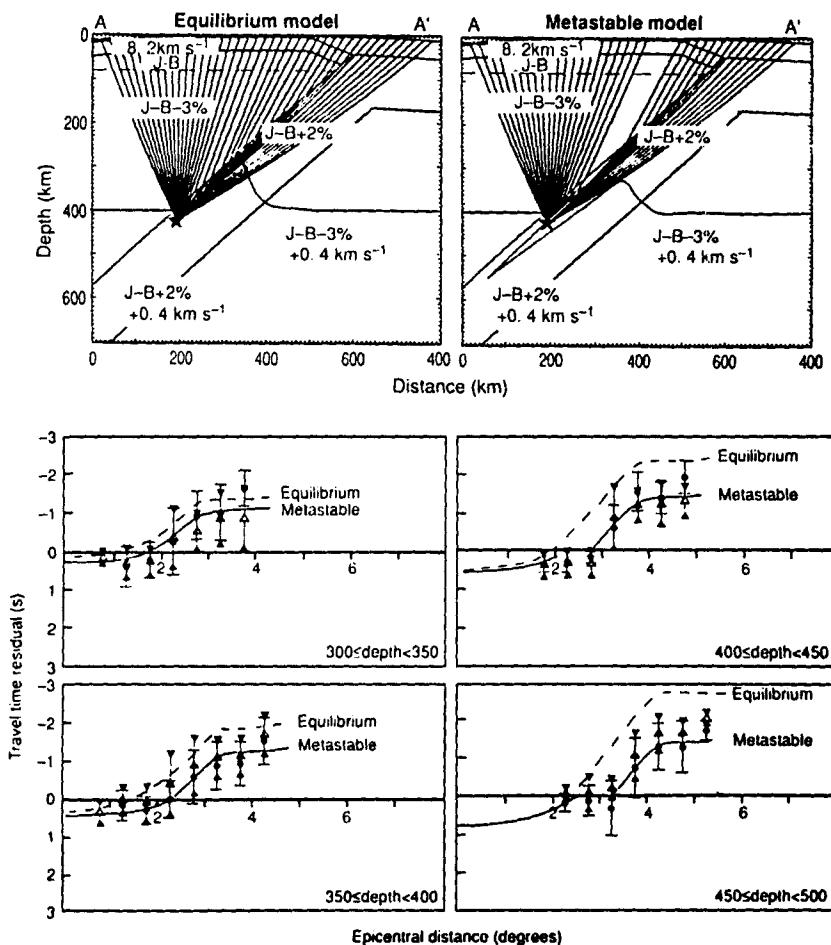


Fig. 33. Schematic of raypaths expected within a slab model for equilibrium and metastable olivine models (top). Below, data from events in the Japan slab are compared with predictions of the two models. Events below 400 km show a preference for the metastable model. Reprinted with permission from Iidaka and Suetsugu (1992).

transformation, rather than being a chemical boundary, but its undulations do provide constraints on the lateral temperature variations near the boundary. Several studies have attempted to detect perturbations of the boundary in the vicinity of an impinging slab, using converted and reflected phases. The main procedure for localized studies has been analysis of teleseismic signals showing down-going S-to-P conversions which arrive after direct P, or underside and topside reflections of ScS and SS waves. Depressions of the phase transition by up to 50 km have been detected under Tonga (Bock and Ha, 1984; Richards and Wicks

1990; Wicks and Richards, 1991; Vidale and Benz, 1992), the Izu-Bonin/Marianas (Barley *et al.*, 1982; Vidale and Benz, 1992; Wicks and Richards, 1993), the southwest Pacific (Revenaugh and Jordan, 1991), South America (Vidale and Benz, 1992), and the Kurils (Shearer, 1991; Shearer and Masters, 1992). Down-going S-to-P conversions can be rather intermittent in nature due to radiation pattern or rupture directivity effects (Barley *et al.*, 1982; Bock and Ha, 1984; Wicks and Richards, 1991), but there are also regional variations in the consistency of the conversions (Richards and Wicks, 1990). The boundary must be rather sharp (<5 km) to account for the frequency content of the converted phases. In the vicinity of the depressed phase boundary the slab may actually be slower than the surrounding mantle if it has only 2–4% thermal velocity anomaly and the phase transition involves a 4–5% velocity increase. This may account for disruption of deep slab velocity signatures in tomographic images right near the 600-km boundary (e.g., Zhou, 1990a).

These studies support the evidence for a negative Clapeyron slope for this phase transition (Ito *et al.*, 1990), but they alone cannot be used to argue convincingly against chemical stratification of the mantle which could prevent the slabs from penetrating. This is because postulated chemical differences between the upper and lower mantles that are needed to account for differences in their average densities (Jeanloz and Knittle, 1989; Stixrude *et al.*, 1992) may not be associated with a strong seismic velocity contrast (Jeanloz, 1991). Subducting slab material may pass through the phase transition but still be prevented from sinking deep into the lower mantle by a chemical contrast between the upper and lower mantles. Numerical calculations (e.g., Christensen and Yuen, 1984) all predict that there should be substantial (100–300 km) downward deflection of any chemical boundary with a large enough density increase to result in stratified convection. There is no compelling argument for the phase transition and any chemical contrast being tightly linked, so the depth at which downwelling material may be deflected is uncertain, if there is chemical layering in the mantle.

The primary application of 660-km boundary topography is as an indicator of cumulative thermal anomaly near the boundary. The observed topography of up to 50 km requires from 600 to 900°C reduction of the ambient temperatures near the downwelling (Vidale and Lay, 1993), using experimental determinations of the Clapeyron slope. This is compatible with many thermal models of the sinking lithosphere. The slab may pass through the transition undeformed, causing a depressed phase transition, or the slab may pile up, cooling the mantle and depressing the phase boundary without requiring that the bulk of the slab ultimately sink into the lower mantle. For example, Shearer and Masters (1992) show a 1500-km broad depression of the 660-km discontinuity landward from the southern Kuril arc. This is consistent with the cooling effect of a horizontally deflected slab, as imaged in the tomographic and differential residual sphere analyses mentioned earlier. If all recently subducted slabs are piled up in the

transition zone, one would expect broad depressions of the 660-km discontinuity around all margins of the Pacific Ocean, which is observed in the western Pacific and South America but not under the Aleutians and Tonga, and there are depressed regions under the Atlantic and East Pacific where no subduction is occurring (Shearer and Master, 1992; Morgan and Shearer, 1993). Current topographic models are very limited in resolution, so it is unclear how to interpret the global patterns.

Three-dimensional seismic velocity models for the mantle have been combined with maps of 660-km phase boundary topography to explore flow patterns in the mantle by Morgan and Shearer (1993). They find that while the topography on the 660-km discontinuity acts to inhibit convection across the boundary, it is two to four times too small to prevent whole mantle convection. The seismic models were used to provide the buoyancy distribution, with several viscosity structures being considered. There is a fairly good general correlation between observed deflections of the 660-km boundary and flow patterns induced by volumetric heterogeneity. Patterns of radial flux versus depth in the resulting models show no reduction near the 660-km boundary, as would be expected for strongly stratified convection. Morgan and Shearer (1993) note that the relatively small volume of slabs tends to inhibit their penetration through the phase boundary, whereas their low temperatures and high viscosity tend to favor their penetration. They suggest that the trade-off between these effects may account for the variable nature of slab deflection or penetration of the lower mantle suggested by seismic tomography.

6. FOCUSING, MULTIPATHING, AND DIFFRACTION EFFECTS OF SLAB STRUCTURE

In addition to seismic wave travel times, amplitude and waveform anomalies have been analyzed to place constraints on deep slab velocity heterogeneity, dating back to the initial investigations of slabs. Some aspects of this have already been discussed, relating to the attenuation characteristics of slabs and the wedge (Section 2), the propagation of high-frequency guided waves in slabs (Section 2.2), and converted and reflected phases (Section 5). In this section we will concentrate on focusing and defocusing effects of the high-velocity, tabular slab structure, as well as diffraction effects that distort long-period waveforms. Observation of such wavefield phenomena can be used to constrain velocity gradients in the slab structure with better resolution than residual sphere modeling or seismic tomography; however, the applications have been limited by the general difficulties of handling the complex three-dimensional geometries involved as well as the many propagation phenomena affecting seismic wave amplitudes in the Earth.

6.1. Short-Period Defocusing and Multipathing Effects

As soon as the first three-dimensional raytracing capabilities were developed (e.g., Julian, 1970; Sorrells *et al.*, 1971; Jacob, 1972), it was recognized that seismic wave amplitudes and waveforms could be used to study shadowing, multipathing, and wave complexity effects of slabs. Because most amplitude studies require some knowledge of the source radiation pattern, the initial applications used data from the nuclear explosion LONGSHOT (Davies and Frasier, 1970; Davies and Julian, 1972). Davies and Julian (1972) used the method of Julian (1970) to perform three-dimensional raytracing for an Aleutian slab model and predicted that a strong P wave shadow zone should cover much of Canada and Europe. This was shown to be consistent with observed patterns of magnitudes and multipathed short-period signals. In fact, for some stations in western Canada, PcP is larger than P . Slab models with velocity anomalies of 5–7% from 0 to 230 km and 10% at intermediate depth were considered, with strong ray deflections being predicted for such heterogeneity. It was suggested that slab heterogeneity contributes to coda arrivals for both teleseismic stations and stations located above slabs, due to reflections, refractions, and scattering.

Sleep (1973) considered short-period and long-period P wave amplitudes at WWSSN stations for events in the Tonga, Kermadec, Kuril, and Aleutian slabs. Corrections were applied for the source radiation patterns, distance, and station anomalies (based on amplitudes from events located in the trenches). He found that other than for the shallow-dipping Aleutian slab, there were rather modest short-period shadowing effects, with less than a factor of 2 amplitude patterns. Some distant stations recording Tonga events show a low-amplitude precursor, which he postulated may be a greatly defocused arrival that traveled down the slab. Raytracing in slab velocity models was used to model amplitude patterns for three nuclear explosions (above the Aleutian slab) and 15 shallow and intermediate-depth earthquakes. The Aleutian explosions show low amplitudes toward the north for both short periods and long periods, but the earthquake data preclude shadow zones with factor of 10 reductions in short-period amplitudes, as predicted by geometric spreading calculations for shadow zones on the down-dip side of the slab. The observed factor of 2.5 short-period amplitude pattern for the Aleutian events was found to be quite sensitive to the velocity model and was used to locate the slab. The intermediate-depth events were found to locate in the colder region of the slab. The Tonga events show very weak evidence for an amplitude pattern in the short period but not in the long periods, and the Kuril event shows only a hint of a pattern as well. Sleep (1973) concluded that there is typically less than a factor of 2 amplitude reduction in the shadow zones but noted that the scatter in amplitudes is large, probably due to station effects. Further analysis of short-period amplitudes for LONGSHOT was presented by Green (1976), who used the relative intensity of rays in one-dimensional and

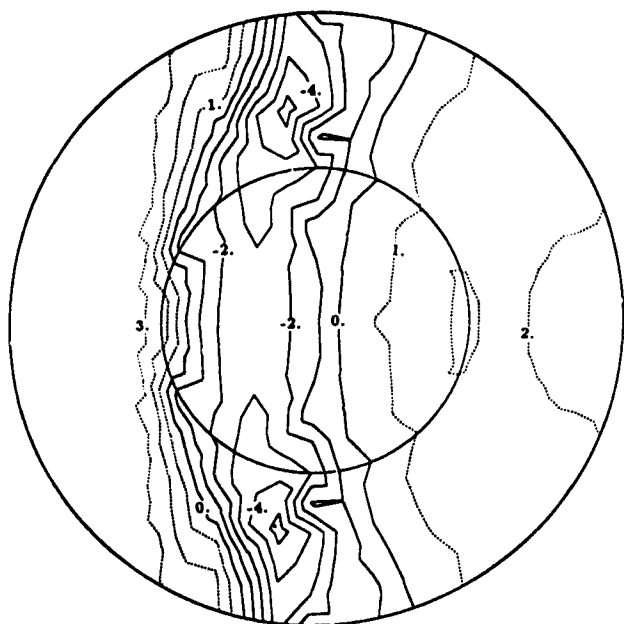
two-dimensional models. This method is similar to the relative intensity calculations of Jacob (1972).

Short-period P wave amplitudes in the western United States for 19 central Aleutian events were analyzed by Nieman *et al.* (1986). These paths travel along the strike of the slab, where raytracing calculations predict rapid variations of focusing and defocusing. Slab model calculations with an 80-km-thick slab extending to 300 km depth were made, providing fair agreement with patterns for events in the forearc and outer rise, but the patterns in the data are not very clear.

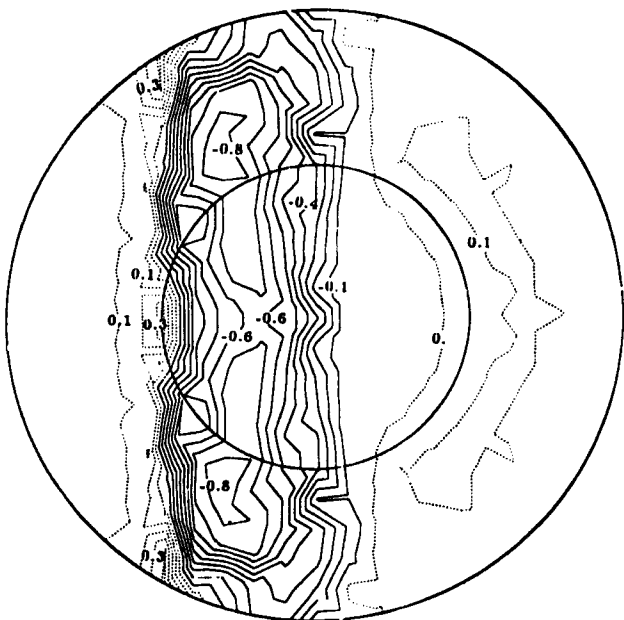
Teleseismic short-period amplitudes for deep events in the Kuril slab were used by Suetsugu (1988, 1989) to help constrain his model for the deep slab. Corrections were made for radiation pattern, geometric spreading, and station anomalies, and the data show factor of 2 amplitude patterns for paths traveling 50–65° down-dip. The data were modeled using a hybrid two-dimensional finite element and optics method. The preferred models have a strong gradient near the upper slab boundary, with slabs extending into the lower mantle to a depth near 1000 km, with 3.5% fast velocity. A tomographic inversion of the deep structure was used (Section 4.1) to interpret the amplitude and travel times simultaneously.

Improved ray methods using dynamic raytracing and Gaussian beams for accurately computing short-period amplitude effects in subducting slabs have been presented by Ha (1978), Cormier (1989, 1990), Weber (1990), Koketsu (1991), and Sekiguchi (1992). Cormier (1990) and Cormier *et al.* (1991) used a modified form of dynamic raytracing to predict travel times, geometric spreading, and high-frequency waveform distortions for S waves in three-dimensional slab models. They considered slabs with and without advective thickening and presented full lower hemisphere calculations of geometric amplitude and travel time patterns. The amplitude and travel time anomalies are not perfectly correlated but do have some general trends in common (Fig. 34). Cormier (1990) shows that for a slab model that steepens in dip in the lower mantle, focusing by the gradients in the lower part of the slab can offset the defocusing effects of the long path. This is particularly relevant for PcP observations like those of Boyd and Creager (1991), which were used in residual sphere modeling. Cormier *et al.* (1990) used the three-dimensional model of Boyd and Creager (1991) in a raytracing exercise to predict the pattern of magnitude anomalies for the Amchitka nuclear tests. The model predicts a broad zone of low P wave amplitudes toward the north at distances greater than 70°, with the average magnitude being

Fig. 34. Synthetic predictions of patterns of S wave travel time anomalies and logarithmic amplitude anomalies due to defocusing, in lower hemisphere projections, for a model with a high-velocity slab dipping steeply toward the left. The earliest times are observed toward the north and south because the raypaths stay in the slab the longest. Defocusing (negative amplitude anomalies) occurs along strike and down-dip, but the correlation with travel time patterns is not perfect. Reprinted with permission from Cormier (1990).



S Travel Time Anomalies



S Amplitude Anomalies

biased by up to 0.1 magnitude unit for a realistic station distribution. Amplitude variations compatible with earlier results of Sleep (1973) and Davies and Julian (1972) were predicted.

Weber (1990) used two-dimensional Gaussian beam synthetics to explore amplitude effects of high-velocity slab models. He considered effects of the maximum slab anomaly, depth of slab penetration, thickness and dip of the slab, and position of the sources in the slab. The models predict caustics and focusing, along with shadow zones and defocusing, with amplitudes ranging over ± 1 magnitude unit in regions with little travel time anomaly. Focusing is produced by both the top and bottom of the slab in his models, although it is probably exaggerated by the sharp edges of the slabs in his models. Small changes in dip of the slab can produce large shifts in the distance of the focusing and defocusing patterns. It is desirable to exploit this sensitivity to improve slab models. Weber (1990) considered the amplitude patterns presented by Suetsugu (1988, 1989), and his calculations led him to favor a model in which high velocities in the slab do not extend below 670 km depth, but he did not show whether the model of Suetsugu (1989) is inconsistent with the data. Differences in the amplitude patterns at close distances for short and long slabs shown by Weber (1990) are difficult to understand, raising some question about how stable the amplitude calculations are.

Three-dimensional Gaussian beam calculations for the effects of slab structure were presented by Sekiguchi (1992), to explore the potential of amplitude patterns for assessing the effects of elevated or depressed 410-km transitions. Incident plane waves with three-dimensional velocity and attenuation structures were considered, as well as geometries with up-going paths in slab models. For future work, amplitude patterns appear to hold some promise for testing the position of the phase boundary in the slab, although there are many contributions to amplitude patterns from the velocity gradients in the slab as well as acute sensitivity to the precise location of the sources in the structure.

6.2. Long-Period Defocusing and Diffraction Effects

The antiwaveguide nature of a high-velocity subducting slab causes frequency-dependent diffraction effects for seismic waves with intermediate and long periods. Davies and Julian (1972) considered long-period amplitude and waveform effects for LONGSHOT to be the result of diffraction by the Aleutian slab. Because ray theory fails to account for such diffractions, more complete wave theories have been developed to handle the propagation of long-period signals in a high-velocity slab. Ward and Aki (1975) developed the first analytical wave theory procedure for calculating short-period and long-period P waveforms in a slab. They explored two-dimensional wave solutions for one-dimensional slabs,

with a 10% P velocity anomaly and a 20% S velocity anomaly with a triangular profile across the slab. For short periods they found a shadow zone consistent with ray theory, and defocusing for long periods could produce a factor of 2 decrease in P wave amplitudes accompanied by substantial broadening. The stronger heterogeneity assigned to the S velocity structure predicts larger multipathing and defocusing effects. It was also found that the position of the source in the high-velocity layer influences the multipathing effects. They only briefly considered any data suggesting that broadening of P waves from aftershocks of an Alaskan earthquake may be associated with slab effects.

Following up on the short-period and long-period amplitude studies of Sleep (1973), long-period amplitudes from 11 earthquakes along the Kuril arc were examined by Engdahl *et al.* (1977). Focal mechanisms were determined using WWSSN observations, and then raytracing in slab models was used to locate the events. It was found that 20° deflections of takeoff angles and 35° deflections of azimuths could be caused by the slab velocity heterogeneity. The amplitude pattern from the deepest event was used to obtain station-distance corrections (implicitly assuming no deep slab heterogeneity), and the corrected amplitude patterns were compared with raytracing predictions of focusing and defocusing effects. No consistent pattern of broadening was found in the period measurements, and the scatter in the data prevented improving the position of the slabs based on matching the patterns.

Characterizing diffraction effects is most promising using broadband seismic data. Choy and Cormier (1986) observed systematic variations in the shape of broadband S and ScS displacement pulses from a deep event in the Kuril slab. The S phases have a broadened tail, an effect that was attributed to frequency dependence of attenuation in the lower mantle. Their model has enhanced attenuation of low-frequency (0.01–0.1 Hz) body waves at depths from 400 to 1600 km, which preferentially affects the S waves. Engdahl and Kind (1986) observed systematic variations in broadening of broadband teleseismic P waves from 11 shallow events in the Aleutians recorded at the Gräfenberg array in Germany, which they attributed to variations in near-source crustal reverberations. Both of these sets of observations may also have some contribution from slab diffraction.

Analysis of broadband SH waves from two deep events in the Kuril slab by Silver and Chan (1986), including the event studied by Choy and Cormier (1986), revealed additional evidence for broadening of direct S signals relative to ScS at paths along the strike of the slab (Fig. 35). The broadened S waves were found to have early arrivals with enhanced pulse areas, and it was concluded that multipathing due to a lower mantle extension of the slab was responsible rather than a lower mantle attenuation structure. This interpretation was supported by raytracing calculations, which show that multipathing to the North American stations that show the anomaly is predicted for a slab model which is similar to the residual sphere model of Creager and Jordan (1986) but which steepens in dip

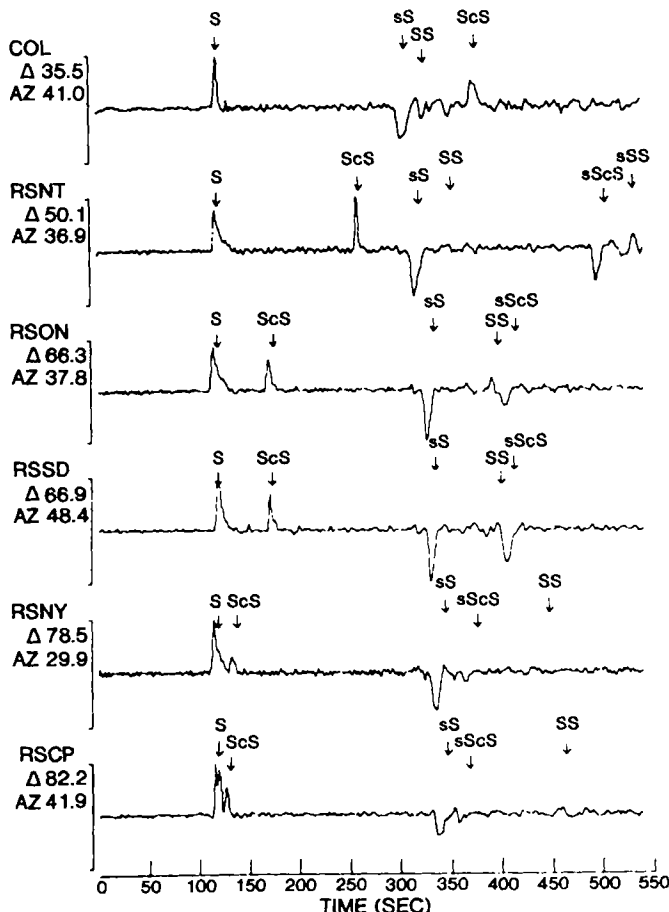


Fig. 35. Examples of teleseismic broadband SH signals recorded at North American stations for a deep-focus earthquake in the Kuril slab. The raypaths are along the slab strike. The first arrival in each trace is the direct S wave, followed by the core reflection, ScS, and the surface reflections, sS and sScS. Note that the pulse width of the S phase tends to be greater than that of the ScS phase, except at COL. RSCP shows an extra arrival between S and ScS that is from lower mantle structure. Reprinted with permission from Silver and Chan (1986).

at 900 km depth. It is unlikely that multipathing is responsible for the broadened S waves, but diffraction by a high-velocity structure in the lower mantle is possible. Silver and Chan (1986) considered a few data for other events in different slabs and argued that broadening is most pronounced along the slab strike for the Kuril arc. If this is the correct explanation, it is surprising that station COL, directly along the arc but at closer distances, does not show broadening of the S waves.

A much larger data set of 70 pairs of broadband S and ScS displacement waveforms from 10 deep-focus events at stations spanning a 110° azimuth range straddling the strike direction of the Kuril slab was analyzed by Beck and Lay (1986). Patterns in the travel times, amplitudes, and relative broadening were considered. The maximum variations in waveform complexity of S and ScS are observed along the Kuril slab strike, but sometimes S is broadened and sometimes it is not. There is substantial scatter in the data, with S sometimes being broadened at azimuths well removed from the slab strike (out the back of the slab). S is found to be broadened relative to ScS in 74% of the observations. The data indicate that there is a source of waveform variability in the lower mantle superimposed on any near-source effect. S and ScS waveform differences and differential travel times were found to correlate only along the slab strike.

Interpretation of the broadened S waveforms has been complicated by the lack of numerical methods for solving the full three-dimensional wave propagation problem. Vidale (1987) used a two-dimensional finite difference program to predict P and S waveforms in the down-dip plane of models for the Kuril slab. A long-period diffracted wave is produced for paths along the slab, as some energy travels within the slab and some in the surrounding medium (Fig. 36). A variety of models were considered, including the thermal slab model of Creager and Jordan (1986). This model predicts a factor of 2 amplitude reduction due to defocusing down-dip and 5-s broadening of the broadband P wave pulses. Assuming $\delta \ln V_s = 2\delta \ln V_p$, a corresponding shear wave model was produced, which predicts factor of 3.3 amplitude reduction with a 20-s broadening in the down-dip direction. Models with flaring velocity heterogeneity or short, very fast velocity models were considered as well, both of which produce weaker diffractions but still a factor of 2.5 defocusing. Additional two-dimensional slab calculations were performed by Witte (1987, 1989), using a pseudospectral method for elastic and anelastic waves. He considered a range in slab models similar to those explored by Vidale (1987) but found somewhat less pronounced effects on the waveforms.

Analysis of broadband waveforms distorted by the high-velocity tabular structure under the Caribbean was performed by Vidale and Garcia-Gonzalez (1988). Using their two-dimensional finite difference method, weak broadening of digital waveforms recorded in North America for events in South America indicates that the lower mantle heterogeneity has a half-width of about 450 km, with a 3000-km lateral extent and 800-km depth extent. The estimated peak velocity anomaly is 1.5% for V_s and 0.6% for V_p . If this model is correct, the feature is about five times broader than shallow slabs and the velocity anomaly is about five times smaller.

Engdahl *et al.* (1988) explored whether the broadband observations of Engdahl and Kind (1986) can be explained by slab diffraction rather than crustal reverberations. Analysis of long-period P waveforms from the nuclear explosion

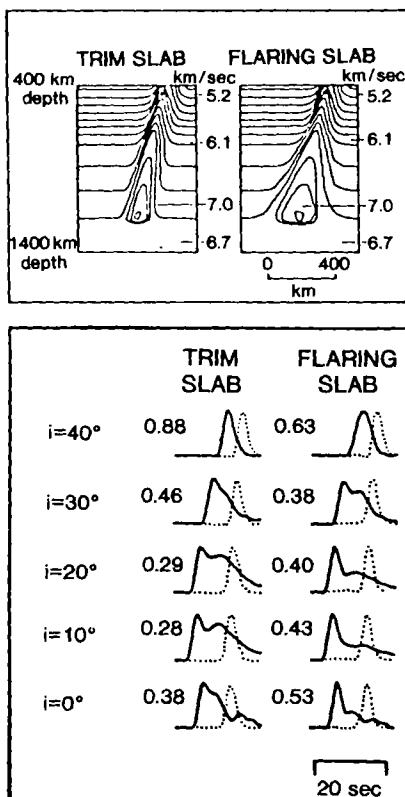


Fig. 36. Numerical calculation of SH waves using a two-dimensional finite difference method for the slab velocity models shown at the top. The synthetics shown below compare reference waveforms (dotted line) with the broadened pulses observed in the down-dip direction. The angle from the vertical toward the slab dip direction is shown for each synthetic case. Note that the paths down the slab arrive very early and have strong waveform distortion. The peak amplitudes of the slab synthetics are shown relative to the reference case. Defocusing by more than a factor of 3 is predicted down-dip for the trim slab model. Reprinted with permission from Vidale (1987).

CANNIKIN shows that defocusing and diffraction effects of the Aleutian slab do appear to be observed in Europe. A slight sharpening of the gradients at the top of the slab velocity model of Engdahl and Gubbins (1987), with almost 10% velocity anomaly at intermediate depth, can match the observed waveforms rather well. Broadening of down-going P waves for shallow events can explain the trends in the data of Engdahl and Kind (1986) as well. Analysis of P waveforms for a 135-km-deep event in the Kuril slab shows modest waveform broadening in the down-dip direction; however, several other events near this depth and an event at 540 km show no evidence of slab diffractions or pulse broaden-

ing. Thickening of the slab or reduced velocity gradients relative to the thermal model of Creager and Jordan (1986) were suggested as explanations for the absence of clear slab anomalies.

Cormier (1989) attempted to construct broadband S wave synthetics for slab models using Gaussian beams but was only partially successful. The basic defocusing effect of the slab could be reproduced, but the long-period diffraction effect was only approximated. Strong azimuthal patterns are predicted, with broadening expected on the entire dipping side of the slab. Raypaths out the back of the slab should have little waveform effect, even just 15° seaward of the slab strike. Cormier (1989) argues that along-strike complexities in broadband waveforms are probably caused by deep slab structure and suggests that observations of waveform complexity modeled by Lay and Helmberger (1983) as resulting from structure near the core–mantle boundary may instead be a near-source effect. Cormier (1989) notes that using a 70° dipping slab model, like that proposed by Creager and Jordan (1986) for the Kuril slab, predicts strong broadening of ScS phases in Europe, which is not observed. Cormier (1990) considered broadened slab models like those of Fischer *et al.* (1988) and Gurnis and Hager (1988), finding that the down-dip effects on ScS can be reduced, so he prefers such models.

Broadband SH wave displacements observed at distances greater than 72° from deep and intermediate-depth events in the Kuril slab were shown by Lay and Young (1989) to be more likely the result of lower mantle triplications, as suggested by Lay and Helmberger (1983), rather than diffractions by near-source structure as suggested by Cormier (1989). This emphasizes that waveform complexities may have several different origins, and caution must be exercised in attributing distortions to near-source effects.

Fischer (1990) and Schwartz *et al.* (1991a) have examined many broadband S and ScS waveforms for events in the Java and Kuril slabs, finding that the waveform complexity does not vary systematically with respect to the slab strike (Fig. 37). Schwartz *et al.* (1991a) find that there is a poor correlation of travel time and amplitude anomalies, but there is a correlation of ScS–S differential time anomalies and ScS/S ratios, indicative of defocusing effects. The lack of a simple pattern with respect to the slab suggests that this is not a near-source effect.

An extensive analysis of shear wave long-period travel times and amplitudes in the down-dip direction for slabs in the northwest Pacific was conducted by Gaherty *et al.* (1991). S, ScS, sS, and sScS observations were corrected for radiation pattern, geometric spreading, attenuation, and empirically determined station amplitude statics. Complete amplitude residual spheres were constructed for two events, but amplitude modeling was restricted to quasi-two-dimensional down-dip geometries. Comparison of finite difference synthetics for slab models from Creager and Jordan (1986) show reasonably good agreement for the Kuril

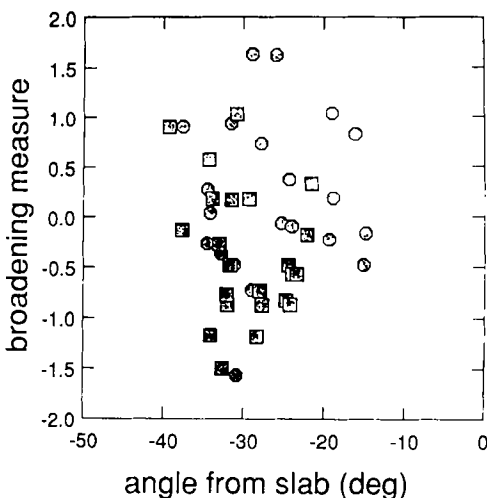


Fig. 37. Graph of normalized integrated pulse area of observed broadband SH pulses as a function of the angle between the takeoff direction of the ray and the plane of the Kuril slab. The boxes are ScS phases and the octagons are S phases. No systematic broadening is observed relative to the slab geometry, but S pulses do tend to be broader than ScS. Reprinted with permission from Schwartz *et al.* (1991a).

and Japan slabs (Fig. 22). Consistent variations of amplitude with takeoff angle relative to the slab dip were observed, but models with broadened slabs are also consistent with the data. Application of corrections based on the sS and sScS amplitude patterns enhances the trends in the down-going amplitudes for the Kuril slab, which holds promise for future complete amplitude residual sphere modeling. Deep events show a pattern, while intermediate events do not.

Synthetic calculations of long-period waveform effects for a kinetically suppressed olivine- β spinel phase transition in the slab interior also hold promise for future work (Vidale *et al.*, 1991). The presence of a low-velocity wedge inside the slab can cause secondary P arrivals from 1 to 4 s later than direct P at distances less than 30° and beyond 60° in the down-dip direction. The average slab velocity anomaly is reduced by the depressed boundary, but the most important effect is that the wedge provides gradients which can produce critical angles for the down-going wave. Secondary arrivals should be more readily detected for events in the upper phase boundary at depths near 400 km. There is as yet no clear evidence for such waveform distortions in teleseismic broadband data.

7. FUTURE DIRECTIONS IN SLAB IMAGING AND SUMMARY

The diverse seismological approaches mentioned in this chapter and the vast corresponding literature in the reference list are an impressive achievement of the

last 25 years of slab investigations. No longer are we constrained to cartoon models of subducting lithosphere; three-dimensional images of elastic velocity heterogeneity consistently reveal high-velocity tabular structures enveloping deep seismicity. Surprisingly sharp boundaries are found at the top of and within the subducting slab, and complex heterogeneity of the overlying wedge has been mapped out in several regions. Aseismic regions of slabs have been imaged, both in the upper mantle and in the uppermost lower mantle, and deformation of the deep slab has been related to seismicity locations and focal mechanisms. Many of the estimates of slab seismic heterogeneity that have been discussed are tabulated in Table 1, with a wide range of absolute velocity anomaly and velocity contrast estimates. Relative travel time anomalies tend to give average slab-wedge contrast estimates on the order of 5–7%, with absolute slab anomalies of 3–5%. Tomographic models indicate 2–4% heterogeneity, usually as a slab-wedge contrast, but are known to underpredict actual heterogeneity. Reflections and conversions indicate stronger, localized contrasts in the upper portions of slabs at intermediate depth, with velocity contrasts as large as 10–12%, but this is enhanced by the presence of a low-velocity channel in the slab. It appears that no single structure is generally representative of all slabs, presumably due to variations in thermal state of different slabs as well as variations in the overlying wedge from arc to arc.

Attaining an understanding of the thermal and chemical state of slabs, as well as their ultimate fate, is the primary objective of these seismological efforts. Clearly, progress has been made, but many fundamental questions persist. A very basic issue which is not resolved is the precise temperature distribution in the slab. Numerical models have many parameters that are poorly constrained, so independent corroboration of the calculations is important. Attempts to define a cutoff temperature for deep earthquakes based on rheological models also seem flawed given our ignorance of the mechanism of deep events. One hope for an absolute temperature determination in the slab would be reliable imaging of the 410-km olivine–spinel transition, but the possibility of kinetic distortion of this boundary complicates the problem. The 660-km transition is perhaps a better thermometer, as kinetic effects are at least not known to be important, and clear imaging of the boundary is viable (Section 5.3). The weakness here is uncertainty of the Clapeyron slope. As the experimental uncertainty is reduced the temperature estimates will be improved, but it will still not necessarily be clear exactly what part of the slab material is undergoing the phase transition.

Laboratory measurements of seismic velocity dependence on temperature in combination with thermal models with little viscous shear heating can produce reasonable seismic velocity anomalies for slabs (e.g., Creager and Jordan, 1986), but this does not constrain the absolute temperature anomalies well, because chemical effects have usually been ignored and the laboratory measurements were not made at high pressure and high temperature. More complete characterization of the phase equilibria in the slab and the associated seismic velocity

variations should allow joint thermal-mineralogical modeling of the observed seismic anomalies, improving the estimates of slab temperature structure. Ita (1992) has attempted a preliminary modeling of slab velocity structure using a differentiated pyrolytic model, a numerical thermal model, and available phase equilibria constraints. This model predicts large slab anomalies of 6–15%, with strong velocity gradients across the slab, and the upper part of the slab is faster than the lower part from 300 to 670 km depth due to chemical effects. The estimated velocities are higher than observed, particularly in the transition zone, but the general approach is promising. The problem is difficult because the phase equilibria are quite sensitive to the thermal model, coupling the parameters. Unfortunately, there are many thermodynamic parameters yet to be measured, particularly involving the shear modulus at high pressure and temperature, as well as persisting arguments over the bulk petrology of the slab (e.g., Ringwood 1993; Anderson, 1987b) so this may be a long process. Another example where experimental work is of great importance is for interpreting the low-velocity region at the top of the Japan slab. Tatsumi *et al.* (1994) have explored seismic velocities in granulite and amphibolite to see whether a low-velocity region in the crust or in the overlying wedge can be produced by hydrous phases. Anisotropy is an additional factor which must be considered in mapping a petrological model into a velocity structure, and one should not base arguments on low-pressure phases such as olivine when considering deep slab anisotropy (Anderson, 1987b).

At present, given a thermal model, there is substantial uncertainty in the relative P and S velocity heterogeneity that will result. There are now numerous reliable high-temperature low-pressure estimates of $dV_{(P,S)}/dT$ (e.g., Isaak *et al.*, 1989). These indicate $\delta \ln V_s/\delta \ln V_p = 1.2$ for forsterite from 300 to 1700 K. For depths down to the transition zone, there is little experimental evidence suggesting that this ratio will increase in the cold slab as a result of compression or exchange of Fe for Mg, so comparable ratios should be used for the seismogenic portion of the slab [higher values should be used in the wedge due to partial melting effects, but the velocity effects of partial melt (e.g., H. Sato *et al.*, 1989) are also still somewhat unclear]. However, there is evidence for higher ratios in the lower mantle (e.g., Jordan and Lynn, 1974; Dziewonski and Woodhouse, 1987). In an interpretation of thermodynamic causes of large shear velocity anomalies relative to P velocity anomalies ($\delta \ln V_s \approx 2\delta \ln V_p$) for deep mantle structure, Anderson (1987a) argues that temperature-induced variations of seismic velocity are inhibited by pressure in the Earth at large depths in the mantle. This occurs because the rigidity assumes a larger role in the temperature effect on velocity than the bulk modulus with increasing pressure. Use of laboratory measurements of temperature derivatives in modeling the deep slab without accounting for the effects of high pressure can thus lead to incorrect mapping of thermal structure into velocity structure, but it is unclear how the velocity scaling

varies with depth. Use of pressure- and temperature-dependent systematics of isochemical compounds rather than isostructural analogues to estimate properties of deep mantle materials has been pursued by Anderson (1988), but ultimately direct experimental determinations of material properties at high pressure and high temperature are very desirable. Empirical calibration of $\delta \ln V_s/\delta \ln V_p$ scaling using comparisons of P and S wave tomography and residual sphere modeling is important for the future. This should be done with careful suppression of deep mantle and near-receiver path effects, as these may tend to bias the anomaly scaling.

The many studies of reflections and conversions of seismic phases from boundaries at the edges and within the subducting slab (Section 5) have proved difficult to explain with thermal and chemical models of the slab. The main difficulty is that the seismically inferred boundaries are often stronger than can be reasonably attributed to thermal or petrological models. It is important that three-dimensional waveform modeling approaches be brought to bear on this problem to ensure that simplified seismic wave theories have not overestimated the boundary properties. There may also be an intrinsic bias in the data toward larger-amplitude observations, possibly enhanced by scattering effects.

A very useful approach to understanding the internal structures of the slab is to model the oceanic lithosphere prior to subduction, constraining the lid structure and any internal boundaries (e.g., Asada and Shimamura, 1976; Shimamura and Asada, 1976; Shimamura *et al.*, 1983; Anderson and Regan, 1983; Graves and Helmberger, 1988). Studies in the old Pacific lithosphere have revealed the presence of 5% internal lithospheric discontinuities and 50–100-km-thick seismic lids.

There is as yet no unambiguous resolution of the fate of deep slabs, but progress has been made in detecting deep aseismic slab material. Relative travel time patterns, residual sphere modeling, and tomographic images of deep slabs (Section 3 and 4) are suggestive of broadening and steeply dipping extension of the north-central Kuril slab to depths of about 1000 km under the Sea of Okhotsk, flattening to subhorizontal for the southern Kuril slab, and flattening and thickening of the Japan slab, with some tabular material dipping steeply into the lower mantle to depths of 800–900 km. Much of the flattening in the southern Kuril and Japan slabs appears to occur above 660 km depth. The northern and central Izu–Bonin slab appears to deflect horizontally well above the 660 km discontinuity, extending across the entire width of the Philippine Sea plate to the Ryukyu arc. Flattening of the deep slab appears to correspond to the syntaxes of the Japan slab, suggesting that kinematic and geometric constraints exert important influence on the fate of the deep slab. A broadened high-velocity anomaly extends vertically below the Marianas subduction zone to depths of about 1200 km. The Middle American slab appears to extend well below the cutoff of seismicity, possibly connecting up to a broad fast velocity region more than 1000

km deep beneath the Caribbean. Large-scale tomographic images of the entire mantle, while lacking resolution of small structures such as slabs, do suggest generally fast lower mantle velocities below the circum-Pacific, but a direct connection of these very large-scale features with slab anomalies is not yet established. Distinguishing continuous downwellings from thermally coupled layered systems is particularly difficult for large-scale tomographic models, but thermal coupling has not been shown to explain continuity of small-scale features.

The collective seismological, geodynamical, and mineralogical evidence summarized here can perhaps best be reconciled with a model of the Earth in which descending slabs do encounter resistance to lower mantle penetration, as a result of increasing viscosity with depth, intrinsic resistance from the endothermic perovskite phase transitions, and possibly a few percent chemical density contrast between the upper and lower mantles. The slab may buckle, imbricate, and deflect above this boundary in some regions. Apparently, the termination of seismicity near 660 km depth can be attributed to combined effects of thermal assimilation and completion of phase transformations in the slab (recall that seismicity in many slabs does not even penetrate this far) and, for seismogenic slabs that do exceed this depth, silicate material transforming to perovskite, extinguishing the mechanisms causing deep earthquakes. The aseismic portion of the slab may further broaden below the phase boundary. Slabs with rapid trench motions, such as the Izu slab, may flatten above the boundary.

Because the thermal inertia of the slab is still high at 660 km depth, the intrinsic chemical buoyancy of the slab components, which would tend to retain the slab in the transition zone if thermal equilibration were achieved, is inadequate to keep the slab from sinking. The lower mantle downwelling appears to be slowed relative to the upper mantle rates, with large slab accumulations and entrained material producing long-wavelength heterogeneities in the lower mantle below active subduction zones. This heterogeneity is imaged in residual sphere and tomographic models. Broadening and perhaps buckling of the slab cause viscous heating of the slab, reducing the lower mantle velocity gradients involved and making the deep slab anomalies inefficient diffractors of seismic waves. The variability of tabular extensions of deep slabs, some lying horizontal and others penetrating vertically, can be attributed to the variable tectonic history and specific geometry of particular zones, as material piles up and deforms near the top of the lower mantle. The slab material may tend to flush out catastrophically; the images of accumulations above and just below the 660 km discontinuity do not show the massive volumes expected for the total history of subduction. Of course, some flushing events may be ongoing, whereas in other places accumulations are just beginning.

Other interpretations can of course be made, but it seems that most of them have serious flaws. Undistorted slab penetration into the lower mantle is implied

by some residual sphere models, but this is hard to reconcile with the abundant evidence for significantly broadened anomalies below 660 km depth, as well as the clear evidence for horizontal deflection of some slabs. A penetrative convection scenario with relatively little deformation of the slab can be invoked to accommodate the duality of slab behavior, but this requires that the Earth system resides within a fairly restrictive range of conditions. If the evidence for a bulk difference in chemistry between the upper and lower mantle holds up, a modified version of the penetrative convection scenario may still be the best option, with significant broadening of deep slab material being included. Horizontal deflection of all slabs in a rigorously stratified model is difficult to reconcile with the evidence for tabular lower mantle velocity anomalies down-dip of several slab trajectories. Although several hundred kilometer deflections of a chemical discontinuity are expected, there is evidence for much deeper slablike structures which cannot be readily explained unless one invokes very tabular downwellings in a thermally coupled convection system. Horizontally deflected slabs are intrinsically more difficult to detect than steeply dipping extensions, but given the large cumulative volumes of subducted material, it is surprising that more dramatic transition zone anomalies near subduction zones are not apparent if this scenario is correct. Improved tomography of the transition zone and mapping of mantle discontinuity topography can contribute significantly to this problem.

Clearly, improved seismic images of deep slab structure, additional experimental work on chemical contrasts between the upper and lower mantles, and three-dimensional spherical convection calculations with phase transitions and temperature-dependent viscosity (to better incorporate slab properties) are all needed before there will be any consensus on the fate of descending slabs. It is also important to better understand the chemistry and rheology of the transition zone and the lower mantle. There is much promise in merging the approaches of residual sphere modeling and tomography, with additional attempts to incorporate *a priori* information about the upper mantle slab thermal and chemical heterogeneity. Initial location of seismicity in models with *a priori* slab structures should reduce mislocation effects and improve the retention of path anomalies in the travel time patterns. In this effort seismologists should draw upon parameterized models of the slab geometry, using kinematic models or surface trend analysis to define the *a priori* geometry in the seismogenic zones. Although there is always some danger when invoking *a priori* information, the last 25 years of analysis have provided good confidence in our basic understanding of subducting slabs, and we should not be afraid to exploit that knowledge. This should enhance our ability to resolve very deep slab structure where we lack *a priori* knowledge other than the total volume of material that has gone down. At the current rate of progress it appears that the next decade will bring about additional great leaps in our understanding of the velocity structure and fate of deep slabs.

ACKNOWLEDGMENTS

This study was supported by the National Science Foundation under grant EAR-9104764 and by facilities support from the W. M. Keck Foundation. Completion of this review was enabled by the Japan Society for Promotion of Science, which provided a visiting scholar fellowship to the author, who visited the Disaster Prevention Research Institute of Kyoto University. I thank Professor Masataka Ando for his very kind hospitality at DPRI and for many stimulating discussions. My understanding of slab tomography was expanded by discussions with Dr. Kazuro Hirahara. I thank K. Hirahara, G. Helffrich, T. Jordan, and R. van der Hilst for preprints. Rob van der Hilst provided the cross sections through his model shown in Figs. 26 and 27. Kristine Eckhardt provided helpful comments on the manuscript. This is contribution number 144 of the Institute of Tectonics and C. F. Richter Seismological Laboratory, University of California, Santa Cruz.

REFERENCES

- Abe, K. (1972). Seismological evidence for a lithospheric tearing beneath the Aleutian arc. *Earth Planet. Sci. Lett.* **14**, 428–432.
- Abe, K., and Kanamori, H. (1970). Mantle structure beneath the Japan Sea as revealed by surface waves. *Bull. Earthq. Res. Inst.* **48**, 1011–1021.
- Abers, G. A., and Roecker, S. W. (1991). Deep structure of an arc-continent collision: Earthquake relocation and inversion for upper mantle P and S wave velocities beneath Papua New Guinea. *J. Geophys. Res.* **96**, 6379–6401.
- Adams, R. D., and Ware, D. E. (1977). Subcrustal earthquakes beneath New Zealand: Locations determined with a laterally inhomogeneous velocity model. *N.Z. J. Geol. Geophys.* **20**, 59–83.
- Agarwal, N. K., Jacoby, W. R., and Berckhemer, H. (1976). Teleseismic P wave travel time residuals and deep structure of the Aegean region. *Tectonophysics* **31**, 33–57.
- Aggarwal, Y. P., Barazangi, M., and Isacks, B. (1972). P and S travel times in the Tonga-Fiji region: A zone of low velocity in the uppermost mantle behind the Tonga Island arc. *J. Geophys. Res.* **77**, 6427–6434.
- Aki, K., and Lee, W. (1976). Determination of three-dimensional velocity anomalies under a seismic array using first P arrival times from local earthquakes. *J. Geophys. Res.* **81**, 4381–4399.
- Aki, K., Christoffersson, A., and Husebye, E. S. (1977). Determination of the three-dimensional seismic structure of the lithosphere. *J. Geophys. Res.* **82**, 277–296.
- Amato, A., Alessandrini, B., and Cimini, G. B. (1993). Teleseismic wave tomography of Italy. In "Seismic Tomography: Theory and Practice" (H. M. Iyer and K. Hirahara, eds.), pp. 361–395. Chapman and Hall, London.
- Anderson, D. L. (1987a). A seismic equation of state. II. Shear properties and thermodynamics of the lower mantle. *Phys. Earth Planet. Inter.* **45**, 307–323.
- Anderson, D. L. (1987b). Thermally induced phase changes, lateral heterogeneity of the mantle, continental roots and deep slab anomalies. *J. Geophys. Res.* **92**, 13968–13980.
- Anderson, D. L. (1988). Temperature and pressure derivatives of elastic constants with application to the mantle. *J. Geophys. Res.* **93**, 4688–4700.
- Anderson, D. L. (1991). Chemical boundaries in the mantle. In "Glacial Isostasy, Sea-Level and the Mantle Rheology" (R. Sabadini et al., eds.), pp. 379–401. Kluwer Academic Publishers, The Netherlands.
- Anderson, D. L., and Bass, J. D. (1986). Transition region of the Earth's upper mantle. *Nature (London)* **320**, 321–328.

- Anderson, D. L., and Regan, J. (1983). Uppermantle anisotropy and the oceanic lithosphere. *Geophys. Res. Lett.* **10**, 841–844.
- Anderson, R. N., DeLong, S. E., and Schwarz, W. M. (1978). Thermal model for subduction with dehydration in the downgoing slab. *J. Geol.* **86**, 731–739.
- Anderson, R. N., DeLong, S. E., and Schwarz, W. M. (1980). Dehydration, asthenospheric convection and seismicity in subduction zones. *J. Geol.* **88**, 445–451.
- Ando, M., Ishikawa, Y., and Yamazaki, F. (1983). Shear wave polarization anisotropy in the upper mantle beneath Honshu, Japan. *J. Geophys. Res.* **88**, 5850–5864.
- Ando, M., Kaneshima, S., Ohtaki, T., and Okura, T. (1989). S to P converted phase from the lower plane of the double-planed deep seismic zone. *EOS* **70**, 1228.
- Andrews, D. J., and Sleep, N. H. (1974). Numerical modeling of tectonic flow behind island arcs. *Geophys. J. Roy. Astron. Soc.* **38**, 237–251.
- Ansell, J. H., and Gubbins, D. (1986). Anomalous high frequency wave propagation from the Tonga Kermadec seismic zone to New Zealand. *Geophys. J. R. Astron. Soc.* **85**, 93–106.
- Ansell, J. H., and Smith, E. G. C. (1975). Detailed structure of a mantle seismic zone using the homogeneous station method. *Nature (London)* **253**, 518–522.
- Aoki, H., and Tada, T. (1973). P wave travel time anomaly in Japan—observation of the Cannikin nuclear explosion. *J. Phys. Earth* **21**, 433–443.
- Apperson, K. D., and Frohlich, C. (1987). The relationship between Wadati–Benioff zone geometry and P, T and B axes of intermediate and deep focus earthquakes. *J. Geophys. Res.* **92**, 13821–13831.
- Asada, T., and Shimamura, H. (1976). Observations of earthquakes and explosions at the bottom of the western Pacific: Structure of oceanic lithosphere revealed by a longshot experiment. In “The Geophysics of the Pacific Ocean Basin and Its Margin” (G. H. Sutton, M. H. Manghnani, and R. Moberly, eds.), pp. 135–153. *Geophys. Monogr. Ser.* **19**, AGU, Washington, DC.
- Astiz, L., Lay, T., and Kanamori, H. (1988). Large intermediate-depth earthquakes and the subduction process. *Phys. Earth Planet. Inter.* **53**, 80–166.
- Barazangi, M., and Isacks, B. (1971). Lateral variations of seismic wave attenuation in the upper mantle above the inclined earthquake zone of the Tonga Island arc: Deep anomaly in the upper mantle. *J. Geophys. Res.* **76**, 8493–8516.
- Barazangi, M., and Isacks, B. L. (1979). A comparison of the spatial distribution of mantle earthquakes determined from the data produced by local and by teleseismic networks for the Japan and Aleutian arcs. *Bull. Seism. Soc. Am.* **69**, 1763–1770.
- Barazangi, M., Isacks, B., and Oliver, J. (1972). Propagation of seismic waves through and beneath the lithosphere that descends under the Tonga Island arc. *J. Geophys. Res.* **77**, 952–958.
- Barazangi, M., Isacks, B. L., Oliver, J., Dubois, J., and Pascal, G. (1973). Descent of lithosphere beneath New Hebrides, Tonga–Fiji and New Zealand: Evidence for detached slabs. *Nature (London)* **242**, 98–101.
- Barazangi, M., Isacks, B., Dubois, J., and Pascal, G. (1974). Seismic wave attenuation in the upper mantle beneath the southwest Pacific. *Tectonophysics* **24**, 1–12.
- Barazangi, M., Pennington, W., and Isacks, B. (1975). Global study of seismic wave attenuation in the upper mantle behind island arcs using pP waves. *J. Geophys. Res.* **80**, 1079–1092.
- Barley, B. J., Hudson, J. A., and Douglas A. (1982). S to P scattering at the 650 km discontinuity. *Geophys. J. R. Astron. Soc.* **69**, 159–172.
- Bass, J. D., and Anderson, D. L. (1984). Composition of the upper mantle: Geophysical tests of two petrological models. *Geophys. Res. Lett.* **11**, 237–240.
- Beck, S. L., and Lay, T. (1986). Test of the lower mantle slab penetration hypothesis using broad-band S waves. *Geophys. Res. Lett.* **13**, 1007–1010.
- Benz, H. M., Zandt, G., and Oppenheimer, D. H. (1992). Lithospheric structure of northern California from teleseismic images of the upper mantle. *J. Geophys. Res.* **97**, 4791–4807.

- Bercovici, D., Schubert, G., and Tackley, P. J. (1993). On the penetration of the 660-km phase change by mantle downflows. *Geophys. Res. Lett.* **20**, 2599–2602.
- Bevis, M., and Isacks, B. L. (1984). Hypocentral trend surface analysis: Probing the geometry of Benioff zones. *J. Geophys. Res.* **89**, 6153–6170.
- Billington, S. (1980). The morphology and tectonics of the subducted lithosphere in the Tonga–Fiji–Kermadec region from seismicity and focal mechanism solutions. Ph.D. Thesis, Cornell Univ., Ithaca, NY, 220 pp.
- Billington, S., and Isacks, B. L. (1975). Identification of fault planes associated with deep earthquakes. *Geophys. Res. Lett.* **2**, 63–66.
- Blanco, M. J., and Spakman W. (1993). The P-velocity structure of the mantle below the Iberian Peninsula: Evidence for subducted lithosphere below southern Spain. *Tectonophysics* **221**, 13–34.
- Bock, G. (1981). The effect of the descending lithosphere beneath the Tonga island arc on P wave travel time residuals at the Warramunga Seismic Array. *Phys. Earth Planet. Inter.* **25**, 360–371.
- Bock, G. (1987). P wave travel times from deep and intermediate depth earthquakes to local seismic stations and the subducted slab of oceanic lithosphere beneath the Tonga Island arc. *J. Geophys. Res.* **92**, 13863–13877.
- Bock, G., and Clements, J. R. (1982). Attenuation of short-period P, PcP, ScP, and pP waves in the Earth's mantle. *J. Geophys. Res.* **87**, 3905–3918.
- Bock, G., and Ha, J. (1984). Short period S–P conversion in the mantle at a depth near 700 km. *Geophys. J. R. Astron. Soc.* **77**, 593–615.
- Bock, G., Eguchi, T., and Fujinawa, Y. (1991). P wave velocity anomalies between the Tonga subducting slab and the overlying mantle beneath the Lau basin. *J. Geophys. Res.* **96**, 18119–18128.
- Bokelmann, G. H. R., and Silver, P. G. (1993). The Caribbean anomaly: Short-wavelength lateral heterogeneity in the lower mantle. *Geophys. Res. Lett.* **20**, 1131–1134.
- Bolt, B. A., and Nutti, O. W. (1966). P wave residuals as a function of azimuthal observations. *J. Geophys. Res.* **71**, 5977–5985.
- Bowman, J. R. (1988). Body wave attenuation in the Tonga subduction zone. *J. Geophys. Res.* **93**, 2125–2139.
- Bowman, J. R., and Ando, M. (1987). Shear-wave splitting in the upper mantle wedge above the Tonga subduction zone. *Geophys. J. R. Astron. Soc.* **88**, 25–41.
- Boyd, T. M., and Creager, K. C. (1991). The geometry of Aleutian subduction: Three-dimensional seismic imaging. *J. Geophys. Res.* **96**, 2267–2291.
- Brodholt, J., and Stein, S. (1988). Rheological control of Wadati–Benioff zone seismicity. *Geophys. Res. Lett.* **15**, 1081–1084.
- Burbach, G. V., and Frohlich, C. (1986). Intermediate and deep seismicity and lateral structure of subducted lithosphere in the circum-Pacific region. *Rev. Geophys.* **24**, 833–874.
- Burnley, P. C., Green, H. W. II., and Prior, D. J. (1991). Faulting associated with the olivine to spinel transformation in Mg_2GeO_4 and its implications for deep-focus earthquakes. *J. Geophys. Res.* **96**, 425–443.
- Cassidy, J. F., and Ellis, R. M. (1993). S wave velocity structure of the northern Cascadia subduction zone. *J. Geophys. Res.* **98**, 4407–4421.
- Chatelain, J.-L., Molnar, P., Prévot, R., and Isacks, B. L. (1992). Detachment of part of the downgoing slab and uplift of New Hebrides (Vanuatu) Islands. *Geophys. Res. Lett.* **19**, 1507–1510.
- Chinn, D., Isacks, B. L., and Barazangi, M. (1980). High frequency seismic wave propagation in western South America along the continental margin, in the Nazca plate, and across the Altiplano. *Geophys. J. R. Astron. Soc.* **60**, 209–244.
- Chiu, J.-M. (1982). Structural features of subduction zones determined by detailed analysis of short

- period seismic waves from earthquakes recorded in the New Hebrides Island arc. Ph.D. Thesis, Cornell Univer., Ithaca, NY.
- Chi, J.-M., Isacks, B. L., and Cardwell, R. K. (1985). Propagation of high frequency seismic waves inside the subducted lithosphere from intermediate-depth earthquakes recorded in the Vanuatu arc. *J. Geophys. Res.* **90**, 12741–12754.
- Chi, J.-M., Isacks, B. L., and Cardwell, R. K. (1991). 3-D configuration of subducted lithosphere in the western Pacific. *Geophys. J. Int.* **106**, 99–111.
- Chopelas, A., and Boehler, R. (1989). Thermal expansion measurements at very high pressure, systematics and a case for a chemically homogeneous mantle. *Geophys. Res. Lett.* **16**, 1347–1350.
- Chopelas, A., and Boehler, R. (1992). Thermal expansivity in the lower mantle. *Geophys. Res. Lett.* **19**, 1983–1986.
- Choy, G. L., and Cormier, V. F. (1986). Direct measurement of the mantle attenuation operator from broadband P and S waveforms. *J. Geophys. Res.* **91**, 7326–7342.
- Christensen, D., Zhao, D., and Pulpian, H. (1992). Tomographic imaging of the Alaska subduction zone. *EOS, Trans. Am. Geophys. Union* **73**, 199. (Abstr.)
- Christensen, U. (1982). Phase boundaries in finite amplitude mantle convection. *Geophys. J. R. Astron. Soc.* **68**, 487–497.
- Christensen, U. R. (1989). Models of mantle convection: One or several layers. *Phil. Trans. R. Soc. London A* **328**, 417–424.
- Christensen, U. R., and Yuen, D. A. (1984). The interaction of a subducting lithospheric slab with a chemical or phase boundary. *J. Geophys. Res.* **89**, 4389–4402.
- Christensen, U. R., and Yuen, D. A. (1985). Layered convection induced by phase transitions. *J. Geophys. Res.* **90**, 10291–10300.
- Christodoulou, A., and Hatzfeld, D. (1988). 3-D crustal and upper mantle structure beneath Chakidiki (N. Greece). *Earth Planet. Sci. Lett.* **88**, 153–168.
- Clayton, R. W., and Comer, R. P. (1983). A tomographic analysis of mantle heterogeneities from body wave travel times. *EOS, Trans. Am. Geophys. Union* **64**, 776. (Abstr.).
- Cleary, J. (1967). Azimuthal variation of the Longshot source term. *Earth Planet. Sci. Lett.* **3**, 29–37.
- Cleary, J., and Hales, A. L. (1966). Azimuthal variation of U.S. station residuals. *Nature (London)* **210**, 619–620.
- Clowes, R. M., Brandon, M. T., Green, A. G., Yorath, C. J., Brown, A., Sutherland, A., Kanasewich, E. R., and Spencer, C. (1987). Lithoprobe–southern Vancouver Island: Cenozoic subduction complex imaged by deep seismic reflection. *Can. J. Earth Sci.* **24**, 31–51.
- Comte, D., and Suárez, G. (1994). An inverted double seismic zone in Chile: Evidence of phase transformation in the subducted slab. *Science* **263**, 212–215.
- Cormier, V. F. (1989). Slab diffraction of S waves. *J. Geophys. Res.* **94**, 3006–3024.
- Cormier, V. F. (1990). Three-dimensional structure of subducted lithospheric slabs. Constraints from the amplitudes and waveforms of S waves. *Tech. Report GL-TR-90-0154*, Geophysics Laboratory, Hanscom AFB, MA.
- Cormier, V. F., Kim, W., Mandal, B., and Harvey, D. (1991). Effects of descending lithospheric slab on yield estimates of underground nuclear tests. *Tech. Report PL-TR-91-2025*, Phillips Laboratory, Hanscom AFB, MA.
- Creager, K. C. (1984). Geometry, velocity structure, and penetration depths of descending slabs in the western Pacific. Ph.D. Dissertation, Univ. of Calif., San Diego, La Jolla.
- Creager, K. C., and Boyd, T. M. (1991). The geometry of Aleutian subduction: Three-dimensional kinematic flow model. *J. Geophys. Res.* **96**, 2293–2307.
- Creager, K. C., and Boyd, T. M. (1992). Effects of earthquake mislocation on estimates of velocity structure. *Phys. Earth Planet. Sci.* **75**, 63–76.

- Creager, K. C., and Jordan, T. H. (1984). Slab penetration into the lower mantle. *J. Geophys. Res.* **89**, 3031–3049.
- Creager, K. C., and Jordan, T. H. (1986). Slab penetration into the lower mantle beneath the Mariana and other island arcs of the northwest Pacific. *J. Geophys. Res.* **91**, 3573–3589.
- Crosson, R. S., and Owens, T. J. (1987). Slab geometry of the Cascadia subduction zone beneath Washington from earthquake hypocenters and teleseismic converted waves. *Geophys. Res. Lett.* **14**, 824–827.
- Cunningham, P., Roecker, S. W., and Hatzfeld, D. (1986). Three dimensional P and S wave velocity structures of southern Peru and their tectonic implications. *J. Geophys. Res.* **91**, 9517–9532.
- Daessler, R., and Yuen, D. A. (1993). The effects of phase transition kinetics on subducting slabs. *Geophys. Res. Lett.* **20**, 2603–2606.
- Davies, D., and Frasier, C. W. (1970). P-wave multipathing, seismic discrimination. *Semi-Annual Technical Summary*, Lincoln Lab., Lexington, MA.
- Davies, D., and Julian, B. R. (1972). A study of short period P-wave signals from Longshot. *Geophys. J. R. Astron. Soc.* **29**, 185–202.
- Davies, D., and McKenzie, D. P. (1969). Seismic travel time residuals and plates. *Geophys. J. R. Astron. Soc.* **18**, 51–63.
- Ding, X., and Grand, S. (1992). Slab related velocity anomaly below Kurile subduction zone. *EOS, Trans. Am. Geophys. Union* **73**, 385. (Abstr.)
- Drakatos, G., and Drakopoulos, J. (1991). 3-D velocity structure beneath the crust and upper mantle of Aegean Sea region. *PAGEOPH* **135**, 401–420.
- Dubois, J. (1971). Propagation of P waves and Rayleigh waves in Melanesia: Structural implications. *J. Geophys. Res.* **76**, 7217–7240.
- Dubois, J., Pascal, G., Barazangi, M., Isacks, B. L., and Oliver, J. (1973). Travel times of seismic waves between the New Hebrides and Fiji Islands: A zone of low velocity beneath the Fiji plateau. *J. Geophys. Res.* **78**, 3431–3436.
- Duffy, T. S., and Anderson, D. L. (1989). Seismic velocities in mantle minerals and the mineralogy of the upper mantle. *J. Geophys. Res.* **94**, 1895–1912.
- Dziewonski, A. M. (1984). Mapping the lower mantle: Determination of lateral heterogeneity in P velocity up to degree and order 6. *J. Geophys. Res.* **89**, 5929–5952.
- Dziewonski, A. M., and Anderson, D. L. (1983). Travel times and station corrections for P waves at teleseismic distances. *J. Geophys. Res.* **88**, 3295–3314.
- Dziewonski, A. M., and Gilbert, F. (1976). The effect of small, aspherical perturbation on travel times and re-examination of the corrections for ellipticity. *Geophys. J. R. Astron. Soc.* **44**, 7–17.
- Dziewonski, A. M. and Woodhouse, J. H. (1987). Global images of the Earth's interior. *Science* **236**, 37–48.
- Ekström, G., Dziewonski, A. M., and Ibanez, J. (1990). Deep earthquakes outside slabs. *EOS, Trans. Am. Geophys. Union* **71**, 1462 (Abstr.)
- Engdahl, E. R. (1973). Relocation of intermediate depth earthquakes in the central Aleutians by seismic ray tracing. *Nature (London) Phys. Sci.* **245**, 23–25.
- Engdahl, E. R. (1975). Effects of plate structure and dilatancy on relative teleseismic P wave residuals. *Geophys. Res. Lett.* **2**, 420–422.
- Engdahl, E. R. (1977). Seismicity and plate subduction in the central Aleutians. *Am. Geophys. Union, Ewing Ser.* **1**, 259–271.
- Engdahl, E. R., and Fujita, K. (1981). Comments on 'Double seismic zone beneath the Marianas Island arc' by I. R. Samowitz and D. W. Forsyth. *J. Geophys. Res.* **86**, 7023–7024.
- Engdahl, E. R., and Gubbins, D. (1987). Simultaneous travel time inversion for earthquake location and subduction zone structure in the central Aleutian islands. *J. Geophys. Res.* **92**, 13855–13862.

- Engdahl, E. R., and Kind, R. (1986). Interpretation of broad-band seismograms from central Aleutian earthquakes. *Ann. Geophys.* **4**, 233–240.
- Engdahl, E. R., and Scholz, C. H. (1977). A double Benioff zone beneath the Central Aleutians and unbending of the lithosphere. *Geophys. Res. Lett.* **4**, 473–476.
- Engdahl, E. R., Sleep, N. H., and Lin, M.-T. (1977). Plate effects in north Pacific subduction zones. *Tectonophysics* **37**, 95–116.
- Engdahl, E. R., Dewey, J. W., and Fujita, K. (1982). Earthquake location in island arcs. *Phys. Earth Planet. Inter.* **30**, 145–156.
- Engdahl, E. R., Vidale, J. E., and Cormier, V. F. (1988). Wave propagation in subducted lithospheric slabs. Proceedings of the 6th course: Digital Seismology and Fine Modeling of the Lithosphere, International School of Applied Geophysics, Majorana Center, Erice, Sicily, pp. 139–155. Plenum Publishing Co., New York.
- Engebretson, D., and Kirby, S. (1992). Deep Nazca slab seismicity: Why is it so anomalous? *EOS, Trans. Am. Geophys. Union* **73**, 379. (Abstr.)
- Fedotov, S. A. (1963). The absorption of transverse seismic waves in the upper mantle and energy classification of near earthquakes of intermediate focal depth. *Izu. Akad. Navk. SSR, Ser. Gephys.* **6**, 509–520. (English trans.).
- Fedotov, S. A., and Slavina, L. B. (1968). An estimate of the longitudinal-wave velocities in the upper mantle under the northwestern part of the Pacific Ocean and Kamchatka. *Izv. Acad. Sci. USSR Phys. Solid Earth* **4**, 70–83.
- Fischer, K. M. (1990). Waveforms from slab earthquakes: Deep slab structure in the Kurils and Java. *EOS, Trans. Am. Geophys. Union* **71**, 1460. (Abstr.)
- Fischer, K. M., and Jordan, T. H. (1991). Seismic strain rate and deep slab deformation in Tonga. *J. Geophys. Res.* **96**, 14429–14444.
- Fischer, K. M., and Yang, X. (1994). Anisotropy in Kuril-Kamchatka subduction zone structure. *Geophys. Res. Lett.* **21**, 5–8.
- Fischer, K. M., Jordan, T. H., and Creager, K. C. (1988). Seismic constraints on the morphology of deep slabs. *J. Geophys. Res.* **93**, 4773–4783.
- Fischer, K. M., Creager, K. C., and Jordan, T. H. (1991). Mapping the Tonga slab. *J. Geophys. Res.* **96**, 14403–14427.
- Fitch, T. J. (1975). Compressional velocity in source regions of deep earthquakes: An application of the master earthquake technique. *Earth Planet. Sci. Lett.* **26**, 156–166.
- Fitch, T. J. (1977). In situ P-wave velocities in deep earthquake zones of the SW Pacific: Evidence for a phase boundary between the upper and lower mantle. In “Island Arcs, Deep Sea Trenches and Back Arc Basins,” Maurice Ewing Ser., Vol. 1 (M. Talwani and W. C. Pitman, eds.), pp. 123–136. AGU, Washington, DC.
- Flanagan, M. P., and Wiens, D. A. (1990). Attenuation structure beneath the Lau back arc spreading center from teleseismic S phases. *Geophys. Res. Lett.* **17**, 2117–2120.
- Flanagan, M. P., and Wiens, D. A. (1993). Radial upper mantle attenuation structure of inactive back-arc basins from differential shear wave measurements. *J. Geophys. Res.*, submitted.
- Forte, A. M., Dziewonski, A. M., and Woodward, R. L. (1993). Aspherical structure of the mantle, tectonic plate motions, nonhydrostatic geoid, and topography of the core-mantle boundary. In “Dynamics of Earth’s Deep Interior and Earth Rotation” (J. L. LeMouél, D. E. Smylie, and T. Herring, eds.). Am. Geophys. Union Geodyn. Ser., **72**, 135–166.
- Frohlich, C. (1987). Aftershocks and temporal clustering of deep earthquakes. *J. Geophys. Res.* **92**, 13944–13956.
- Frohlich, C., and Barazangi, M. (1980). A regional study of mantle velocity variations beneath eastern Australia and the southwestern Pacific using short-period recordings of P, S, P_cP, S_cP and S_cS waves produced by Tonga deep earthquakes. *Phys. Earth Planet. Inter.* **32**, 1–14.

- Frohlich, C., and Grand, S. P. (1990). The fate of subducting slabs. *Nature (London)* **347**, 333–334.
- Frohlich, C., Billington, S., Engdahl, E. R., and Malahoff, A. (1982). Detection and location of earthquakes in the central Aleutian subduction zone using island and ocean bottom seismograph stations. *J. Geophys. Res.* **87**, 6853–6864.
- Fujita, K., and Kanamori, H. (1981). Double seismic zones and stresses of intermediate depth earthquakes. *Geophys. J. R. Astron. Soc.* **66**, 131–156.
- Fujita, K., Engdahl, E. R., and Sleep, N. H. (1981). Subduction zone calibration and teleseismic relocation of thrust zone events in the central Aleutian Islands. *Bull. Seism. Soc. Am.* **71**, 1805–1828.
- Fukao, Y. (1977). Upper mantle P structure on the ocean side of the Japan–Kurile arc. *Geophys. J. R. Astron. Soc.* **50**, 621–642.
- Fukao, Y., Kanjo, K., and Nakamura, I. (1978). Deep seismic zone as an upper mantle reflector of body waves. *Nature (London)* **272**, 606–608.
- Fukao, Y., Hori, S., and Ukawa, M. (1983). A seismological constraint on the depth of the basalt–eclogite transition in a subducting oceanic crust. *Nature (London)* **303**, 413–415.
- Fukao, Y., Yamaoka, K., and Sakurai, T. (1987). Spherical shell tectonics: Buckling of the subducted lithosphere. *Phys. Earth Planet. Inter.* **45**, 59–67.
- Fukao, Y., Obayashi, M., Inoue, H. and Nenbui, M. (1992). Subducting slabs stagnant in the mantle transition zone. *J. Geophys. Res.* **97**, 4809–4822.
- Funamori, N., and Yagi, T. (1993). High pressure and high temperature in situ x-ray observation of $MgSiO_3$ perovskite under lower mantle conditions. *Geophys. Res. Lett.* **20**, 387–390.
- Furumura, T., and Moriya, T. (1990). Three-dimensional Q structure around the Hidaka Mountains, Hokkaido, Japan, *Zisin*, **43**, 121–132. (In Japanese with English abstract.)
- Gaherty, J. B., and Hager, B. H. (1994). Compositional vs. thermal buoyancy and the evolution of subducted lithosphere. *Geophys. Res. Lett.* **21**, 141–144.
- Gaherty, J., Lay, T., and Vidale, J. E. (1991). Investigation of deep slab structure using long period S waves. *J. Geophys. Res.* **96**, 16349–16367.
- Galea, P. (1992). Observation of very high P-velocities in the subducted slab, New Zealand, and their relation with the slab geometry. *Geophys. J. Int.* **110**, 238–250.
- Geller, R. J. (1990). Metastable phases confirmed. *Nature (London)* **347**, 620–621.
- Giardini, D. (1992). Space–time distribution of deep seismic deformation in Tonga. *Phys. Earth Planet. Inter.* **74**, 75–88.
- Giardini, D., and Woodhouse, J. H. (1984). Deep seismicity and modes of deformation in Tonga subduction zone. *Nature (London)* **307**, 505–509.
- Giardini, D., and Woodhouse, J. H. (1986). Horizontal shear flow in the mantle beneath the Tonga arc. *Nature (London)* **319**, 551–555.
- Glennon, M. A., and Chen, W.-P. (1993a). Systematics of deep-focus earthquakes along the Kuril–Kamchatka arc and their implications on mantle dynamics. *J. Geophys. Res.* **98**, 735–769.
- Glennon, M. A., and Chen, W.-P. (1993b). Ruptures of deep-focus earthquakes in the northwestern Pacific: Constraints from broadband seismic data. *Geophys. J. Int.*, submitted.
- Goto, K., and Hamaguchi, H. (1983). Characteristics of distribution of thermal stress and stress due to phase changes in descending plate beneath island arc. *Zisin* **36**, 31–41. (In Japanese.)
- Goto, K., Hamaguchi, H., and Suzuki, Z. (1983). Distribution of stress in descending plate in special reference to intermediate and deep focus earthquakes. I. Characteristics of thermal stress distribution. *Tohoku Geophys. J.* **29**, 81–105.
- Goto, K., Hamaguchi, H., and Suzuki, Z. (1985). Earthquake generating stresses in a descending slab. *Tectonophysics* **112**, 111–128.
- Goto, K., Suzuki, Z., and Hamaguchi, H. (1987). Stress distribution due to olivine–spinel phase transition in descending plate and deep focus earthquakes. *J. Geophys. Res.* **92**, 13811–13820.

- Goula, X., and G. Pascal (1979). Structure of the upper mantle in the convex side of the New Hebrides island arc. *Geophys. J. R. Astron. Soc.* **58**, 145–167.
- Grand, S. P. (1987). Tomographic inversion for shear velocity beneath the North American plate. *J. Geophys. Res.* **92**, 14065–14090.
- Grand, S. P. (1990). A possible station bias in travel time measurements reported to ISC. *Geophys. Res. Lett.* **17**, 17–20.
- Grand, S. P., and Ding, X.-Y. (1989). Residual spheres and slab penetration into the lower mantle. *EOS, Trans. Am. Geophys. Union* **70**, 1322. (Abstr.)
- Grand, S. P., and Engebretson, D. C. (1992). The relation between subduction history and lower mantle heterogeneity. *EOS, Trans. Am. Geophys. Union* **73**, 385. (Abstr.)
- Granet, M., and Trampert, J. (1989). Large-scale P-velocity structure in the Euro Mediterranean area. *Geophys. J. Int.* **99**, 583–594.
- Grasso, J. R., Cuer, J., and Pascal, G. (1983). Use of two inverse techniques. Application to a local structure in the New Hebrides island arc. *Geophys. J. R. Astron. Soc.* **75**, 437–472.
- Graves, R. W., and Helmberger, D. V. (1988). Upper mantle cross section from Tonga to Newfoundland. *J. Geophys. Res.* **93**, 4701–4711.
- Green, A. G. (1976). Ray paths and relative intensities in one- and two-dimensional velocity models. *Bull. Seism. Soc. Am.* **66**, 1581–1607.
- Green, A. G., Clowes, R. M., Yorath, C. J., Spencer, C., Kanasewich, E. R., Brandon, M. T., and Brown, A. S. (1986). Seismic reflection imaging of the subducting Juan de Fuca plate. *Nature (London)* **319**, 210–213.
- Green, H. W. II, and Burnley, P. C. (1989). A new, self-organizing mechanism for deep-focus earthquakes. *Nature (London)* **341**, 733–737.
- Green, H. W. II, Young, T. E., Walker, D., and Scholz, C. H. (1990). Anticrack-associated faulting at very high pressure in natural olivine. *Nature (London)* **348**, 720–722.
- Green, H. W. II, Scholz, C. H., Tingle, T. N., Young, T. E., and Koczynski, T. A. (1992a). Acoustic emissions produced by anticrack faulting during the olivine \rightarrow spinel transformation. *Geophys. Res. Lett.* **19**, 789–792.
- Green, H. W. II, Young, T. E., Walker, D., and Scholz, C. H. (1992b). The effect of nonhydrostatic stress on the $\alpha \rightarrow \gamma$ olivine phase transformations. *Geophys. Monog.*, in press.
- Gregerson, S. (1977). P wave travel time residuals caused by a dipping plate in the Aegean arc in Greece. *Tectonophysics* **37**, 83–93.
- Griggs, D. T. (1972). The sinking lithosphere and the focal mechanism of deep earthquakes. In "The Nature of the Solid Earth" (E. C. Robertson, ed.), pp. 361–384. McGraw-Hill, New York.
- Gubbins, D., and Snieder, R. (1991). Dispersion of P waves in subducted lithosphere: Evidence for an eclogite layer. *J. Geophys. Res.* **96**, 6321–6333.
- Gudmundsson, O., Davies, J. H., and Clayton, R. W. (1990). Stochastic analysis of global traveltimes data: Mantle heterogeneity and random errors in the ISC data. *Geophys. J. Int.* **102**, 25–43.
- Gurnis, M. (1986). The effects of chemical density differences on convective mixing in the Earth's mantle. *J. Geophys. Res.* **91**, 11407–11419.
- Gurnis, M., and Hager, B. H. (1988). Controls on the structure of subducted slabs. *Nature (London)* **335**, 317–321.
- Ha, J. (1978). A parabolic propagation model for the propagation of precursory signals through the subducted lithosphere. M.Sc. Thesis, Victoria, Univ. of Wellington.
- Hager, B. H. (1984). Subducted slabs and the geoid. *J. Geophys. Res.* **89**, 6003–6015.
- Hager, B. H., and Clayton, R. (1989). Constraints on the structure of mantle convection using seismic observations, flow models, and the geoid. In "Mantle Convection: Plate Tectonics and Global Dynamics" (W. R. Peltier, ed.), pp. 657–763. Gordon and Breach, New York.
- Hager, B. H., and Richards, M. A. (1989). Long-wavelength variations in Earth's geoid: Physical models and dynamical implications. *Phil. Trans. R. Soc. Lond. A* **328**, 309–327.

- Hager, B. H., Clayton, R. W., Richards, M. A., Comer, R. P., and Dziewonski, A. M. (1985). Lower mantle heterogeneity, dynamic topography and the geoid. *Nature (London)* **313**, 541–545.
- Hamada, K. (1973). The upper mantle beneath Japan inferred from P travel time anomalies by means of three-dimensional ray tracing, Part I. *J. Phys. Earth* **21**, 463–474.
- Hamaguchi, H., Goto, K., and Suzuki, Z. (1983). Double planed structure of intermediate depth seismic zone and thermal stress in the descending plate. *J. Phys. Earth* **31**, 329–347.
- Hamburger, M. W., and Isacks, B. L. (1987). Deep earthquakes in the Southwest Pacific: A tectonic interpretation. *J. Geophys. Res.* **92**, 13841–13854.
- Hanks, T. C., and Whitcomb, J. H. (1971). Comments on paper by J. W. Minear and M. Nafi Tokosoz: 'Thermal regime of a downgoing slab and new global tectonics'. *J. Geophys. Res.* **76**, 613–616.
- Harris, R. A., Iyer, H. M., and Dawson, P. B. (1991). Imaging the Juan de Fuca plate beneath southern Oregon using teleseismic P wave residuals. *J. Geophys. Res.* **96**, 19879–19889.
- Hasebe, K., Fujii, N., and Uyeda, S. (1970). Thermal processes under island arcs. *Tectonophysics* **10**, 335–355.
- Hasegawa, A., and Sacks, I. S. (1981). Subduction of the Nazca plate beneath Peru as determined from seismic observations. *J. Geophys. Res.* **86**, 4971–4980.
- Hasegawa, A., Umino, N., and Takagi, A. (1978a). Double-planed structure of the deep seismic zone in the northeastern Japan arc. *Tectonophysics* **47**, 43–58.
- Hasegawa, A., Umino, N., and Takagi, A. (1978b). Double-planed deep seismic zone and upper mantle structure in the northeastern Japan arc. *Geophys. J. R. Astron. Soc.* **54**, 281–296.
- Hasegawa, A., Umino, N., Takagi, A., and Suzuki, Z. (1979). Double-planed deep seismic zone and anomalous structure in the upper mantle beneath northeastern Honshu (Japan). *Tectonophysics* **57**, 1–6.
- Hasegawa, A., Zhao, D., Hori, S., Yamamoto, A., and Horiuchi, S. (1991). Deep structure of the northeastern Japan arc and its relationship to seismic and volcanic activity. *Nature (London)* **352**, 683–689.
- Hasemi, A. H., Ishii, H., and Takagi, A. (1984). Fine structure beneath the Tohoku district, northeastern Japan arc, as derived by an inversion of P wave arrival times from local earthquakes. *Tectonophysics* **101**, 245–265.
- Hashida, T. (1989). Three dimensional seismic attenuation structure beneath the Japanese Islands and its tectonic and thermal implications. *Tectonophysics* **159**, 163–180.
- Hashida, T., and Shimazaki, K. (1985). Seismic tomography: 3-D image of upper mantle attenuation beneath the Kanto district, Japan. *Earth Planet. Sci. Lett.* **75**, 403–409.
- Hashida, T., and Shimazaki, K. (1987). Determination of seismic attenuation structure and source strength by inversion of seismic intensity data: Tohoku district, northeastern Japan arc. *J. Phys. Earth* **35**, 67–92.
- Hashida, T., Stravrakakis, G., and Shimazaki, K. (1988). Three dimensional seismic attenuation structure beneath the Aegean region and its tectonic implications. *Tectonophysics* **145**, 43–54.
- Hauksson, E. (1985). Structure of the Benioff zone beneath the Shumagin Islands, Alaska: Relocation of local earthquakes using three dimensional ray tracing. *J. Geophys. Res.* **90**, 635–649.
- Helffrich, G., and Stein, S. (1993). Study of the structure of the slab–mantle interface using reflected and converted seismic waves. *Geophys. J. Int.* **115**, 14–40.
- Helffrich, G. R., Stein, S., and Wood, B. J. (1989). Subduction zone thermal structure and mineralogy and their relationship to seismic wave reflections and conversions at the slab/mantle interface. *J. Geophys. Res.* **94**, 753–763.
- Herrin, E. (1968). Seismological tables for P phases. *Bull Seism. Soc. Am.* **58**, 1193–1241.
- Hirahara, K. (1977). A large-scale three-dimensional seismic structure under the Japan islands and the Sea of Japan. *J. Phys. Earth* **25**, 393–417.

- Hirahara, K. (1980). Three-dimensional shear velocity structure beneath the Japan Islands and its tectonic implications. *J. Phys. Earth* **28**, 221–241.
- Hirahara, K. (1981). Three-dimensional seismic structure beneath southwest Japan: The subducting Philippine Sea plate. *Tectonophysics* **79**, 1–44.
- Hirahara, K. (1988). Detection of three-dimensional velocity anisotropy. *Phys. Earth Planet. Inter.* **51**, 71–85.
- Hirahara, K. (1993). Tomography using both local earthquakes and teleseisms: Velocity and anisotropy. In "Seismic Tomography: Theory and Practice" (H. M. Iyer and K. Hirahara, eds.), pp. 493–518, Chapman and Hall, London.
- Hirahara, K., and Hasemi, A. (1993). Tomography of subduction zones using local and regional earthquakes and teleseisms. In "Seismic Tomography: Theory and Practice" (H. M. Iyer and K. Hirahara, eds.), pp. 519–562, Chapman and Hall, London.
- Hirahara, K., and Ishikawa, Y. (1984). Travel time inversion for three-dimensional P wave velocity anisotropy. *J. Phys. Earth* **32**, 197–218.
- Hirahara, K., and Mikumo, T. (1980). Three-dimensional seismic structure of subducting lithospheric plate under the Japan Islands. *Phys. Earth Planet. Inter.* **21**, 109–119.
- Hirahara, I., Ikami, A., Ishida, M., and Mikumo, T. (1989). Three-dimensional P wave velocity structure beneath central Japan: Low velocity bodies in the wedge portion of the upper mantle above high velocity subducting plates. *Tectonophysics* **163**, 63–73.
- Honda, S. (1985). Thermal structure beneath Tohoku, northeast Japan—a case study for understanding the detailed thermal structure of the subduction zone. *Tectonophysics* **112**, 69–102.
- Honda, S. (1987). Two-layer convection with a soft boundary—slab penetration and mantle convection. *Zisin* **40**, 575–592. (In Japanese with English abstract.)
- Honda, S., Yuen, D. A., Balachandar, S., and Reuteler, D. (1993). Three-dimensional instabilities of mantle convection with multiple phase transitions. *Science* **259**, 1308–1311.
- Honda, T. (1984). Travel time analysis of PS-converted waves at the upper plane of the Pacific plate beneath the northern Kanto, Japan. Graduation Thesis, Chiba Univ. (In Japanese.)
- Hori, S. (1990). Seismic waves guided by untransformed oceanic crust subducting into the mantle: The case of the Kanto district, central Japan. *Tectonophysics* **176**, 355–376.
- Hori, S., Inoue, H., Fukao, Y., and Ukawa, M. (1985). Seismic detection of the untransformed 'basaltic' oceanic crust subducting into the mantle. *Geophys. J. R. Astron. Soc.* **83**, 169–197.
- Horie, A., and Aki, K. (1982). Three dimensional velocity structure beneath the Kanto district, Japan. *J. Phys. Earth* **30**, 255–281.
- Horie, A., and Shibuya, K. (1979). P wave velocity structure down to 150 km in the Kanto district—simultaneous determination of velocity structure, hypocenter parameters and station corrections by using inversion technique. *Zisin Ser. 2* **32**, 125–140. (In Japanese with English abstract.)
- Horiuchi, S., Yamamoto, A., Ueki, A., Tachibana, K., Konoj, T., and Takagi, A. (1982). Two-dimensional depth structure of the crust beneath the Tohoku district, the northeast Japan arc, Part II. Moho discontinuity and P-wave velocity. *J. Phys. Earth* **30**, 71–86.
- House, L. S., and Jacobs, K. H. (1982). Thermal stresses in subducting lithosphere can explain double seismic zones. *Nature (London)* **295**, 587–589.
- Houston, H., and Williams, Q. (1991). Fast rise times and the physical mechanism of deep earthquakes. *Nature (London)* **352**, 520–522.
- Hovland, J., and Husebye, E. S. (1981). Three-dimensional seismic velocity image of the upper mantle beneath southeastern Europe. In "Identification of Seismic Sources—Earthquake or Underground Explosion" (E. S. Husebye and S. Mykkeltveit, eds.), pp. 589–605. Reidel, Dordrecht.
- Hovland, J., and Husebye, S. (1982). Upper mantle heterogeneities beneath eastern Europe. *Tectonophysics* **90**, 137–151.

- Hsui, A. T., and Toksöz, M. N. (1979). The evolution of thermal structures beneath a subduction zone. *Tectonophysics* **60**, 43–60.
- Hsui, A. T., Marsh, B. D., and Toksöz, M. N. (1983). On melting of the subducted oceanic crust: Effects of subduction induced mantle flow. *Tectonophysics* **99**, 207–220.
- Huppert, L., and Froehlich, C. (1981). The P velocity within the Tonga Benioff zone determined from trace rays and observations. *J. Geophys. Res.* **86**, 3771–3782.
- Hurukawa, N. (1987). Simultaneous determination of hypocenters and P velocities in source regions of subcrustal earthquakes in the Tokai district, central Japan. *J. Seism. Soc. Jpn.*, Ser. 2, **40**, 551–560. (In Japanese with English abstract.)
- Hurukawa, N., and Hirahara, K. (1980). Structure of the Philippine Sea plate subducting beneath the Kii Peninsula. *J. Seism. Soc. Japan* **33**, 303–316. (In Japanese.)
- Hurukawa, N., and Imoto, M. (1987). P and S velocities in the source region of subcrustal earthquakes in the Tokai district, central Japan. *J. Phys. Earth* **36**, 1–17.
- Hurukawa, N., and Imoto, M. (1992). Subducting oceanic crusts of the Philippine Sea and Pacific plates and weak-zone-normal compression in the Kanto district, Japan. *Geophys. J. Int.* **109**, 639–652.
- Iidaka, T., and Mizoue, M. (1991). P wave velocity structure inside the subducting Pacific plate beneath the Japan region. *Phys. Earth Planet. Inter.* **66**, 203–213.
- Iidaka, T., and Obara, K. (1991). The upper boundary of the subducting Pacific plate estimated from ScSp waves beneath the Kanto region. Preprint.
- Iidaka, T., and Suetsugu, D. (1992). Seismological evidence for metastable olivine inside a subducting slab. *Nature (London)* **356**, 593–595.
- Iidaka, T., Mizoue, M., and Suyehiro, K. (1989a). Seismological evidence on velocity structure inside the subducting Pacific plate. *Phys. Earth Planet. Inter.* **58**, 249–254.
- Iidaka, T., Nakamura, I., and Mizoue, M. (1989b). The upper mantle boundary of the Pacific beneath the Kanto region estimated from PS converted waves. *Bull. Earthq. Res. Inst.* **64**, 37–50. (In Japanese with English abstract.)
- Iidaka, T., Mizoue, M., Nakamura, I., Tsukuda, T., Sakai, K., Kobayasi, M., Haneda, T., and Hashimoto, S. (1990). The upper boundary of the Philippine Sea plate beneath the western Kanto region estimated from S-P converted wave. *Tectonophysics* **179**, 321–326.
- Iidaka, T., Mizoue, M., Nakamura, I., Tsukuda, T., Sakai, K., Kobayasi, M., Haneda, T., and Hashimoto, S. (1991). The upper boundary of the Philippine Sea plate beneath the western Kanto region estimated from S-P and P-S converted waves. Preprint.
- Iidaka, T., Mizoue, M., and Suyehiro, K. (1992). Seismic velocity structure of the subducting Pacific plate in the Izu–Bonin region. *J. Geophys. Res.* **97**, 15307–15319.
- Inoue, H., Fukao, Y., Tanabe, K., and Ogata, Y. (1990). Whole mantle P wave travel time tomography. *Phys. Earth Planet. Inter.* **59**, 294–328.
- Irifune, T., and Ringwood, A. E. (1993). Phase transformations in subducted oceanic crust and buoyancy relationships at depths of 600–800 km in the mantle. *Earth Planet. Sci. Lett.* **117**, 101–110.
- Isak, D. G., Anderson, O. L., Goto, T., and Suzuki, I. (1989). Elasticity of single-crystal forsterite measured to 1700 K. *J. Geophys. Res.* **94**, 5895–5906.
- Isacks, B. L., and Barazangi, M. (1973). High frequency shear waves guided by a continuous lithosphere descending beneath western South America. *Geophys. J. R. Astron. Soc.* **33**, 129–139.
- Isacks, B. L., and Barazangi, M. (1977). Geometry of Benioff zones: Lateral segmentation and downwards bending of the subducted lithosphere. In “Island Arcs, Deep Sea Trenches, and Back-Arc Basins,” Maurice Ewing Ser., vol. 1 (M. Talwani and W. C. Pitman III, eds.), pp. 99–114. Am. Geophys. Union, Washington, DC.
- Isacks, B., and Molnar, P. (1971). Distribution of stresses in the descending lithosphere from a global

- survey of focal mechanisms solutions of mantle earthquakes. *Rev. Geophys. Space Phys.* **9**, 103–174.
- Isacks, B., Oliver, J., and Sykes, L. R. (1968). Seismology and the new global tectonics. *J. Geophys. Res.* **73**, 5855–5899.
- Ishida, M. (1970). Seismicity and travel time anomaly in and around Japan. *Bull. Earthq. Res. Inst.* **48**, 1023–1051.
- Ishida, M. (1984). The spatial distribution of earthquake hypocenters and the three dimensional velocity structure in the Kanto–Tokai district, Japan. *J. Phys. Earth* **32**, 399–422.
- Ishida, M. (1992). Geometry and relative motion of the Philippine Sea plate and Pacific plate beneath the Kanto–Toaki district, Japan. *J. Geophys. Res.* **97**, 489–513.
- Ishida, M., and Hasemi, A. (1984). The three-dimensional P wave velocity structure in the Kanto–Tokai district, Japan. *Res. Notes NRCDP* **58**, 1–11. Natl. Res. Cent. for Disaster Prev., Tsukuba, Japan. (In Japanese.)
- Ishida, M., and Hasemi, A. (1988). Three-dimensional fine velocity structure and hypocentral distribution of earthquakes beneath the Kanto–Tokai district, Japan. *J. Geophys. Res.* **93**, 2076–2094.
- Ishikawa, Y. (1985). Double seismic zone beneath Kyushu, Japan. *Zisin* **38**, 265–269. (In Japanese.)
- Ita, J. J. (1992). Petrology, density and velocity structure of subducting lithosphere and the mantle. Ph.D. Thesis, University of California, Berkeley, 108 pp.
- Ito, E., and Takahashi, E. (1989). Postspinel transforms in the system Mg_2SiO_4 – Fe_2SiO_4 and some geophysical implications. *J. Geophys. Res.* **94**, 10637–10646.
- Ito, E., and Yamada, H. (1982). Stability relations of silicate spinels, ilmenites, and perovskites. In “High Pressure Research in Geophysics” (S. Akimoto and M. H. Manghani, eds.), pp. 405–419. Center for Academic Publishing, Tokyo.
- Ito, E., Akaogi, M., Topor, L., and Navrotsky, A. (1990). Negative pressure–temperature slopes for reactions forming $MgSiO_3$ perovskite from calorimetry. *Science* **249**, 1275–1278.
- Iyer, H. M., and Hirahara, K. (Eds.). “Seismic Tomography: Theory and Practice.” Chapman and Hall, London. 842 pp.
- Iyer, H. M., and Rite, A. (1981). Teleseismic P-wave delays in the Oregon Cascades. *EOS, Trans. Amer. Geophys. Union* **62**, 1089. (Abstr.)
- Iyer, H. M., Rite, A., and Green, S. M. (1982). Search for geothermal heat sources in the Oregon Cascades by means of teleseismic P residual technique. Paper presented at 52nd Annual International Meeting and Exposition, Soc. of Explor. Geophys., Tulsa, OK.
- Jacob, K. H. (1970). Three-dimensional seismic ray tracing in a laterally heterogeneous spherical earth. *J. Geophys. Res.* **75**, 6675–6689.
- Jacob, K. H. (1972). Global tectonic implications of anomalous seismic P travel times from the nuclear explosion LONGSHOT. *J. Geophys. Res.* **77**, 2556–2573.
- James, D. E., and Snook, J. A. (1990). Seismic evidence for continuity of the deep slab beneath central and eastern Peru. *J. Geophys. Res.* **95**, 4989–5001.
- Jarrard, R. D. (1986). Relations among subduction parameters. *Rev. Geophys.* **24**, 217–284.
- Jeanloz, R. (1991). Effects of phase transitions and possible compositional changes on the seismological structure near 650 km depth. *Geophys. Res. Lett.* **18**, 1743–1746.
- Jeanloz, R., and Knittle, E. (1989). Density and composition of the lower mantle. *Phil. Trans. R. Soc. Lond. A* **328**, 377–389.
- Jordan, T. H. (1975). Lateral heterogeneity and mantle dynamics. *Nature (London)* **257**, 745–750.
- Jordan, T. H. (1977). Lithospheric slab penetration into the lower mantle beneath the Sea of Okhotsk. *J. Geophys.* **43**, 473–496.
- Jordan, T. H., and Lynn, W. S. (1974). A velocity anomaly in the lower mantle. *J. Geophys. Res.* **79**, 2679–2685.
- Jordan, T. H., Lerner-Lam, A. L., Creager, K. C. (1989). Seismic imaging of mantle convection:

- The evidence for deep circulation. In "Mantle Convection: Plate Tectonics and Global Dynamics" (W. R. Peltier, ed.), pp. 87–201. Gordon and Breach Science Publishers, New York.
- Jordan, T. H., Puster, P., Glatzmaier, G. A., and Tackley, P. J. (1993). Comparisons of seismic earth structures and mantle flow models using radial correlation functions. *Science* **261**, 1427–1431.
- Julian, B. R. (1970). Ray tracing in arbitrary heterogeneous media. *Tech. Note 1970* **45**. Lincoln Lab, Cambridge MA.
- Julian, B. R., and Gubbins, D. (1977). Three dimensional raytracing. *J. Geophys.* **43**, 95–113.
- Kaila, K. L. (1969). A new analytical method for finding the upper mantle velocity structure from P and S wave travel times of deep earthquakes. *Bull. Seism. Soc. Am.* **59**, 755–769.
- Kaila, K. L., and Krishna, V. G. (1978). Upper mantle velocity structure in the Tonga–Kermadec island arc region. *J. Phys. Earth* **26 Suppl.**, S155–S180.
- Kaila, K. L., Krishna, V. G., and Narain, H. (1971). Upper mantle P wave velocity structure in the Japan region from travel-time studies of deep earthquakes using a new analytical method. *Bull. Seism. Soc. Am.* **61**, 1549–1570.
- Kaila, K. L., Krishna, V. G., and Narain, H. (1974). Upper mantle shear wave velocity structure in the Japan region. *Bull. Seism. Soc. Am.* **64**, 355–374.
- Kamiya, S. (1991a). Three dimensional P-wave velocity structure beneath the Japanese Islands estimated from Japan University Network Earthquake Catalog data. *Bull. Earthq. Res. Inst., Univ. Tokyo* **66**, 383–417. (In Japanese with English abstract.)
- Kamiya, S. (1991b). Three dimensional P-wave velocity structure beneath the Japanese Islands estimated from the seismological bulletin of the Japan Meteorological Agency. *Zisin* **44**, 185–201. (In Japanese with English abstract.)
- Kamiya, S., Miyatake, T., and Hirahara, K. (1988). How deep can we see the high velocity anomalies beneath the Japan Islands? *Geophys. Res. Lett.* **15**, 828–831.
- Kamiya, S., Miyatake, T., and Hirahara, K. (1989). Three dimensional P wave velocity structure beneath the Japanese Islands. *Bull. Earthq. Res. Inst., Univ. Tokyo* **64**, 457–485.
- Kanamori, H. (1968). Travel time to Japanese stations from Longshot and their geophysical implications. *Bull. Earthq. Res. Inst., Univ. Tokyo* **46**, 841–859.
- Kanamori, H. (1970). Mantle beneath the Japanese arc. *Phys. Earth Planet. Inter.* **3**, 475–483.
- Kanamori, H., and Abe, K. (1968). Deep structure of the Japanese arc as revealed by surface waves. *Bull. Earthq. Res. Inst.* **46**, 1001–1025.
- Kaneshima, S., and Silver, P. G. (1992). A search for source side mantle anisotropy. *Geophys. Res. Lett.* **96**, 1049–1052.
- Kanjo, K. (1987). The existence of seismic-wave velocity discontinuity in the Sagami Bay region estimated from converted SP waves. *Q. J. Seism.* **50**, 61–64. (In Japanese.)
- Kao, H., and Chen, W.-P. (1993). Transition from interplate slip to double seismic zone along the Kuril–Kamchatka arc. *J. Geophys. Res.*, submitted.
- Kao, H., and Chen, W.-P. (1994). The double seismic zone in Kuril–Kamchatka: The tale of two overlapping single zones. *J. Geophys. Res.* **99**, 6913–6930.
- Kasahara, J., and Harvey, R. R. (1977). Seismological evidence for the high-velocity zone in the Kuril trench area from ocean bottom seismometer observations. *J. Geophys. Res.* **82**, 3805–3814.
- Katsumata, M. (1953). On the deep-focus earthquake of July 10, 1940. *Q. J. Seism.* **18**, 141–150. (In Japanese.)
- Katsumata, M. (1960). The effect of seismic zones upon the transmission of seismic waves. *Q. J. Seism.* **25**, 89–95. (In Japanese.)
- Kawakatsu, H. (1985). Double seismic zone in Tonga. *Nature (London)* **316**, 53–55.
- Kawakatsu, H. (1986a). Double seismic zones: kinematics. *J. Geophys. Res.* **91**, 4811–4825.
- Kawakatsu, H. (1986b). Downdip tensional earthquakes beneath the Tonga arc: A double seismic zone? *J. Geophys. Res.* **91**, 6432–6440.

- Kayal, J. R. (1986). Analysis of strong phases other than P and S from a microearthquake survey in the Wellington region, New Zealand. *Bull. Seism. Soc. Am.* **76**, 1347–1354.
- Kayal, J. R., and Smith, E. (1984). Upper mantle P wave velocities in the southeast North Island, New Zealand. *Tectonophysics* **104**, 115–125.
- Kendall, J.-M., and Thomson, C. J. (1993). Seismic modeling of subduction zones with inhomogeneity and anisotropy—I. Teleseismic P-wavefront tracking. *Geophys. J. Int.* **112**, 39–66.
- Kincaid, C., and Olson, P. (1987). An experimental study of subduction and slab migration. *J. Geophys. Res.* **92**, 13832–13840.
- King, S. D., and Hager, B. H. (1993). Subducted slabs and the geoid: I. Numerical calculations with temperature dependent viscosity. *J. Geophys. Res.*, in press.
- Kirby, S. H., Durhan, W. B., and Stern, L. A. (1991). Mantle phase changes and deep earthquake faulting in subducting lithosphere. *Science* **252**, 216–225.
- Kissling, E., and Lahr, J. (1991). Tomographic image of the Pacific slab under southern Alaska. *Eclogae Geol. Helv.* **84**, 297–315.
- Knittle, E., Jeanloz, R., and Smith, G. L. (1986). The thermal expansion of silicate perovskite and stratification of the Earth's mantle. *Nature (London)* **319**, 241–216.
- Koketsu, K. (1991). Three-dimensional ray tracing in a subduction zone. *Zisin* **44**, 165–176. (In Japanese.)
- Krishna, V. G., and Kaila, K. L. (1984a). Upper mantle velocity structure in the Ryukyu and Taiwan–Luzon arcs. *J. Phys. Earth* **32**, 63–81.
- Krishna, V. G., and Kaila, K. L. (1984b). Upper mantle velocity structure in the New Guinea and Solomon Islands regions. *J. Phys. Earth* **32**, 339–371.
- Kuge, K., and Satake, K. (1987). Lateral segmentation within the subducting lithosphere: Three-dimensional structure beneath the North Island, New Zealand. *Tectonophysics* **139**, 223–237.
- Langston, C. A. (1981). Evidence for the subducting lithosphere under southern Vancouver Island and western Oregon from teleseismic P wave conversions. *J. Geophys. Res.* **86**, 3857–3866.
- Lapp, D. B., Owens, T. J., and Crosson, R. S. (1990). P waveform analysis for local subduction geometry south of Puget Sound, Washington. *Pure Appl. Geophys.* **133**, 349–365.
- Lay, T. (1983). Localized velocity anomalies in the lower mantle. *Geophys. J. R. Astron. Soc.* **72**, 483–516.
- Lay, T. (1993). The fate of descending slab. *Ann. Rev. Earth and Planet. Sci.*, in press.
- Lay, T., and Helmberger, D. V. (1983). A lower mantle S wave triplication and the shear velocity structure of D''. *Geophys. J. R. Astron. Soc.* **75**, 799–838.
- Lay, T., and Young, C. J. (1989). Waveform complexity in teleseismic broadband SH displacements: Slab diffractions or deep mantle reflections? *Geophys. Res. Lett.* **16**, 605–608.
- Lay, T., Astiz, L., Kanamori, H., and Christensen, D. H. (1989). Temporal variation of large intraplate earthquakes in coupled subduction zones. *Phys. Earth Planet. Inter.* **54**, 258–312.
- Lees, A. C., Bukowinski, M. S. T., and Jeanloz, R. (1983). Reflection properties of phase transition and compositional change models of the 670-km discontinuity. *J. Geophys. Res.* **88**, 8145–8159.
- Ligdas, C. N., and Main, I. G. (1991). On the resolving power of tomographic images in the Aegean area. *Geophys. J. Int.* **107**, 197–203.
- Ligdas, C. N., Main, I. G., and Adams, R. D. (1990). 3-D structure of the lithosphere in the Aegean region. *Geophys. J. Int.* **102**, 219–229.
- Liu, M., Yuen, D. A., Zhao, W., and Honda, S. (1991). Development of diapiric structures in the upper mantle due to phase transitions. *Science* **252**, 1836–1839.
- Louat, R., Isacks, B. L., and Dubois, J. (1979). Anomalous propagation of seismic waves through the zone of shearing contact between the converging plates of the New Hebrides arc. *Nature (London)* **281**, 293–295.

- Lundgren, P. R., and Giardini, D. (1992a). Seismicity, shear failure and modes of deformation in deep subduction zones. *Phys. Earth Planet. Inter.* **74**, 63–74.
- Lundgren, P. R., and Giardini, D. (1992b). Isolated deep earthquakes and the fate of subduction in the mantle. *EOS, Trans. Am. Geophys. Union* **73**, 386. (Abstr.)
- Machetel, P., and Weber, P. (1991). Intermittent layered convection in a model mantle with an endothermic phase change at 670 km. *Nature (London)* **350**, 55–57.
- Mao, H. K., Hemley, R. J., Fei, Y., Shu, J. F., Chen, L. C., Jephcoat, A. P., Wu, Y., and Bassett, W. A. (1991). Effect of pressure, temperature and composition on lattice parameters and density of $(\text{Mg}, \text{Fe})\text{SiO}_3$ -perovskite to 30 GPa. *J. Geophys. Res.* **96**, 8069–8079.
- Marthelot, J.-M., Chatelain, J.-L., Isacks, B. L., Cardwell, R. K., and Coudert, E. (1985). Seismicity and attenuation in the central Vanuatu (New Hebrides) Islands: A new interpretation of the D'Entrecasteaux fracture zone. *J. Geophys. Res.* **90**, 8641–8650.
- Matsuzawa, T., Umino, N., Hasegawa, A., and Takagi, A. (1986). Upper mantle velocity structure estimated from PS-converted wave beneath the northeastern Japan arc. *Geophys. J. R. Astron. Soc.* **86**, 767–787.
- Matsuzawa, T., Umino, N., Hasegawa, A., and Takagi, A. (1987). Estimation of thickness of a low-velocity layer at the surface of the descending oceanic plate beneath the northeastern Japan arc by using synthesized PS-wave. *Sci. Rep. Tohoku Univ., Ser. 5* **31**, 19–28.
- Matsuzawa, T., Kono, T., Hasegawa, A., and Takagi, A. (1990). Subducting plate boundary beneath the northeastern Japan are estimated from SP converted waves. *Tectonophysics* **181**, 123–133.
- McKenzie, D. P. (1969). Speculations on the consequences and causes of plate motions. *Geophys. J. R. Astron. Soc.* **18**, 1–32.
- McKenzie, D. P. (1970). Temperature and potential temperature beneath island arcs. *Tectonophysics* **10**, 357–366.
- McKenzie, D. P. (1971). Comments on paper by J. W. Minear and M. Nafi Toksoz: 'Thermal regime of a downgoing slab and new global tectonics.' *J. Geophys. Res.* **76**, 607–609.
- McKenzie, D. P., and Julian, B. (1971). Puget Sound, Washington, earthquake and the mantle structure beneath the northwestern United States. *Geol. Soc. Am. Bull.* **82**, 3519–3524.
- McKenzie, D. P., and Sclater, J. G. (1968). Heat flow inside the island arcs of the northwest Pacific. *J. Geophys. Res.* **73**, 3173–3179.
- McLaren, J. P., and Frohlich, C. (1985). Model calculations of regional network locations for earthquakes in subduction zones. *Bull. Seism. Soc. Am.* **75**, 397–413.
- Meade, C., and Jeanloz, R. (1990). The strength of mantle silicates at high pressures and room temperature: Implications for the viscosity of the mantle. *Nature (London)* **348**, 533–535.
- Meade, C., and Jeanloz, R. (1991). Deep focus earthquakes and recycling of water into the Earth's mantle. *Science* **252**, 68–72.
- Michaelson, C. A., and Weaver, C. S. (1986). Upper mantle structure from teleseismic P-wave arrivals in Washington and northern Oregon. *J. Geophys. Res.* **91**, 2077–2094.
- Minear, J. W., and Toksöz, M. N. (1970a). Thermal regime of a downgoing slab. *Tectonophysics* **10**, 367–390.
- Minear, J. W., and Toksöz, M. N. (1970b). Thermal regime of a downgoing slab and new global tectonics. *J. Geophys. Res.* **76**, 1397–1419.
- Minear, J. W., and Toksöz, M. N. (1971). Reply. *J. Geophys. Res.* **76**, 617–626.
- Mitronovas, W., and Isacks, B. (1971). Seismic velocity anomalies in the upper mantle beneath the Tonga–Kermadec island arc. *J. Geophys. Res.* **76**, 7154–7180.
- Mitronovas, W., Isacks, B. L., and Seeber, L. (1969). Earthquake locations and seismic wave propagation in the upper 250 km of the Tonga island arc. *Bull. Seism. Soc. Am.* **59**, 1115–1135.
- Miyamachi, H., and Moriya, T. (1984). Velocity structure beneath the Hidaka mountains in Hokkaido, Japan. *J. Phys. Earth* **31**, 13–42.

- Miyatake, T., and Hirahara, K. (1989a). Three dimensional P wave velocity structure beneath Tonga Islands. *Abstr. Fall Meet. Seism. Soc. Jpn.* 1, P05. (Abstr. in Japanese.)
- Miyatake, T., and Hirahara, K. (1989b). Three dimensional seismic velocity structure beneath the Japan Islands (3). *Abstr. Fall Meet. Seism. Soc. Jpn.* 288. (Abstr. in Japanese.)
- Mizoue, M. (1976). Some remarks on the characteristics of subcrustal earthquake activities. *Proc. National Symposium on Earthquake Prediction Research in Japan*, pp. 9–105. (In Japanese.)
- Mizoue, M., Nakamura, I., Chiba, H., Yoshida, M., Hagiwara, H., and Yokota, T. (1981). The structure of the upper part of the crust in the regions of Sagami Bay, the Izu Peninsula and Suruga Bay as found by the observation of the earthquake swarm east of Izu Peninsula in 1980. *Bull. Earthq. Res. Inst.* **56**, 139–160.
- Molnar, P., and Oliver, J. (1969). Lateral variations in attenuation in the upper mantle and discontinuities in the lithosphere. *J. Geophys. Res.* **74**, 2648–2682.
- Molnar, P., Freedman, D., and Shih, J. S. F. (1979). Lengths of intermediate and deep seismic zones and temperatures in downgoing slabs of lithosphere. *Geophys. J. R. Astron. Soc.* **56**, 41–54.
- Mooney, H. M. (1970). Upper mantle inhomogeneity beneath New Zealand: Seismic evidence. *J. Geophys. Res.* **75**, 285–309.
- Morgan, J. P., and Shearer, P. M. (1993). Seismic constraints on mantle flow and topography of the 660-km discontinuity: Evidence for whole mantle convection. *Nature (London)* **365**, 506–511.
- Nagamune, T. (1971). Seismic waves associated with the anomalous zone in the upper mantle. *Geophys. Mag.* **35**, 123–135.
- Nagamune, T. (1973). Seismic wave velocities in the deep earthquake zone. *Pap. Meteorol. Geophys.* **24**, 139–156. (In Japanese.)
- Naguchi, S., and Okada, H. (1976). Anomalous seismic wave transmission and the upper mantle structure in and around Hokkaido. In “Symposium on Subterranean Structure in and around Hokkaido and Its Tectonic Implications,” Hokkaido University, Sapporo, 28–43. (In Japanese.)
- Nagumo, S., and Ouchi, T. (1990). An effect of source on Po/So generation evidenced by a deep-focus earthquake. *Geophys. Res. Lett.* **17**, 965–968.
- Nagumo, S., Hasegawa, S., Koresawa, S., and Kobayashi, H. (1970). Ocean bottom seismographic observation at the outside of Japan Trench near the Erimo seamount. *Bull. Earthq. Res. Inst. Tokyo Univ.* **48**, 769–792.
- Nakamura, M., Ando, M., and Ohkura, T. (1992a). The plane-like distribution of deep earthquakes below 300 km and the sharp upper and lower slab–asthenosphere boundaries. *Nature (London)*, submitted.
- Nakamura, M., Ando, M., and Ohkura, T. (1992b). Reflected waves from the lower plate boundary. *Abstr. Annual Meeting Seism. Soc. Jpn.*, in press.
- Nakanishi, I. (1980). Precursors to ScS phases and dipping interface in the upper mantle beneath southwestern Japan. *Tectonophysics* **69**, 1–35.
- Nakanishi, I. (1985). Three dimensional structure beneath the Hokkaido–Tohoku region as derived from a tomographic inversion of P arrival times. *J. Phys. Earth* **33**, 241–256.
- Nakanishi, I., and Horie, A. (1980). Anomalous distributions of seismic intensities due to the descending Philippine Sea plate beneath the southern Kanto district, Japan. *J. Phys. Earth* **28**, 333–360.
- Nakanishi, I., and Yamaguchi, K. (1986). A numerical experiment on nonlinear image reconstruction from first arrivals for two-dimensional island arc structure. *J. Geophys. Earth* **34**, 194–201.
- Nakanishi, I., Suyehiro, K., and Yokota, T. (1981). Regional variations of amplitudes of ScSp phases observed in the Japanese Islands. *Geophys. J. R. Astron. Soc.* **67**, 615–634.
- Neele, F., VanDecar, J., and Snieder, R. (1993). The use of P wave amplitude data in a joint inversion with travel times for upper mantle velocity structure. *J. Geophys. Res.* **98**, 12033–12054.

- Nenbai, M. (1990). How deep does a lithospheric slab descend into the mantle? M.S. Thesis, Nagoya Univ.
- Ni, J. F., Ibenbrahim, A., and Roecker, S. W. (1991). Three-dimensional velocity structure and hypocenters of earthquakes beneath the Hazara arc, Pakistan: Geometry of the underthrusting Indian plate. *J. Geophys. Res.* **96**, 19865–19877.
- Niazi, M. (1971). Seismic dissipation in deep seismic zones from the spectral ratio of pP/P. *J. Geophys. Res.* **76**, 3337–3343.
- Nieman, T. L., Fujita, K., and Rogers, W. J. (1986). Teleseismic mislocation of earthquakes in island arcs—theoretical results. *J. Phys. Earth* **34**, 43–70.
- Nolet, G. (1985). Solving or resolving inadequate and noisy tomographic systems. *J. Comp. Phys.* **61**, 463–482.
- Nolet, G. (1987). Seismic wave propagation and seismic tomography. In "Seismic Tomography" (G. Nolet, ed.), pp. 1–23. Reidel, Dordrecht.
- Obara, K. (1989). Regional extent of the S wave reflector beneath the Kanto district, Japan. *Geophys. Res. Lett.* **16**, 839–842.
- Obara, K. and Sato, H. (1988). Existence of an S wave reflector near the upper plane of the double seismic zone beneath the southern Kanto district, Japan. *J. Geophys. Res.* **93**, 15037–15045.
- Obara, K., Hasegawa, A. and Takagi, A. (1986). Three dimensional P and S wave velocity structure beneath the northeastern Japan arc. *Zisin Ser. 2* **39**, 201–215. (In Japanese.)
- Oda, H., Tanaka, T., and Seya, K. (1990). Subducting oceanic crust on the Philippine Sea plate in southwest Japan. *Tectonophysics* **172**, 175–189.
- Ohtaki, T., and Kaneshima, S. (1994). Continuous high velocity aseismic zone beneath the Izu-Bonin arc. *Geophys. Res. Lett.* **21**, 1–4.
- Okada, H. (1971). Forerunners of ScS waves from nearby deep earthquakes and upper mantle structure in Hokkaido. *Zisin Ser. 2* **24**, 228–239. (In Japanese.)
- Okada, H. (1973). Converted P phase from the ScS phase at the inclined deep seismic zone. *Yearb. Carnegie Inst. Wash.* **72**, 238–245.
- Okada, H. (1977). Fine structure of the upper mantle beneath Japanese island arcs as revealed from body wave analyses. D.Sc. Thesis, Univ. of Hokkaido, 129 pp.
- Okada, H. (1980). New evidence of the discontinuous structure of the descending lithosphere as revealed by ScSp phase. *Adv. Earth Planet. Sci.* **8**, 53–63.
- Okano, K., and Suetsugu, D. (1992). Search for lower mantle high velocity zones beneath the deepest Kurile and Mariana earthquakes. *Geophys. Res. Lett.* **19**, 745–748.
- Okino, K., Ando, M., Kaneshima, S., and Hirahara, K. (1989). The horizontally lying slab. *Geophys. Res. Lett.* **16**, 1059–1062.
- Okura, T., and Takeuchi, F. (1989). Structure of the upper surface of the Philippine Sea plate estimated by later phases from earthquakes occurring beneath Iyonada. *Program and Abstracts, Seismol. Soc. Jpn., No 1*, **A49**, 49. (Abstr. in Japanese.)
- Oliver, J., and Isacks, B. (1967). Deep earthquake zones, anomalous structures in the upper mantle, and the lithosphere. *J. Geophys. Res.* **72**, 4259–4275.
- Oliver, J., Isacks, B., Barazangi, M., and Mitronovas, W. (1973). Dynamics of the down-going lithosphere. *Tectonophysics* **19**, 133–147.
- Olson, P. (1988). Fate of subducted lithosphere. *Nature (London)* **331**, 113–114.
- Olson, P., Silver, P. G., and Carlson, R. W. (1990). The large-scale structure of convection in the Earth's mantle. *Nature (London)* **344**, 209–215.
- Oncescu, M. C. (1984). Three-dimensional P-wave velocity image under the Carpathian arc. *Tectonophysics* **106**, 305–319.
- Owens, T. J., Crosson, R. S., and Hendrickson, M. A. (1988). Constraints on the subduction

- geometry beneath western Washington from broadband teleseismic waveform modeling. *Bull Seism. Soc. Am.* **78**, 1319–1334.
- Oxburgh, E. R., and Turcotte, D. L. (1970). Thermal structure of island arcs. *Bull Geol. Soc. Am.* **81**, 1665–1688.
- Parise, J. B., Wang, Y., Yeganeh-Haeri, A., Cox, D. E., and Fei, Y. (1990). Crystal structure and thermal expansion of (Mg,Fe)SiO₃ perovskite. *Geophys. Res. Lett.* **17**, 2089–2092.
- Pascal, G., Dubois, J., Barazangi, M., Isacks, B. L., and Oliver, J. (1973). Seismic velocity anomalies beneath the New Hebrides island arc: Evidence for a detached slab in the upper mantle. *J. Geophys. Res.* **78**, 6998–7004.
- Pascal, G., Isacks, B. L., Barazangi, M., and Dubois, J. (1978). Precise relocations of earthquakes and seismotectonics of the New Hebrides island arc. *J. Geophys. Res.* **83**, 4957–4973.
- Peacock, S. (1987). Creation and preservation of subduction-related inverted metamorphic gradients. *J. Geophys. Res.* **92**, 12763–12781.
- Peltier, W. R., and Solheim, L. P. (1992). Mantle phase transitions and layered chaotic convection. *Geophys. Res. Lett.* **19**, 321–324.
- Prasad, G., and Bock, G. (1987). P wave travel times from the Tonga subduction zone to stations on the oceanic side of the Tonga-Kermadec trench. *Geophys. Res. Lett.* **14**, 9–12.
- Prévôt, R., Roecker, S. W., Isacks, B. L., and Chatelain, J. L. (1991). Mapping of low P wave velocity structures in the subducting plate of the central New Hebrides, Southwest Pacific. *J. Geophys. Res.* **96**, 19825–19842.
- Pulliam, R. J., Vasco, D. W., and Johnson, L. R. (1993). Tomographic inversions for mantle P wave velocity structure based on the minimization of l² and l¹ norms of International Seismological Centre travel time residuals. *J. Geophys. Res.* **98**, 699–734.
- Puspito, N. T., Yamanaka, Y., Miyatake, T., Shimazaki, K., and Hirahara, K. (1993). Three-dimensional P-wave velocity structure beneath the Indonesian region. *Tectonophysics* **220**, 175–192.
- Rasmussen, J., and Humphreys, E. (1988). Tomographic image of the Juan de Fuca plate beneath Washington and western Oregon using teleseismic P wave travel times. *Geophys. Res. Lett.* **15**, 1417–1420.
- Rees, B. A., and Okal, E. A. (1987). The depth of the deepest historical earthquakes. *Pure Appl. Geophys.* **125**, 699–715.
- Revenaugh, J., and Jordan, T. H. (1991). Mantle layering from ScS reverberations. 2. The transition zone. *J. Geophys. Res.* **96**, 19763–19780.
- Reyners, M., and Coles, K. S. (1982). Fine structure of the dipping seismic zone and subduction mechanics in the Shumagin islands, Alaska. *J. Geophys. Res.* **87**, 356–366.
- Richards, M. A., and Davies, G. E. (1989). On the separation of relatively buoyant components from subducted lithosphere. *Geophys. Res. Lett.* **16**, 831–843.
- Richards, M. A., and Engebretson, D. C. (1992). Large-scale mantle convection and the history of subduction. *Science* **355**, 437–440.
- Richards, M. A., and Wicks, C. W. (1990). S–P conversion from the transition zone beneath Tonga and the nature of the 670 km discontinuity. *Geophys. J. Int.* **101**, 1–35.
- Richter, F. M. (1979). Focal mechanisms and seismic energy release of deep and intermediate earthquakes in the Tonga-Kermadec region and their bearing on the depth extent of mantle flow. *J. Geophys. Res.* **84**, 6783–6795.
- Ringwood, A. E. (1976). Phase transformations in descending plates: Implications for mantle dynamics and differentiation. *Am. Geophys. Union Monograph* **19**, 391–398.
- Ringwood, A. E. (1982). Phase transformations and differentiation in subducting lithosphere—implications for mantle dynamics, basalt petrogenesis and crustal evolution. *J. Geol.* **90**, 611–643.

- Ringwood, A. E. (1986). Dynamics of subducted lithosphere and implications for basalt petrogenesis. *Terra Cognita* **6**, 67–77.
- Ringwood, A. E. (1990). Slab–mantle interactions. 3. Petrogenesis of intraplate magmas and structure of the upper mantle. *Chem. Geol.* **82**, 187–207.
- Ringwood, A. E. (1993). Role of the transition zone and 660 km discontinuity in mantle dynamics. Unpublished manuscript.
- Ringwood, A. E., and Irfune, T. (1988). Nature of the 650 km seismic discontinuity: Implications for mantle dynamics and differentiation. *Nature (London)* **331**, 131–136.
- Robinson, R. (1976). Relative teleseismic travel time residuals, North Island, New Zealand and their relation to upper-mantle structure. *Tectonophysics* **31**, T41–T48.
- Robinson, R. (1983). Velocity structure of the Wellington region, New Zealand, from local earthquake data and its implications for subduction tectonics. *Geophys. J. R. Astron. Soc.* **75**, 335–359.
- Robinson, R. (1986). Seismicity, structure and tectonics of the Wellington region, New Zealand. *Geophys. J. R. Astron. Soc.* **87**, 379–409.
- Roecker, S. W. (1982). Velocity structure of the Pamir–Hindu Kush region: Possible evidence of subducted crust. *J. Geophys. Res.* **87**, 945–959.
- Roecker, S. W. (1985). Velocity structure in the Izu–Bonin seismic zone and the depth of the olivine–spinel phase transition in the slab. *J. Geophys. Res.* **90**, 7771–7794.
- Roecker, S. W., Yeh, H. and Tsai, Y. B. (1987). Three dimensional P and S wave velocity structure beneath an arc–continent collision. *J. Geophys. Res.* **92**, 10547–10570.
- Romanowicz, B. A. (1980). A study of large-scale lateral variations of P velocity in the upper mantle beneath western Europe. *Geophys. J. R. Astron. Soc.* **63**, 217–232.
- Ross, N. L., and Hazen, R. M. (1989). Single-crystal x-ray diffraction study of MgSiO₃ perovskite from 77 to 400 K. *Phys. Chem. Minerals* **4**, 299–305.
- Sacks, I. S. (1969). Distribution of absorption of shear waves in South America and its tectonic significance. *Yearb. Carnegie Inst. Washington* **67**, 339–344.
- Sacks, I. S. (1971). The Q structure of South America. *Yearb. Carnegie Inst. Washington* **69**, 340–343.
- Sacks, I. S., and Okada, H. (1974). A comparison of the anelasticity structure beneath western South America and Japan. *Phys. Earth Planet. Inter.* **9**, 211–219.
- Sacks, I. S., and Snook, J. A. (1977). The use of converted phases to infer the depth of the lithosphere–aethenosphere boundary beneath South America. *J. Geophys. Res.* **82**, 2011–2017.
- Samowitz, I. R., and Forsyth, D. W. (1981). Double seismic zone beneath the Mariana Island arc, *J. Geophys. Res.* **86**, 99–117.
- Satake, K., and Hashida, T. (1989). Three-dimensional attenuation structure beneath North Island, New Zealand, *Tectonophysics* **159**, 181–194.
- Sato, H., Sacks, I. S., and Murase, T. (1989). The use of laboratory data for estimating temperature and partial melt fraction in the low velocity zone: Comparison with heat flow and electrical conductivity studies. *J. Geophys. Res.* **94**, 5689–5704.
- Sato, T., Nakayama, K., Tanaka, K., and Hasemi, A. (1989). Three dimensional P wave velocity structure beneath northern part of the Tohoku district, northern Honshu, Japan. *Zisin* **42**, 419–437. (In Japanese with English abstract.)
- Scarpa, R. (1982). Travel time residuals and three dimensional velocity structure of Italy. *Pure Appl. Geophys.* **120**, 583–606.
- Schneider, J. F., and Sacks, I. S. (1987). Stress in the contorted Nazca plate beneath southern Peru from local earthquakes. *J. Geophys. Res.* **92**, 13887–13902.
- Schubert, G., and Turcotte, D. L. (1974). Phase changes and mantle convection. *J. Geophys. Res.* **76**, 1424–1432.

- Schubert, G., Turcotte, D. L., and Oxburgh, E. R. (1970). Phase change instability in the mantle. *Science* **169**, 1075–1077.
- Schubert, G., Yuen, D. A., and Turcotte, D. L. (1975). Role of phase transitions in a dynamic mantle. *Geophys. J. R. Astron. Soc.* **42**, 705–735.
- Schwartz, S. Y., Lay, T., and Beck, S. L. (1991a). Shear wave travel time, amplitude, and waveform analysis for earthquakes in the Kurile slab: Constraints on deep slab structure and mantle heterogeneity. *J. Geophys. Res.* **96**, 14445–14460.
- Schwartz, S. Y., Lay, T., and Grand, S. (1991b). Seismic imaging of subducted slabs: Trade-offs with deep path and near-receiver effects. *Geophys. Res. Lett.* **18**, 1265–1268.
- Scrivner, C., and Anderson, D. L. (1992). The effect of post Pangea subduction on global mantle tomography and convection. *Geophys. Res. Lett.* **19**, 1053–1056.
- Sekiguchi, S. (1991). Three-dimensional Q structure beneath the Kanto–Tokai district, Japan. *Tectonophysics* **195**, 83–104.
- Sekiguchi, S. (1992). Amplitude distribution of seismic waves for laterally heterogeneous structures including a subducting slab. *Geophys. J. Int.* **111**, 448–464.
- Shearer, P. M. (1991). Constraints on upper mantle discontinuities from observations of long-period reflected and converted phases. *J. Geophys. Res.* **96**, 18147–18182.
- Shearer, P. M., and Masters, T. G. (1992). Global mapping of topography on the 660-km discontinuity. *Nature (London)* **355**, 791–796.
- Shimamura, H., and Asada, T. (1976). Apparent velocity measurements on an oceanic lithosphere. *Phys. Earth Planet. Inter.* **13**, 15–22.
- Shimamura, H., Asada, T., Suyehiro, K., Yamada, T., and Inatani, H. (1983). Long shot experiments to study velocity anisotropy in the oceanic lithosphere of the northwestern Pacific. *Phys. Earth Planet. Inter.* **31**, 348–362.
- Shiono, K. (1974). Travel time analysis of relatively deep earthquakes in southwest Japan with special reference to the underthrusting of the Philippine Sea plate. *J. Geosci., Osaka City Univ.* **18**, 37–59.
- Shiono, K., and Sugi, N. (1985). Life of an oceanic plate: Cooling time and assimilation time. *Tectonophysics* **112**, 35–50.
- Shurbet, D. H. (1962). The high frequency P and S phases from the West Indies. *Bull. Seism. Soc. Am.* **52**, 957–962.
- Shurbet, D. H. (1964). The high frequency S phase and the structure of the upper mantle. *J. Geophys. Res.* **69**, 2065–2070.
- Silver, P. G., and Chan, W. W. (1986). Observations of body wave multipathing from broadband seismograms: Evidence for lower mantle slab penetration beneath the Sea of Okhotsk. *J. Geophys. Res.* **91**, 13787–13802.
- Silver, P., Carlson, R. W., and Olson, P. (1988). Deep slabs, geochemical heterogeneity and the large-scale structure of mantle convection: Investigation of an enduring paradox. *Annu. Rev. Earth Planet. Sci.* **16**, 477–541.
- Sleep, N. H. (1973). Teleseismic P-wave transmission through slabs. *Bull. Seism. Soc. Am.* **63**, 1349–1373.
- Sleep, H. M. (1975). Stress and flow beneath island arcs. *Geophys. J. R. Astron. Soc.* **42**, 827–857.
- Sleep, N. H. (1979). The double seismic zone in downgoing slabs and the viscosity of the mesosphere. *J. Geophys. Res.* **84**, 4565–4571.
- Smalley, R. F., Jr., and Isacks, B. L. (1987). A high-resolution local network study of the Nazca plate Wadati–Benioff zone under western Argentina. *J. Geophys. Res.* **92**, 13903–13912.
- Smith, A. T., and Toksöz, M. N. (1972). Stress distribution beneath island arcs. *Geophys. J. R. Astron. Soc.* **29**, 289–318.
- Snieder, R. (1988). Large scale waveform inversions of surface waves for lateral heterogeneity—II:

- Application to surface waves in Europe and the Mediterranean. *J. Geophys. Res.* **93**, 12067–12080.
- Snoke, J. A., Sacks, I. S., and Okada, H. (1974a). Empirical models for anomalous high frequency arrivals from deep focus earthquakes in South America. *Geophys. J. R. Astron. Soc.* **37**, 133–139.
- Snoke, J. A., Sacks, I. S., and Okada, H. (1974b). A model not requiring continuous lithosphere for anomalous high frequency arrivals from deep focus South American earthquakes. *Phys. Earth Planet. Inter.* **9**, 199–206.
- Snoke, J. A., Sacks, I. S., and Okada, H. (1977). Determination of the subducting lithosphere boundary by use of converted phases. *Bull. Seism. Soc. Am.* **67**, 1051–1060.
- Snoke, J. A., Sacks, I. S., and James, D. E. (1979). Subduction beneath western South America: Evidence from converted phases. *Geophys. J. R. Astron. Soc.* **59**, 219–225.
- Solheim, L. P., and Peltier, W. R. (1994). Avalanche effects in phase transition modulated thermal convection. *J. Geophys. Res.* **99**, 6997–7018.
- Solomon, S. C., and Butler, R. G. (1974). Prospecting for dead slabs. *Earth Planet. Sci. Lett.* **21**, 421–430.
- Solomon, S. C., and U, K. T. P. (1975). Elevation of the olivine–spinel transition in subducted lithosphere: Seismic evidence. *Phys. Earth Planet. Inter.* **11**, 97–108.
- Sondgereld, C. H., Isacks, B. L., Barazangi, M., and Billington, S. (1977). A search for velocity anomalies near the deep portions of the inclined seismic zone of Tonga island arc. *Bull. Seism. Soc. Am.* **67**, 537–541.
- Sorrells, G. G., Crowley, J. B., and Veith, K. F. (1971). Methods for computing ray paths in complex geological structures. *Bull. Seism. Soc. Am.* **61**, 27–53.
- Spakman, W. (1986a). Subduction beneath Eurasia in connection with the Mesozoic Tethys. *Geol. Mijnbouw* **65**, 145–153.
- Spakman, W. (1986b). The upper mantle structure in the Central European–Mediterranean region. In “European Geotraverse (EGT) Project, the Central Segment” (R. Freeman, St. Mueller, and P. Giese, eds.), pp. 215–222. European Science Foundation, Strasbourg, France.
- Spakman, W. (1988). Upper mantle delay time tomography. Ph.D. Thesis, Univ. of Utrecht, Utrecht, Netherlands, 200 pp.
- Spakman, W. (1990). Tomographic images of the upper mantle below central Europe and the Mediterranean. *Terra Nova* **2**, 542–553.
- Spakman, W. (1991). Delay time tomography of the upper mantle below Europe, the Mediterranean, and Asia Minor. *Geophys. J. Int.* **107**, 309–332.
- Spakman, W., and Nolet, G. (1988). Imaging algorithms, accuracy and resolution in delay time tomography. In “Mathematical Geophysics: A Survey of Recent Developments in Seismology and Geodynamics” (N. J. Vlaar *et al.*, eds.), pp. 155–188. Reidel, Dordrecht.
- Spakman, W., Wortel, M. J. R., and Vlaar, N. J. (1988). The Hellenic subduction zone: A tomographic image and its geodynamic implications. *Geophys. Res. Lett.* **15**, 60–63.
- Spakman, W., Stein, S., van der Hilst, R., and Wortel, R. (1989). Resolution experiments for NW Pacific subduction zone tomography. *Geophys. Res. Lett.* **16**, 1097–1100.
- Spakman, W., van der Lee, S. and van der Hilst, R. (1993). Travel-time tomography of the European Mediterranean mantle down to 1400 km. *Phys. Earth Planet. Inter.* **79**, 3–74.
- Spencer, C. P., and Engdahl, E. R. (1983). A joint hypocentre location and velocity inversion technique applied to the central Aleutians. *Geophys. J. R. Astron. Soc.* **72**, 399–415.
- Spencer, C. P., and Gubbins, D. (1980). Travel-time inversion for simultaneous earthquake location and velocity structure determination in laterally varying media, *Geophys. J. R. Astron. Soc.* **63**, 95–116.
- Stark, P. B., and Frohlich, C. (1985). The depth of the deepest deep earthquakes. *J. Geophys. Res.* **90**, 1859–1869.

- Stefani, J. P., Geller, R. J., and Kroeger, G. C. (1982). A direct measurement of the distance between a hypocenter in a Benioff-Wadati zone and the slab-asthenosphere contact. *J. Geophys. Res.* **87**, 323-328.
- Steinbach, V., and Yuen, D. A. (1992). The effects of multiple phase transitions on Venusian mantle convection. *Geophys. Lett.* **19**, 2243-2246.
- Stixrude, L., Hemley, R. J., Fei, Y., and Mao, H. K. (1992). Thermoelasticity of silicate perovskite and magnesiowüstite and stratification of the earth's mantle. *Science* **257**, 1099-1101.
- Su, W.-J., and Dziewonski, A. M. (1991). Predominance of long-wavelength heterogeneity in the mantle. *Nature (London)* **352**, 121-126.
- Su, W.-J., and Dziewonski, A. M. (1992). On the scale of mantle heterogeneity. *Phys. Earth Planet. Inter.* **74**, 29-54.
- Su, W.-J., Woodward, R. L., and Dziewonski, A. M. (1994). Degree-12 model of shear velocity heterogeneity in the mantle. *J. Geophys. Res.*, **99**, 6945-6980.
- Suetsugu, D. (1987). Recent seismological studies on lower mantle slab penetration. *Zisin Ser. 2* **40**, 633-644. (In Japanese with English abstract.)
- Suetsugu, D. (1988). Lower mantle slab penetration as inferred from P wave travel time and amplitude analysis. Sc.D. Thesis, Hokkaido Univ.
- Suetsugu, D. (1989). Lower mantle high velocity zone beneath the Kurils as inferred from P wave travel time and amplitude data. *J. Phys. Earth* **37**, 265-295.
- Sugi, N., Kikuchi, M., and Fukao, Y. (1989). Mode of stress release within a subducting slab of lithosphere: Implication of source mechanism of deep and intermediate-depth earthquakes. *Phys. Earth Planet. Inter.* **55**, 106-125.
- Sung, C. M. (1979). Kinetics of the olivine-spinal transition under high pressure and temperature: Experimental results and geophysical implications. In "High-Pressure Science and Technology" (K. D. Timmerhaus and M. S. Barber, eds.), pp. 31-41. Plenum, New York.
- Sung, C. M., and Burns, R. G. (1976). Kinetics of high pressure phase transformations: Implications to the evolution of the olivine-spinal transition in the downgoing lithosphere and its consequences on the dynamics of the mantle. *Tectonophysics* **31**, 1-32.
- Suyehiro, K., and Sacks, I. S. (1978). An anomalous low velocity region above the deep earthquakes in the Japan subduction zone. *Carn. Inst. Wash. Yearbook* **77**, 505-511.
- Suyehiro, K., and Sacks, I. S. (1979). P and S wave velocity anomalies associated with the subducting lithosphere determined from travel time residuals in the Japan region. *Bull. Seism. Soc. Am.* **69**, 97-114.
- Suyehiro, K., and Sacks, I. S. (1983). An anomalous low velocity region above the deep earthquakes in the Japan subduction zone. *J. Geophys. Res.* **88**, 10429-10438.
- Suzuki, S., Sasatani, T., and Motoya, Y. (1983). Double seismic zone beneath the middle of Hokkaido, Japan, in the southwestern side of the Kurile arc. *Tectonophysics* **96**, 59-76.
- Sykes, L. R. (1966). The seismicity and deep structure of island arcs. *J. Geophys. Res.* **71**, 2981-3006.
- Sykes, L. R., Isacks, B. L., and Oliver, J. (1969). Spatial distribution of deep and shallow earthquakes of small magnitudes in the Fiji-Tonga region. *Bull. Seism. Soc. Am.* **59**, 1093-1114.
- Tackley, P. J. (1993). Effects of strongly temperature-dependent viscosity on time-dependent, three-dimensional models of mantle convection. *Geophys. Res. Lett.* **20**, 2187-2190.
- Tackley, P. J., Stevenson, D. J., Glatzmaier, G., and Schubert, G. (1993). Effects of an endothermic phase transition at 670 km depth on spherical mantle convection. *Nature (London)* **361**, 699-704.
- Tada, T. (1972). P wave velocity distribution in the downgoing slab. *Zisin* **25**, 310-317.
- Takanami, T. (1982). Three dimensional seismic structure of the crust and upper mantle beneath the orogenic belts in southern Hokkaido, Japan. *J. Phys. Earth* **30**, 87-103.
- Takei, Y., and Suetsugu, D. (1989). A high velocity zone in the lower mantle under the Japan

- subduction zone inferred from precise measurements of P wave arrival times. *J. Phys. Earth* **37**, 225–231.
- Tanaka, T. (1987). Seismic structure of the crust and the upper mantle beneath the Shikoku and the Chugoku region, Japan. M.S. Thesis, Kyoto University. 307 pp.
- Tanaka, T., and Oda, H. (1988). A prominent later phase observed for the subcrustal earthquakes beneath southwest Japan. *Program and Abstracts, Seism. Soc. Jpn., No. 1*, **B3**, 107. (Abstr. in Japanese.)
- Taniyama, H., Shimazaki, K., and Hirahara, K. (1990). Corrections for receiver structure in teleseismic travel time inversion: 3-D P wave velocity structure of the New Hebrides. *EOS, Trans. Am. Geophys. Union* **71**, 897. (Abstr.)
- Matsumi, Y., Ito, K., and Goto, A. (1994). Elastic wave velocities in isochemical granulite and amphibolite: Origin of a low-velocity layer at the slab/mantle wedge interface. *Geophys. Res. Lett.* **21**, 17–20.
- Toksöz, N., Minear, J. W., and Julian, B. R. (1971). Temperature field and geophysical effects of a downgoing slab. *J. Geophys. Res.* **76**, 1113–1138.
- Toksöz, M. N., Sleep, N. H., and Smith, A. T. (1973). Evolution of the downgoing lithosphere and mechanisms of deep focus earthquakes. *Geophys. J. R. Astron. Soc.* **35**, 285–310.
- Toy, K. M. (1989). Tomographic analysis of ISC travel time data for earth structure. Ph.D. Thesis, Univ. of California, San Diego.
- Tsujiura, M. (1972). Spectra of body waves and their dependence on source depth. I. Japanese arc. *J. Phys. Earth* **20**, 251–266.
- Tsukahara, H. (1980). Physical conditions for double seismic planes of the deep seismic zone. *J. Phys. Earth* **28**, 1–15.
- Tsumura, K. (1973). Microearthquake activity in the Kanto district. *Publication for the 50th anniversary of the Great Kanto Earthquake, 1923*, 67–87. (In Japanese.)
- Turcotte, D. L., and Schubert, G. (1971). Structure of the olivine–spinel phase boundary in the descending lithosphere. *J. Geophys. Res.* **76**, 7980–7987.
- Turcotte, D. L., and Schubert, G. (1973). Frictional heating of the descending lithosphere. *J. Geophys. Res.* **78**, 5876–5886.
- Ukawa, M., and Fukao, Y. (1982). Simultaneous determination of P and S velocities of the crust and sub-Moho mantle with earthquake hypocenters in central Honshu, Japan. *J. Phys. Earth*, **30**, 171–189.
- Umino, N., and Hasegawa, A. (1975). On the two-layered structure of deep seismic plane in northeastern Japan arc. *Zisin* **28**, 125–139. (In Japanese.)
- Umino, N., and Hasegawa, A. (1984). Three-dimensional Q, structure in the northeastern Japan arc. *Zisin Ser. 2*, **37**, 217–228. (In Japanese.)
- Umino, N., Matsuzawa, T., and Hasegawa, A. (1990). Abstr. Annu. Meet. Seism. Soc. Japan, No. 2, 200. (Abstr.)
- Utsu, T. (1966). Regional differences in absorption of seismic waves in the upper mantle as inferred from abnormal distributions of seismic intensities, *J. Fac. Sci. Hokkaido Univ. Ser. 7 (Geophysics)* **2**, 359–374.
- Utsu, T. (1967). Anomalies in seismic wave velocity and attenuation associated with a deep earthquake zone, *I. J. Fac. Sci. Hokkaido Univ. Ser. 7* **3**, 1–25.
- Utsu, T. (1969). Anomalous seismic intensity distributions in western Japan. *Bull. Geophys. Hokkaido Univ.* **21**, 45–52. (In Japanese.)
- Utsu, T. (1971). Seismological evidence for anomalous structure of island arcs with special reference to the Japanese region. *Rev. Geophys. Space Phys.* **9**, 839–890.
- Utsu, T. (1975). Regional variation of travel-time residuals of P waves from nearby deep earthquakes in Japan and vicinity. *J. Phys. Earth* **23**, 367–380.

- Utsu, T., and Okada, H. (1968). Anomalies in seismic wave velocity and attenuation associated with a deep earthquake zone. 2. *J. Fac. Sci., Hokkaido Univ., Ser. 7* **3**, 65–84.
- VanDecar, J. C. (1991). Upper mantle structure of the Cascadia subduction zone from nonlinear teleseismic travel time inversion. Ph.D. Thesis, Univ. of Washington, Seattle.
- van der Hilst, R. (1990). Tomography with P, PP and pP delay-time data and the three-dimensional mantle structure below the Caribbean region. Ph.D. Thesis, Univ. of Utrecht, 200 pp.
- van der Hilst, R., and Engdahl, E. R. (1991). On the ISC PP and pP data and their use in delay time tomography. *Geophys. J. Int.* **106**, 169–188.
- van der Hilst, R., and Engdahl, E. R. (1992). Step-wise relocation of ISC earthquake hypocenters for linearized tomographic imaging of slab structure. *Phys. Earth Planet. Inter.* **75**, 39–54.
- van der Hilst, R., and Seno, T. (1993). Effects of relative plate motion on the deep structure and penetration depth of slabs below the Izu-Bonin and Mariana Island arcs. *Earth Planet. Sci. Lett.* **120**, 375–407.
- van der Hilst, R., and Spakman, W. (1987). A tomographic image of the Lesser Antilles subduction zone. *EOS, Trans. Am. Geophys. Union* **68**, 1376. (Abstr.).
- van der Hilst, R. D., and Spakman, W. (1989). Importance of the reference model in linearized tomography and images of subduction below the Caribbean plate. *Geophys. Res. Lett.* **16**, 1093–1096.
- van der Hilst, R., Engdahl, E. R., Spakman, W., and Nolet, G. (1991). Tomographic imaging of subducted lithosphere below northwest Pacific island arcs. *Nature (London)* **353**, 37–43.
- van der Hilst, R. D., Engdahl, E. R., and Spakman, W. (1992). What can we learn about deep slab structure and mantle dynamics from tomographic images? *EOS, Trans. Am. Geophys. Union* **73**, 385. (Abstr.).
- van der Hilst, R. D., Engdahl, E. R., and Spakman, W. (1993). Tomographic inversion of P and pP data for aspherical mantle structure below the northwest Pacific region. *Geophys. J. Int.* **115**, 264–302.
- Van der Sluis, A., and van der Vorst, H. A. (1987). Numerical solution of large, sparse linear systems arising from tomographic problems. In "Seismic Tomography" (G. Nolet, ed.), pp. 53–87. Reidel, Dordrecht.
- Vasco, D. W. (1991). Imaging the mantle: A weighted least squares approach. *J. Adv. Comp. Lab.* LANL, Oct. 4–13.
- Vasco, D. W., Pulliam, R. J., and Johnson, L. R. (1993). Formal inversion of ISC arrival times for mantle P-velocity structure. *Geophys. J. Int.* **113**, 586–606.
- Vassiliou, M. S. (1984). The state of stress in subducting slabs as revealed by earthquakes analyzed by moment tensor inversion. *Earth Planet. Sci. Lett.* **69**, 195–202.
- Vassiliou, M. S., and Hager, B. H. (1988). Subduction zone earthquakes and stress in slabs. *Pure Appl. Geophys.* **128**, 574–624.
- Vassiliou, M. S., Hager, B. H., and Raefsky, A. (1984). The distribution of earthquakes with depth and stress in subducting slabs. *J. Geodyn.* **1**, 11–28.
- Veith, K. F. (1974). The relationship of island arc seismicity to plate tectonics. Ph.D. dissertation, Southern Methodist Univ., Dallas, TX, 162 pp.
- Veith, K. F. (1975). Refined hypocenters and accurate reliability estimates. *Bull. Seism. Soc. Am.* **65**, 1199–1222.
- Vidale, J. E. (1987). Waveform effects of a high velocity, subducted slab. *Geophys. Res. Lett.* **14**, 542–545.
- Vidale, J. E., and Benz, H. M. (1992). Upper-mantle seismic discontinuities and the thermal structure of subduction zones. *Nature (London)* **356**, 678–683.
- Vidale, J. E., and Garcia-Gonzalez, D. (1988). Seismic observation of a high velocity slab 1200–1600 km in depth. *Geophys. Res. Lett.* **15**, 369–372.

- Vidale, J. E., and Houston, H. (1993). The depth dependence of earthquake duration and implications for rupture mechanisms. *Nature (London)* **365**, 45–47.
- Vidale, J. E., and Lay, T. (1993). Phase boundaries and mantle convection. *Science* **261**, 1401–1402.
- Vidale, J. E., Williams, Q., and Houston, H. (1991). Waveform effects of a metastable olivine tongue in subducting slabs. *Geophys. Res. Lett.* **18**, 2201–2204.
- Vlaar, N. J., and Wortel, M. J. R. (1976). Lithospheric aging, instability and subduction. *Tectonophysics* **32**, 331–351.
- von Huene, R., and Scholl, D. W. (1991). Observations at convergent margins concerning sediment subduction, subduction erosion, and the growth of continental crust. *Rev. Geophys.* **29**, 279–316.
- Wadati, K., Hirono, T., and Yumura, T. (1969). On the attenuation of S-waves and the structure of the upper mantle in the region of Japanese Islands. *Meteorol. Geophys.* **20**, 49–78.
- Wang, Y., Weidner, D. J., Liebermann, R. C., Liu, X., Ko, J., Vaughan, M. T., Zhao, Y., Yeganeh-Haeri, A., and Pacalo, R. E. G. (1991). Phase transition and thermal expansion of MgSiO_3 perovskite. *Science* **251**, 410–413.
- Ward, R. W., and Aki, K. (1975). Synthesis of teleseismic P waves from sources near sinking lithospheric slabs. *Bull. Seism. Soc. Am* **65**, 1667–1680.
- Watanabe, I. (1977). The upper mantle structure beneath Japan and its vicinity derived from P-wave travel time residuals. M.S. Thesis, Nagoya Univ., 49 pp.
- Weber, M. (1990). Subduction zones—their influence on traveltimes and amplitudes of P waves. *Geophys. J. Int.* **101**, 529–544.
- Weinstein, S. A. (1993). Catastrophic overturn of the earth's mantle driven by multiple phase changes and internal heat generation. *Geophys. Res. Lett.* **20**, 101–104.
- Whitman, D., Isacks, B. L., Chatelain, J.-L., Chiu, J.-M., and Perez, A. (1992). Attenuation of high-frequency seismic waves beneath the central Andean plateau. *J. Geophys. Res.* **97**, 19929–19947.
- Wickens, A. J., and Buchbinder, G. G. R. (1980). S wave residuals in Canada. *Bull. Seism. Soc. Am.* **70**, 809–822.
- Wicks, C. W. Jr., and Richards, M. A. (1991). Effects of source radiation patterns on the phase $S_{670}\text{P}$ beneath the Tonga subduction zone. *Geophys. J. Int.* **107**, 279–290.
- Wicks, C. W. Jr., and Richards, M. A. (1993). A detailed map of the 660-kilometer discontinuity beneath the Izu-Bonin subduction zone. *Science* **261**, 1424–1427.
- Wiens, D. A., McGuire, J. J., and Shore, P. J. (1993). Evidence for transformational faulting from a deep double seismic zone in Tonga. *Nature* **364**, 790–793.
- Witte, D. (1987). Numerical simulations of seismic waves distorted by subducting slabs. *EOS. Trans. Am. Geophys. Union* **68**, 352. (Abstr.).
- Witte, D. (1989). The pseudospectral method for simulating wave propagation. Ph.D. Dissertation, Columbia Univ., New York.
- Woodward, R. L., and Masters, G. (1991). Global upper mantle structure from long period differential travel times. *J. Geophys. Res.* **96**, 6351–6377.
- Wortel, M. J. R. (1982). Seismicity and rheology of subducted slabs. *Nature (London)* **296**, 553–556.
- Wortel, M. J. R. (1986). Deep earthquakes and the thermal assimilation of subducting lithosphere. *Geophys. Res. Lett.* **13**, 34–37.
- Wortel, M. J. R., and Spakman, W. (1992). Structure and dynamics of subducted lithosphere in the Mediterranean region. *Proc. Kon. Ned. Akad. V. Wetensch.* **95**, 325–347.
- Wortel, M. J. R., and Vlaar, N. J. (1988). Subduction zone seismicity and the thermomechanical evolution of downgoing lithosphere. *PAGEOPH* **128**, 625–659.
- Wortel, M. J. R., Goes, S. D. B., and Spakman, W. (1990). Structure and seismicity of the Aegean subduction zone. *Terra Nova* **2**, 554–562.

- Wyss, M. (1973). The thickness of deep seismic zones. *Nature (London)* **242**, 255–256.
- Wyss, M., and Molnar, P. (1972). Source parameters of intermediate and deep focus earthquakes in the Tonga arc. *Phys. Earth Planet. Inter.* **6**, 279–292.
- Yamamizu, F. (1973). P travel time anomaly in Japan as deduced from three dimensional seismic ray tracing. *Geophys. Bull. Hokkaido Univ. Sapporo* **30**, 33–56. (In Japanese with English abs.)
- Yamanaka, Y. (1990). Configuration of the high-velocity slab beneath the Kuril arc. Thesis, Univ. Tokyo, Tokyo, 24 pp.
- Yamanaka, Y., Miyatake, T. and Hirahara, K. (1992). Fingering and lower mantle penetration of the Kurile slab. Preprint.
- Yamaoka, K., Fukao, Y. and Kumazawa, M. (1986). Spherical shell tectonics: Effects of sphericity and inextensibility on the geometry of the descending lithosphere. *Rev. Geophys.* **24**, 27–55.
- Yamazaki, F., and Ooida, T. (1985). Configuration of subducted Philippine Sea plate beneath the Chubu district, central Japan. *Zishin* **38**, 193–201. (In Japanese.)
- Yoshii, T. (1977). Structure of the earth's crust and mantle in northeast Japan. *Kagaku* **47**, 170–176. (In Japanese.)
- Yoshii, T. (1979). A detailed cross-section of the deep seismic zone beneath northeastern Honshu, Japan. *Tectonophysics* **55**, 349–360.
- Zandt, G. (1975). Three-dimensional inversion of travel time residuals recorded in southwest Japan—confirmation of the downgoing slab. Unpublished manuscript.
- Zandt, G., and Carrigan, C. R. (1993). Small-scale convective instability and upper mantle viscosity under California. *Science* **261**, 460–463.
- Zhang, S., and Christensen, U. (1993). Geoid anomalies from Cenozoic subduction in semi-dynamical flow models including a phase boundary. *Geophys. Res. Lett.* **20**, 2383–2386.
- Zhao, D. (1991). A tomographic study of seismic velocity structure in the Japan Islands. Ph.D. Thesis, Tohoku Univ., 301 pp.
- Zhao, D., and Hasegawa, A. (1993). P wave tomographic imaging of the crust and upper mantle beneath the Japan Islands. *J. Geophys. Res.* **98**, 4333–4353.
- Zhao, D., Horiuchi, S., and Hasegawa, A. (1990a). 3-D seismic velocity structure of the crust and uppermost mantle in the northeastern Japan arc. *Tectonophysics* **181**, 135–149.
- Zhao, D., Horiuchi, S., and Hasegawa, A. (1990b). P-wave velocity of the uppermost mantle off the Japan Sea coast, *Tohoku Geophys. J.* **33**, 177–183.
- Zhao, D., Hasegawa, A., and Horiuchi, S. (1992a). Tomographic imaging of P and S wave velocity structure beneath northeastern Japan. *J. Geophys. Res.* **97**, 19909–19928.
- Zhao, D., Horiuchi, S., and Hasegawa, A. (1992b). Seismic velocity structure of the crust beneath the Japan Islands. *Tectonophysics* **212**, 289–301.
- Zhao, D., Rogers, G., and Wang, K. (1992c). Tomographic imaging of Cascadia subduction zone in and around Vancouver island. *EOS, Trans. Am. Geophys. Union* **73**, 199. (Abstr.).
- Zhao, D., Hasegawa, A., and Kanamori, H. (1993a). Deep structure of Japan subduction zone as derived from local, regional and teleseismic events. *J. Geophys. Res.*, in press.
- Zhao, D., Christensen, D., and Pulpan, H. (1993b). Tomographic imaging of the Alaska subduction zone. *J. Geophys. Res.*, submitted.
- Zhao, W., Yuen, D. A., and Honda, S. (1992). Multiple phase transitions and the style of mantle convection. *Phys. Earth Planet. Inter.* **72**, 185–210.
- Zhong, S., and Gurnis, M. (1993). Role of plates and temperature dependent viscosity in phase change dynamics. *J. Geophys. Res.*, in press.
- Zhou, H.-W. (1988) How well can we resolve the deep seismic slab with seismic tomography? *Geophys. Res. Lett.* **15**, 1425–1428.
- Zhou, H.-W. (1988). Travel time tomographic studies of structures around subducted lithospheric slabs. Ph.D. Thesis, California Inst. of Technol., 397 pp.

- Zhou, H.-W. (1990a). Mapping of P wave slab anomalies beneath the Tonga, Kermadec and New Hebrides arcs. *Phys. Earth Planet. Inter.* **61**, 199–229.
- Zhou, H.-W. (1990b). Observations on earthquake stress axes and seismic morphology of deep slabs. *Geophys. J. Int.*, **103**, 377–401.
- Zhou, H.-W., and Anderson, D. L. (1989a). Search for deep slabs in the northwest Pacific mantle. *Proc. Natl. Acad. Sci. USA* **86**, 8602–8606.
- Zhou, H.-W., and Anderson, D. L. (1989b). Teleseismic contributions to focal residual spheres and Tangshan earthquake sequence. *EOS, Trans. Am. Geophys. Union* **70**, 1322. (Abstr.).
- Zhou, H.-W., and Clayton, R. W. (1990). P and S wave travel time inversions for subducting slab under the island arcs of the northwest Pacific. *J. Geophys. Res.* **95**, 6829–6851.
- Zhou, H.-W., Anderson, D. L., and Clayton, R. W. (1990). Modeling of residual spheres for subduction zone earthquakes. I. Apparent slab penetration signatures in the NW Pacific caused by deep diffuse mantle anomalies. *J. Geophys. Res.* **95**, 6799–6827.
- Zielhuis, A. (1992). S-wave velocity below Europe from delay time and waveform inversion. Ph.D. Thesis, Univ. of Utrecht, Utrecht, 148 pp.

Index

A

- Aleutians, tomographic inversion studies, 112–113
Aleutians slab, residual sphere modeling, 78–79
Anisotropy
 effects on block inversion formulation, 92
 as indicator of shear flow, 35
 in mapping petrological models into velocity structure, 150
Anomaly, slab, *see* Slab anomaly
Arrivals, late high-frequency, in seismograms, 27–31
Assimilation, thermal, *see* Thermal assimilation
Attenuation
 on concave side of island arc, variations, 31
 heterogeneity, mapping, 35
 slab, *see* Slab attenuation
 tin, mapping in wedge lithosphere, 34–35
Attenuation zone, in shallow wedge, 33
Australia, Warramunga seismic array, 63–64

B

- Basalt, crustal transformation to eclogite, 45–47
Benioff zone, double, 40
 and slab seismicity, 117–121
Buoyancy
 chemical, slab, 45–48
 negative
 slab, 3
 subducting slab, 43

C

- CANNIKIN, 57, 78, 145–146
 near-source and teleseismic travel times, 25

- Caribbean, high-resolution tomographic inversion studies, 109–110
Cascadia, mantle velocity structure studies, 110–112
Central America, high-resolution tomographic inversion studies, 109–110
Chemical reaction, within slab, 4
Contrast, slab–wedge, *see* Slab–wedge contrast
Convection
 phase transitions with, models, 48–51
 slabs and mantle, 2–6
Convergent zone
 Hindu Kush, tomographic studies, 116–117
 Indonesia, slab tomographic studies, 108
 Tonga–Kermadec, tomographic inversions, 104–106
Conversion
 P and S
 for sources above slab, 131–132
 for waves traveling within slab, 125–131
 results, modeling slab structure from, 132–134
 slab related, 121–125
Crust
 basaltic, 3
 transformation from basalt to eclogite to garnetite, 45

D

- Defocusing
 long-period, and diffraction effects, 142–148
 short-period, and multipathing effects, 139–142
Dehydration, in slab thermal models, 39
Diffraction effects, and long-period defocusing, 142–148
Downwelling
 depth of deflection, 137
 shape, in modeling slab kinematics, 11
tabular geometry, imaging, 7

E**Earthquake**

- Cascadia arc, mantle velocity structure studies, 112
- deep
 - information on thermal and chemical state of deep slabs provided by, 8–10
 - maximum depth as constraint on deep slab processes, 10
 - production by slab transformational faulting, 4
 - distribution in slab, 39–41
- Hindu Kush, located in low-velocity material, 117
- intermediate- and deep-focus, 1
- Sakhalin, 124
- in slabs, 7–12
- in studies of slab travel time patterns, 53
- Eclogite**, crustal transformation to garnetite, 45–47
- Explosion**, nuclear, underground, *see* CANNIKIN; LONGSHOT; MILROW

F

- Flattening**
 - Kuril and Japan slabs, 151
 - Pacific slabs, 100
- Flow model, numerical modeling, 2

G

- Garnetite**
 - crustal transformation from eclogite, 45–47
 - transition zone, 43
- Gorda plate, mantle velocity structure studies, 110–111

H

- Harzburgite**, from megalith, effects of thermal equilibration, 46–47
- Heterogeneity**
 - attenuation, mapping, 35
 - long-wavelength, in lower mantle below active subduction zones, 152

mantle, 79

- near-source, smearing into deep parts of model, 88–89
- seismic, interpretation, 52
- slab, measurements, 26–27
- thermal, in slab thermal models, 36
- tin propagation, 30
- velocity
 - elastic, 149
 - flaring, 145
 - in mantle under Japan, 32
 - near-source, 54
 - seismic, three-dimensional, 1

Hindu Kush

- convergent zone, tomographic studies, 116–117
- earthquake, located in low-velocity material, 117

I**Imaging**

- high-resolution, crust structure, 35
- seismic, phase boundaries in slabs, 134–138

slab, *see* Slab imaging

- tabular geometry of downwellings, 7
- tomographic, *see* Tomography

Indonesia, convergent zone, slab tomographic studies, 108**Island arc**

- Aleutians, and LONGSHOT, 24–25
- concave side, variations in attenuation, 31
- Pacific, 13

Izu slab

- deep events, three-dimensional raytracing, 67–68
- deep seismicity in, 11

J**Japan**

- localized studies, 90–97
- strong velocity heterogeneity in mantle, 32
- travel time patterns, 57, 66–67

Japan slab

- residual sphere analysis for events, 86
- straight orientations to 660 km depth, 11

Juan de Fuca plate, mantle velocity structure studies, 111–112

Juan de Fuca slab, deep velocity structure, 55–56

K

Kuril slab

deep-focus event, analysis, 72–73

differential residual sphere, 87

and large-scale regional inversions, 97–104

thickening, 76

Kuril trench, travel time patterns, 60–61

L

Lau basin, 33–34

Lithosphere

oceanic

denification-induced dynamic instability, 3

thermodynamic parameters, 35–51

wedge, mapping of tin attenuation, 34–35

LONGSHOT, 24–25, 32, 33, 53–55, 59, 78, 139

Love wave, group velocities, 32

M

Magmatism, volcanic arc, 37

Mantle

chemical stratification, convective models, 41–44

convection, 2–6

heterogeneity, 79

lower

perovskite structure, predominance, 4

waveform variability, 145

Marianas slab, residual spheres for events, 74–75

Mediterranean, large-scale inversion of P velocity structure, 114–116

Megalith, deformed slab products, fate, 46–47

MILROW, near-source and teleseismic travel times, 25

Model, *see also specific model*

convective

with chemical and viscous stratification,

41–44

with phase transitions, 48–51

olivine, metastable, 135–137

slab thermal, 36–39

thermal and mechanical, 35–51

Modeling

numerical

flow models, 2

quasi-dynamic, for slab thermal problem,

36

residual sphere, 70–88

Multipathing effects, short-period defocusing and, 139–142

N

Nazca plate

deep focus events, analysis of broadband P wave recordings, 129–130

tin propagation, 35

New Britain, block tomography inversion, 106–107

New Hebrides, block tomography inversion, 106–107

New Hebrides arc, seismicity, 58

New Zealand, local events, clear converted phases between P and S, 127

New Zealand slab, tomographic inversions, 104–106

O

Olivine

metastable

model, 135–137

in slab central core, 4

in phase transitions, 8–10

polymorphs, in mantle, 41–43

velocity anisotropy, 25

P

Pacific Ocean

northwest, 90–104

southwest, 104–108

Penetration

slab, extent, 43

- slab material, below 660-km phase transition, 10–11
- Perovskite, structure, in lower mantle, 4
- Phase boundaries, in slabs, seismic imaging, 134–138
- Phase equilibrium, within slab, 4
- Phase transformation
- exothermic, 4
 - mineralogical, within slab, 4
 - slab, effects of chemical buoyancy, 45
 - spinel–perovskite, 135–137
- Phase transition
- olivine in, 8–9
 - olivine– β spinel, in double Benioff zone, 121
 - olivine-modified spinel, in convection models, 48–51
 - 660-km, penetration of slab material below, 10–11
- Philippines, tomographic studies, 108
- Philippine Sea slab, S-to-P conversions, 128–129
- Propagation, tin, heterogeneity, 30–31
- Pyroxene, polymorphs, in mantle, 41–43
- R**
- Rayleigh wave
- dispersion in wedge, 33
 - group velocities, 32
- Raytracing analyses, and relative travel time patterns, 53–70
- Reflection
- occurrence near upper surface of Nazca slab, 130
 - results, modeling slab structure from, 132–134
 - slab related, 121–125
- Relocation
- events, 72–74, 83–86
 - in tomographic inversion studies, 109
- Rheology, non-Newtonian, temperature-dependent, 41–43
- S**
- Sagging, slab, 119–120
- Seismic array, Warramunga, Australia, 63–64
- Seismic discontinuity, 660-km, in mantle, 41–43
- Seismicity
- slab, and double Benioff zones, 117–121
 - thermal controls, 39–41
- Seismic wave, localized sensitivity, in seismological study, 6
- Seismology, information about slabs from, 6–7
- Shear heating, viscous, in generating large wedge temperatures, 38
- Shear strain, deformation, 3
- Shear velocity, slow, wedge above Japan slab, 32
- Sinking
- old oceanic lithosphere at subduction zone, 3
 - slabs into lower mantle, 6
- Slab, *see specific slab*
- Slab anomaly, first-order, 12–27
- Slab attenuation, 25–26
- Slab boundaries
- constraints, and internal structure, 121–134
 - converted and reflected phases, 117–138
- Slab imaging
- future directions, 148–154
 - introduction, 1
- Slab structure
- focusing, multipathing, diffraction effects, 138–148
 - modeling using results from reflections and conversions, 132–134
- Slab-wedge contrast, 32
- Japanese events, 57
- Solomon Islands, block tomography inversion, 106–107
- South America
- high-resolution tomographic imaging studies, 108–110
 - wedge lithosphere near, 34
- Spinel transition, within slab, 4
- Stratification
- chemical and viscous, convective models with, 41–44
 - viscous, models, 51
- Stress, in slabs, finite-element models, 40–41
- Structure, wedge, 31–35
- Subduction zone
- sinking of old oceanic lithosphere at, 3
 - volcanism, 4
- Subjection zone, 30

T

Taiwan, velocity structure, three-dimensional, 107–108

Temperature distribution, in slab, unresolved issue, 149

Thermal assimilation

role in deep activity, 10–11
and seismicity, 40

Thickening

slab, 147
by thermal conduction, 75–77

Tin

attenuation, mapping in wedge lithosphere, 34–35

efficiency across arcs, 31

propagation, heterogeneity, 30

Tomography

block

high-resolution inversions, 98
inversion, for Tonga–Kermadec–New Zealand, 104

seismic, 95

slab velocity structure, 88–117

waveform, 89

wedge structure, 35

Tonga

earthquake energy release, 10–12

slab thermal model, 36

Tonga–Kermadec

convergent zone, tomographic inversions, 104–106

events, relative travel times, 60

ridge, path travel time curves, 34

Tonga slab

buckling and imbrication in, 11–12

geometry and deformation analyses, 77–78

Transition zone

garnetite, 43

improved tomography, 153

phase transitions within, 4

Travel time

anomalies, 64, 70–72

along different paths, 88

relative, 149

curves, for paths along Tonga–Kermadec ridge, 34

near-source and teleseismic, 25

patterns

constraints on slab velocity structure, 51–88

relative, and raytracing analyses, 53–70

retention of path anomalies in, 153

in seismological study, 6

shear wave long-period, 147–148

U

Unbending, slab, 119–121

V

Velocity model, one-dimensional, in location of earthquakes, 7

Velocity structure

elastic, three-dimensional, 7

seismic, internal layered, models, 1

slab

tomographic imaging, 88–117

travel time constraints on, 51–88

wave, elastic, 1

Viscosity

high

lower mantle, 4

slab, 4

subducting slab, 43–44

Volcanic arc, magmatism, 37

W

Wave

guided, 27–31

seismic, *see* Seismic wave

traveling within slab, P and S conversions, 125–131

Waveshape, in seismological study, 6

Wedge

above Japan slab, slow shear velocity, 32

accretionary, 3

flow, slab thermal models, 38–39

lithosphere, mapping of tin attenuation, 34–35

low-velocity, inside slab, 148.

low-velocity regions, 101

structure, 31–35

ISBN 0-12-018835-X



9 780120188352

A standard barcode representation of the ISBN 0-12-018835-X. It consists of two separate vertical barcode patterns. The first barcode on the left represents the ISBN number, and the second barcode on the right represents a library or institutional identifier, labeled '90065' above it.